STUDIES CONCERNING SOME NOVEL FLAMES AND SPECTRAL SOURCES AND THEIR USE IN ATOMIC SPECTROSCOPY

by

MICHAEL SARGENT, B.Sc., A.R.C.S., A.R.I.C.

A thesis submitted for the degree of

Doctor of Philosophy

in the University of London

Department of Chemistry,
Imperial College of Science and Technology,
London, S.W.7.

June, 1970

Abstract

A study of some flames and spectral light sources has been carried out in order to determine possible improvements for their use in the trace analysis techniques of atomic emission, absorption and fluorescence spectroscopy.

Flame characteristics which show significant changes on flame separation were examined in considerable detail, with particular emphasis on the spectra of the flame radiation and the flame temperature. The latter has been measured by novel adaptations of two spectroscopic methods. The use of nitrogen or argon separated flames as free atom sources in both atomic emission and absorption spectroscopy was investigated. Some examples of improvements to determinations of trace metals by both techniques are reported for the air-acetylene and nitrous oxide-acetylene flames.

A Fabry-Perot interferometer system has been assembled in a form suitable for the routine testing and evaluation of spectral light sources used in atomic absorption and fluorescence spectroscopy. The high resolving power of the instrument was used to record the profiles of lines emitted by the light sources. The theory, construction and use of the instrument is fully described. Techniques for measurement of the relative intensities of hyperfine structure components and of actual line widths were investigated. Examples are given of their use for the evaluation of thallium and calcium hollow cathode lamps, electrodeless discharge tubes and a vapour discharge lamp. Possible means of improving the sources are suggested on the basis of these results.

Preface

The volume of research into the use for chemical analysis of atomic emission, absorption and fluorescence spectroscopy has grown enormously during recent years and now encompasses a very wide range of techniques and skills. The work described here naturally reflects the interests of the author and the Analytical Chemistry Group at Imperial College. However, this thesis attempts as far as possible to discuss in general terms the implications of the research carried out into the flames and spectral sources which form such an important part of the three techniques.

Some explanation is necessary concerning the general arrangement of this thesis. I firmly believe that a research project such as that described here cannot be presented in isolation with merely a few short references to the ideas and work which have preceded it. In view of this, the reader will find a fairly detailed discussion of the theoretical and historical background to the present research. Unfortunately, the wide range of topics covered would result in an epic work indeed if all were given an equal treatment of this kind. I have, therefore, attempted a compromise between the desirable and the practical; a framework is presented which includes most of the relevant topics and within this framework several items of particular interest to the author are described in detail. Thus it has been possible to discuss comprehensively the theory which is necessary for a full understanding of the most important aspects of the practical work. It is hoped that this approach has resulted in a personal treatment of the subject which avoids the common pitfall of close resemblance to large sections of well-known textbooks.

Finally, I must apologize for the inconsistencies which appear from time to time in the units used. This is the result of the varied editorial policies of the journals in which some of the diagrams and tables originally appeared; it would have been uneconomic to redraw them merely to change the units. The most common example lies in the variation between Å, nm and mμ for the unit of wavelength. In spite of the recommendations of the CGPM and IUPAC on the use of SI units, I feel, in common with many other workers in this field, that the angstrom remains the most useful unit of wavelength in the optical region of the spectrum. It has, therefore, been used throughout this work except for the special cases mentioned above.

Acknowledgements

The work described in this thesis was carried out in the Chemistry Department of Imperial College between October 1967 and June 1970. It is entirely original except where due reference is made and no part has been previously submitted for any other degree.

I wish to express my gratitude to my supervisor, Dr. G.F. Kirkbright, and to the Head of the Analytical Chemistry Department, Professor T.S. West, for their assistance and encouragement given throughout this project. Thanks are also due to the other members of the Analytical Research team for many helpful discussions during the past three years.

I am also grateful to the Science Research Council for the provision of a Research Studentship and a grant for the purchase of the apparatus from which the Fabry-Perot interferometer was constructed.

M.S.

Imperial College,

June, 1970.

Contents

			Page
CHAPTER I	INTRODUCTION		
1.1	History		11
	1.1.1	General	
	1.1.2	Atomic emission spectroscopy	
	1.1.3	Atomic absorption spectroscopy	
	1.1.4	Atomic fluorescence spectroscopy	
1.2	Spectroscopic Theory		14
	1.2.1	General	
	1.2.2	Atomic energy levels and atomic spectra	
	1.2.3	Emission and absorption of energy	
	1.2.4	The width of spectral lines	
1.3	Analytical Spectroscopy		32
	1.3.1	General	
	1.3.2	Instrumentation	
	1.3.3	Distribution of atomic population	
	1.3.4	The theory and practice of quantitative spectroscopy	
	1.3.5	Comparison of AES, AAS and AFS	
	1.3.6	Comparison with other techniques	
1.4	Flames		47
	1.4.1	General	
	1.4.2	Structure and propagation of premixed flames	
	1.4.3	Radiation from flames	
	1.4.4	Equilibrium in flames	
	1.4.5	Flame temperature	
	1.4.6	Burner design and shape	
	1.4.7	Introduction of the sample into the flame	

Page

1.5 Spectral Sources 62
1.5.1 General
1.5.2 Vapour discharge lamps
1.5.3 Hollow cathode lamps
1.5.4 Electrodeless discharge tubes
1.5.5 Continuum sources
1.5.6 Other sources

CHAPTER II SEPARATED FLAMES

2.1 Introduction 68
2.2 Historical 69
2.2.1 Glass or quartz tube separated flames
2.2.2 Nitrogen or argon separated flames
2.2.3 Flame shielded flames
2.2.4 Air or oxygen shielded flames
2.3 Previous work at Imperial College 83
2.3.1 The quartz tube separated air - acetylene flame
2.3.2 The long path quartz tube separated air-acetylene flame
2.3.3 The quartz tube separated nitrous oxide - acetylene flame
2.4 The Development of Burners For Nitrogen and Argon Separated Flames 88
2.4.1 The original nitrogen separated emission burners
2.4.2 The shortened nitrogen separators for emission burners
2.4.3 The improved nitrous oxide-acetylene burner
2.4.4 Nitrogen separated, long path absorption burners

Page

2.5 A Versatile Burner For Flame Shielded Flames 99

CHAPTER III THE EFFECT OF SEPARATION ON FLAME BACKGROUND AND TEMPERATURE

3.1 The Effect of Changing Flame Shape and Instrumental Characteristics 103

3.2 The Background Emission Spectrum of The Air - Acetylene Flame 107

3.3 The Background Emission Spectrum of The Nitrous Oxide - Acetylene Flame 108

3.4 The Background Absorption Spectrum of The Nitrous Oxide - Acetylene Flame 116

3.5 Flame Temperature Determinations By The 'Iron-Two-Line Method' 120

3.5.1 Introduction

3.5.2 Theory

3.5.3 Implementation of the method

3.5.4 SABCO: A computer programme to calculate self-absorption coefficients

3.5.5 IRTEMS: A computer programme to calculate temperatures corresponding to line intensity ratios

3.5.6 Results

3.6 The CN Vibrational Temperature of The Nitrous Oxide - Acetylene Flame 136

3.6.1 Introduction

3.6.2 Theory

3.6.3 Results

3.6.4 Conclusions

Page

CHAPTER IV THE APPLICATION OF SEPARATED FLAMES TO ATOMIC EMISSION SPECTROSCOPY

4.1 The Nitrogen Separated Air - Acetylene Flame For The Determination of Bismuth 148
- 4.1.1 Introduction
- 4.1.2 Experimental
- 4.1.3 Results
- 4.1.4 Conclusions

4.2 The Nitrogen or Argon Separated Nitrous Oxide-Acetylene Flame For Determination of The Refractory Elements 155
- 4.2.1 Introduction
- 4.2.2 Experimental
- 4.2.3 Results
- 4.2.4 Conclusions

4.3 The Use of The Separated Nitrous Oxide-Acetylene Flame For The Removal of Interferences In Flame Emission Spectroscopy 173
- 4.3.1 Introduction
- 4.3.2 Experimental
- 4.3.3 Results
- 4.3.4 Conclusions

CHAPTER V THE APPLICATION OF SEPARATED FLAMES TO ATOMIC ABSORPTION SPECTROSCOPY

5.1 The Nitrogen Separated Air-Acetylene Flame For The Determination of Arsenic and Selenium 185
- 5.1.1 Introduction
- 5.1.2 Experimental
- 5.1.3 Results
- 5.1.4 Conclusions

Page

5.2 The Nitrogen or Argon Separated Nitrous Oxide-Acetylene Flame For The Determination of The Refractory Elements 194

5.2.1 Introduction

5.2.2 Experimental

5.2.3 Results

5.2.4 Conclusions

CHAPTER VI HIGH RESOLUTION SPECTROSCOPY WITH A FABRY - PEROT INTERFEROMETER

6.1 Introduction 204

6.2 Historical 205

6.2.1 High resolution spectroscopy

6.2.2 The Fabry - Perot interferometer

6.2.3 The Fabry - Perot spectrometer

6.3 Interferometry Theory 216

6.3.1 Interference spectroscopy

6.3.2 Theoretical resolving power

6.3.3 The Fabry - Perot finesse

6.4 The Apparatus 226

6.4.1 The basic interferometer

6.4.2 Arrangement of optical components

6.4.3 Electrical system of the spectrometer

6.5 Adjustment and Use of The Interferometer 238

6.5.1 Setting up

6.5.2 Scanning spectra

6.5.3 Attainable finesse

CHAPTER VII THE EVALUATION OF SPECTRAL SOURCES BY MEASUREMENT OF LINE PROFILES

7.1 Introduction 247

		Page
7.2	Estimation of Self-Absorption Effects In Thallium Sources From The Relative Intensities of The Hyperfine Components	249
	7.2.1 General	
	7.2.2 Results	
	7.2.3 Discussion	
7.3	Accurate Measurements of Changes In Line Width	263
	7.3.1 General	
	7.3.2 Results	
	7.3.3 Discussion	
7.4	Conclusions	275
REFERENCES		278
PUBLICATIONS		288
ERRATA		289

Chapter I

Introduction

1.1 History

1.1.1 General

The work to be described in this thesis is concerned with one small section of the electromagnetic spectrum: the range from approximately 1000 to 10000 Å (10^{-5} to 10^{-4}cm) embracing the region of visible light. Thus when terms such as spectrum, spectroscopy, spectroscoper are encountered, it should be remembered that they are to be interpreted only in this most limited sense. Much of what is to be discussed does hold true for a considerable region on either side of the chosen range, but this should not be taken for granted.

Abiding by these somewhat arbitrary limits, it may be said that the history of spectroscopy dates back over two centuries to the discovery of the visible spectrum by Newton[1]. Since that time, spectroscopers at any given period have concentrated their efforts on one of two fields: analytical chemistry and the interpretation of physical and atomic properties. Over the years, both of these fields have experienced periods of outstanding interest and progress, usually as the result of an innovation in theory or instrumentation. At the present time, the increasing sophistication of analytical spectroscopy has brought the two projects much closer and any distinction between them is becoming less clear.

Three closely related branches of atomic spectroscopy are usually recognized in this field - emission, absorption and fluorescence (proper definitions will be given later). They have probably been of equal importance in the interpretation of physical properties, but until very recently (about the last fifteen years) only emission spectroscopy was used as an analytical tool. This situation is being rapidly rectified.

1.1.2 Atomic emission spectroscopy

Following Newton's study of the spectrum of the sun was a period almost entirely concerned with analytical flame spectroscopy, since no other means of exciting spectra existed. Chemists such as Melvill (1752) and Talbot (1836) were able to relate colours imparted to flames by metallic salts to particular materials, while physicists such as Wollaston (1802) and Fraunhofer (1820) were able to relate the solar and flame spectra of elements such as sodium.

However, the progress of all of these workers was limited by their use of simple, luminous diffusion flames. It was only after the development by Bunsen in 1855 of the Bunsen burner with its colourless, premixed hot flame that real progress could be made. This flame enabled Kirchoff and Bunsen to develop an instrument which must be considered the forerunner of all modern spectroscopes[2,3]. They were able to demonstrate that the visible spectral lines were due to the elements and not to the compounds added to the flame. This gave rise to the foundations of qualitative analytical spectroscopy with the identification of the spectra of many elements (some of which were previously unknown).

Shortly after this, in 1869, the possibility of quantitative analysis using a flame as spectral source was suggested by Janssen. The principles announced by Janssen were first put into practice in 1873 by Champion, Pellet and Grenier[4], who compared the intensity of sodium emission from two flames using a blue glass wedge. Improvement of flames and atomization systems was continued for some time after this by spectroscopers such as Gouy, but gradually the flame was replaced by various electrical devices which were developed towards the end of the nineteenth century. Thus, by the early 1900's the flame had virtually been replaced as a source of emission spectra. The arc and spark reigned supreme in analytical spectroscopy, emission spectrographic analysis now becoming of major importance. Meanwhile, the field of theoretical and atomic spectroscopy had seen the development of low pressure discharge sources such as the Geissler tube.

These were ideal for many purposes, producing spectra at low temperatures and unaffected by the contaminations associated with open air and flames.

Interest in flame emission spectroscopy was restored from 1928 onwards, when the work of the Swedish chemist Lundegardh[5] laid the basis of modern flame spectrophotometry. His development of the air-acetylene flame fed by a pneumatic atomizer together with the spectral analysis of the emission using a spectrograph and photoelectric densitometer was the real beginning of quantitative analytical spectroscopy. Today, the requirements of direct reading, photoelectric spectrophotometers for a stable noise-free emission source have once again centred interest on the flame rather than the conventional arc and spark sources.

1.1.3 Atomic absorption spectroscopy

The phenomenon of atomic absorption has been known as long as emission, being first observed as the now famous Fraunhofer lines of the solar spectrum. By the 1860's, the work of Bunsen and Kirchoff had allowed these observations to be correctly interpreted and reproduced in flames. This work was continued and placed on a sound theoretical basis by the physicists and astronomers of the early twentieth century. This research, which has been summarized by Mitchell and Zemansky[6], was mainly performed at low pressures in enclosed vessels. The main objectives were the interpretation of atomic structure and spectra, with occasional practical application to the study of solar and stellar atmospheres.

Unlike emission spectroscopy, virtually no attempt was made to apply these discoveries to practical chemical analysis (except for the rather exceptional case of mercury vapour in air). Thus, when belated attempts were made to introduce atomic absorption spectroscopy as an analytical tool by Walsh[7] in 1953 and Alkemade and Milatz[8] in 1955, they found that emission methods of analysis were firmly established and

difficult to replace. However, their combination of modern instrumentation and a high temperature flame as the atom reservoir finally succeeded in overcoming the objections of the emission spectrographers and the analysts using simple flame photometers. Today, a wide range of instruments is available commercially and new publications on AAS greatly outnumber those on the emission methods.

1.1.4 Atomic fluorescence spectroscopy

The development of this branch of spectroscopy resembles in many ways that of AAS. It was first reported in 1905 when Wood[9] succeeded in exciting fluorescence of the D lines of sodium vapour. This, and much other early work, was concerned with fundamental studies in enclosed cells of atomic vapour (see Mitchell and Zemansky[6] and Pringsheim[10]). Although a number of workers reported atomic fluorescence from flames[11, 12, 13] there was no real interest until Boers, Alkemade and Smit[14] studied quenching processes in flames by AFS and Alkemade[15] suggested using it for analysis. This suggestion was followed up in 1964 by Winefordner, Vickers and Staab[16, 17] and since then a number of workers have used AFS for a variety of determinations.

1.2 Spectroscopic Theory

1.2.1 General

It is proposed to discuss the basic theory necessary for a proper understanding of the experimental work to follow. Obviously, in view of the restricted space available, the treatment can be of only a cursory nature, except for one or two particularly relevant topics. For a more comprehensive coverage along the same lines, the reader is referred to the very readable treatise by Mavrodineanu and Boiteux[18].

Sources of even more detailed information on particular subjects will be indicated as the discussion proceeds.

Radiation in the region with which we are concerned is generally divided into three basic classes of spectra, depending on the source of the energy changes producing it.

(1) Atomic or line spectra. This type of spectrum is associated with quantized changes in atomic energy produced by variation in the orbital motions of the valence electrons. The wavelengths transporting the energy appear, in general, to be isolated and without any order. Hence the name "line spectra". In the present work we shall be concerned almost entirely with spectra of this type. Indeed, the survey of early experimental work given in Section 1.1 has foreshadowed this by dealing only with the three types of atomic spectra. In view of this, a fairly detailed discussion can be found in the following pages.

(2) Molecular or band spectra. This type of spectrum is associated with the energy changes of molecules and gives rise to closely packed groups of spectral lines. Hence the name "band spectra". They will be encountered in this work in the form of the intense background radiation produced by the molecules present in flame gases. Their great complexity usually means that with conventional flame spectroscopic equipment one can only treat them as unproductive regions where measurements of atomic spectra are impossible. This complexity extends to their theoretical analysis and arises because the energy of a molecule comprises three independent parts:

(i) The electronic excitation energy, corresponding to that of an atom. As in atoms, the electrons can make certain quantum jumps between different orbits.

(ii) The vibrational energy, due to vibration of the atomic nuclei comprising the molecule. As with electronic excitation, only discrete vibrational states are possible.

Even a simple diatomic molecule can exhibit a large variety of vibrational possibilities for any given electronic state.

(iii) The rotational energy, caused by the possibility of groups of atoms rotating about axes within the molecule. Again, only discrete values of the rotational energy are possible, each corresponding to a distinct rotational frequency. The energy differences between two consecutive rotational states are generally quite small and rotational spectra may be thought of as the fine structure of a vibrational band (which, in turn, is said to belong to a system corresponding to a given electronic transition of the molecule).

Clearly, the possibilities for energy transitions and the selection rules governing them will give rise to an extremely intricate theoretical analysis. This is unnecessary for our present purposes and no more will be said here, except to mention that the flame band spectra observed in the visible and ultraviolet regions are mostly due to electronic transitions, associated with superposed rotational and vibrational transitions. Pure rotation and vibration-rotation spectra are, of course, possible but the energy transitions are so small that radiation is produced chiefly in the infrared region, although a few vibration-rotation bands in the orange and red regions are observed in flames.

(3) Continuum spectra.* In these spectra the energy is distributed in an uninterrupted manner between all wavelengths within a given domain. A continuum of this kind is most commonly observed as the

---

* This type of spectrum is often referred to as continuous. The correct definition of continuous spectral sources will be found in Section 1.5.1 and to avoid confusion it should not be used as an alternative to continuum.

black body radiation from a hot solid or liquid (e.g. the anode of a carbon arc). This type of continuum spectrum can be produced in flames by the presence of incompletely vaporized particles, such as carbon or high melting oxides. Another type of continuum commonly observed for flames is the result of an energy transition in which one of the energy states is unquantized; the continuous nature of the energy state is the result of free kinetic energy in some part of the atomic or molecular system. Thus these spectra correspond to processes such as ionization, dissociation or association; e.g. the recombination of K^+ ions and electrons. Once again, although both types of continuum will be noted in the experimental work to follow, a more detailed theoretical treatment is unnecessary here. The subject has been discussed fully by Gaydon; continuum spectra due to hot solids in Ref. 19, Ch. VIII-IX, and those due to reaction processes in Ref. 20, pp. 66-72. It should also be noted that from time to time in the literature one finds an extensive, rather diffuse band system referred to as "a continuum". This should be treated as a description rather than a definition.

Finally, a note of caution must be added. The distinction between emission and absorption of radiation often appears to be reserved for atomic spectra. This is not so, and band and continuum (process) spectra in absorption are just as common as the emission variety. Indeed, continua due to dissociation, ionization and association are probably more common in absorption than emission. Furthermore, experimental work on the absorption band spectra of OH and CN molecules will be found in Chapter III of this thesis.

1.2.2 Atomic energy levels and atomic spectra

As was mentioned in Section 1.1, the existence of atomic emission and absorption spectra with a fixed, characteristic pattern for each element was recognised well before the end ot the last century. Empirical studies by a number of workers showed that the

spectrum of any element could be represented by a set of values, or spectral terms, calculated in inverse wavelength units, or wave numbers; each line of the spectrum was found to correspond to the difference between two of the terms. Further, many of the simple elements were found to give rise to spectral series of lines in which one of the two terms was common to all of the lines. The lines of such a series could be represented by a simple empirical equation.

During the early part of this century, efforts continued to group empirically the lines of ever more complicated spectra and to find simple equations or series to represent the lines of each group. Simultaneously with this empirical progress, workers such as Bohr attempted to explain the experimental grouping of the spectral lines on a sound theoretical basis involving the structure of the atom. The culmination of these efforts was reached during the period 1920 to 1930. In an era of quite remarkable progress, the spectra were systematically classified according to the set of rules known as the quantum theory. The "quantum numbers" and "selection rules" introduced artificially for this purpose were explained in a logical manner by quantum mechanics based on the wave equation.

A detailed study of the consequences of the wave equation becomes rather abstract when attempting to relate results to the actual "appearance" of the atom. For most purposes of practical spectroscopy, it is sufficient to combine the results proved by quantum mechanics with a simple vector model of atomic structure. This has been discussed by authors such as White[21] but even this simplified treatment would be out of place here. However, it is proposed to give a brief summary of the most important details. This will avoid repeated explanations of spectroscopic notation later in this work and introduce many of the principles needed to discuss the hyperfine structure of spectral lines in Chapter VII. The summary will be given in a series of short, numbered paragraphs for ease of reference.

1. Spectral lines are caused by transitions from one fixed energy level of an atom to another, the energy change and wavelength being related by

$$E = h\nu = hc\sigma = \frac{hc}{\lambda} \qquad (1\text{-}1)$$

The quantitative study of the energy changes will be dealt with in Section 1.2.3. For the moment we are only concerned with deciding just which energy levels are fixed for a single atom and then which transitions between the set of levels can actually occur.

2. The energy of the atom is governed by the interaction of the nucleus and the electrons. Changing the position (or orbit) of an electron (or electrons) will therefore change the energy of the atom. Unless a change occurs the atom cannot emit or absorb light and it is said to be in a stationary state.

3. The orbit of each electron may be defined by a set of four quantum numbers:

n, the principal quantum number with values

1, 2, 3, 4, ...

l, the orbital quantum number with values

0, 1, 2, ...n-2, n-1.

j, the inner quantum number with the values

l + s, where s is the spin quantum number of the electron and is $\pm\frac{1}{2}$.

m, the magnetic quantum number which may take the values

j, j-1, ...0, ...1-j, -j

when the atom is in a strong magnetic field.

4. Electrons with different values of l are designated with letters according to:

l =	0	1	2	3	4	...
Electron is	s	p	d	f	g	...

The value of n is placed immediately in front of this symbol.
e.g. n = 3, l = 2 gives 3d.

The optical spectra originate only from the positional changes of electrons in the outermost subshell which with most elements is incompletely filled. These are known as the optical electrons.

6. The different energy levels (or states) possible for any atom are found by calculating the different orbital possibilities of its optical electrons. This is done by adding vectorally certain of their quantum numbers. Each possibility obtained corresponds to a different discrete energy of the atom as a whole.

7. The result of a vector addition often depends on the order in which it is performed so it is essential to decide on the correct vector coupling scheme. The two commonly used are LS coupling (works best for light elements) and jj coupling (more important with the heavier elements).

8. LS coupling involves vector addition of the individual l values of the optical electrons (resultant L); the s values (resultant S); and finally L and S (resultant J). For two electrons with l_1 and l_2, L may take the values

$$l_1 + l_2,\ l_1 + l_2 - 1,\ l_1 + l_2 - 2,\ \ldots\ |l_2 - l_1|$$

With a third electron present, this is repeated using L as an intermediate (etc.).

The spin values s_1, s_2, etc. (each of which is $\frac{1}{2}$) are added in the same way but the limit is reaches at $\frac{1}{2}$ or 0.

The possible values of J are now given by

$$L + S,\ L + S - 1,\ L + S - 2,\ \ldots\ |L - S|$$

All states with the same value of L are called a term and designated according to:

L =	0	1	2	3	4	...
Term is	S	P	D	F	G	...

The sum (2S + 1) is called the multiplicity of the term and is shown as a superscript to the left of this symbol. e.g. S = 1, L = 2 gives a ^{3}D term. The terms are thus classified as singlets, doublets, triplets, etc.

Each value of J corresponds to a separate state

(or energy level) and to signify this the value of J for a particular term is written to the right as a subscript. e.g. if J = 1 in the term shown above, the state is designated $^3D_1$.

9. If only one optical electron is present, as with the alkali metals, exactly the same system is used with the l, s and j values of the particular electron being used instead of L, S and J. e.g. if l = 1, s = $\frac{1}{2}$ (the only possible value) and j = $\frac{3}{2}$, the state would be shown as $^2P_{\frac{3}{2}}$.

10. Since the same term can be obtained from different electron configurations, it is customary to show the configuration of the optical electrons to the left of the term symbol. Thus if the $^2P_{\frac{3}{2}}$ state mentioned above arose from an electron in a 3p orbit it would be written 3p $^2P_{\frac{3}{2}}$. Similarly, if the state $^3D_1$ arose from two optical electrons having n = 3, l = 2 and n = 4, l = 1 it would be written as 3d4p $^3D_1$.

11. <u>jj coupling</u> involves adding the l and s values for each electron vectorally to give a vector j for the electron, then adding these values (again vectorally) to give a resultant J for the atom. Since s = $\pm \frac{1}{2}$, each electron will give j = l + $\frac{1}{2}$ and l - $\frac{1}{2}$.

For values j_1 and j_2 from two different electrons, J can take the values

$$j_1 + j_2,\ j_1 + j_2 - 1,\ j_1 + j_2 - 2,\ \ldots\ |j_1 - j_1|$$

If a third electron is present, these values are taken as intermediates and each is added to j_3 in the same way, etc.

Each set of $(j_1, j_2 \ldots)$ is a term, the different values of J giving the different states. These states are written in the form $(j_1, j_2 \ldots)_J$ e.g. $(\frac{5}{2}, \frac{3}{2})_3$ or $(\frac{3}{2}, \frac{1}{2})_1$

12. LS and jj coupling both give the same total number of states in a given case and the same values of J the same number of times. However, the grouping of these states into terms will not be the same. For example, a dp configuration is found to give three triplet and three singlet terms by LS coupling but two quartets and two doublets by jj coupling.

13. Pure jj coupling never occurs, the heavier elements giving a greater and greater proportion of it mixed with LS coupling. In view of this, and because the LS coupling symbols for states and terms are much easier to print in tables, almost all spectral tables show the LS coupling notation for all elements.

14. It will be observed that neither the LS nor jj coupling schemes make any use of the fourth quantum number, m. This means that if they are used with two or more electrons having the same values of n and l (so-called equivalent electrons) they cannot take into account the exclusion principle. Therefore, only some of the predicted states are actually permitted: e.g. two p electrons give ten states but only five could actually exist if they were, say, both 3p electrons. The problem can be avoided by using a second set of quantum numbers normally only required when studying magnetic splitting of spectra. The calculations are laborious, but fortunately results for many combinations of equivalent electrons are tabulated in the literature[22].

15. The parity of the electron configurations giving rise to a term is often indicated with it in spectral tables. It is said to be odd if the sum of the l values of the optical electrons is odd and is indicated by writing a small letter o as a superscript to the right of the term symbol. Even parities are indicated by omitting the o. For example a dp configudation ($l_1 = 2$, $l_2 = 1$) has an odd parity so we should write $3d4p\ {}^3D_1^o$, etc. The parity is useful in formulating the selection rules which predict the transitions between energy levels (states) of an atom which can actually occur (see Section 16.3 of Ref. 18 for details).

16. Intercombination lines are lines which are forbidden by the selection rules of LS coupling but permitted by those of jj coupling. They are very faint for the light elements, but can be among the strongest lines of the heavy elements where jj coupling is important (e.g. Hg 2537Å).

17. Multiplicity of spectral lines. We have already defined the multiplicity of a term as (2S + 1). The same word multiplet is applied to a group of lines corresponding to transitions between initial levels belonging to one term only and final levels belonging to one other term: i.e. the upper (or lower) levels differ only in their value of J. It should be noted that the group of lines is designated, say, a triplet if the terms are triplets but the actual number of lines will often be greater than this. e.g. the calcium triplet at 4400Å ($4p\,^3P^o \leftrightarrow 4d\,^3D$) is actually composed of six lines.

18. Intervals between states (energy levels) of a term. In the case of LS-coupling, the Landé interval rule states that the energy difference between any two levels designated by J and J + 1 is proportional to J + 1. This applies whether the terms are normal (smallest J = lowest energy) or inverted (largest J = lowest energy) but not if only partial inversion occurs.

The rule does not apply to jj coupling, so that the deviation of the energy levels of any term from the rule is a measure of the amount of jj coupling applying to that term.

19. Relative intensities of lines of a multiplet. These are controlled by a sum rule which states:

The sum of the intensities of all lines of a multiplet which start (or finish) on the same level is proportional to the quantum weight (2J + 1) of the initial (or final) level.

The value (2J + 1) is often designated the statistical weight, g.

The sum rule alone is insufficient to calculate the relative intensities but this is possible by using L and S (or j_1 and j_2) as well as J. It is not necessary to use these equations because all of the results have been tabulated in the literature[23].

N.B.1. The tables will not give accurate results for coupling intermediate between LS and jj.

N.B.2. Unless all the lines of the multiplet are very close together, the intensities obtained from the table will need temperature and wavelength corrections before comparison with experimental results.

20. Grotrian diagrams The easiest way to summarize the terms and states of a particular element and to indicate the values of the energy levels corresponding to them is on a diagram. These diagrams are commonly referred to as Grotrian diagrams (after their originator), term diagrams or energy level diagrams. In many cases, for reasons of clarity, only some of the levels and the most intense lines are indicated.

1.2.3 The emission and absorption of energy

We have so far discussed the effects of atomic energy levels and selection rules on spectral transitions. From this it should be clear that the intensity of a spectral line produced by a gas comprising a group of emitting or absorbing atoms will depend on two main factors.

First, given a fixed population for all levels, the chance of any particular transition occurring will depend on the intrinsic properties of the atom as expressed by the quantum mechanics. Thus, in a group of atoms, the greater the probability of a particular transition the greater the intensity of the corresponding spectral line. Since this probability is a fundamental property of the atom itself it will be discussed below.

Secondly, the number of times a particular transition occurs will depend on the number of atoms existing at any given time with the energy of its initial level. The population of any level will depend on the properties of the group of atoms as a whole; for example, on the temperature and pressure. This particular factory controlling the

intensity of the spectral lines will, therefore, vary with the means used to obtain a population of free atoms or to excite emission lines. In view of this its discussion will be deferred to Section 1.3.3.

The Einstein probabilities The probability of transitions from given energy levels of a fixed population was expressed by Einstein in the form of three coefficients. There are usually written A_{ij}, B_{ji} and B_{ij} and are denoted the transition probabilities of spontaneous emission; absorption; and stimulated emission respectively. The meaning of the subscripts should be clear from Fig. 1-1.

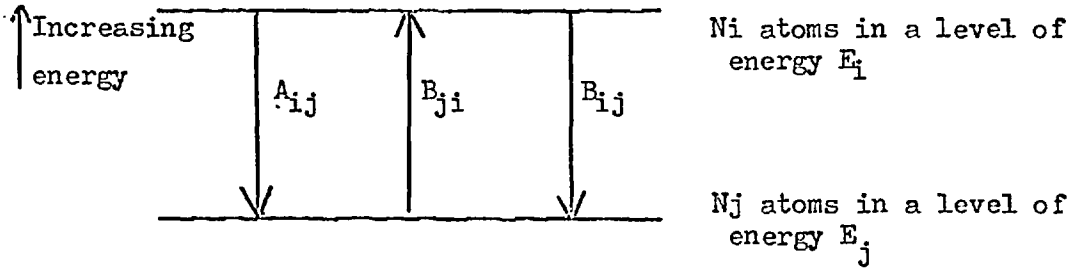


Fig. 1-1 The Einstein Transition Probabilities

The correct definitions of these three probabilities can be found on p.513 of reference 18 but for our purposes it is sufficient to consider them as representing the ratio of the number of atoms undergoing a transition to the number in the initial level.

The intensity of a spontaneous emission line is related to A_{ij} by the equation

$$I_{em} = A_{ij} \cdot h \cdot \nu \cdot N_i \qquad (1\text{-}2)$$

where ν is the frequency of the line.

The intensity of absorption and of stimulated emission will depend on the intensity, I_o, of the incident light. If the resultant reduction in I_o (after allowing for any stimulated emission) is dI, it may be shown that

$$\frac{dI}{I_o} = \frac{h\nu}{c} (B_{ji}N_j - B_{ij}N_i) \qquad (1\text{-}3)$$

(This naturally ignores any spontaneous emission which is quite independent of I_o).

Use of the transition probabilities. Any quantitative expression relating the intensity of an emission or absorption line to the number of atoms must be based on equations (1-2) or (1-3). Hence A_{ij}, B_{ji} and B_{ij} will be extremely important practical quantities. Because of this, it is useful to list some formulae relating them to other spectral quantities.

If we denote the statistical weights of the levels E_i and E_j as g_i and g_j (see Section 1.2.2, para. 19 for definition) it may be shown that the following expressions hold true:

$$g_i B_{ij} = g_j B_{ji} \qquad (1\text{-}4)$$

$$\frac{A_{ij}}{B_{ji}} = \frac{8\pi h\nu^3}{c^3} \cdot \frac{g_j}{g_i} \qquad (1\text{-}5)$$

$$\frac{A_{ij}}{B_{ij}} = \frac{8\pi h\nu^3}{c^3} \qquad (1\text{-}6)$$

These equations show clearly just how closely related are the emission and absorption processes of a gas. They will also prove useful for substitutions into formulae defined only in terms of A_{ij}.

For example, in practical spectroscopy it is frequently advantageous to replace the transition probability with another coefficient called the oscillator strength, f. The emission oscillator strength f_{ij}, is defined by

$$A_{ij} = \frac{8\pi^2 e^2}{\lambda^2 mc} \cdot f_{ij} \qquad (1\text{-}7)$$

where e and m are the electron charge and mass.
Substituting the values of the constants gives

$$A_{ij} = \frac{0.6670 \times 10^8}{\lambda^2} \cdot f_{ij} \qquad (1\text{-}8)$$

where A_{ij} is in sec^{-1} and λ is microns.

The absorption oscillator strength, f_{ji}, is related to f_{ij} by

$$g_j f_{ji} = g_i f_{ij} \qquad (1\text{-}9)$$

In view of this tables of values of f are usually given as "gf" values which may be used for emission or absorption.

Although it is theoretically possible to calculate the value of A_{ij} (and hence all the related coefficients) from the coordinates of the atomic electrons and the wave functions of the energy levels, this is not practical for atomic spectra. Most values found in the literature are measured experimentally from the intensities of emission and absorption lines.

Observed spectra As mentioned previously, we are concerned with three types of spectra. Emission spectra occur when the atom is raised to an excited level by a non-radiative process (e.g. due to a high temperature or collisions with high speed electrons) and then drops back to a lower level by emission of a quantum of energy as radiation. With absorption spectra, the atom is actually raised to a higher level by absorption of a quantum of energy from light with which it is irradiated. The wavelength corresponding to an absorption transition between two energy levels is the same as that of an emission transition.

An atom which has been excited by absorption in this way may lose its excess energy by a non-radiative process, but if instead it re-emits a quantum of energy as light, the process is known as fluorescence. The re-emission of light may often occur by a number of different transitions (each corresponding to different energy differences and hence wavelengths), so that each absorption line could give rise to more than one fluorescence line. The different types of fluorescence spectra have been discussed in detail elsewhere by the author[24] but AFS most commonly uses a line at the wavelength of the main absorption line and this is known as resonance fluorescence.

The observed emission spectra are usually much more complex (i.e. they have more lines) than the other two types. This is because absorption lines usually only originate from energy levels at or near the ground state (due to the tiny populations of higher levels in most sources) and this in turn limits the number of fluorescence lines. On the other hand, emission lines can be detected at much lower intensities and it is possible to observe lines from higher energy levels with very low populations of atoms. In addition to this, some of the emission lines will have their lower levels well above the ground state but their upper levels no higher than other lines which are observed in absorption and emission. Also, some of the sources used for emission are capable of giving anomalously high populations for excited levels (i.e. higher than the Boltzmann distribution for the actual temperature of thesource; this is explained in Section 1.3.4).

1.2.4 The width of spectral lines

A brief introduction to the subject of spectral line widths is given here. A more detailed, mathematical treatment of certain aspects will be found in Chapter 7 in connection with the work on the Fabry-Perot interferometer.

Even the sharpest line that can be produced has a finite width so a line can bever be considered as represented by a unique frequency (or wavelength). A common notation of the intensity distribution of an emission line is shown in Fig. 1-2.

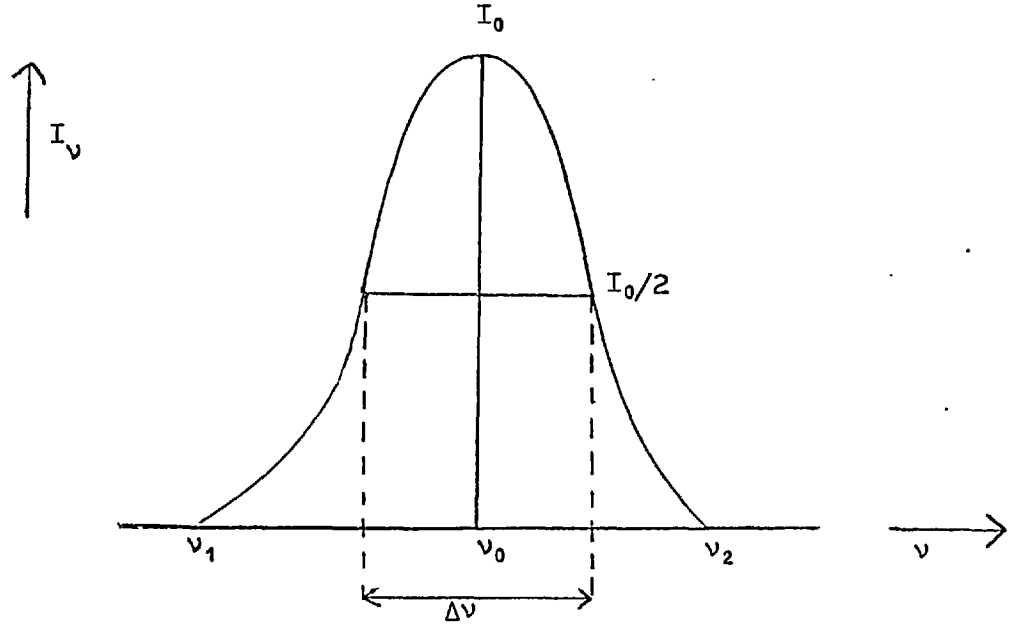


Fig. 1-2 Nomenclature of a Spectral Line Profile

The intensity is written as I_ν, which is a function of frequency, ν. Since the value of $\nu_1 \rightarrow \nu_2$ cannot be measured accurately, it is customary to define the breadth of any line in terms of its half-width, $\Delta\nu$. i.e. the distance between the two points where $I_\nu = I_o/2$. Some authors define the half-width as $\Delta\nu/2$ so care must be taken to avoid confusion. The same nomenclature is used for absorption lines with I replaced by the absorption coefficient k_ν.

A spectral line from any source will be broadened by a number of factors, although the contributions of different factors will vary with the source. All of the factors listed below apply to both emission and absorption lines, except for self-reversal broadening.

Natural broadening is the result of the finite lifetime of any atom in an excited state. By Heisenberg's principle this leads to an uncertainty in the energy of the level and hence in the frequency of a transition to that level. Thus the line corresponding to the transition has a finite width, $\Delta\nu_N$. This is negligible, being of the order of 10^8 sec^{-1} which is about 0.0001Å at 3000Å.

Doppler broadening is caused by the thermal motion of the emitting or absorping atoms. The observed frequency of a transition depends on the relative velocity between the atom and the observer. Since atoms in a gas move in random directions, the observed line is broadened and has the shape of a probability distribution curve. The half-width, $\Delta\nu_D$ or $\Delta\lambda_D$, depends on the atomic weight, the temperature and the frequency of the line and in flames is generally in the range 0.005 to 0.05Å.

Lorentz broadening depends on collisions with other particles of a different kind. It is also known as collisional or pressure broadening and increases rapidly as the foreign gas pressure is increased. In flames at atmospheric pressure, $\Delta\nu_L$ is of the same order as $\Delta\nu_D$.

Holtsmark broadening is produced by collisions with atoms of the same kind as those emitting or absorbing radiation. It is also known as resonance broadening and collisional or pressure broadening. For a given pressure, $\Delta\nu_H$ is generally much greater than $\Delta\nu_L$. It will still be negligible in flames (unless very strong solutions are sprayed) but can be important inside some spectral sources.

Stark and Zeeman broadening are caused by splitting of an atomic line due to the effect on the energy levels of electric and magnetic fields respectively. The latter will not be present in analytical chemistry but strong electric fields may give line broadening in arcs and sparks. The Stark broadening is generally considered fairly small in spectral lamps such as HCL's and EDT's.

Self-reversal broadening is caused by self-absorption of spectral lines and therefore only applies to emission lines (with absorption lines this effect would be considered simply as the expected shape of the line at a given level of absorption). It occurs because, as explained earlier, the proportion of the light absorbed under given conditions decreases as the distance from the line centre increases (since k_ν has the same distribution as I_ν). Thus, the greater the (self-) absorption the "flatter" the line profile becomes and the greater is its effective half-width. Since this multiplication factor is applied to the sum of all the other broadening factors, self-reversal broadening may be more important than any one of them alone. When self-absorption does occur to any extent inside a spectral lamp, this factor may well be the most serious cause of line broadening.

The hyperfine structure (hfs) is often observed as a number of closely packed lines when a single spectral line is examined under high resolution. It may be the result of the presence of more than one isotope (i.e. just as if the lines of several elements almost coincided) and/or the interaction of a nuclear spin with the spins of the electrons (i.e. an extra quantum number is required to explain further orbital possibilities). Some detailed examples of the calculation of hfs and their effects on observed profiles are given in Chapter VII. Meanwhile it must be realised that they have a variable and complicated effect on line width. Each hfs line is really a single spectral line and will be broadened by all of the above factors. If this results in a line width much greater than the hfs separation so that complete overlap occurs the line may still be treated as a single line for most purposes. In cases where the hfs separation is much wider (e.g. mercury 5461Å line has its extreme components about 0.45Å apart), any calculations will be extremely complicated and depend on the amount of overlap (i.e. on the amount of broadening). A normal monochromator used in AAS would not resolve any of the hfs components but unless they are completely overlapped they will still

have an effect on the light absorbed. This is because the equations of Sections 1.2.3 and 1.3.4 must be applied to each hfs line individually and the results summed. The value obtained will be different from that using a "total" value of k_ν for the whole line in a single equation and will depend on the separation of the components. The difference is usually negligible unless certain special cases apply (e.g. if the source hfs components were Stark broadened by a strong electric field which did not affect the flame absorption line hfs).

The total line width is a complicated function of all the above factors especially since the profile caused by say collision broadening is a different type of function from the Gaussian distribution of Doppler broadening. Any generalisation is, therefore, rather misleading. A useful equation to calculate widths for AAS or AFS expressions (i.e. assuming that there is no hfs, that it is completely overlapped, or that it has no effect on the calculations) is

$$\Delta\lambda_{Total} = \left[(\Delta\lambda_D)^2 + (\Delta\lambda_L + \Delta\lambda_H)^2\right]^{\frac{1}{2}} \qquad (1\text{-}10)$$

This may only be used for these restricted purposes and also assumes no self-absorption. It will not be the same as the actual width of many lines encountered in AAS.

1.3 Analytical Spectroscopy

1.3.1 General

In the previous pages we have reviewed the historical aspects of atomic emission, absorption and fluorescence spectroscopy and discussed in some detail the basic theory underlying these techniques. It should be clear from this that qualitative analysis is largely confined to the emission techniques and the basis on which emission

spectroscopy allows the identification of individual elements has been explained.

We must now introduce the extra theory necessary for everyday use of all three techniques as methods of quantitative analysis. At this "practical" level, the theory required depends to a certain extent on the apparatus used. We shall, therefore, take the somewhat unusual step of first giving a brief résumé of the instrumen tation. This will allow us to begin the discussion in Sections 1.3.3 and 1.3.4 with a background knowledge of both the basic theory and the practical requirements of the techniques.

1.3.2 Instrumentation

The instrumentation necessary for quantitative analytical atomic emission, absorption and fluorescence spectroscopy will be discussed in general terms. The flame and spectral sources with which this thesis is particularly concerned, are described in more detail in Sections 1.4 and 1.5 respectively.

The basic arrangement of the apparatus for the three techniques is shown in Fig. 1-3.

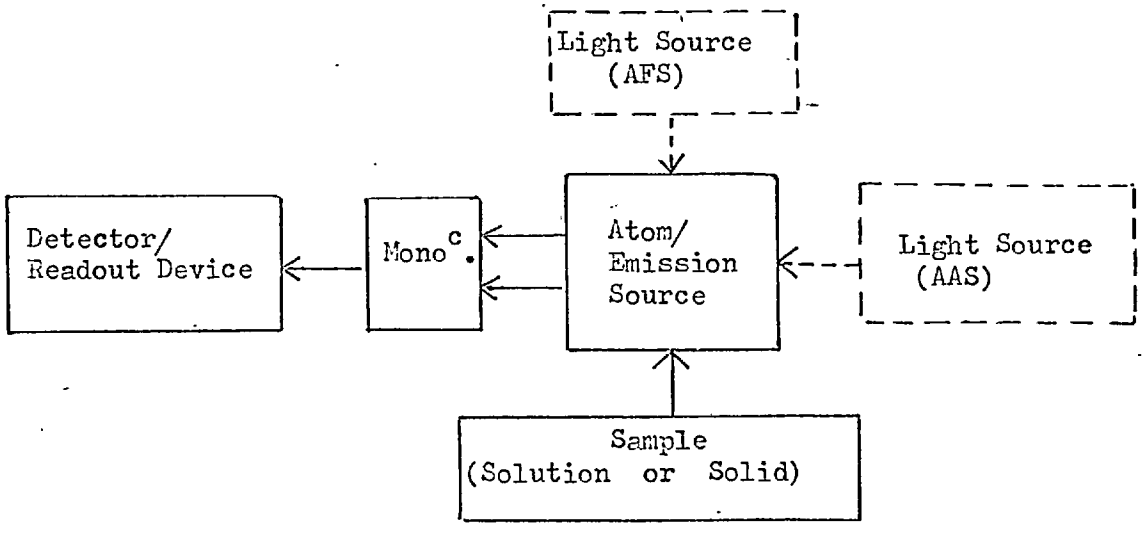


Fig. 1-3 Basic Apparatus for Analytical Spectroscopy

Going from left to right in the diagram, the apparatus may be broken down into the following components.

(a) Detector/readout device. The traditional method of recording and measuring the signal is with the photographic plate and the microdensitometer. Although these are still useful when measurements are required simultaneously at a large number of spectral lines, they have serious disadvantages for rapid, quantitative analysis and would be most impracticable for AAS. Therefore, they have been generally superceded by direct-reading photoelectric devices. Most instruments use a photomultiplier tube, usually coupled with an amplifier which provides sufficient current to drive a chart recorder or meter, allows backing off of unwanted signals and allows the tuned detection of modulated light sources (see below).

(b) Monochromator. It is usually necessary to separate the spectral line(s) of interest before passing the light to the detector. Filters are only suitable for the most simple instruments and, since the introduction of AAS, the grating (rather than the quartz prism) monochromator has become the most popular. This is mainly due to the uniform dispersion and linear wavelength scale which it provides (and also the considerable reduction in price of high quality replicate gratings). Most of the commercial AAS instruments use monochromators of this type with dispersions in the range 10 to 100A/mm, the better ones also being well suited to AES.

(c) Atom/emission source. All three techniques require a means of vaporizing the sample and obtaining a population of free atoms of the element to be determined. In AES the device used for atomization is also used (in most cases) to excite the emission spectrum. At the present time, the flame is the most widely used for these purposes. A large part of the work described in this thesis is concerned with flames and they are discussed in some detail in Section 1.4. Other sources used for AES are arcs, plasmas, sparks and lasers. At the

present time, the first three are most widely used for spectrography (especially qualitative work). A number of devices have been used as free atom cells for AAS and AFS. Furnaces (especially those with long tubes for AAS cells) offer some advantages but have not been very widely used, mainly because of difficulties over memory effects, interferences and lack of reproducibility. Graphite crucibles and rods heated by a high electric current are capable of vaporizing many samples and at the present time are gaining popularity as AAS and AFS cells. Their main advantages lie in the lack of background emission and noise and the very tiny samples which may be used.

(d) Sample. Solid samples were used for many years in arc spectrography but have largely been superseded in AES, AAS and AFS by solution techniques. This is principally due to the ease with which solutions may be nebulized into flames (see Section 1.4.7) or added as small drops to other atomisation cells. The disadvantage of sample dissolution is readily offset by the ease of obtaining homogeneous and reproducible samples, of carrying out chemical pretreatment and of preparing standards. At the present time it would appear that the most likely reason for a return to widespread use of solid samples lies in the field of laser probe analysis. With this technique it is possible to sample and analyse tiny areas from individual layers of a solid sample.

(e) Light source. Both AAS and AFS require a source independent of the means of atomising the sample which can emit spectra of the elements to be determined (or of a suitable alternative). Although the requirements of both techniques can sometimes be met by the same source, they are not in general the same. As far as sharp line sources are concerned, AAS requires extremely narrow lines which need not be particularly intense, whereas AFS requires extremely intense lines which need not be particularly sharp. (The reasons for this will be discussed later). The other types of sources may usually be applied equally well to both techniques because they provide optimum

conditions for neither, although continuum sources are an exception to this. All types of spectral sources are described in some detail in Section 1.5 because of their use with the Fabry-Perot interferometer.

1.3.3 Distribution of atomic population

We have already seen that spectra arise because atoms or molecules may assume a number of discrete energy levels, and that the intensity of a line depends, among other things, on the population of its initial level. If the particular type of energy in question (e.g. electronic or, say, vibrational for a molecule) has attained equilibrium the relative populations of the quantized levels may be easily found using the Maxwell-Boltzmann law. The conditions under which the law can be applied are discussed in detail for flames (with which we are most concerned) in Sections 1.4.3 and 1.4.4.

The law states that if at an absolute temperature T there are N_i particles with energy E_i and N_j with energy E_j, then

$$\frac{N_i}{N_j} = \exp. \quad \frac{-(E_i - E_j)}{kT} \tag{1-11}$$

provided that the two levels are both nondegenerate. As was explained in Section 1.2.2, most energy levels which we look on as a single level are in fact degenerate because they split into $(2J + 1)$ sublevels on application of a magnetic field. When there is no magnetic field, each of these sublevels has the same energy. Therefore, in the example above the number of particles with energy E_i is actually given by $(2J_i + 1)\, n_i$, etc. If we revert to our "single" levels as shown in Fig. 1-1 we now have $N_i = g_i n_i$ and $N_j = g_j n_j$. The law then becomes

$$\frac{N_i}{N_j} = \frac{g_i}{g_j} \cdot \exp. \quad \frac{-(E_i - E_j)}{kT} \tag{1-12}$$

This equation is extremely useful as it stands and is used for calculations involving relative line intensities - e.g. for calculations of "population" temperatures as explained in Section 1.4.5. However for AES and AAS it is often more convenient if the population of any one level can be expressed in terms of the total number, N, of particles present. This is easily done by expressing N as the sum of the populations of all levels, i.e. $N = \sum_i N_i$, (or $\sum_j N_j$, etc.). Since from (1-12)

$$\frac{N_i}{N_j} = \frac{g_i \exp[-E_i/kT]}{g_j \exp[-E_j/kT]} \qquad (1\text{-}13)$$

we have

$$\frac{N_i}{N} = \frac{g_i \exp[-E_i/kT]}{\sum_j g_j \exp[-E_j/kT]} = \frac{g_i \exp[-E_i/kT]}{F(T)} \qquad (1\text{-}14)$$

This equation applies quite generally to both atoms and molecules and to all types of energy levels. The $\sum_j$ is the partition function, F(T), for the type of energy in question and the difficulty of calculating it varies enormously with specific cases.

A number of expressions for the partition function under different circumstances and also some approximations are given in Ch. 20-4 of Flame Spectroscopy[18]. However, for our purposes it is usually more convenient with atomic spectra to simply perform the summation manually using the published g_i and E_i values for the energy levels. This is especially true with flames since it should be obvious from equation(1-14)that for normal temperatures (say, less than 3000°K), the value of N_i will be very small if E_i is more than a few electron volts; e.g. if T = 3000°K and E_i = 2 eV, $\exp[-E_i/kT] = 4 \times 10^{-4}$ so that N_i will be negligible compared with N. It is, therefore, rarely necessary to consider levels more than about 1 eV above the ground state when carrying out the summation.

It has already been explained in Section 1.2.3 that AAS determinations are not automatically much more sensitive than AES ones, even though the initial level of the absorption line has a much higher population than that of the corresponding emission line. This is largely for experimental reasons, but two other common fallacies in AAS are connected directly with the Boltzmann law.

First, it is often stated that, assuming a constant free atom population, the number of atoms absorbing at a ground state line will always be independent of temperature. In fact this is only true for atoms giving simple spectra where the only low lying level is the ground state. When a number of levels lie below about 1 eV, changes of population (and hence absorption) at any level will occur with temperature. These changes are usually quite small but in some cases fortuitous combinations of statistical weights and energies can make them much more serious. This is illustrated for the $5p^2\ ^3P$ triplet ground state of tin in Table 1-1. It can be seen that the population N_j of the true ground state level drops rapidly with increasing temperature.

			N_j/N				
J	E_j(eV)	g_j	1000°	1500°	2000°	2500°	3000°
0	0.000	1	0.772	0.563	0.433	0.354	0.302
1	0.210	3	0.200	0.332	0.384	0.400	0.407
2	0.425	5	0.028	0.105	0.184	0.246	0.291

Table 1-1: Relative Populations of ^3P Levels of Tin.

The second fallacy is that the most highly populated level at flame temperatures will always be the lowest one. This is actually disproved by some of the results in Table 1-1, but illustrated much more clearly with aluminium as shown in Table 1-2. The two levels of

the ground state doublet ($3p\ ^2P_{\frac{1}{2},1\frac{1}{2}}$) are separated by only 0.0139eV and even at 1000° the upper one is almost twice as highly populated.

Finally in this section, we must note that although N is the total number of free neutral atoms present it often does not represent the total amount of sample present. This is because some atoms may be ionized and others present as stable compounds formed by the element. Ionization presents no problem since when in equilibrium it obeys the Boltzmann law. However, the theoretical treatment of compound formation and dissociation is very complex, involving advanced thermodynamic principles. It is generally more convenient to discuss the subject from an experimental point of view and this is done later for flames.

			N_j/N				
J	E_j(eV)	g_j	1000°	1500°	2000°	2500°	3000°
$\frac{1}{2}$	0.0000	2	0.370	0.358	0.351	0.348	0.345
$1\frac{1}{2}$	0.0139	4	0.630	0.642	0.648	0.652	0.655

Table 1-2: Relative Populations of ^2P Levels of Aluminium

1.3.4 Theory and practice of quantitative spectroscopy

In order to place quantitative spectroscopy on a sound basis, it is essential to have an expression which relates the observed emission or absorption of light to the concentration of atoms producing it. It might appear that we already have such expressions in the first two equations of Section 1.2.3, but these are of little use for analytical calibration curves in the form shown. This results from a number of practical difficulties, the most important of which is that every

spectral line has a finite width. As explained in Section 1.2.4, this means that rigorous expressions can only be obtained by using complex functions to represent the line profile or by integrating the radiation with respect to the total line width.

With emission, the integration is simply

$$\int I_\nu d\nu = I_{em} = A_{ij} h\nu N_i \text{ (i.e. eqtn. (1-2)).}$$

In fact this is performed automatically when emission signals are measured with a conventional monochromator and equation (1-2) may be used to relate the signal to the atom concentration.

With absorption (and this includes self-absorption of emission signals) the fundamental equation is

$$I_\nu = I_\nu^0 \exp(-k_\nu L) \qquad (1\text{-}15)$$

where I_ν^0 and I_ν are the initial and final intensities of radiation of frequency ν, k_ν is the absorption coefficient at the same frequency and L is the length of the absorption cell. The equivalent of the emission integration would be

$$K = \int k_\nu \, d\nu = \frac{dI}{I} = \frac{h\nu}{C} (B_{ji} N_j - B_{ij} N_i) \qquad (1\text{-}16)$$

(from eqtn. (1-3)).

However, K (the integrated absorption coefficient) can only be measured practically by plotting the actual line profile using an ultra-high resolution monochromator. Conventional instruments only allow measurement of $\int I_\nu \, d\nu$ and $\int I_\nu^0 \, d\nu$. These are not related to K by a simple integration of equation (1-15) because k_ν is also a variable. Therefore, not only must a complex expression for k_ν in terms of the line profile be used, but also k_ν will still appear in the final result (since $\int e^x \, dx$ is e^x). In view of this, the integration is usually only carried out for a few relevant approximations. Those used for AAS and AFS have been discussed in detail elsewhere by the author[24] and only the most useful results are summarized below.

AES calibration curves. If self-absorption is neglected, we may use equation (1-2) and substitute for N_i in terms of the total number of atoms present provided that there is thermal equilibrium (see Section 1.3.3). This gives

$$I_{em} = A_{ij}.\ h.\ \nu.\ N.\ \frac{g_i.\ \exp.\left[-E_i/kT\right]}{F(T)} \qquad (1\text{-}17)$$

i.e. a plot of I_{em} versus N (or sample concentration in most cases) should give a straight line calibration.

This equation applies whenever there is no self-absorption - that is for non-ground state lines or for resonance lines at very low concentrations - and is extremely useful. For example, it is the basis of several methods of flame temperature measurement (see Section 1.4.5).

When self-absorption is not negligible, the decrease in I_{em} obviously depends on the length of the flame. The expression for the received intensity is therefore of the form

$$I = \propto \int_0^{\nu} \left[\int_0^{L} I_{em} \exp.\ (-k_\nu x)\,dx \right] d\nu \qquad (1\text{-}18)$$

where $\propto$ is a factor depending on the instrument used.

The evaluation of this expression is extremely complicated (see, for example, the textbook by Penner[25]) and depends on the nature of the line broadening. It is usually found that after initially varying linearly with N (i.e. no self-absorption), I is proportional to $N^{\frac{1}{2}}$. At very high concentrations, resonance broadening may occur and result in a further change in the calibration curve.

AAS calibration curves. In view of the difficulties mentioned above of using K or k_ν, it is more practical to define two other quantities in terms of the total amount of light passing through the absorption cell within the "bandpass" of the spectral line used.

The total absorption factor, A_T is defined as

$$A_T = \frac{I_o - I}{I_o} \qquad (1\text{-}19)$$

(where I_o and I are intensities integrated over the whole line). The percent absorption commonly used in AAS is simply $A_T \times 100$.

The absorbance, A is defined as

$$A = \log_{10}\left(\frac{I_o}{I}\right) \qquad (1\text{-}20)$$

The relationship between A_T or A and N_j can be found with certain special conditions for the widths of the source and absorption lines and the value of $k_\nu L$. $k_\nu L$ is usually referred to as the optical density; k_ν incorporates all the factors affecting the amount of light absorbed, such as the number of atoms, the width of the absorbing line and its transition probability).

One or more of the following conditions are normally invoked:

(i) Source line much wider than absorption line, i.e. a continuum source.

(ii) Source line much narrower than absorption line. i.e. a sharp-line source.

(iii) Very small optical density.

(iv) Very large optical density.

These give the following special cases:

(a) For (i) + (iii) : $A_T \propto (N_j.L)$

(b) For (i) + (iv) : $A_T \propto (N_j.L)^{\frac{1}{2}}$

(c) For (ii) + (iii) : $A_T \propto (N_j.L)$

(d) For (ii) + (iv) : A_T = a constant value

(e) For (ii) only : $A \propto (N_j.L)$

The situation arising from these results is as follows. If a contimuum source is used, plots of percent absorption against concentration will be linear at low concentrations. As the sample concentration is increased, a point is reached where the relation changes (fairly sharply) so that the percent absorption is proportional to the square root of the concentration. The position of this change-over depends on the bandpass of the monochromator; generally the narrower the bandpass the higher the concentration at which it occurs.

This is useful, because a narrow bandpass also helps to increase the size of the absorption for any concentration. However, it may not always be desirable to use a very narrow bandpass because the situation under (d) may be reached at high concentrations and the calibration curve will slope off to a horizontal line. Plots of absorbance against concentration should not be used with continuum sources since there is no simple relationship.

For sharp line sources, cases (c) and (d) cover only the extremes of the concentration range, so that there is no simple relationship between A_T and N_j in the concentration range most important for AAS. Plots of A against N_j are much more useful in this case, since (e) was obtained without placing a limit on the value of the optical density. Such plots should, therefore, be linear over the whole concentration range. In practice, the source line is never really narrow and an error is introduced into (e). However, this usually only becomes serious at values of A greater than about 0.5

AFS calibration curves. These are even more complex than those for atomic absorption, since fluorescence involves both absorption and emission and energy. Fortunately, under most standardized AFS conditions the fluorescence signal is directly proportional to the amount of light absorbed. Also AFS is usually carried out with low concentrations of solutions and with cells of small path length. Hence conditions (a) and (c) above will apply and plots of fluorescence signal against concentration should be linear. If stronger solutions are used, bending of the curves will occur due to factors such as exceeding the range of (a) and (c) or absorption of radiation before it leaves the fluorescence cell (i.e. the fluorescence signal is no longer proportional to the absorbed light by a factor independent of the concentration).

Relationship between concentration and N or N_j. In the above discussion it has been assumed that the proportionality between sample solution concentration and number of free atoms in the cell

remains constant over the whole concentration range provided the experimental conditions are kept constant. In practice this may not always be so and the shape of the calibration curve may be altered. For example, the nebulizer efficiency may change at high concentrations so that less sample enters the flame. Ionization is an important effect with elements such as the alkali metals. The percentage ionization becomes progressively smaller with increasing concentration (due to the higher population of free electrons) and the free atom population therefore increases faster than sample concentration.

Detection limits and sensitivity. The only realistic method of defining detection limits for AES, AAS and AFS and which allows comparisons to be made between different methods is on the basis of the signal noise level. The detection limit is usually defined as the amount of the element which gives a ratio of signal to peak to peak noise of 2 : 1 or 1: 1.

The signal to noise ratio is usually measured at concentrations somewhat above the detection limit, which is then calculated by simple proportion. This may be done for AAS as well as AES (and AFS) provided that the signal is kept below about ten percent absorption (i.e. 0.04 absorbance). This is because case (c) above then holds and the absorption is linearly proportional to the concentration.

In AAS, it is also common to find sensitivity values quoted as well as detection limits. These are a measure of the signal change which can be expected for a given concentration change and take no account of signal noise levels. The sensitivity is usually defined as the concentration in ppm (μg/ml) which gives an absorption of 1% (or an absorbance of 0.0044). It may therefore be measured directly from the slope of the calibration curve.

1.3.5 Comparison of AES, AAS and AFS.

It must first be stated that, in the opinion of the author, all three techniques are complementary and, contrary to popular belief, none has any outstanding advantage over the other two. This is true whether based on the criterion of "limit of detection" or that of ease and convenience of analysis. First, at the present time each technique has a group of elements for which it provides the most sensitive method of analysis. There also remain many elements which are equally sensitive by two or even all three techniques. Assuming equal advances (and research effort) in all three arts, this state of affairs is likely to remain with us for some time, although the individual elements in the groups may change. Secondly, each technique has its own instrumental and experimental advantages and disadvantages. Since many of these overlap it is rather difficult to make a direct comparison. However the following points may be noted:-

1. AES requires no extra spectral light source whereas this is essential with the other two techniques.

2. AES is much more easily adaptable to non-standard determinations and may more easily be used for qualitative analysis.

3. AAS requires less operator skill and the performance deteriorates less rapidly when cheaper instruments are used.

4. AAS is particularly easily adapted to automation and digital readout for computers because of the reference provided by the background source and the simplicity of using double beam operation.

5. Although it gives good sensitivity for several elements, AFS appears to combine many of the disadvantages of the other two methods.

6. Many of the best detection limits by AFS are obtained only in cool flames where chemical interferences are very serious.

To summarise, AAS is the best suited to rapid routine analysis by relatively unskilled operators and to automation. AES is the more versatile method for use by a skilled analytical chemist in a laboratory where small numbers of non-routine determinations are required, often at short notice. Finally, it should be realised that, apart from the spectral sources, essentially the same equipment is required for all three techniques. Thus, in such a laboratory it will often be possible to select one of the three techniques on its own merits as the optimum for a particular determination.

1.3.6 Comparison with other techniques for inorganic analysis

In general, AES, AAS and AFS have the same advantages over classical chemical methods of analysis as most other instrumental techniques. For example, they allow determinations at much lower concentrations while maintaining good accuracy and routine analysis of large numbers of samples is much quicker. On the other hand, results are relative to the standards used rather than absolute values and much more expensive apparatus is needed. Since these advantages and disadvantages of all instrumental methods are well known, we are more concerned with the factors distinguishing AES, AAS and AFS from other instrumental techniques.

Perhaps the biggest advantage of the three techniques over most of the others is their relative freedom from interferences and the need for extensive sample pretreatment. This may sound a little optimistic in view of the need to prepare solutions and standards and the interferences quoted in the experimental part of this thesis. However, a much more realistic picture is obtained if one considers for a moment some of the other techniques. With electrochemical methods such as polarography and coulometry most types of samples require dissolution and a preliminary separation (in one or even more stages). Similar disadvantages apply to the solution spectrophotometric

techniques, which also require stocks of many different reagents in a laboratory covering a wide range of analyses. Even more sophisticated techniques such as those of radiochemistry require extensive sample treatment, usually by skilled technicians. Xray techniques allow the use of solid samples in much the same way as arc spectrography but the complicated matrix effects mean that both require the extensive use of accurately prepared solid standards. Usually the best results are obtained for the routine examination of large numbers of samples with only small variations in composition. Although solid sampling often sounds attractive, it should be remembered that any pretreatment is much more complicated than with a solution which is merely to be sprayed into a flame.

Obviously, there are also some disadvantages. These include the difficulty of determining major sample constituents without a large degree of dilution (with its attendant errors) and of measurement of non-metallic constituents by direct methods. At the present time, a number of specific metals and sample types also present difficulties for routine analysis. However, the current intensification of research seems to be removing these problems more quickly than is the case for those inherent in other instrumental methods of inorganic analysis.

1.4 Flames

1.4.1 General

A brief survey is given of the theoretical and practical aspects of flames, but many of the topics are covered in much greater detail in later chapters.

A flame is obtained by burning a mixture of a fuel and an oxidant; with all of the flames described here both are in gaseous

form when they reach the burner. The most important gases for flame spectroscopic applications are :-

Fuels: coal gas, propane, acetylene, hydrogen and bottled gas (butane).

Oxidants: Air, oxygen, oxygen + inert gas, and nitrous oxide.

These gases may be used to obtain four main groups of flames.

(a) Diffusion flames in air are obtained when only the fuel gas is supplied to the burner and burns with the surrounding air. Hydrogen is the best fuel for spectroscopic purposes since the flames are very fuel rich and hydrocarbons form too much soot. The hydrogen flame gives exceptionally low background emission but is cool, limited to air as oxidant and solutions must be nebulized using hydrogen (unless an inert gas is added, making the flame even cooler).

(b) Diffusion flames with additional oxidant have the oxidant as well as the fuel supplied via the burner, which has outlets designed so that all mixing occurs by diffusion above the burner. This allows the oxidant to be used to nebulize solutions and its type and quantity may be varied.

(c) Turbulent flames are a logical development of (b) in which the burner jets are shaped to give forced mixing of the gases above the burner. The flames obtained are just as safe from flash-back as diffusion flames but much hotter. Unfortunately, their turbulent nature results in loud accoustic noise, noisy signals and no distinct flame zones, large areas being equivalent to a reaction zone with consequent high background emission.

(d) Premixed flames have an explosive mixture containing the correct proportions of fuel and oxidant leaving the top of the burner. This results in a quiet, stable flame with well-defined zones. Flashback into the burner must be avoided by careful design (see Section 1.4.6) but these flames are widely used in flame spectroscopy because of their many advantages: they are as hot as turbulent flames

with much lower background and noise outside the reaction zone; the flame shape is easily varied; and the temperature and composition of different flames is well documented and easily reproduced. Much of what follows will be particularly concerned with premixed flames.

1.4.2 Propagation and structure of premixed flames

The propagation of a stable flame using a particular combination of gases and burner depends basically on three factors:-

The limits of inflammability are the upper and lower limits of fuel to oxidant ratio between which combustion will spread through a gas mixture that has been ignited.

The ignition temperature is the lowest temperature at which combustion propagates spontaneously through a gas mixture.

The burning velocity is the speed at which a flame moves through a combustible gas mixture by propagation of the reaction by thermal conductivity between adjacent layers of the mixture.

For a given combination of gases, all three factors vary enormously with experimental conditions. The gas mixtures used in flame spectroscopy must obviously lie within the limit of inflammability and have ignition temperatures well above room temperature (so that they can only be ignited by supplying heat in the form of a match, spark, etc.), but the factor of greatest interest to the flame spectroscoper is the burning velocity. The burner must be carefully designed to match this to the upward gas velocity through the burner head so that the flame will neither "lift-off" and extinguish itself nor flash back into the burner and cause an explosion. This is discussed in Section 1.4.6.

The gases leaving the top of the burner are raised to their ignition temperature in a small preheating zone by the heat of the

existing flame. Immediately above lies the brightly luminous primary reaction zone, whose outer surface forms the flame front. The shape of this is governed by the fact that the burning velocity of the gas mixture always equals the component of the gas velocity perpendicular to its surface. For a circular burner (or holes in a burner head) its shape is conical, although somewhat distorted (see Gaydon and Wolfhard[19], for a detailed discussion). This distortion is the result of a back pressure caused by the heating, expansion and acceleration of gases in the flame front. (It is for this reason that with nebulizers fitted with a constant head of water at their drain outlet one can observe a change in water level on lighting the flame). Also, the quenching effect of the burner reduces the burning velocity just above the burner head.

The hot gases leaving the flame front enter a region known as the interconal zone. In some flames this may be a dark region extending for several millimetres around the front; in others it is much larger and a source of strong emission (see Section 1.4.3). The interconal zone can only be studied properly using a flame separator and this is described in Chapter II. Except in the most fuel lean flames, the gases in the interconal zone are not completely combusted to their ultimate oxidation products. Therefore, with flames burning in the atmosphere, the interconal zone is surrounded by a secondary reaction zone. This region is in fact a diffusion flame where the gases burn further using the surrounding air as oxidant. It is generally much larger than the other zones as is due mainly to the combustion of CO and H_2 and species such as OH and NO (depending on the flame).

1.4.3 Radiation from flames.

Discussion of the radiation from flames involves two approaches. First, we must list the species from which it originates and compare the intensities and types of radiation from different regions of the flame. This is mainly a straightforward matter of

quoting known experimental facts. Secondly, we must attempt to interpret the excitation mechanisms responsible responsible for radiation from different species and different parts of the flame. Here the situation is much more confused with a notable scarcity of experimental data and rigorous theory.

The most intense radiation from the flame originates in the primary reaction zone, as might be expected, and is mainly due to molecular band spectra. However, atomic lines (due to C and to metal atoms if these are added to the flame) and a continuum background (due to incandescent carbon particles or nonquantized transitions) are also observed. The species producing the bands obviously vary with the gases used, but some of the more common ones are C_2, CH, CHO, OH, CN and NH. Radiation from the interconal zone is much less intense due to low populations of many of the species giving strong band spectra. Probably the most common emission from this region is due to OH. However, there are one or two notable exceptions, especially when fuel rich flames are used as higher concentrations of carbon-containing species then persist into the interconal zone. For example, the interconal zone of the fuel rich nitrous oxide-acetylene flame is a bright pink colour due to the high concentration of CN radicals (see Chapter 3). The secondary reaction zone also gives much less intense radiation than the primary zone, the main bands arising from OH (usually much more intense than in the interconal zone). The characteristic blue colour of the outer cone of hydrocarbon flames is caused by a continuum due to the reaction.

$$CO + O \rightarrow CO_2 + h\nu$$

A similar reaction with NO produces the whitish yellow-green colour at the tip of some hydrogen flames. The orange colour of the outer cone of these flames is mainly due to vibration-rotation bands of H_2O (and also of OH).

Radiation from flames may, in the first instance, be separated into two categories - thermal and non-thermal. The latter is often referred to as simply chemiluminescence without further explanation, but this can be misleading; the reader will appreciate

that all energy and radiation from flames is essentially chemical in origin.

With thermal excitation, the emitting species is raised to its excited state by virtue of the high temperature of its surroundings. In other words, energy is transferred between species and converted to electronic excitation by collision processes. This energy is that responsible for the heat of the flame and released during the reactions of the fuel and oxidant. It is contained in the flame species by virtue of their motions (both internal and external) and should not be confused with the flame species actually existing in a high excited state. Gaydon and Wolfhard have suggested [19] that energy transfers of this type which result in electronic excitation are unlikely to be due to the translational motion of the flame species but more probably occur via the rotations and vibrations of the molecular species.

The total radiation from a given region of the flame can only be called thermal if complete thermal equilibrium is present. (This is discussed in detail in Section 1.4.4). However, in flame spectroscopy it is more usual to refer to the emission from each individual species. It is then possible to indicate whether a minority of species are giving non-thermal radiation when the rest of the hot gases are, for practical purposes, in thermal equilibrium. By convention, a particular emission is referred to as "non-thermal" if more than a small amount is produced as such, although obviously some part of it (however small) will still be thermal in origin. The best indication of non-thermal origins for a particular emission is to use that radiation to determine a spectroscopic temperature and compare it with the true equilibrium temperature. (This is discussed further in the following sections).

Excitation of species sufficiently to emit radiation may be produced by many factors other than the heat of their surroundings. For example, the intense emission from discharges results from the presence of large numbers of fast-moving electrons. However, in flames by far the most common source of non-thermal radiation is

chemiluminescence. This arises when the emitting species is formed directly in an excited state as the result of a chemical reaction. For example, chemiluminescence in the flame gases themselves may result from reactions such as

$$CH + O_2 \rightarrow CO + OH^*$$

or

$$O + ClO_2 \rightarrow ClO + O_2^*$$

(* denotes an electronic excited state).
Similar processes may be obtained with metals added to the flame:

$$C + MO \rightarrow CO + M^*$$

or

$$H + H + M \rightarrow H_2 + M^*$$

(This second example is really an induced chemiluminescence, not a true one, since M is not chemically modified by the reaction).
It is also possible that instead of an excited flame species losing its excess energy by radiation as chemiluminescence, it could transfer it to another flame species or a metal atom by collision

e.g. $OH^* + M \rightarrow OH + M^*$.

The emission from the metal atom in a case like this is often termed chemiluminescent, but "energy transfer" would be more accurate.

In many cases, although non-thermal emission from a flame can be identified as such, it may not be clear whether it is due to true chemiluminescence, induced chemiluminescence or an energy transfer. It is then much more satisfactory to term the radiation "non-thermal" or "overexcitation" rather than "chemiluminescent".

Discussion of the regions of the flame giving thermal and non-thermal radiation will be postponed until the next section, since it is closely related to equilibria in flames.

1.4.4 Equilibrium in flames

Three types of equilibrium may be considered in flames: chemical, thermal and radiational. The most significant failure to

reach equilibrium will be through incomplete combustion. However, the main chemical reactions involved in flames are normally completed in a very short time and chemical disequilibrium is generally restricted to the reaction zone. Thus, in the premixed flames considered in this work it is possible to calculate the flame gas composition assuming complete equilibrium and obtain a very good approximation to the actual situation outside of the reaction zone. The minor chemical changes giving rise to phenomena such as chemiluminescence will be considered in conjunction with thermal equilibrium since they have a much greater effect on the radiation from the flame gases than on their composition.

When thermal equilibrium exists in a region of the flame, the light emitted by all species will be a function of the flame temperature. Conversely, if radiation from the flame is used to measure its temperature the same value will always be obtained. Even if we assume chemical equilibrium, thermal equilibrium does not correspond to a state of complete equilibrium, which would also require radiative equilibrium. The latter is only achieved if all radiation emitted by the flame is replaced by absorption of light. This is only true for a black body and clearly the situation in a flame is usually very far from this. However, Gaydon and Wolfhard have shown[19] that in flames at atmospheric pressure, the flame species experience far more deactivations by collision than by emission of light. Thus, radiation of light has a negligible effect on the thermal equilibrium. (This is probably not true in very low pressure flames where radiation may cause a significant drop in flame temperature).

As might be expected, most overexcitation in flames originates from the primary reaction zone, since the greatest release of energy occurs there and thermal equilibrium cannot be expected. Radicals such as OH, CH, C_2 and HCO are well known for their non-thermal emission from this region of the flame. Similarly, overexcitation of metal atoms added to hydrocarbon flames occurs mainly in the reaction zone. At the other extreme, the outer cone a few

centimetres above the reaction zone is a region where for most purposes thermal equilibrium has been achieved (minor variations do occur, because as discussed below some equilibria, such as ionization, take longer to achieve than others). The observed radiation is then for all practical purposes entirely thermal. Between these two well-defined regions is a transition zone where overexcited particles achieve sufficient collisions to reach equilibrium. Thus, it is often possible to observe some non-thermal radiation from the interconal zone. The amount and the height in the flame to which it occurs will vary with the flame and the species considered. For example, C_2 and CH chemiluminescence will persist higher up in a fuel rich flame. OH chemiluminescence generally persists much longer than that from metal atoms.

Two facts should be clear from what we have discussed so far. First, for a study of flame spectroscopy, the equilibrium with which we are most concerned is the thermal one. Secondly, thermal equilibrium is best studied by considering the equilibrium of individual flame species; their state of equilibrium is directly dependent on the number of collisions they have undergone since formation in the reaction zone. Equilibrium of this type is indicated by whether the energy of a species obeys the Maxwell-Boltzmann Law. In its simplest form this merely states that if a species has possible energy levels E_0, E_1, E_2, etc., then the number of atoms/molecules with these energies will be very proportional to

$$e^{-E_0/kT},\ e^{-E_1/kT},\ \text{etc.}$$

Each type of energy requires different numbers of collisions to reach this state of equilibrium, since different degrees of freedom are involved. The approximate numbers are:

Translational	10
Rotational	10^3
Vibrational	10^5
Excitation and dissociation	10^7
Ionization	10^9

This merely means that if all species start their life in the flame out of equilibrium, translational energy will be the first class to reach equilibrium within its own class, i.e. to obey a Maxwell-Boltzmann distribution. This will be followed by rotational energy, and so on until after sufficient collisions equilibrium is achieved between all classes and the flame gases are in thermal equilibrium. The result of the finite number, of collisions which have occurred by any point in the flame is that we may be able to obtain, for example, an OH rotational temperature in the reaction zone because at that point the rotational energy levels (i.e. the rotational spectral lines) obey the Maxwell-Boltzmann Law. If we attempted to obtain the OH vibrational temperature at the same point we might find that the vibrational levels did not obey the Law. In this case, it would be impossible to solve the equations, graphs, etc. used to calculate the temperature from the vibrational spectral lines (see Section 1.4.5). However, the OH rotational temperature that we did obtain bears no relation to the "actual" temperature of the flame - it is just a function of the reactions forming the OH, the point of measurement, etc.

In the region of the flame where most species have suffered enough collisions to equilibrate all types of energy, it is usually acceptable to speak of "thermal equilibrium" even if this is not strictly true. For example, the same temperature might have been measured in the outer cone of the flame using different iron lines or a thermocouple, but the OH rotational temperature was much higher. This would mean that some OH chemiluminescence was still being observed

due to a persistent reaction, but the amount of energy involved would not be enough to make any difference to the practical level of equilibrium of metal atoms added to the flame. Similarly, the ionization of, say, potassium added to the flame might not have reached equilibrium because of the high number of collisions required. Thus a temperature measured using the ionization distribution in the Maxwell-Boltzmann law might be erroneous. In most cases, the energy involved would be too small to prevent the flame gases as a whole having an "actual" equilibrium temperature.

1.4.5 Flame temperature

The usual concepts of temperature and conventional methods of measuring high temperatures are not, in general, applicable to flames. Devices such as thermocouples, resistance thermometers and optical pyrometers can only be used with special precautions and for certain restricted applications. The most widely used, and the most informative, means of measuring flame temperature are spectroscopic; that is they utilise radiation emitted or absorbed by discrete particles present in the flame gases or added to them. In this thesis we are concerned only with the spectroscopic methods.

It should be clear from the discussion of Sections 1.4.3 and 1.4.4 that unless the whole flame were in thermal equilibrium we could not expect the temperature to be the same in all regions. Further, unless each region of the flame studied is in complete thermal equilibrium, different spectroscopic methods will indicate different temperatures. Thus, it is possible to talk of translational, rotational, electronic, etc. temperatures. As long as their limitations are realised, such temperatures are still very useful. Indeed, in many cases they provide more information about the flame processes than can be obtained under equilibrium conditions.

Most spectroscopic temperatures are measured by applying the Maxwell-Boltzmann Law to the populations of the energy levels of the

species concerned. Thus, they are often referred to as "population" temperatures. This applies even to the translational temperature which depends on the distribution of kinetic energy and ultimately on the Maxwellian distribution of the velocities of the atoms or molecules.

For the quantized energy levels of line and band spectra the law is usually applied in the form of equation (1-14)(Section 1.3.3). The required populations may be measured from emission or absorption spectra. Most work has been done with emission spectra because of the low concentrations of many flame species, the difficulties of making the required quantitative absorption measurements (see Section 1.3.4) and because chemiluminescence will only be revealed by emission temperatures. The main disadvantage of emission methods is the difficulty in avoiding the effects of self-absorption. This problem is discussed in detail in Chapter III, together with a rather empirical absorption method for molecular spectra which avoids self-absorption effects completely.

In general, there are two widely used methods of measuring population temperatures from spectral lines or bands. The line reversal method involves matching the brightness of an emission line from the flame against that of a calibrated continuum background source at the same wavelength. When the line is seen in neither emission nor absorption against the continuum the two temperatures will be identical. Since the continuum originates from a black body (or something of known emissivity such as a tungsten filament lamp) its temperature is easily measured with a pyrometer. Really, this amounts to an indirect method of measuring the absolute intensity for substitution into equation (1-14) and energy level populations may be deduced from the result. It may be applied to both atomic and molecular spectra but is best known with the yellow doublet emitted by sodium added to the flame.

The other common method involves the elimination of N and F(T) from equation (1-14) by measuring the relative intensities of two or

more lines from the same element or flame species. If the species are atomic, equation (1-14) applies directly and the measured temperature will be an electronic one. This is discussed in detail using iron lines in Section 3.5 . With molecular species, appropriate transition probabilities (involving further powers of ν) must be substituted into the equation, depending on whether the spectral lines used are rotational, vibrational, etc. The appropriate expressions are derived in "Flame Spectroscopy"[18] and their use is illustrated with CN in Section 3.6 . The method requires an accurate knowledge of transition probabilities and because of this has been used much more widely with molecular species than atomic species (since there is ample molecular emission from the flame gases and accurate relative transition probabilities may often be calculated).

1.4.6 Burner design and shape

Although it is of fundamental importance in flame spectroscopy, burner design has been given relatively little attention by analytical chemists. The main requirements for the burners used with premixed, laminar flames are:-

1. Complete mixing of the fuel and oxidant gases.
2. Laminar flow of these gases as they leave the top of the burner.
3. Minimum loss of analytical sample within the burner and ease of cleaning.
4. Burner port(s) designed to give a stiff, stable flame with the required gas flows and to prevent flash-back of the flame into the burner.
5. If a flash-back should occur it must be contained within the burner.
6. The burner should run for long periods without overheating or clogging.
7. The flame obtained should be of a convenient size, quiet, and usable over a wide range of stoichiometry.

The main part of the burner may be constructed to meet most of these requirements without too much difficulty, but the design of the burner head and its port(s) is rather more critical. Each port must be narrow enough to quench combustion by the cooling action of the walls if the flame should strike back. At the same time, the total area of the port(s) must give an upward gas velocity (at the required flow rates) which will balance the burning velocity and give a stiff, stable flame. Usually the gas velocity is chosen in a range three to ten times greater than the burning velocity (which does not act parallel to the gas flow, but perpendicular to the flame front). The usual choice for the burner port(s) is between a set of small holes and a narrow slit. The latter is more convenient to produce, since the holes must either be drilled in a steel plate or obtained using a set of capillary tubes. Holes are also more liable to clogging, more difficult to clean, and give a more untidy appearance to the flame but it is usually easier to obtain the correct combination of quenching diameter and total area for a given size of flame.

In addition to these requirements the burner must provide a flame of the optimum shape for the instrument and technique to be used with it. This simply means that it must put as many as possible of the atoms in the flame within the optical path of the detector. Since most modern detection systems are based on a narrow entrance slit (giving a narrow solid angle and optical path) and since hollow cathode lamps give narrow light beams, a long, flat flame end-on is the obvious choice for AAS. Given the same detector system, the same shape would also be optimum for AES if it were not for the fact that the effect of self-absorption on emission signals increases rapidly with increasing path length.

If a new instrument were designed for AES it would be best to have an optical path wide enough to allow a circular burner which gives much less self-absorption. This would also have the advantage of being optimized for AFS as well (the circular flame is needed to get as large an area as possible within the solid angles of both the

light source and detector and to reduce self-absorption of the fluorescence signal). It would give the same AAS results as a long flame if the background source could provide a light beam wide enough to cover the full width of the flame (note that the link between path length and absorbance via Beer's Law is a fallacy in AAS).

With modern flame spectrophotometers, a long flame also gives the best AES detection limits, because it matches the optical system, but self-absorption will bend the calibration curves at higher concentrations. Provided there is sufficient emission intensity, this curvature may be greatly reduced by turning the flame side-ways on to the monochromator. Under these conditions, a long rectangular flame is a better choice for emission work than the traditional circular flame.

1.4.7 Introduction of the sample into the flame.

Many different methods of adding solid or liquid samples to the flame have been devised. In practice, by far the most common technique is to dissolve up the sample, convert the solution to a mist and use one (or more) of the flame gases to carry it into the flame. Even within this restricted field, there is a wide choice of nebulizers which may be used to atomize the solution.

The simplest nebulizer, and still the most popular in flame spectroscopy, is the pneumatic type. This is usually made of narrow concentric tubes machined to a jet shape at one end. The gas is forced through one tube and creates a suction which draws the liquid up the other. When they meet at the jet, the liquid is dispersed into a suspension of fine droplets in the gas stream. This may be introduced directly into the flame, but normally contains too high a proportion of large droplets which give rise to noisy signals. It is more common practice to pass the mist through a cloud chamber which allows the larger drops to fall out and run to waste. A simple

chamber with perhaps one or two baffles is quite suitable for most purposes but rather inefficient, allowing a maximum of about 5% of the solution to reach the flame. More recently work has been carried out with much more complicated cloud chambers. For example, heating and condensing units may be fitted with the object of removing a large proportion of the solvent (but not the solute) before it reaches the flame.

Although these devices help to improve the efficiency, they detract from the basic advantage of the pneumatic nebulizer - its simplicity and reliability. Under these circumstances, other types of nebulizer may become more attractive alternatives. For example, ultrasonic nebulizers produce fine droplets by the action of sound waves generated by a vibrating crystal. They allow much more precise and easy control of solution uptake and droplet size independent of gas flow rate. If all the droplets can be produced to a fine, uniform size by this technique an elaborate cloud chamber is no longer required to obtain good efficiency and low signal noise.

1.5 Spectral Sources

1.5.1 General

Most of the spectral sources described here have been known for many years but it is only since the introduction of AAS (and AFS) that most of them have become of widespread commercial interest; probably more hollow cathode lamps have been manufactured in the last five years than in the previous fifty. In view of this, and also because of the applications described in this thesis, the main emphasis in the following descriptions will be on the suitability of each source for AAS and AFS.

Before describing any individual sources, it is useful to emphasize the basic categories into which they may be placed. This

classification may be done on the basis of the type of spectra emitted and on the way in which the source is prepared and used.

(a) Spectral distinctions. First, the source may emit light continuously with respect to time whenever it is in use or it may be pulsed so that light is emitted only in short, specific bursts of energy. Sources which are merely modulated (so as to provide a tuned amplifier system for AAS or AFS) are generally referred to as continuous. At the present time, pulsed sources have not been used very much for AAS and AFS and they will not be described here. However, they offer considerable promise for the future both because greater intensity is obtainable and because of the possibility of time resolved techniques. Secondly, either of these types of source may emit a line spectrum or a continuum spectrum. These terms have been defined in Section 1.2.1.

(b) Practical distinctions. The most common class of sources encountered in AAS and AFS are permanently sealed-off. This offers considerable advantages for ease of use, good reproducibility and simplicity, especially if the source is at very low or very high pressure. The second class is known as demountable. These generally have similar forms to the sealed-off types but allow alterations to the contents to be made at any time after manufacture. This is most commonly done simply by fitting a tap instead of a seal and these sources are much more versatile for research purposes. Most of the sources described below as sealed-off can be used in demountable form with virtually no change in characteristics. Finally we must recognise a class of consumable sources in which the element whose emission is required must be continually replaced. Sources such as flames, arcs, plasmas and flow-through microwave discharges fall into this category.

1.5.2 Vapour discharge lamps (VDL)

These lamps have been widely used as sources of line spectra from the volatile elements (Cd, Cs, He, Hg, K, Na, Ne, Rb, Tl and Zn). For many years VDL's such as those made by Phillips and Osram (Wotan) were the only widely available commercial lamps for line spectra. They give intense outputs with very low background levels and are ideal for purposes such as spectrograph calibration, since they are easy to use, robust and require only simple power supplies. Unfortunately, when run at the currents recommended by the manufacturer (1.0 to 1.5 amp.) the lines are very broad and strongly self-absorbed or even self-reversed. A few of them may be run at currents below 0.5 amp. to give lines which are sufficiently sharp for AAS (see Chapter VII) but only with a considerable loss in intensity.

1.5.3 Hollow cathode lamps (HCL).

The hollow cathode lamp is one of the most important sources of intense, sharp-line spectra and has been widely used by spectroscopers since its introduction in 1916. Many different designs have been described over the years and they can generally be placed into two classes. For ultra-high resolution studies of hyperfine structure, especially of resonance lines, the cathode is usually cooled with water or liquid air giving extremely sharp lines. When line width is less critical or for studies of high energy lines, a hot hollow cathode may be used. Apart from greater simplicity, the latter gives a much higher intensity. The line widths are still sufficiently small for measurements of peak absorption and all commercial lamps used for AAS are of this type.

In most lamps used for AAS, the cathode is a hollow cylinder, 10 to 20mm long and less than 10mm in diameter, made of the required element or lined with it. The cathode is sealed inside the lamp together with an anode whose exact position and size is unimportant,

and the lamp is filled with an inert gas at a pressure of about 1 torr When a voltage of 500 to 1000 volts is applied between the electrodes, the inert gas is ionized and a stream of positive ions is directed into the hollow cathode by the field. These ions cause a strong sputtering action on the cathode surface so that particles are ejected into the discharge which is concentrated in this region. The atoms are then excited into strong spectral emission by collisions with the excited atoms and ions of the inert gas. Helium is not often used as the filler gas because it is too light to produce sufficient sputtering and its high excitation potential (19.7 eV) results in spark spectra. Until recently argon was the normal filler gas, but a number of the most modern lamps use neon (mainly to reduce the background spectrum around the resonance lines of some elements). Most commercial lamps are operated at the relatively low currents of 5 to 25mA. Use of higher currents leads to increased Doppler broadening and self-absorption and also shortens the life-time of HCL's made with the more volatile elements.

A large number of improvements have been made in hollow cathode lamps over the last few years because of the growth in AAS. These can be placed into two groups. First, significant advances in stability, line width and intensity have been made by using auxillary electrodes; electrode shields; improved shapes of electrodes and lamps; different types of chemical matrices within the cathode; etc. Secondly, much work has been done on the production of multi-element lamps to reduce the number required for the average laboratory. Originally, multicathode lamps were produced but more recently better results have been obtained with several elements inside one cathode. In either case, the elements to be used together must be carefully chosen with respect to the spectra, volatility etc.

1.5.4 Electrodeless discharge tubes (EDT)

The high frequency electrodeless discharge tube has been used as a source of sharp, line spectra even longer than the hollow cathode lamp. It has a number of advantages for basic work, including studies of hyperfine structure: the discharge can be maintained at pressures as low as 0.001 torr (very little pressure broadening); only tiny quantities of the element are required; there is no contamination from electrodes or difficulty with their high vacuum seals; and the tubes are easily cooled. In spite of this, EDT's have been less widely used than HCL's. Perhaps the main reason for this is the difficulty of obtaining a stable discharge in the lamp and a reproducible spectral output, except for a few elements. When the tubes are used for basic studies of spectra, the emitting element is present only as an impurity and no real problem arises. However, in order to obtain sources bright enough for AAS and particularly AFS, it has been the practice to use much larger quantities. The metal or its compound will then condense on the walls of the tube unless they are kept at a sufficiently high, uniform temperature. This requirement is often not met, the bulb having cold areas outside of the discharge, and the particular way in which condensation occurs at any time governs the nature of the spectrum obtained. Because of these difficulties, EDT's have not been as widely available commercially as HCL's. The construction and use of the modern type of microwave frequency EDT used in a resonant cavity is described in Chapter VII .

1.5.5 Continuum sources

In theory continuum sources would appear to offer one outstanding advantage for AAS and AFS over the sources already described - it would no longer be necessary to provide a separate lamp for each element studied. Unfortunately, there are many practical difficulties and continuum sources have not been widely used for these

purposes. As explained in Section 1.3.4 , the sensitivity for AAS will only be as good as with a sharp line source if a high resolution monochromator is used. Although this problem does not arise with AFS, it is still difficult to obtain sufficient intensity, especially in the U.V., with the continuum sources available at present. Obviously, the conventional tungsten lamp will be of little use for this type of work, but the newer quartz-iodine lamps are much more intense. The well-known hydrogen lamps give a much greater output, but even they cannot compare with the best line sources in the U.V. and much of the visible region. (It must be remembered that for AFS, it is the output of the continuum source over the width of the spectral line which is important not that over the bandpass of the monochromator; hence, with many instruments these sources appear misleadingly intense). Several recently developed pulsed sources offer the promise of much greater continuum intensities.

1.5.6. Other sources

A number of other sources, such as Geissler tubes and atomic beams, have been developed over the years to provide sharp line spectra of individual elements. However, none of them are of any interest for AAS or AFS at the present time. More important are the consumable sources mentioned earlier. A number of workers have tried using flames, arcs and plasmas as light sources for AAS and AFS because, like continuum sources, they do not require a separate lamp for each element. The main difficulty is to obtain lines sharp enough for AAS. Sources, such as the plasmas, which give sufficient intensity for AFS are generally too noisy for good results, and they are also rather expensive. The most detailed work on consumable sources for AAS has been carried out by Strasheim, Butler and co-workers[26]. They report that the best results are obtained with a Kranz-arc. This is nitrogen stabilized and the signal is taken from a region outside the electric field (thus avoiding Stark broadening of the lines).

Chapter II

Separated Flames

2.1 Introduction

As explained in Section 1.4.2, premixed flames generally consist of an inner reaction zone and an outer diffusion zone separated by an interconal zone containing an appreciable concentration of the atoms and radicals produced in the reaction zone. These are readily attacked by the same atmospheric oxygen which supports the secondary diffusion flame so that their presence is usually only apparent in quite fuel rich flames. If the flame could be stabilised in the absence of this secondary air, then the outer zone of the flame would disappear and the atom/radical concentration of the interconal zone would greatly increase. Further, it would be possible to view (spectroscopically) and study the radicals in the interconal zone without spectral or chemical interference from the outer diffusion flame.

Over the years, several different ways of achieving some or all of these aims have been devised. This has led to considerable ambiguity in the nomenclature used to describe the results obtained. To avoid this in the present work, the terms defined below will be used throughout the following discussion even if they differ from the description assigned to a particular flame by its originator.

a) A separated flame is one in which the secondary diffusion zone is physically moved some distance from the primary zone leaving a greatly extended interconal zone between the two. This separation may be obtained by surrounding the lower part of the flame with either a solid wall or a wall of an inert gas.

b) A shielded flame is one in which the flame is protected in some way from the surrounding atmosphere without physically separating its zones. Examples include a sheath of filtered air(to protect the

flame from dust); a sheath of oxygen (to increase the temperature at the edge of the flame); and a sheath of another flame (to protect species normally attacked by atmospheric oxygen).

Although the author's work has been mainly concerned with (a), a brief literature survey is given of both types. This is necessary because many of the advantages described above can be achieved by separating or by shielding the flame and the final choice of method is often quite arbitrary.

2.2 Historical

Since Smithells' pioneering work on flame separation (see below) many descriptions of separated or shielded flames have appeared in the literature. The majority of these have been concerned with fundamental studies on flames, although some analytical applications are also described. However, in either case the relevant papers are extremely difficult to trace, especially in the older literature. This situation has arisen because the separation or shielding of the flame was usually considered a minor part of the work and is, therefore, not recorded in the abstracts and indexes used for literature surveys. In view of this, the reader should remember that a method of separating a flame is not necessarily new just because no previous record of it comes readily to hand. In fact, the few examples quoted below cover almost every possible means of separating or shielding a flame. Usually only a particular application is new and even some of these have been "discovered" several times. For convenience, the examples are grouped under the type of separation or shielding used rather than chronologically.

2.2.1 Glass or quartz tube separated flames.

The first recorded separation of any flame was that of the

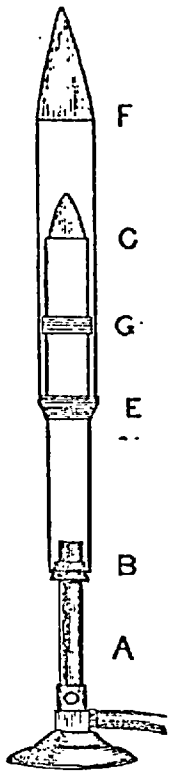
inner and outer cones of a Bunsen-type flame, achieved independently ca. 1891 by Smithells[27] and by Teclu[28]. Both of these workers found that if they fitted a glass tube over the top of the Bunsen burner and lit an ordinary luminous flame at the top they could reduce the fuel (or increase the air) until a critical value was reached when the flame struck back leaving the outer cone burning at the top of the glass tube while the inner cone burnt at the top of the Bunsen tube. A slightly improved version is shown in Fig. 2-1, which was taken from Smithells' original paper[27].

Using a separator identical to this, except for a more versatile gas control unit than the Bunsen burner, Smithells and Ingle[27] and Smithells and Dent[29] carried out a considerable amount of research into the structure and appearance of various hydrocarbon and cyanogen flames. The main part of their work was concerned with the analysis of the gases in the three zones; a task which would have been impossible without their flame separator.

In 1917, Hemsalech published several papers dealing with the spectra of iron and in one of these [30] he described the use of a glass tube separated air-coal gas flame to determine which part of the flame gave the most intense iron emission. He also mentioned (Ref. 30, p. 233) that this type of separated flame was in common use at that time.

Smith and Pickering [31] used glass tube separation of Bunsen-type air-propane, oxygen-propane and air-acetylene flames to study the effect of excess fuel on flame shape in the absence of secondary air.

Some years after this, Ludlam[32] also used a separated flame to study flame spectra. He separated an air-hydrogen flame with a silica tube in order to study the green band emission obtained when phosphorus vapour is sprayed into a cool flame and reported that use of a separator greatly enhanced this emission. Thirty years later this discovery was put to commercial use for the analysis of phosphorus and also sulphur and boranes (which give similar band emissions) with the



A = Bunsen burner
BC = Inner glass tube
EF = Outer glass tube
B: Joint is cork
E: Joint is a rubber ring
G: Asbestos ring

Fig. 2-1

The Original Smithells Flame Separator

introduction of a number of monitoring devices (see below).

The next important development of the quartz-tube separator was described by Honma and Smith in 1954[33]. They separated a natural gas-air flame in order to use it as a source for the flame spectroscopic determination of nitrogen in organic compounds by the CN band emission obtained at 3883Å. This appears to be one of the first practical, analytical applications of a separated flame.

A number of relatively cool hydrocarbon-air flames were also burnt on a Smithells-type separator by Street and Thomas[34] for a study of carbon formation in flames, the separator being used to prevent atmospheric oxygen attacking the carbon particles. An interesting development for these cool flames was that the top of the separator was covered with brass gauze to stabilise the secondary diffusion flame.

In 1959, Drager[35] described a novel separated flame for quantitative determinations of halogens in gases by an adaption of the Beilstein test. He used the burner arrangement shown in Fig. 2-2 to separate two diffusion flames. The lower flame atomises the halogen compounds and heats the copper necessary for the Beilstein test; the copper halide formed then passes into the upper flame where it is excited to give the characteristic green emission. Several years later, this method was improved by Gilbert[36], who used the more conventional Smithells-separated air-hydrogen flame and replaced copper by indium. Recently, this design has been further improved by Herrmann and co-workers[37] for the analysis of chlorine in organic pesticides. Their burner is shown in Fig. 2-3 and incorporates an extra tube to protect the secondary zone from draughts and dust.

The separated air-hydrogen flame has also been used extensively in the phosphorus and sulphur monitors mentioned earlier. The first of these was disclosed in 1962 by Drager[38] and the burner used is shown in Fig. 2-4. It was rather more elaborate than an ordinary separated flame because the outer tube was cooled by a water jacket to increase the chemiluminescent emission obtained in the flame. A similar burner for the same purpose was produced shortly afterwards in the United States[39]. At about the same time a quartz-tube separated air-hydrogen flame without water cooling was developed for a pentaborane monitor[40] and in 1965 this same burner was used by Crider[41] as a monitor for sulphur dioxide in air, apparently without knowledge of the previous work on phosphorus and sulphur. His burner incorporated a light-tight exhaust tube and he did not mention whether the secondary zone of the flame was actually supported inside this chimney by atmospheric air.

In 1966 Brody and Chaney[42] used a phosphorus and sulphur detector of this type in conjunction with gas chromatography, the nitrogen from the column being mixed with oxygen and used to support a glass tube separated hydrogen flame of the now familar type. Sulphur and phosphorus band emission in this type of flame has also been

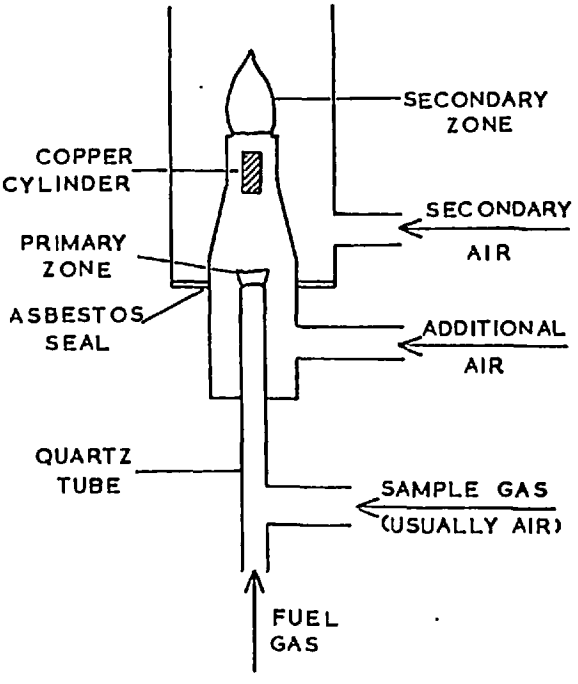


Fig. 2-2

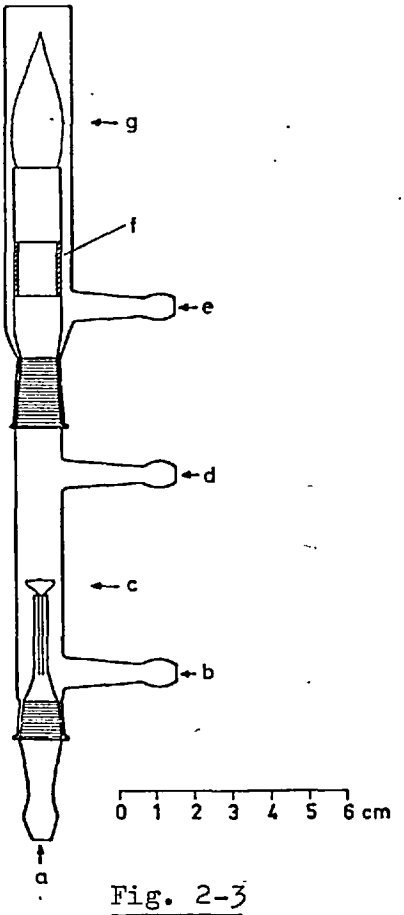


Fig. 2-3

a Hydrogen
b Primary air
c Primary zone
d Nitrogen stream with atomised sample
e Secondary air
f Beryllium-bronze cylinder with inner layer of indium
g Secondary zone of the separated flame

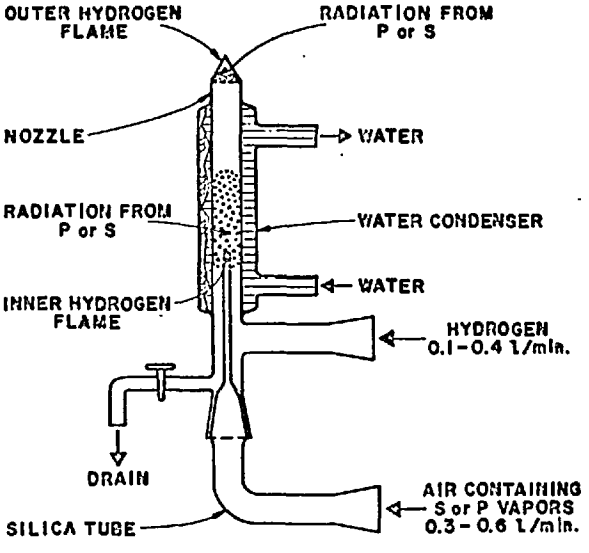


Fig. 2-4

Burners For Separated Air-Hydrogen Flames

described by Dagnall, Thompson and West[43] and by Syty and Dean[44].

Finally, mention must be made of the work of Mavrodineanu, who has advocated the use of separated flames in analytical flame spectroscopy for a number of years. In what is probably his longest discussion of the topic (Ref. 45, particularly pp. 382-387) he described in detail the separation of the premixed air-acetylene flame with a quartz tube and anticipated much of the early work at Imperial College on separated flames. This included: spectrographic identification of the species present in the three zones of the separated air-acetylene flame; the effect of separation on the flame background emission and its interference in flame spectrophotometry; the separation of molecular and atomic emission (specifically of MgO and Mg); the enhanced emission from refractory elements in the reducing interconal zone (specifically of Cr and Mo); the provision of side arms with flat quartz windows to facilitate optical measurements through the quartz separator; and the possibility of "application to practical analytical measurements in atomic emission or atomic absorption mode "(Op. cit. p. 385, lines 3-5). Some of these conclusions on separated air-acetylene flames are repeated together with a large selection of results, flame spectra and colour photographs in the massive textbook by Mavrodineaunu and Boiteux[18] (pp. 21, 168-169, Plates 21-23 and Figs. 1-15, 12-13 and 12-14).

2.2.2 Nitrogen or argon separated flames.

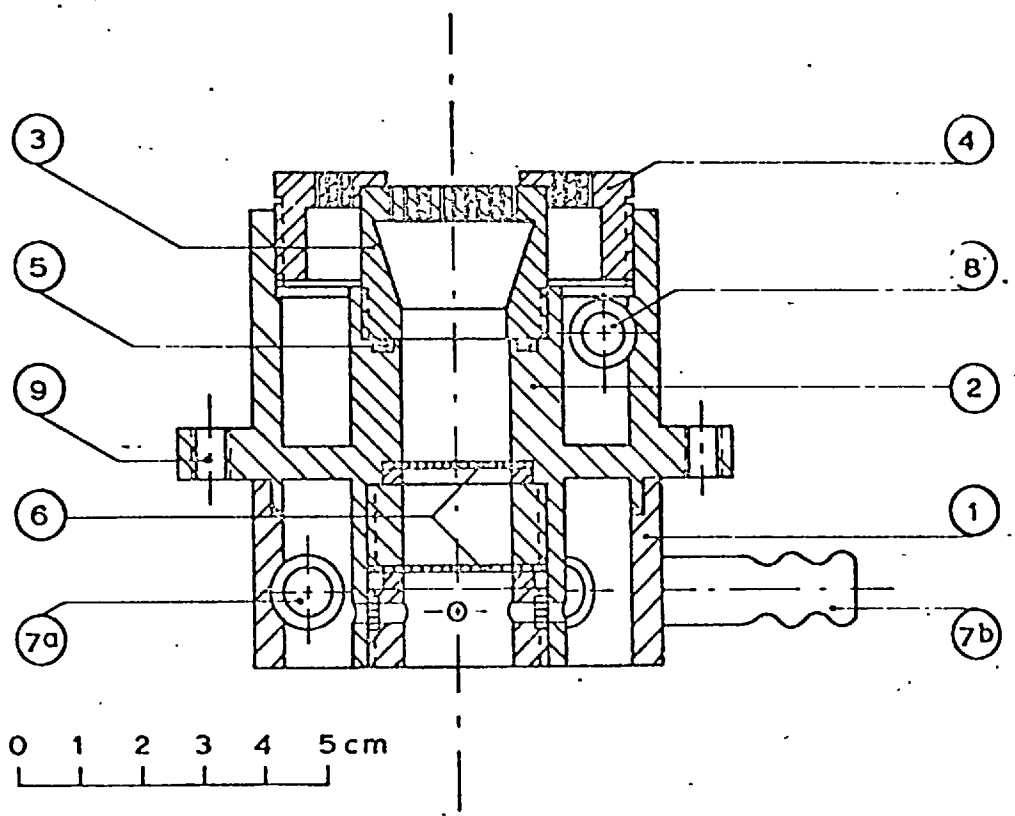
The practice of shielding an arc or spark discharge with nitrogen or argon to reduce the background spectrum and increase the emission line intensities has been well known in spectrography for many years (for reviews of this subject see Refs. 46, 47). However, there appear to be no previous applications of nitrogen/argon shielded flames to analytical spectroscopy and only one or two descriptions of nitrogen separated flames in the literature. Several workers have sheathed low pressure flames with nitrogen to stabilize them[48,49]

and other workers have used nitrogen sheathed flames to maintain a uniform gas flow and an upward flow at the flame boundary in particle track studies [50,51]. These flames were not actually separated, since separation requires that the glass or quartz tube be replaced with a vertical wall of an inert gas exhibiting laminar flow. Egerton[52] showed that such a flow of nitrogen could be obtained by passing it through a coil of corrugated metal strip (see Section 2.4.1), but used it to stabilize a flat flame burning on a Powling-type burner rather than for flame separation. Padley and Sugden[53] have described a flame sheathed H_2-O_2-N_2 flame in which the outer flame is further protected by a wall of nitrogen (see also Section 2.2.3). This burner has also been used by Jenkins[54] for H_2-O_2 flames with a variety of inert diluents.

The only true separation of a flame using an inert gas stream in the way described in the present work appears to have been by Alkemade and Zeegers at the University of Utrecht. They have described the separation of premixed, cylindrical air-acetylene flames[55, 56, 57] and also air-hydrogen and air-carbon monoxide flames[58] using a stream of cold nitrogen gas. The construction of the burner has been described in detail by Zeegers[59] and a diagram of it fitted with a burner plate suitable for hydrogen-air flames is shown in Fig. 2-5.

The exit channels for the nitrogen stream are 0.5cm long and their outlets were placed 0.2cm higher than the top of the combustion cones in order to prevent blowing-off and turbulence of the flame. The nitrogen sheath provided was 1.2cm thick around a flame 2.0cm in diameter and gave a stable, cylindrical, laminar flame undisturbed by secondary combustion at the flame border up to heights about 8cm above the reaction zone.

These flames were used for a prolonged study of the formation, recombination and electronic excitation of flame radicals (especially OH) and it was necessary to exclude additional OH radicals normally formed by secondary combustion at the flame border as well as



1 outer wall; 2 wall separating mixing chamber for H_2 and air and the chamber for N_2; 3 burner top with exit canals; 4 ring-shaped plate with exit canals for N_2; 5 package ring of teflon; 6 grids to prevent back fire; 7a and b inlets for H_2 and air, respectively; 8 inlet for N_2; 9 hole with screw-thread for adjustment to bottom plate.

Fig. 2-5 Burner For Nitrogen-Separated Flames

entrained atmospheric oxygen. Although no mention is made of the reason for choice of nitrogen separation instead of quartz tube, the latter would probably have introduced considerable experimental difficulties into their absorption measurements and their measurements of very small chemiluminescent emission signals. Also, the solid wall would have a more serious effect on the flame equilibria than a nitrogen sheath. No doubt these considerations have influenced other workers and it is probable that other references to this type of flame

separation may be found in the literature.

2.2.3 Flame shielded flames

So many different types of flame shielded flames have been described by different workers that in the space available here it is only possible to quote the work of one or two important contributors as examples. Basically, the fundamental work with this type of flame has been for two purposes.

a) To maintain the temperature of the inner flame at its "normal" value right across the flame (in the unshielded flame, the edge is cooled by contact with the atmosphere and temperature measurements by methods such as sodium line reversal are affected accordingly[60]).

b) To protect unstable species formed in the flame from attack (oxidation and/or quenching) by the surrounding atmosphere.

A great deal of work on flame shielded flames providing optical paths of uniform temperature has been carried out by Kohn and his associates in the course of their studies on optical cross sections of spectral lines emitted by species in flames[61, 62, 63, 64]. The flames used included air-acetylene, air-nitrous oxide-acetylene and oxygen-acetylene and they have described burners with both partial shielding (i.e. a long path flame with an extra flame at each end) and complete shielding (i.e. two concentric burners, either rectangular or circular). The burners were all constructed by supporting a large number of steel capillaries between two brass plates, the capillaries being pressed into holes drilled in the plates. This is an extremely versatile and safe mthod of burner construction since:

(i) The capillaries provide laminar gas flow and anti-flashback protection and can be easily cut to the optimum length.

(ii) Different width capillaries may be provided for different combustion mixtures (if necessary in the same burner).

(iii) The spacing between the capillaries is easily altered.

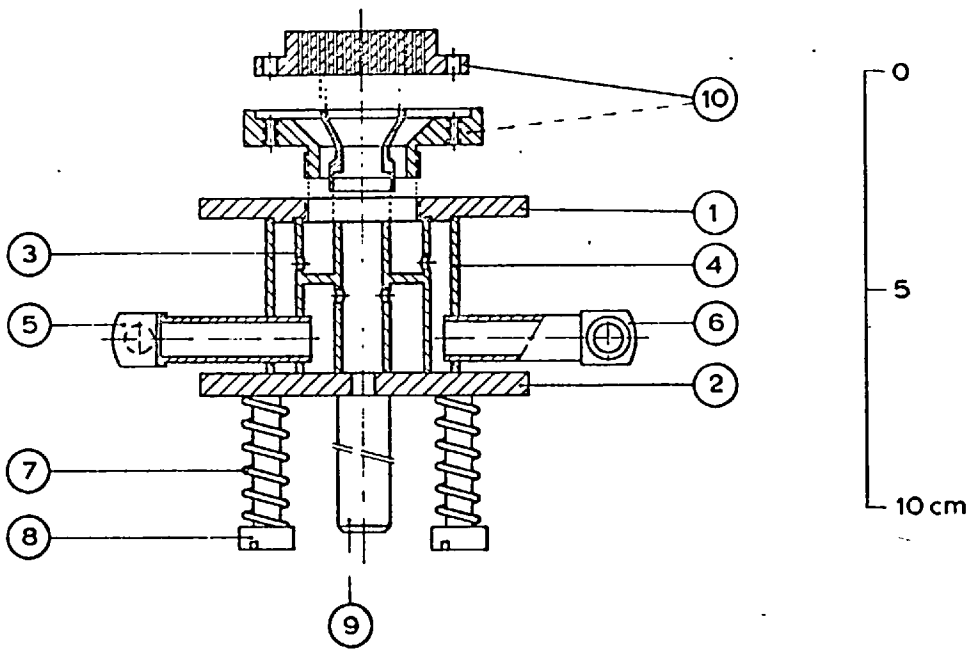
(iv) It is very easy to add the species being studies to the inner flame independently of the outer one (which is nearly always required when flame shielded flames are used in this way).

(v) The relative sizes and shapes of the inner and outer flames are easily altered, merely by connecting the capillaries to common gas inputs as required.

Alkemade and his co-workers have produced a range of concentric Meker-type burners over a number of years for flame sheathing air-acetylene, air-propane, air - or oxygen-hydrogen and air-carbon monoxide flames. The ultimate result of this work is the simple burner unit produced by Hollander[65] and shown in Fig. 2-6. This particular burner uses premixed gases for both the inner and outer flames, but the same author has also described a much larger burner incorporating gas mixing chambers and a heated chamber for vaporizing solid salts into the flame.

Although a concise review of the work with these flames has not been published, mention should be made of their use for accurate line reversal temperature measurements and resonance fluorescence studies[55, 66, 67, 68]; measurement of the ionization of the alkali metals and of the dissociation energies of the alkaline earth metal oxides[65, 69, 70, 71, 72]; and measurement of α' line broadening parameters[73].

Sugden and his co-workers at Cambridge have also made extensive use of flame shielded flames in their studies of radicals and ions in flames during the past fifteen years. Their papers are far too numerous to list here, but details and references for their earlier work (Meker-type burners) are given in Ref. 74 and for their later work (burners constructed with hypodermic needles) in Refs. 53 and 75.



1 = upper plate; 2 = base plate (serving as safety-outlet); 3 = wall separating outer and inner chamber; 4 = outer wall; 5 and 6 are inlet tubes for central flame and outer zone gases, respectively; 7 = spring pressing base plate (2) against burner walls (3) and (4); 8 = screw adjusting spring (7) and fixed in plate (1); 9 = holder; 10 = burner top with exit holes.

Fig. 2-6

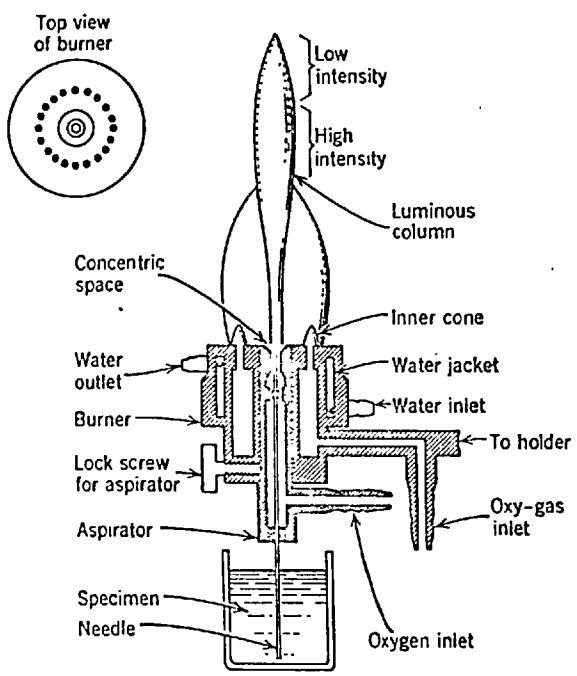


Fig. 2-7

Burners For Flame Shielded Flames

A similar burner for sheathed oxygen hydrogen flames, allowing independent aspiration to the inner and outer flames, has been described by Bogdan and Zinman[76] and is available commerically (Bethlehem Apparatus Co., Burner Model A-PM20).

The sheathed flame is of considerable importance in flame emission spectroscopy since the outer flame sheath effectively increases the temperature of the inner flame (into which solutions are sprayed for analysis) and, hence, the emission signal. Even more important is the protection it afford to excited species in the inner flame from quenching and/or oxidation. Unfortunately, the flame sheath increases the flame background rather than decreasing it as does flame separation; conversely, flame separation decreases the temperature rather than increasing it.

An earlier application to flame photometry was the Weichselbaum-Varney atomizer burner shown in Fig. 2-7[77].

This unit has a premixed oxygen-coal gas flame surrounding a stream of oxygen carrying the nebulized sample. The result is an oxygen-coal gas diffusion flame sheathed by a premixed flame. A more modern and convenient unit giving a similar effect is the Gilbert atomizer-burner described in Section 2.2.4. Although this is classed as an oxygen sheathing burner, it effectively provides two concentric, turbulent diffusion flames with the sample added to the inner flame.

2.2.4 Air or oxygen shielded flames.

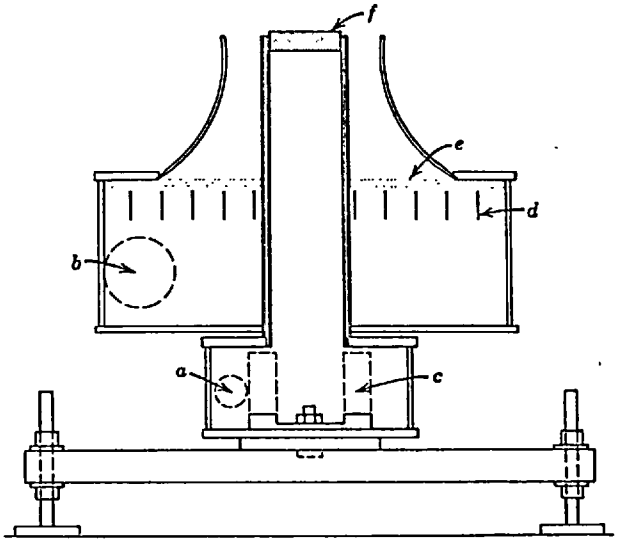
The construction of a burner providing air or oxygen shielding of a flame is rather more simple than that required for the nitrogen separation described in Section 2.2.2, since there is no real necessity for laminar flow of the shielding gas. The main advantages of an air shield are increased stability of the flame and protection from atmospheric pollution (e.g. dust particles), and a number of commercial flame spectrophotometers have included burners with

filtered air shields. A simple and efficient burner of this type is shown in Fig. 2-8. It was designed by Ramsay[78] for an air-coal gas flame used with micro-determinations by flame photometry.

Recently, P.T.Gilbert has strongly advocated the use of oxygen shielded fuel rich air-hydrogen and oxygen-acetylene flames. His principal concern has been the ability of these flames to produce chemiluminescent excitation of a variety of elements[79,80,81,82], but he has also suggested that sheathing the fuel-rich oxygen-acetylene flame with oxygen enhances its utility as a source of atoms of elements forming refractory oxides (Ref. 81, p.177). This latter effect apparently occurs because the oxygen sheath allows a much more fuel rich flame to be supported on the burner, thus increasing the reducing atmosphere at the centre of the flame.

The original oxygen shielded burner produced by Gilbert is shown in Fig. 2-9. It can be seen that it is basically the well known Beckman turbulent, total consumption atomizer-burner with a simple modification. In use the fuel (hydrogen or acetylene) emerging from the burner forms a turbulent diffusion flame with the oxygen on both sides of it - i.e. the result is really one diffusion flame sheathed by another with sample added to the inner flame only. Gilbert has suggested (Ref. 81, p.174) that high levels of chemiluminescence can be obtained only with this type of flame because of its large area corresponding to the small reaction zone of a premixed flame.

Apart from chemiluminescence possibilities, the increase in temperature afforded by the oxygen sheath is often useful in general flame emission spectrophotometry. Webb and Wordingham[83] have reported a premixed oxygen-propane flame shielded with oxygen which suppressed the interference of phosphate on strontium and calcium emission. More recently Mavrodineanu[45] has adopted an oxygen sheathing device produced many years ago by Hemsalech[30] to increase the thermal emission from flames by raising the temperature. This simple arrangement consists of a quartz tube separator of the type described in Section 2.2.1 placed around a normal premixed burner



a Coal gas - air in
b Filtered air in
c Radial vanes
d Honeycomb
e Brass gauze
f Porous plate

Fig. 2-8 Burner For Shielding A Premixed Air - Coal Gas Flame With Filtered Air

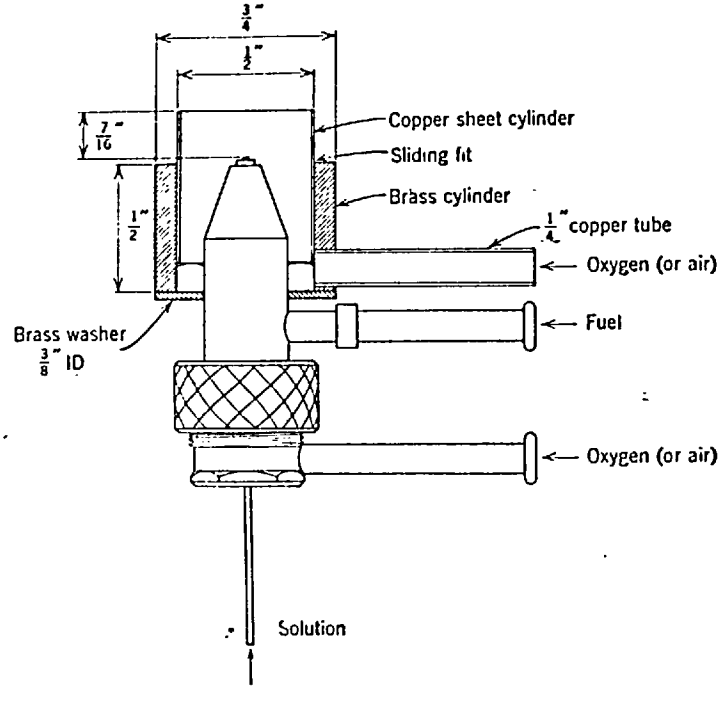


Fig. 2-9 Sheathed Atomiser - Burner Developed By Gilbert

(e.g. air-acetylene) and with an oxygen inlet tube near the bottom of the separator. If necessary, the shielding oxygen can be used to atomize the sample and the shield may be used with a premixed oxygen-acetylene flame (use of this arrangement allows a tiny burner jet for the premixed flame without the possibility of atomized sample causing clogging). A similar, but more versatile, sheathing arrangement has also been described by Byrne[84]. He used a pyrex tube resting on a perforated brass block fitted around the burner head so that he could study the effect on methane, propane and carbon monoxide-flames of different ambient atmospheres (ranging from almost pure nitrogen to pure oxygen).

2.3. Previous Work AtImperial College

The work carried out by the author and described in this thesis followed on directly from an extensive development of quartz tube separated flames by Dr. A. Semb and Dr. D.N. Hingle. This was the first systemmatic study of the use of high temperature separated flames for analytical flame spectroscopy and because of its importance to the logical development of nitrogen/argon separated flames it will be described in some detail.

2.3.1 The quartz tube separated air-acetylene flame[85]

The burner constructed for separating air-acetylene flames is shown in Fig. 2-10. It is basically a Unicam Meker type burner of the usual premixed type fitted with a "Vitreosil" transparent fused silica tube, 20mm internal bore and 120mm long. The Unicam air-acetylene stainless steel burner head has thirteen orifices of about 1.2mm diameter arranged in a square of side 9mm. The most convenient separation was obtained with the top of the silica tube 60-80mm above the top of the burner. It was found that distances

much greater than this caused instability of the flame and that instability also resulted if the gas mixture was made too lean or too rich. Provided these limits were observed, the flame was easily separated into a stable primary zone on the burner head inside the silica tube, and a secondary diffusion flame burning at the top of the silica tube.

Dr. Semb found that this separation greatly reduced the flame background emission from all species present, but especially that from OH and CO (which occur mainly in the secondary combustion zone). Unfortunately, the temperature drop occuring on separation also caused a reduction in the emission from metal atoms nebulized into the flame, so that an improvement in detection limit was obtained only from those elements giving their principal emission lines in the regions of highest flame background (e.g. Bi and Mg). The flame was enriched with 15% oxygen in an attempt to overcome this difficulty, but such a measure is not really suitable for routine use. Other difficulties encountered were the inability to support fuel rich separated flames on the burner and the tendency for dirt to accumulate on the walls of the separator (especially if concentrated solutions or organic solvents were nebulized).

2.3.2 The long path quartz tube separated air-acetylene flame.[86]

The long tube burner described here differs from most other devices of this type produced for atomic absorption spectroscopy in that the suction used to draw the air-acetylene flame into the tube does not suck in extra air at the same time. This arises because the long tube is attached directly to a quartz tube separator and the effective result is a separated flame turned through 90^0, i.e. the light path passes through a horizontal interconal zone extended to some 30cm while the secondary zone burns vertically above it as usual. The burner used to achieve this is shown in Fig. 2-11.

A normal air-acetylene flame was burned on a standard Unicam

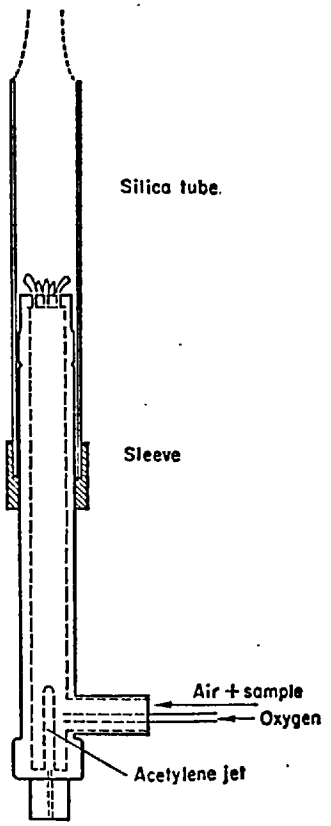


Fig. 2-10

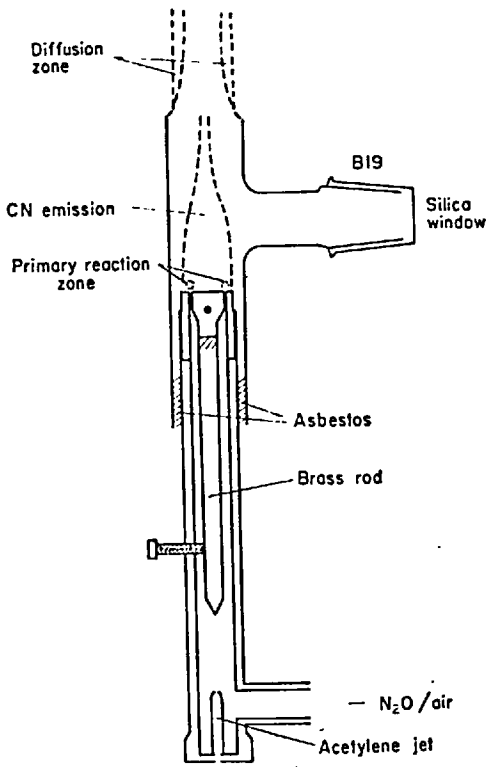


Fig. 2-12

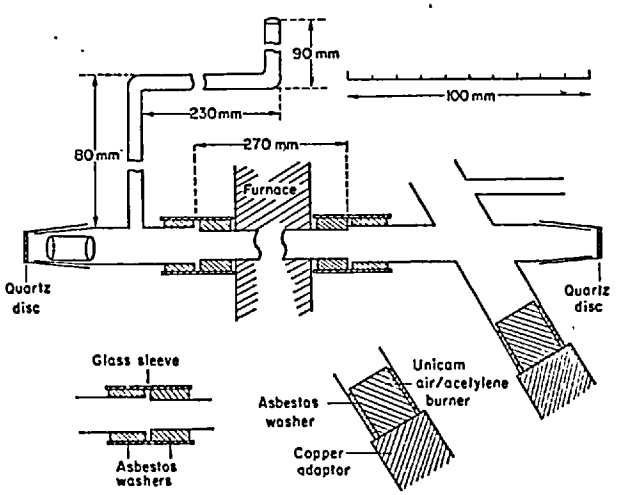


Fig. 2-11

Mechanically Separated Burners

burner head at the base of the separator. The long tube was placed inside a furnace operating at 1100°C to maintain an even temperature along its length. Suction was provided at the side arm to the left of the long tube so that the interconal gases would be drawn through the furnace. The system worked well with most mixture strengths, but in order to separate lean flames it was necessary to add hydrogen at the top of the separator through the extra tube shown. This stabilised the secondary diffusion flame burning at the top of the separator,

In use, the burner arrangement was found to give a considerably reduced background absorbance below 3300Å in spite of the long path length. This contributed to the good sensitivity obtained with Ag, Cu, Fe, Hg, Mg and Zn, all of which are relatively easily atomised and give principal absorbance lines below 3300Å.

2.3.3 The quartz-tube separated nitrous oxide-acetylene flame[87,88]

The first nitrous oxide-acetylene flames used in analytical flame spectroscopy were all long path flames burnt on 5cm. slot burners similar to that designed by Amos and Willis for atomic absorption (see Section 5.2). However, it was felt that the high temperature and reducing atmosphere of this flame would be just as useful for flame emission spectroscopy of refractory elements if the intense background emission due to OH and CO could be removed. i.e. if the flame could be separated. This was not practical, nor desirable, at the time with a long path flame and so Dr. Semb designed the first circular nitrous oxide-acetylene "emission" burner. This is shown in Fig. 2-12.

The original burner was based on the usual Unicam premixed burner stem with the conventional Meker-type head replaced with a stainless steel head with a circular slot 0.50mm wide and 11mm internal diameter. The central steel plug used to obtain this slot was held in place by

three small grub screws near the top of the burner. A brass rod was attached to the steel plug and centred in the burner stem by three brass screws. The main object of this arrangement was to conduct heat away from the centre of the burner head.

Preliminary separations of the flame were obtained using a simple quartz tube as described in Section 2.3.1. However, because of the very high temperature of the nitrous oxide-acetylene flame, this soon became opaque and it was replaced with the quartz tube plus side arm shown in Fig. 2-12. The clear silica window at the end of this side arm could be used for long periods without becoming too dirty. It also gave the advantage that the cone and window could be removed to unseparate the flame and could thus be cleaned without extinguishing the flame.

The most important observation made with this flame was that although the background emission due to OH and CO was reduced on separation, the emission from species such as CN and C_2 actually increased. It was realised that this was due to their protection from oxidation by atmospheric oxygen. Thus separation of the flame increased its reducing nature and extended the reducing atmosphere to a much larger region of the flame. This could be seen visually by the intense red CN emission obtained within the separator. In view of this, the flame emission analysis studies were restricted to elements which form refractory oxides in less reducing flames and very good results were obtained for Al, Be, Mo, Ti, V and W.

The main problems encountered with the burner were: the difficulty of lighting the flame with the separator in place; the difficulty of changing from separated to unseparated flames (or vice versa) for comparitive measurements; and reductions in the transparency of the quartz window after the flame had been operating for some time.

The burner shown in Fig. 2-12 was modified by Dr. Hingle so that it could be used for atomic fluorescence studies on a Techtron AA4[89].

This involved removing the brass cooling stem from the centre of the burner head, so that just the short nitrous oxide head could be fitted to the Techtron burner base with an adaptor, and fitting a second side-arm and window to the quartz separator at 90° to the first side-arm. This burner was initially used for the determination of Be by thermal emission and atomic fluorescence spectroscopy[89]. Later, the same instrument/burner combination was applied to an extensive study of the atomic emission spectroscopy of the rare earths[90].

2.4 The Development of Burners for Nitrogen and Argon Separated Flames.

The burners described in this section are placed in the chronological order in which they were envisaged and constructed. This provides a clearer idea of the gradual development which occurred than if they were to be listed in the same way as the results in later chapters. Also, describing all of the burners in this section, rather than individually with the results obtained with them, avoids a great deal of unnecessary duplication. This would result from the use of the same basic burner for several different purposes with only slight modification. Reference to this section will be made frequently in the experimental parts of later chapters.

2.4.1 The original nitrogen separated emission burners.

The initial nitrogen separation experiments were based on a completely standard Unicam (air-acetylene) burner (as supplied with the SP 900). This is made up of a stem (about 12.5 cm long and 1.75cm outside diameter) with a side arm fitted near the base to act as an air inlet. Acetylene is supplied through a fine jet fitted into an anti-blowback valve unit screwed to the base and a Meker-type burner head (about 3cm long and with 13 holes) is screwed into the top.

The first successful separator constructed was simply this burner fitted into a pyrex glass tube about 10cm long and 3cm wide and attached to the burner using a large cork. Nitrogen was added through a single glass side-arm attached to the glass tube just above the cork and some glass beads were placed inside the tube to give a uniform nitrogen flow right around the burner. The secondary zone of the air-acetylene flame was lifted about 2-3cm. above the level of the burner head. However, a rather high nitrogen pressure was required and to avoid this the glass beads were replaced with a special "laminar flow" packing placed near the top of the glass tube. This packing has been used for many years by chemical engineers and physicists requiring laminar gas flows and is simply a tightly wound coil of alternate layers of plain and crimped metal strip. The result is the same as a solid block with hundreds of tiny holes drilled through it and, provided a suitable ratio of diameter to length is chosen, any gas forced through it must exhibit laminar flow. These initial experiments were conducted using stainless steel strip 3/4 inch wide, but better results were later obtained using strips 1 to 1½ inches wide made of a cupro-nickel alloy. This metal was less springy than the stainless steel and allowed much tighter coils to be wound more easily.

Although various angles were tried with the glass side-arm, a really uniform flow of nitrogen could not be obtained and a relatively high pressure was still needed. Also, the glass separators with side-arms were rather fragile and rather difficult to make. All of these problems were overcome with the separator design shown in Fig. 2-13. This uses a 13.5cm long brass tube fitted to the burner stem with a rubber bung. The nitrogen was admitted through four narrow brass pipes spaced evenly around the rubber bung (only two pipes are shown in Fig. 2-12 for clarity). Excellent results were obtained with this separator - with the same nitrogen flow rate as before, practically the whole outer cone of the air-acetylene flame could be made to "disappear". Using the lower, optimum flow rate

(about 10 l./min) the secondary cone could be lifted 5-7cm above the burner head without any difficulty. Further, the flame was much more stable because of the more even and laminar nitrogen flow.

The same basic burner was used for a nitrogen separated nitrous oxide-acetylene flame by replacing the air-acetylene burner head with a special one of our own design. This was essentially the head shown in Fig. 2-12 except that the long piece of brass screwed into the steel centre piece was removed and the lower part of the centre piece turned into a cone shape. It was found that the three grub screws holding the centre piece in position were adequate to remove heat from the centre piece without the extra brass column and screws. The width of the circular slot in the burner head was found to be extremely critical in obtaining a stable, easily separated flame. Good results were obtained with a slot 0.75mm wide and 11mm internal diameter, a nitrogen flow of about 15 l./min. lifting the secondary diffusion zone to a height of approximately 7cm. above the primary zone.

As well as lifting the secondary zone, nitrogen separation also greatly increases the size of the red interconal zone obtained with the slightly fuel rich flame. Replacing nitrogen with argon gives an even larger red zone (see Section 3.3). The effect of separation on the zones of the flame is shown diagramatically in Fig. 2-14.

2.4.2 The shortened nitrogen separators for emission burners.

Although the separator described in Section 2.4.1 worked extremely well, it was found to have two short-comings:-

(a) Its rather large overall height (about 22cm) meant that it could only be used conveniently with a Unicam SP 900. Its use with the Techtron AA4 required the removal of the optical bench of that instrument and supporting the monochromator some distance above bench level.

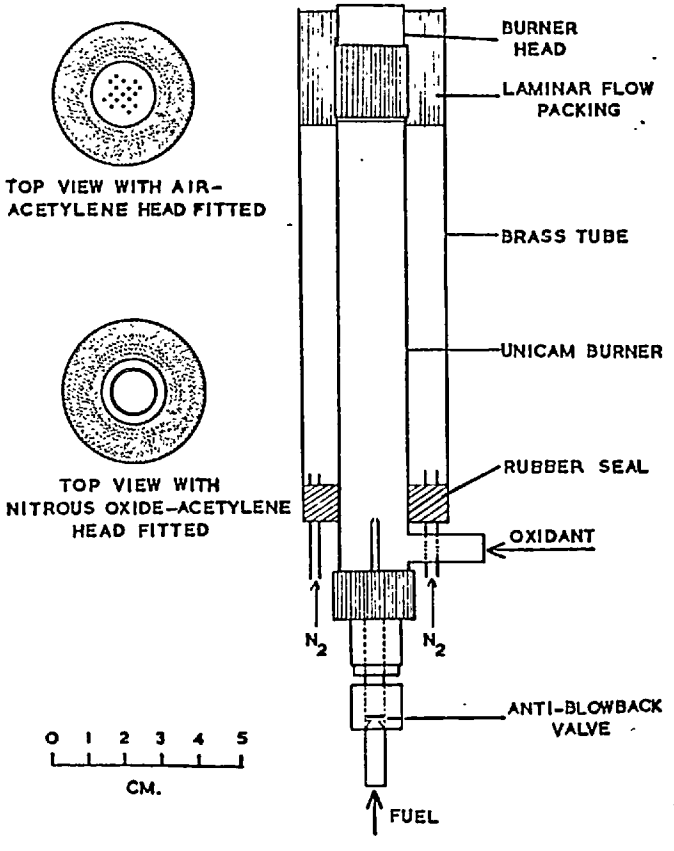
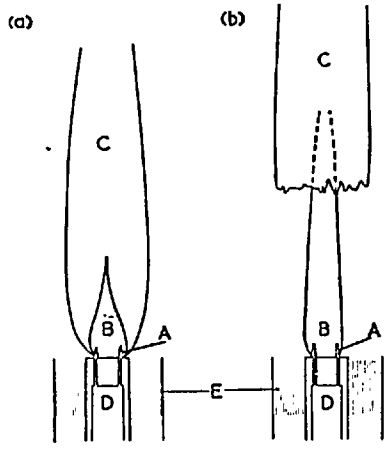


Fig. 2-13 The Original Nitrogen Separator



(a) Conventional flame
(b) Separated flame

A: Primary zone
B: Red (interconal) zone
C: Secondary zone
D: Burner head
E: Laminar flow packing

Fig. 2-14 Effect of Separating Nitrous Oxide - Acetylene Flame

(b) When the separator was used with nitrous oxide-acetylene, both it and the burner head tended to become overheated. This was dangerous (because the hotter the burner, the more likely is a flash-back) and also inconvenient (because the burner slot was found to soot-up more quickly when hot). With the quartz-separated flame this problem was overcome by fitting a water cooling tank around the burner head (see Ref. 89). However, to obtain similar cooling of the burner head with the nitrogen separator (and not just cooling the outside of the separator) would have been impossible without completely redesigning it anyway.

The redesigned separator is shown in Fig. 2-15. It can be seen that the height was reduced to only 3.75cm and that the diameter was increased slightly to 6.25cm to allow an inner brass core to be incorporated. The whole tank was constructed with brass tubing and plates soldered (or braised in later models) together. Winding the packing (D) around the brass core instead of directly round the burner head meant that the separator was independent of the burner and could easily be removed at any time. However, the main purpose of the brass core was that in conjunction with the small water tank at the base of the separator it provided efficient cooling of the burner head. It was found that a small flow of cold water through this tank was sufficient to keep the whole unit cool, even when a nitrous oxide-acetylene flame was burnt for long periods. The sheathing gas was introduced through four pipes (A) as before, but this time they were horizontal rather than vertical (both to reduce the overall height and because of the water tank at the base). The other, minor, modification to the design was the incorporation of three steel pins (E) to support the packing inside the separator. This overcame the problem experienced with the previous design of accidentally pushing the packing in too far when handling the separator.

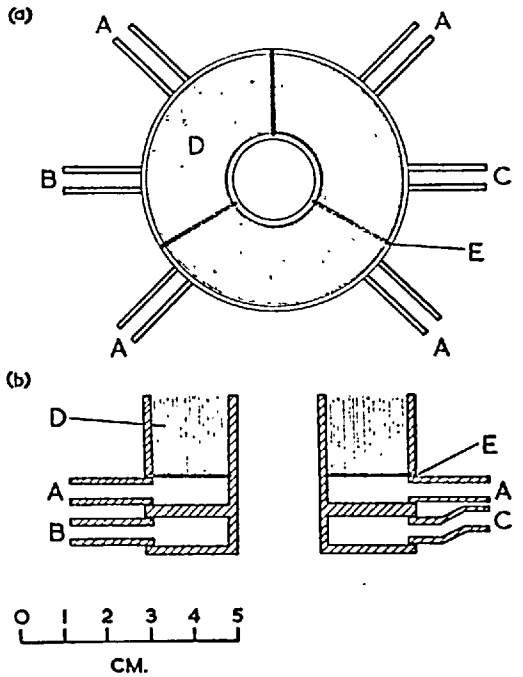
The hole in the centre of the separator was made to give a good

fit around the burner heads and stem used previously. To allow the separator to be used easily with a Techtron AA4 as well, new air-acetylene and nitrous oxide-acetylene burner heads were produced to the same design as before but with the same height as the new separator. Using a small brass adaptor (see Ref. 89), the burner and separator unit could then be plugged directly into the Techtron atomiser/burner unit in place of the standard absorption head.

Although the new design gave adequate separation for most purposes, it only lifted the secondary zone about half the height achieved with the tall separator. This was mainly because of the reduced sheathing gas velocity resulting from introducing it horizontally (it was found that the height of separation depended more on the velocity of the sheathing gas than on its volume, presumably because the higher the velocity the further above the separator the laminar flow persists). Also, even this separation could only be obtained by using a larger volume of nitrogen and the separated flame was slightly less stable. However, a compromise between height and efficiency was essential if a separator was to be fitted directly to a Techtron AA4. It was also considered that water cooling was most desirable for the nitrous oxide-acetylene separator because of the reduction in "sooting-up", so this design was also used with nitrous oxide-acetylene flames on the SP900. However, for air - acetylene flames on this instrument the original design of separator was retained because of its greater efficiency.

2.4.3 The improved nitrous oxide-acetylene burner.

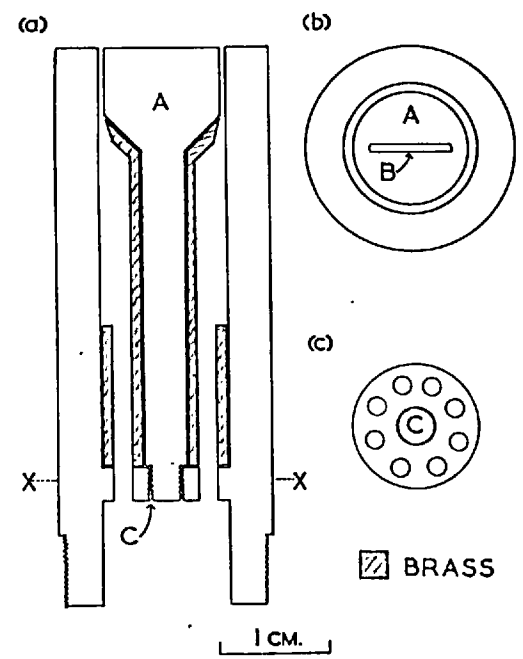
The determination of refractory metals by thermal emission spectroscopy in a separated nitrous oxide-acetylene flame (see Section 4.2) was carried out using a burner of the type described above, i.e. with a small stainless steel centre piece held in position by three 6BA grub screws placed at 120° intervals around



(a) Top view
(b) Side view

A: Nitrogen inlet
B: Cooling water inlet
C: Cooling water outlet
D: Laminar flow packing
E: Steel pin to support packing

Fig. 2-15 The Shortened Nitrogen Separator



(a) Vertical section
(b) Plan view of top
(c) Plan view of section X - X (showing inside only)

A: Stainless steel central core
B: Screwdriver slot
C: Tapped hole for central core

Fig. 2-16 The Improved Nitrous Oxide - Acetylene Burner Head

the rim. During the course of this work it became apparent that the burner, although adequate, had certain practical disadvantages:-

(a) The position of the three grub screws near the top of the burner caused the gas stream at the base of the flame to become turbulent as it passed around them. This resulted in a primary zone divided into three sections and in the infusion of atmospheric oxygen into the red (reducing) zone of the flame. As a result of this the red zone of the unseparated flame was reduced in size and its reducing properties were decreased.

(b) The relatively high temperature of the centre piece of the burner (even when water cooling was employed) meant that the slit was easily "sooted-up" if a rich flame was burnt.

(c) The three grub screws corroded rapidly, making removal of the centre piece difficult. Further, once the burner had been cleaned accurate relocation of the centre piece was also difficult and could take some time to accomplish.

These difficulties were also experienced by Dr. D.N. Hingle during his work on beryllium[89] and the rare earths[90]. A new type of nitrous oxide-acetylene burner head was, therefore, designed jointly[91] and a diagram of the final result is shown in Fig. 2-16. In the new design the centre piece (A) of the burner has a long, narrow spindle tapped (6BA) at the bottom. This allows it to be screwed into a central hole (C) near the base of the burner head. This hole is drilled through a steel insert left when the main burner body is drilled out (see Fig. 2-16 (C). This insert also carries seven other holes so that the fuel gases can flow freely to the flame. The centre piece is held rigidly in position by a brass inset fitting tightly around it and specially shaped to give smooth gas flow (shown shaded in Fig.2-16 (a). Holes are drilled through the base of this brass insert to match those in the steel one below it. The main purpose of the brass insert is to conduct heat from the centre piece to the main body of the burner which

is water cooled (either by a separate water tank or by one incorporated in a nitrogen separation tank). The size of the inner piece was chosen to give a burner slit width of 0.43mm. A screw driver slot (B) cut in the top of the centre piece allows it to be easily unscrewed. A second, smaller, centre piece was also produced giving a slit width of 1.15mm. This allowed a completely stable air-acetylene flame to be supported on the burner and nitrogen separated if desired.

The nitrous oxide-acetylene flame supported on this burner was a considerable improvement on any obtained previously. It was much more stable and regular in structure, with an unbroken primary zone and a much larger red zone when unseparated. This was entirely due to the reduction in turbulence and, hence, the entrainment of atmospheric oxygen. It was found to give an improvement in detection limits over unseparated flames used previously for refractory elements.

2.4.4 Nitrogen separated long path absorption burners.

After the success of the round nitrogen separated burners in flame emission spectroscopy, it was felt that the separation of a long path flame might prove useful in atomic absorption spectroscopy. This is particularly true with the determination of refractory elements in the nitrous oxide-acetylene flame, since the sensitivity is reduced by the influx of atmospheric oxygen along the long, exposed sides of the flame. In view of this the first separator constructed was based on the Techtron 5cm slot nitrous oxide burner. The construction is shown in Fig. 2-17. Two small, brass boxes were cemented on to the large top plate of the burner (using "Araldite" epoxy-resin). Each box had fine copper gauze framing the inside wall and copper nitrogen inlet pipes at each end. It can be seen from Fig. 2-17 that no shielding was provided at the ends of the burner. In use, the device was found to separate the flame to a small extent but also to make it rather unstable. However, in a comparitive test with an unmodified

burner, separation was found to give a useful improvement in aluminium absorption. It was also found that even without the nitrogen turned on a small increase in absorption was obtained, presumably because the presence of the shielding tanks helped to reduce the influx of atmospheric oxygen. This was a major factor in the decision not to proceed with a properly constructed separator of this type, since the ability to switch from a separated flame to a completely conventional flame would have been lost. There were also considerable constructional difficulties.

A much more satisfactory solution to the problem of constructing a burner for long path separated flame was found by adapting the Unicam absorption burners which had been in use in the laboratory for some time. These were based on the same stem as the emission burners but the round head was replaced by a much larger rectangular head (approx. 7.5 x 2cm cross section and 3cm deep). For air-acetylene flames, this was used with the Unicam Meker burner plate with a row of 17 holes 5cm long. For nitrous oxide-acetylene flames, this burner plate was replaced by two stainless steel plates and spacers giving a slot approximately 0.40 x 5cm. Both burners had been tested over a considerable period of time and found to give safe, quiet, stable flames. However, it was felt that if the burners were to be enclosed by shielding tanks, some form of water cooling would be desirable, especially with nitrous oxide-acetylene flames. Since the burners were so large anyway, it was decided to incorporate the water cooling tank with the burner (rather than with the shield as in Section 2.4.2). The first separated burners constructed were based on existing burners and the water cooling was provided by two small brass tanks screwed to the flat base of the burner head on either side of the stem.

A later design incorporating these water tanks inside the steel burner head is shown diagrammatically in Fig. 2-18. This diagram does not show the actual construction of the shielding tank. It is simply a double walled steel box with no top and held together by a base which is welded to the inner box but screwed to the outer box so

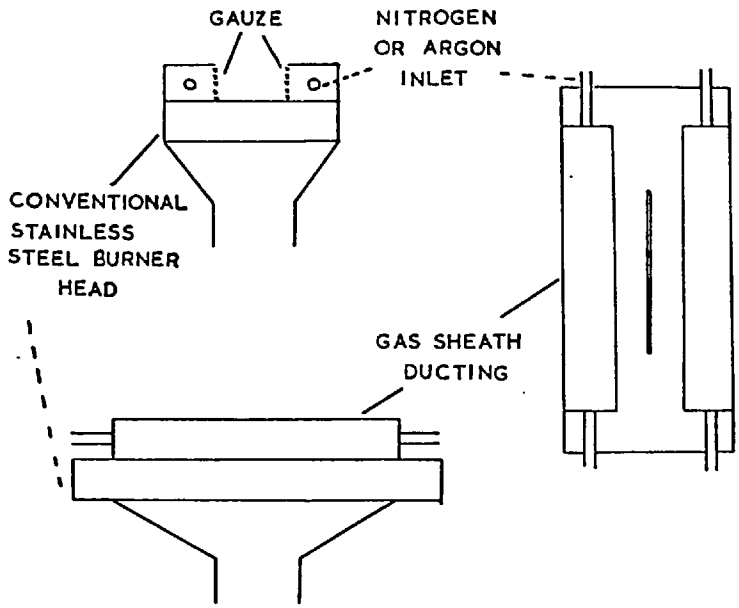
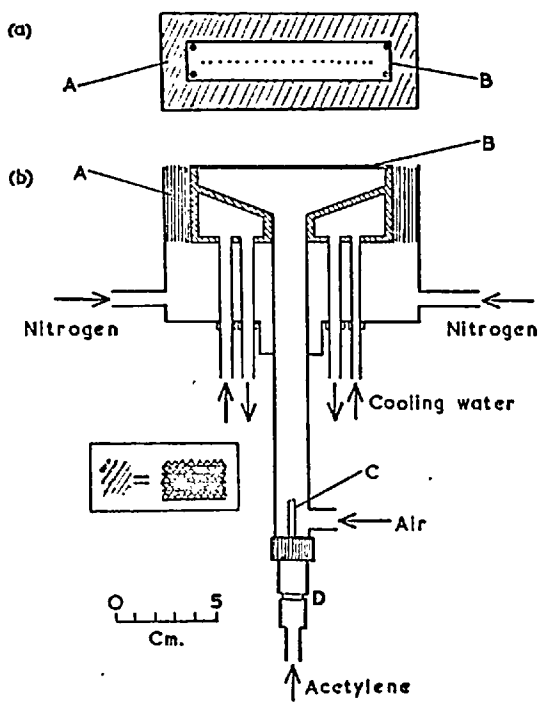


Fig. 2-17 The Nitrogen Separated Techtron Burner



(a) Top view
(b) Vertical cross section

A: Laminar flow packing
B: Removable burner plate
C: Acetylene jet
D: Anti - flashback valve

Fig. 2-18 The First Successful Long Path Separated Burner

that the two can be separated if necessary. This construction was adopted so that the burner could be removed easily from the inner box without disturbing the laminar flow packing. This packing could not be wound as with the round burners and was placed in cut strips along the sides of the boxes. To facilitate this, the front of the outer box was made removable. The large size of the burner and water tanks meant that there was no problem over space and a packing depth of 1.5 inches was used. There was also room to leave a large mixing space beneath the packing and only two nitrogen inlet pipes were necessary. The four pipes for the water cooling tanks were taken out through holes in the base of the separator.

In use, the separator was found to be extremely efficient with both air-acetylene and nitrous oxide-acetylene flames. With the former, the secondary combustion zone could be lifted 5cm with no difficulty using about 20 l./min. of nitrogen. The same flow rate of nitrogen or argon lifted the secondary zone of the nitrous oxide-acetylene flame 3-4cm. above the burner plate and also gave a very large increase in the size of the red interconal zone. A separation of this order has been found to be more than adequate for all atomic absorption purposes. It was also found that the separation was extremely stable with both flames, especially in the region normally used for absorption measurements (up to 2cm above the burner head). Whether used conventionally or separated, the water cooling of the nitrous oxide-acetylene flame was found to give a considerable improvement in its "sooting-up" characteristics, allowing it to be run for long periods of time without attention.

2.5 A Versatile Burner For Flame Shielded Flames.

Many of the advantages of flame separation may be obtained by shielding the flame with an outer flame. Such a device is also necessary for fundamental studies on flames. Usually the burner is

arranged so that solutions are nebulized only into the centre flame. Any emission observed will then originate from an area of uniform temperature. This allows the temperature of the centre of the flame to be accurately measured by the two line, line reversal, etc. techniques. It also prevents self-reversal of spectral lines and this type of burner is almost always used for high resolution studies of spectral lines emitted by flames. In view of the interest in this work of protecting the inner zones of flames; of measuring flame temperatures; and of using a Fabry-Perot interferometer to study spectral lines, the construction of a flame shielded burner seemed most desirable.

The construction of the burner is shown diagrammatically in Fig. 2-19. It is a rather complicated design but the burner was intended for purely experimental purposes and it was desirable to make it as versatile as possible. The inner burner is very closely based on the designs described in previous sections; the burner stem and the acetylene inlet/anti-flashback valve are copied from the standard Unicam SP900 burner. The inner burner head is very similar to that described in Section 2.4.3 but a number of improvements were incorporated. The outside diameter of the burner slot was increased to 0.600" (15.23mm) to give a larger flame area. Interchangeable centre-pieces were used to vary the slit width so that different gas mixtures could be used with the same burner. The initial order specified centre pieces giving slit widths of 0.017" (0.43mm) for nitrous oxide-acetylene, 0.035" (0.89mm) for air-hydrogen flames, and 0.054" (1.37mm) for air-acetylene flames. The different slit widths gave stable flames with all gas mixtures used but care was needed to select the correct centre piece on each occasion.

The design of the outer burner for the flame shield presented more problems. In order to encompass the inner burner it must obviously cover a large area but the total area of the actual burner ports must be small enough to prevent flashback. It was also nccessary to leave space for a water cooling tank, which the author

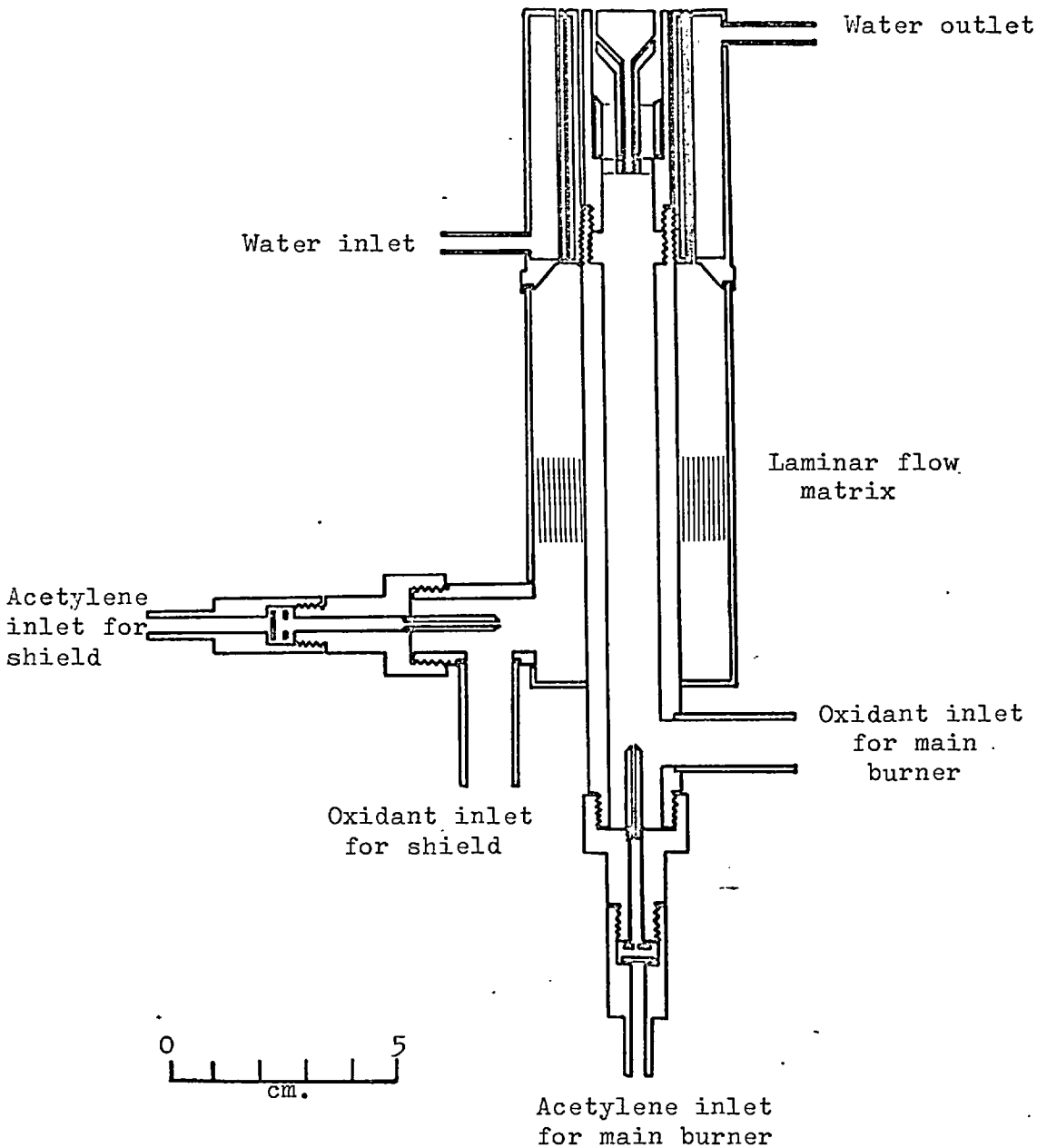


Fig. 2-19 A Burner For Flame Shielded Flames

has found essential for use with fuel rich nitrous oxide-acetylene flames. In view of this, a design using steel capillary tubes was chosen. As shown in Fig. 2-19 these are mounted in a brass tank which fits around the inner burner head. In use the tank is filled with water which therefore serves to cool both the inner burner and the capillary tubes of the shielding flame. Two inch long (50.7mm) capillary tubes were used as this allowed the brass tank to be the same height as the inner burner head. It was intended to burn nitrous oxide or even oxygen flames on the outer burner so the area of the capillary tubes needed to be kept fairly small (even though the quenching capacity of a two inch long, water-cooled capillary tube is very high). After some calculation it was decided to use 110 capillary tubes with an inside diameter of 0.017" (0.43mm). These were arranged on two concentric circles of 1.050" (26.00mm) and 1.130" (28.65mm) diameter respectively. 55 tubes were placed on the inner row at a centre-to-centre distance of 0.060" (0.152mm) and 55 on the outer row at a distance of 0.0646" (0.164mm).

The brass tank forming the outer burner head was screwed into place using a thread on the outside of the inner burner stem. It then formed a gas-tight seal with a brass tube braised on to the inner burner stem. This tube acted as a premixing space for the gases producing the outer flame. To ensure uniform mixing and distribution of the gases, a laminar flow matrix of the type used for flame separation (see Section 2.4.1) was placed near the base. Gases were passed into the outer tube using standard Unicam-type inlets of the same type as on the inner burner stem (see Fig. 2-19). The outer flame shield worked well, especially with the nitrous oxide-acetylene mixture. Use of slightly wider capillary tubes would probably have given better stability with slow burning flames (such as fuel rich air-acetylene) without any lowering of safety standards.

Chapter III

The Effect of Separation On Flame Background and Temperature

The effects of separation on the structure and physical appearance of the flame and on its utility in analytical chemistry have been discussed in general, qualitative terms in Chapter 2. It is now proposed to describe in detail the changes in the emission and absorption spectra of the flame gases produced by separation. The flame temperatures have also been measured, since their knowledge is important if a correct interpretation of the changes in the spectra is to be obtained.

3.1 The Effect of Changing Flame Shape and Instrumental Characteristics.

Since two different flame shapes and two different types of instrument have been used, it is necessary to discuss briefly the differing effects they have on the background radiation received from the flame and the way in which it changes on separation of the flame.

First, the shape of the flame. This has a relatively small effect on the phenomena to be discussed in this chapter and is certainly much less important than the type of instrument chosen. The most noticeable effect of changing from a circular flame to a long flat one is the resulting increase in path length. This gives much greater self absorption of species present in the flame in high concentrations. An example of this is the change in the relative intensities of the CN bands discussed in Section 3.6. It should also be noted that with the nitrous oxide-acetylene flame there is a much greater increase of path length for species present in the red zone when the circular flame is separated than with the flat one.

Conversely, when the circular flames are separated, there is a much greater drop in the CO and OH emission than is observed with the flat flames, since the thickness of the secondary zone at the ends if the flat flame is very small (this effect is even more noticeable if the optical system is such that only a small area of the flame is observed).

The only other effects of flame shape which need concern us are those of entrainment of air and flame temperature. It seems likely that the flat flame allows more air to reach the centre of the flame than does the circular one. This effect is particularly important with the nitrous oxide-acetylene flame which is used for its highly reducing atmosphere. Probably, in the conventional flames more CN, CH, etc. are present in the circular flame than the flat one for a given fuel: oxidant ratio (this should not be the case in the separated flames, where the species are protected from the surrounding air). The extra air (or nitrogen/argon) entrainment, together with the flame shape itself, probably also results in the flat flames having a lower temperature than the circular ones. This would also result in slightly different background radiation from the two types of flames.

The type of instrument used to make measurements can have a profound effect on the background radiation observed from the flame and the way in which it changes on separation. It is important to understand these limitations if the observations reported in this chapter are to be interpreted correctly. Leaving aside the conventional spectrograph, two basic types of instrument are used in analytical flame spectrophotometry. These are represented in this work by:

a) The Unicam SP900A flame spectrophotometer. This type of instrument is now beginning to disappear from the manufacturers' catalogues; it is designed for emission spectroscopy and therefore has a prism monochromator of fairly low resolution but good light gathering power and an optical system without lenses so that light is received from the whole

area of the flame. It is intended to be used with a small circular burner.

b) The Techtron AA4 atomic absorption spectrophotometer. This type of instrument is now the most popular for all types of flame spectroscopy and a far larger range is on the market than was ever available with the old flame (spectro-)photometers. Almost all of them use a grating monochromator of good resolution but relatively poor light gathering power (often due to the small maximum slit width). Generally, the optical system incorporates lenses and is designed for an image of a long flat flame to be focussed on to the monochromator slit.

For our purposes, the differences between these two groups of instruments can be summarized into two factors.

(i) Using a monochromator of higher resolution results in a completely different appearance for many of the molecular bands obtained frome the flame species and, in most cases, alters the readings obtained for the relative intensities of the various peaks. This is illustrated in Fig. 3-1 with the spectrum of the C_2 4737 Å Swan band emitted by a nitrous oxide-acetylene flame. Spectrum a) was obtained with the Unicam SP900A and b) with the Techtron AA4. It can be seen that a much more accurate reading of the intensity of, say, the 4737.1Å peak can be obtained with the high resolution monochromator. This is true whether you want to measure the absolute intensity of the peak or its intensity relative to the immediate background. (in this case, the CO continuum). Thus when studying a list of peak intensities or a printed spectrum, it is important to note the type of monochromator used as well as the flame.

(ii) When an instrument such as the Unicam SP900A is used with the conventional flames, background radiation is received from the whole area of the flame. This means that when the secondary zone is lifted out of the optical path by flame separation there

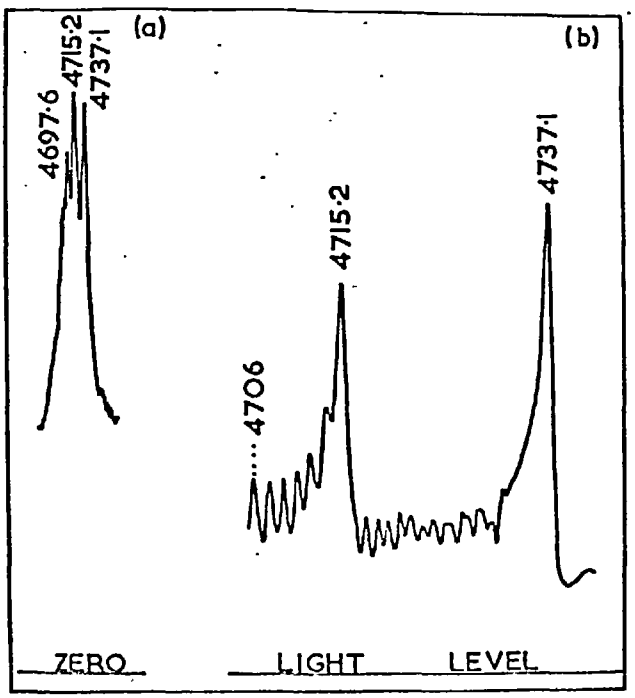


Fig. 3-1 C_2 4737.1A Band : (a) With a Unicam SP900A, (b) With a Techtron AA4

is a very large drop in the amount of OH and CO radiation received. On the other hand, with the nitrous oxide-acetylene flame, the instrument is capable of receiving all of the radiation from the considerably enlarged red zone obtained on separating the flame. Thus there is a considerable increase in the signal from CN, CH, C_2, etc. which are present in the interconal zone. With the more sophisticated optical systems used in instruments such as the Techtron AA4, radiation is received only from a small area of the flame, usually near the centre. Thus, these changes are much less marked, particularly when a flat flame is used with the optical path along the centre of the interconal zone.

3.2 The Background Emission Spectrum of the Air-Acetylene Flame.

The spectra of the conventional and nitrogen separated flames are shown in Fig. 3-2. They were recorded using the circular burner and separator described in Section 2.4.1 and a Unicam SP900A spectrophotometer and ancillary apparatus described in Section 4.1.2.

With the conventional flame, only two features may be distinguished. These are the continuum due to the reaction $CO + O \rightarrow CO_2 + h\nu$ and OH bands with heads at 2811Å and 3064Å. It may be seen that between them they result in a strong background radiation over the whole of the visible and near ultraviolet regions of the spectrum. This emission is particularly intense at the head of the second OH band, between 3064Å and about 3100Å. The radiation due to CO and OH is so intense over the whole region studied that emission cannot be detected from other species present in the flame. Fortunately, most of the CO and OH emission originates from the secondary combustion zone of the flame. Thus, when the flame is separated only a very small amount of CO and OH radiation is observed from the interconal zone. However, the other species present in the flame have much higher concentrations within the interconal zone. Therefore, in the separated flame it is possible to identify a number of C_2 and CH bands which were previously obscured by the CO continuum. This is shown by the second spectrum in Fig. 3-2.

It is important to note that the changes in intensity which occur with the various band systems on separation depend on the air: acetylene ratio selected. The effect of acetylene flow-rate on the OH emission from the nitrogen separated flame at 3068Å is shown in Fig. 4-2(a). It may be seen that the intensity increases rapidly as the mixture is made more fuel lean. The change with fuel flow in the conventional flame is much less rapid. Thus, a greater reduction in OH emission intensity is obtained on separating a stoichiometric flame than a lean one.

As mentioned earlier, the background radiation measured using

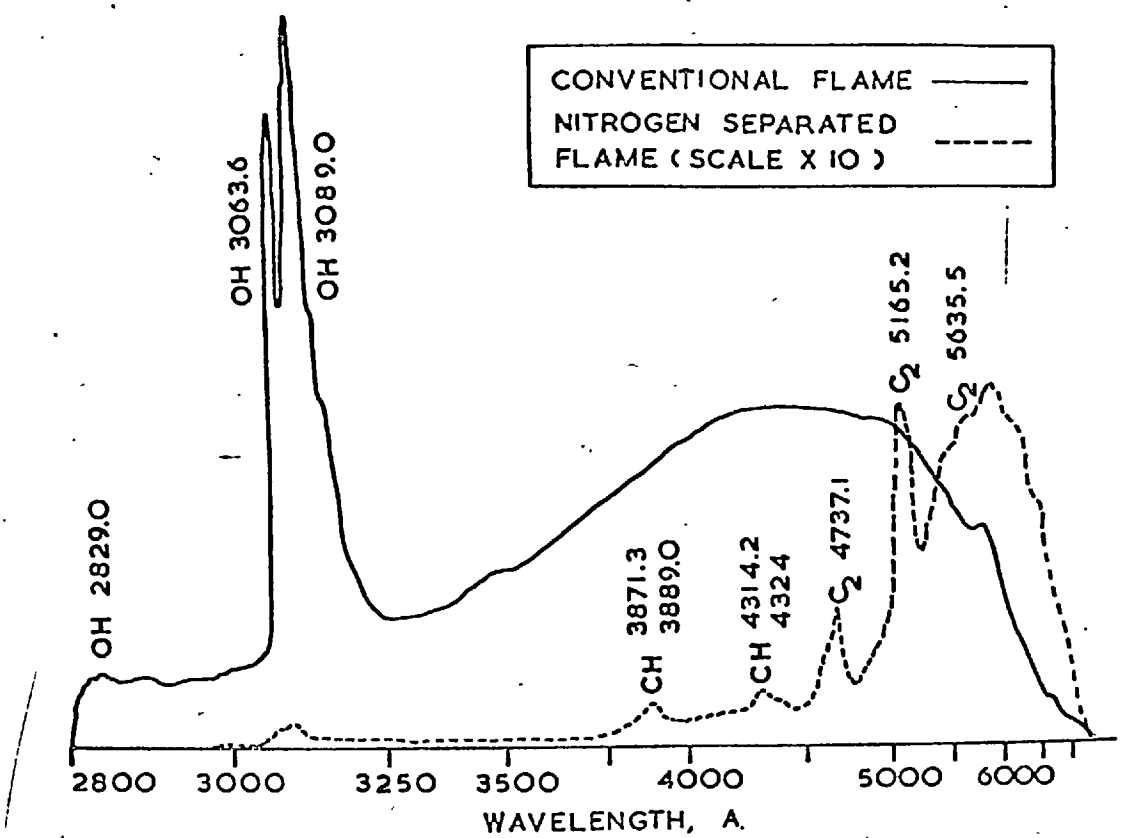


Fig. 3-2 Effect of Separation on Background Spectrum of The Air - Acetylene Flame

an instrument such as the Techtron AA4 is somewhat different. The biggest difference is the much smaller drop in OH and CO radiation observed on separating the flame. It is also easier to distinguish the CH and C_2 bands emitted by the interconal zone from the radiation from the secondary zone.

3.3 The Background Emission Spectrum of the Nitrous Oxide-Acetylene Flame.

The background spectrum of the nitrous oxide-acetylene flame is far more complicated than that of air-acetylene and a simple scan such

as that shown in Fig. 3-2 would not be very helpful. This is because the variations in intensity between the different bands make it very difficult to show them all clearly on a single diagram. Instead, the information is presented in the form of tables of wavelengths and intensities.

The main features of the background emission spectrum from the conventional and separated slightly fuel-rich nitrous oxide-acetylene flames burning on the circular slot burner and observed with a Unicam SP900A are listed in Table 3-1. All of the intensities were measured as the absolute peak heights above zero light level. In view of this, some of the values include contributions from species other than the main one indicated in column two. The measurements were made with radiation from the primary zone excluded, so that the species contributing most to this "overall" background level is CO.

The most noticeable differences from the air-acetylene flame are the presence of intense emission from CN and NH, and the increase in intensity is obviously partly due to the higher flame temperature, but also indicates the absence of atomic oxygen in the interconal zone of the slightly rich flame. As with air-acetylene, the other species making major contributions to the flame background are the OH and CO present in the secondary zone.

In the argon- or nitrogen- shielded flame, the background emission from OH and CO is suppressed due to the separation of the secondary zone, just as with the air-acetylene flame. A slight reduction in the CH emission intensity is also observed on shielding, whereas the CN and C_2 background emission is considerably increased. These results agree with the visual observation (Section 2.4.1) of the "lifting-off" of the secondary oxidising mantle and also the extension and protection of the reducing atmosphere of the interconal zone which is achieved on separation. The background emission from all species is greater in the argon-shielded flame than in the nitrogen-shielded flame. This is partly because nitrogen cools the flame more than argon, owing to their different thermal capacities (see Section 4.2), and

Table 3-1

Wavelength, nm	Emitting species	Type of emission	Overall relative intensity in unshielded flame*	Relative intensities of lines in the three flames		
				No shield	Argon shield	Nitrogen shield
665·66	CN	Red system	2·5	100	382	147
650·23	CN	Red system	5·5	100	351	162
635·51	CN	Red system	9·5	100	346	185
619·12	C_2	Swan band	11	100	360	192
601·25	CN	Red system	14	100	270	160
587·76	CN	Red system	39	100	233	110
574·87	CN	Red system	27	100	422	198
563·55	C_2	Swan band	28	100	420	187
549·02	CN	Red system	30	100	231	119
536·50	CN	Red system	30	100	231	122
525·49	CN	Red system	29	100	219	132
516·52	C_2	Swan band	63	100	335	134
473·71	C_2	Swan band	170	100	122	69
460·61	CN	Violet band	160	100	141	72·5
444·0	CO	Continuum	105	100	57	35
436·52	C_2	Swan band	160	100	74	53
431·42	CH		220	100	84	35·5
425·0	CO	Continuum	110	100	64·6	38·5
422·5	CO	Continuum	110	100	83·3	42·1
421·60	— CN	Violet system	1320	100	253	85·5
419·72	CN	Violet system	1080	†		
418·10	CN	Violet system	742	†		
416·78	CN	Violet system	512	†		
388·34	CN	Violet system	10000	100	268	102·3
387·14	CN	Violet system	5710	†		
386·19	CN	Violet system	3905	†		
359·04	CN	Violet system	1050	100	377	117
358·59	CN	Violet system	1020	†		
358·39	CN	Violet system		†		
343·5	CO	Continuum	92	100	28	12·7
336·00	NH		400	100	8·3	5·3
314·34	CH		‡	‡	100	82·3
308·90	OH	Band peak	6050	25000§	100	76
306·36	OH	Band head	5900		100	73
289·27	OH + NO	Partly β-NO system	380	100	7	5·1
282·90	OH	Band peak	510	100	4·5	3·0

* These values have *not* been corrected for the variation of instrumental sensitivity with wavelength.
† Relative intensities are not given for these peaks because they are the same as those quoted for the corresponding band-head.
‡ This peak could not be measured in the unshielded flame because of interference from the intense OH emission; in the argon-shielded flame the intensity ratio $CH_{314\cdot3} : OH_{306\cdot4} = 100:61$ was measured.
§ The reduction on shielding is so enormous at this wavelength that this value for the relative emission from the unshielded flame can only be an approximate estimate.

it is also possible that diatomic nitrogen molecules have a greater quenching effect on emission excitation than monatomic argon. However, the interconal zone is much larger in the argon-shielded flame than the nitrogen-shielded one with a circular burner so that instrument was able to receive radiation from a larger area. It seems likely that this is due to argon disturbing the flame gases less than nitrogen and thus entraining even less atmospheric oxygen.

This change in the size of the interconal zone between the different flames makes it considerably more difficult to interpret the results in Table 3-1. In border-line cases where the change in emission intensity on shielding is relatively small, it is difficult to separate the effect of the temperature reduction known to occur on shielding from actual changes in the number of emitting species

observed (either due to actual changes in concentration, or to changes in the volume of flame in which they may be observed). This results in several species in Table 3-1 giving apparently anomalous results. For example, all of the C_2 (Swan) bands show an increase in emission intensity on argon-shielding, except that with the shortest wavelength (4365.2Å) which shows a decrease. Since the effect of a temperature drop on emission intensity is greater at shorter wavelengths, it is reasonable to assume that this example is a case of the temperature effect predominating. An effect of this type might explain why the CH emission at 4314Å decreases on shielding (when it would be expected to increase in the same way as C_2 and CN), and why certain of the CN peaks show an increase in intensity with argon-shielding but a decrease with nitrogen shielding.

The additional results given in Table 3-2 should help to make the relative importance of these different factors more clear. Both sets of results give the heights of the peaks above the immediate background level for all species except OH and CO. These values are given as heights above the zero light level measured with the shutter shut (as in Table 3-1) because there is no other discernable background at those wavelengths. The two sets of results in Table 3-2 represent the two extremes discussed earlier; i.e. radiation received from the whole area of the flame with large changes in size on shielding the flame, and radiation received mainly from the very centre of the interconal zone with no significant changes in the size. It may be seen that the magnitude of the changes occurring on shielding is considerably reduced in the latter case, proving that a large part of the changes recorded in Table 3-1 results from variations in the volume of the flame being observed.

First, the reduction in intensity of OH and CO emission on shielding is much less marked in the flat flame. This is because there is only a tiny length of secondary zone at the end of the flame and the detector mainly views the centre of the flame along its axis. Secondly, the emission intensities of CN and C_2 which showed large

Table 3-2

Wavelength (Å)	Species	Relative Emission With Circ. Flame/Unicam SP900A			Relative Emission With Flat Flame/Techtron AA4		
		No Shield	Argon Shield	Nitrogen Shield	No Shield	Argon Shield	Nitrogen Shield
5877.6	CN	100	164	54			
4606.1	CN	100	275	136	100	129	100
4216.0	CN	100	277	91	100	124	86
3883.4	CN	100	268	102	100	113	82
3590.4	CN	100	430	132	100	186	100
5635.5	C_2	100	684	189	100	133	87
5165.2	C_2	100	366	116	100	160	82
4737.1	C_2	100	170	100	100	125	83
4365.2	C_2	100	92	95	100	54	35
4314.2	CH	100	82	27	100	28	17
3143.4	CH	-	100	96	100 -	34 100	31 90
3360.0	NH	100	4.2	3.9	100	1.8	1.3
3089.0	OH	25000	100	76	100	16	11
2829.0	OH	100	4.5	3.0	100	16	10
~ 4440	CO	100	57	35	100	105	64
~ 4225	CO	100	83.3	42.1	100	93	62
~ 3435	CO	100	28	12.7	100	48	30

increases on shielding the circular flame now show much smaller increases on argon shielding and usually decreases on nitrogen shielding. This is consistent with an increase in population and a

decrease in temperature, the latter effect predominating on nitrogen shielding, plus the fact that the area of flame seen by the detector no longer increases on shielding. Finally, the CH and NH emission show a much larger decrease on shielding the flat flame. This is because these species are found in the centre of the flame (like CN and C_2) so that without the effect of an increased flame size on shielding the temperature decrease becomes more noticeable. These results also suggest that there is no increase in the actual concentration of CH and NH, or else it is only small.

To help in the interpetation of these results, the effect of changing the acetylene flow rate on the emission from the main flame species was measured. The results are given graphically in Fig. 3-3. They were measured using the circular slot burner with a nitrous oxide flow rate of 4.0 l./min. and the Unicam SP900A, as before. Measurements were made so that only radiation from the interconal zone (and the surrounding secondary zone with the conventional flame) was received by the monochromator entrance slit. The sensitivity of the instrument was adjusted for each curve so that the maximum emission recorded on it gave full scale deflection of the meter. Thus the curves show only the relative behaviour in the three flames. The shapes of the curves and the positions of the peaks are the important points illustrated showing the net effect of change in flame temperature and in concentration of emitting species as the fuel flow changes.

The argon- and nitrogen- shielded flames produce curves almost identical in shape, confirming that the greater emission intensity obtained with argon is mainly a physical effect (since all species are affected in the smae way). For CN, C_2, CO and CH the curves for the shielded and unshielded flames are very similar except for the degree of fuel-richness at which certain features occur. Each of these species contains carbon, of which there is an increasing abundance as the flame is made more fuel-rich, so shielding of the flame mainly results in slightly less fuel-rich conditions being required to obtain the same emission (since shielding protects the

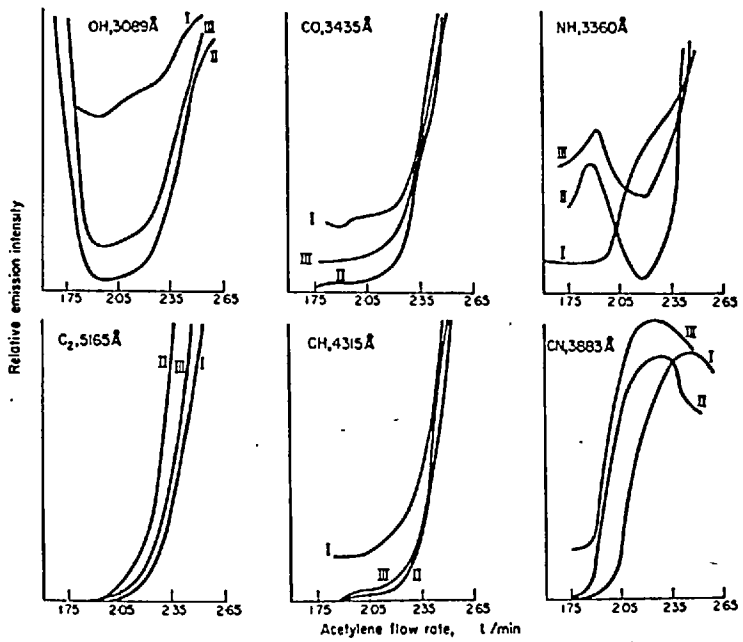


Fig. 3-3 Effect of fuel flow-rate on relative emission intensity from the flame species in the nitrous oxide–acetylene flame.
I = Unshielded flame.
II = Nitrogen-shielded flame.
III = Argon-shielded flame.

---

reducing atmosphere from oxygen in the surrounding air), cf. results for CN and C_2. However, with OH and NH emission, shielding the flame produces a curve of completely different shape. It is significant that these are the only two important species in the flame that do not contain carbon. The minimum in the OH curve for the unshielded flame becomes a very sharp trough on shielding.

It is possible that the trough arises from the OH emission from the inner cone of the flame (i.e. from the OH formed by primary combustion) and in the ordinary flame this is masked by the much greater quantity of OH formed by secondary combustion at the outside of the flame. However, it is less satisfactory to apply such

a simple explanation to the NH curves. Reference to Table 3-2 shows that shielding with the flat flame/Techtron AA4 produces a greater reduction in NH emission than shielding with the circular flame/ Unicam SP900A. It is, therefore, unlikely that a sufficiently large portion of the NH emission originates from the secondary zone for the above explanation to hold for NH. Further, a very interesting result is obtained if the NH and CN curves from Fig. 3-3 are redrawn so as to show the two curves for each flame alongside each other. This is done in Fig. 3-4. It may be seen that in the unshielded flame the CN and NH emission increase together from an acetylene flow rate of about 2.0l./min. upwards. As the CN emission starts to level off and then decrease (from about 2.2 l./min.) the NH emission starts to rise quite steeply (even though the fuel-rich flame is cooler). This strongly suggests a link between the fall in the CN signal and the rise in the NH. The graphs for the two shielded flames, which are almost identical, illustrate this point even more clearly. The most noticeable feature is that the NH maximum at around 1.9 l./min. almost exactly coincides with the CN minimum and the NH minimum at about 2.2 l./min. coincides with the CN maximum. Further, a sharp fall in NH emission coincides with a sharp rise in CN, and vice versa.

This would seem to be almost conclusive proof that the CN and NH populations are rigidly linked; i.e. in the shielded flame with constant nitrous oxide flow rate, there is a given amount of atomic N available (from the N_2O) and if we make conditions more favourable for CN formation, the extra N needed must be obtained by dissocation of some of the NH (or possibly by its not being formed in the first place). The nitrogen used for sheathing is unlikely to take any part in this equilibrium because of its high dissociation energy (9.76 eV), and this is in agreement with the fact that argon gives exactly the same shaped curves.

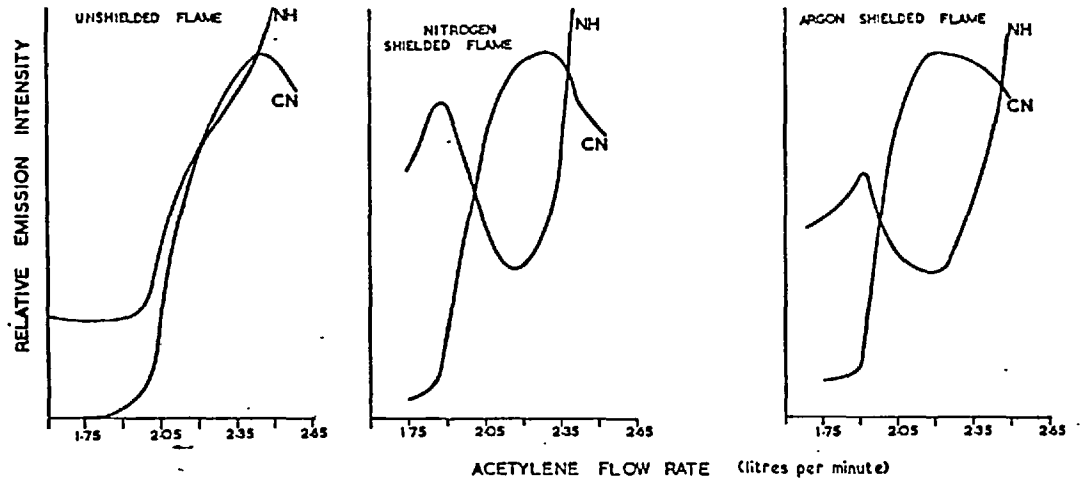


Fig. 3-4 Effect of Fuel Flow on CN and NH Emission

3.4 The Background Absorption Spectrum of The Nitrous Oxide-Acetylene Flame

Although the emission results quoted above had proved extremely useful in interpreting the equilibria of the nitrous oxide-acetylene flame, there still remained some doubt as to how faithfully the radiation emitted by each species reflected changes in the concentration of that species. A more satisfactory criterion of the concentration changes is provided by absorption measurements. These have been made for CN and OH, no absorption being detectable for the other species.

The absorption measurements were made using a 150 watt xenon arc lamp as the background light source, together with the Techtron AA4 spectrophotometer. The circular emission burner used previously was used as the absorption cell. (It would have been desirable to make some comparison measurements with the flat flame, but the long path shielded burner had not been constructed when this work was done, and subsequently a xenon arc was not available). The light beam from the xenon arc was modulated at 285 cps using the standard Techtron

emission chopper and then focussed through the flame on to a pinhole placed on the far side of the flame. Another lens was used to focus the light from the pinhole on to the monochromator entrance slit. This arrangement was used so that the radiation reaching the detector from the flame itself was kept to a minimum; even though it is unmodulated, the CN emission from the flame is so intense that without this arrangement it gives a large, noisy signal. The light beam was adjusted in size so that it was about 2mm square on the side where it entered the flame and 1mm square where it left it. The same nitrous oxide flow rate was used as for the emission results (4.0 l./min).

The absorption spectrum of the CN 3883Å band is shown in Fig. 3-5 for each of the three flames. Only the first part of the band with the four main vibrational peaks is illustrated; the rotational fine structure continues for some time on the violet side of the band but is of no interest. These spectra were obtained from a region of the flame 2mm above the burner, with the acetylene flow rate of 2.15 l./min. (approximately the "best red zone"). It can be seen that the absorption does increase on separating the flame, but this is due to the increased path length as well as to any increase in CN concentration.

The effect of acetylene flow rate of the CN absorbance is shown graphically in Fig. 3-6 at three different heights above the burner. It may be seen that the shapes of the curves are very similar to those previously obtained for CN emission. This would suggest that the CN emission is a good indicator of CN concentration and that the CN emission is largely thermal in origin within the red interconal zone (although some chemiluminescence cannot be ruled out in the region immediately above the primary zone where no measurements have been made). Unlike the emission results, the absorbance values are absolute quantities so that direct comparisons may be made between the three graphs and all the different curves. The difference in absorption recorded between the nitrogen and argon

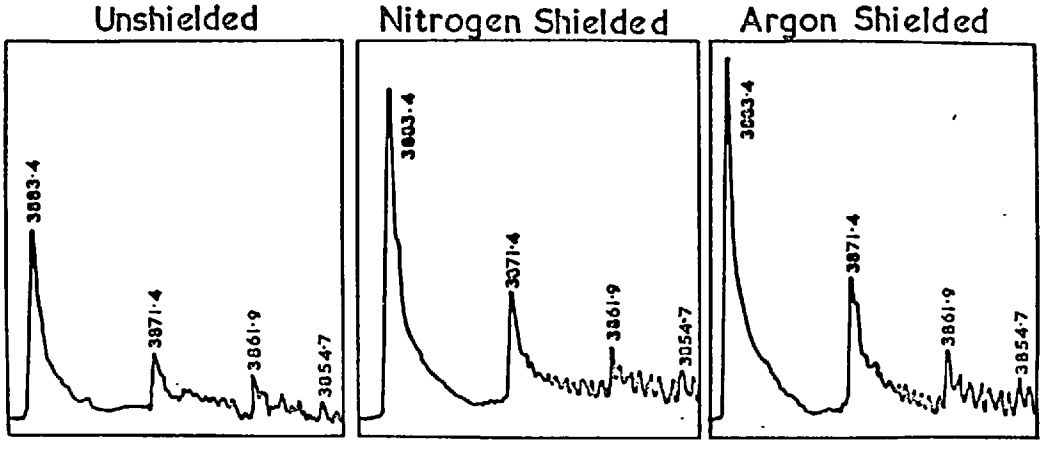


Fig. 3-5 Absorption Spectrum of CN 3883Å Band In The Nitrous Oxide - Acetylene Flame

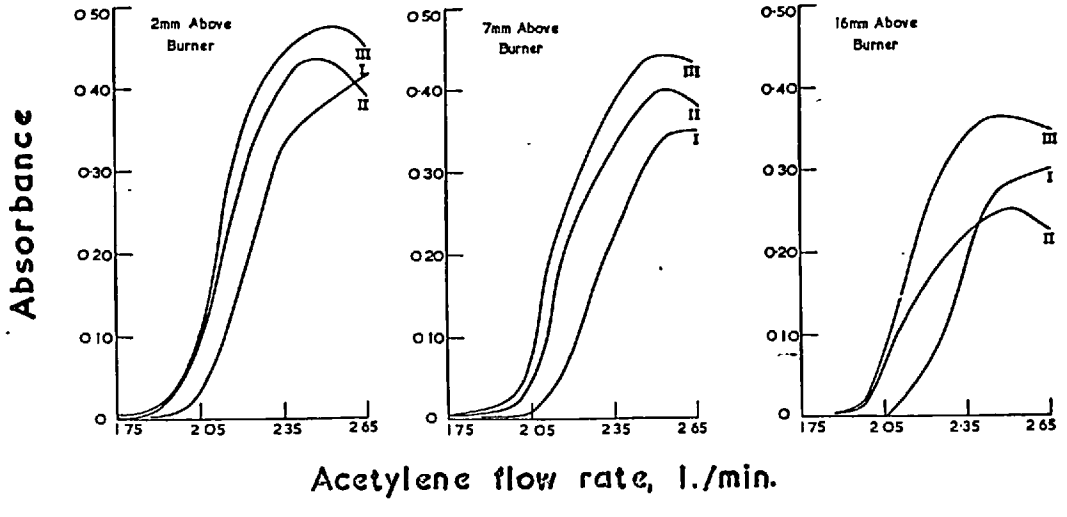


Fig. 3-6 Effect of Fuel Flow on CN Absorbance at 3883.4Å

shielded flames is probably largely one of path length. This is born out by the fact that the difference is quite small at 2mm and 7mm above the burner but becomes quite large at 16mm; the argon

shielded flame retains a cylindrical red zone for some distance above the burner, but in the nitrogen shielded flame the red zone has a distinctly conical shape. The conventional flame generally gives a much smaller CN absorption than the two separated ones, except at high fuel flows. However, at 16mm above the burner the absorbance from the conventional flame at high fuel flows is considerably larger than that from the nitrogen shielded flame.

The OH absorbance from the nitrous oxide-acetylene flame is much smaller than that from CN, and a measurable amount of absorption could only be obtained with the unseparated flame. The effect of acetylene flow rate on the absorbance at 3089Å in this flame is shown in Fig. 3-7. The most important feature of this curve is that it is quite different from the corresponding emission one in Fig. 3-3. Over most of the range studied, the absorbance decreases with increasing fuel flow whereas the emission increases. It is very difficult to explain this other than by assuming that a large portion of the OH emission is chemiluminescent in origin. This would also account for the intense OH emission from the conventional flame when the absorption can only just be measured. The concentration of OH would be expected to drop as the fuel flow is increased (since the disoocation energy of OH is much lower than that of species such as CN and CO) and this is in agreement with the absorption result. We must, therefore, look for a chemiluminescent reaction involving a carbon-containing species as the most likely way to account for the increase in emission intensity. Gaydon has suggested (Ref. 20, p.195) that the most likely reaction of this type in the reaction zone of oxy-acetylene flames is

$$CH + O_2 \rightarrow CO + OH^*.$$

Although it is by no means certain that this provides the complete answer in the present case, it is interesting to refer again to Fig.3-3. The OH emission from the two separated flames starts to rise steeply at the same fuel flows as that at which a sharp increase is obtained from the emission of all of the carbon containing species. Prior to

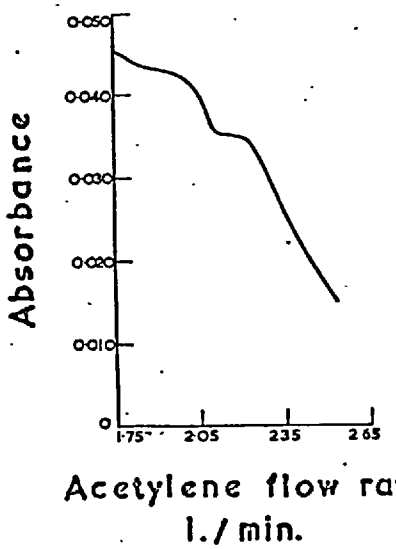


Fig. 3-7

Effect of Fuel Flow on OH Absorbance at 3089A In The Conventional Air - Acetylene Flame

this, the OH emission had been falling steeply, as expected if the OH concentration decreases with increasing fuel flow. Probably the much slower change in the conventional flame is due to the fact that the detector is receiving a large amount of thermal OH radiation from the secondary zone as well as any chemiluminescent emission.

3.5 Flame Temperature Determinations By The "Iron-Two-Line Method"[92]

3.5.1 Introduction

The problems associated with flame temperature determination have been outlined in Section 1.4.5, together with the most important methods. If a method applicable to a wide range of flames is required, these techniques must be applied to the atomic spectra of elements added to the flame. The sodium line-reversal method is the most popular in this respect and is capable of giving accurate results for medium temperature flames. Unfortunately at higher

temperatures (2800°K or above) the selection and calibration of a suitable background source becomes difficult. It is also difficult to obtain spacial resolution good enough for flame temperature profiles unless a spectrograph or scanning monochromator is used to detect the reversal point, but the determination of the reversal point then becomes rather tedious.

In view of these difficulties, the author several years ago investigated a method involving the use of equation 1-14 with the relative intensities of pairs of iron lines[93, 94]. This provides an electronic excitation temperature which should be identical to that obtained by the line reversal method but requires no background light source and only a conventional spectrograph or monochromator to make measurements. However, if it is to be used as a general method over a wide range of temperatures, the element chosen must emit a complex spectrum with a large number of lines whose relative transition probabilities are known with good accuracy. At that time, the only logical choice from this point of view was to use iron. Since then, the publication by the National Bureau of Standards of an extensive list of oscillator strengths and transition probabilities for iron[95] has made this choice even more satisfactory. The NBS values were derived from a critical evaluation of the data available in the literature and probably form the best single set for a large number of spectral lines to be published to date. Iron also shows a number of other desirable features for two-line temperature measurements in flames. Many of the lines have sufficiently low excitation energy to be detectable even in cool flames; a high population of free atoms is obtained in the flame as iron does not form thermally stable oxides extensively even in moderate temperature flames; and the ionisation potential of iron is 7.9 e.V. so that the degree of ionisation is insignificant in most flames.

In spite of this, there is still a serious difficulty in using the method with flames. Any self-absorption of the iron lines may lead to large errors in the intensity ratio and hence in the

measured temperature. As a result of this, the method has been applied in the past mainly to plasma sources which are optically thin (i.e. give low absorption) with respect to many useful lines (see, for example, Section VI of the review by Robinson and Lenn[96]). With optically dense sources, such as flames, the problem may be overcome either by empirically choosing lines and/or line pairs whose intensity ratios are unaffected by self-absorption under the conditions of measurement, or by correcting a graphical solution for self-absorption. The former method is the easier and was used by the author and also by several other workers[97, 98, 99, 100]. Simplified methods of correcting graphical solutions for self-absorption have been described[101,102,103] but these methods still involve the calculation of the curves of growth of self-absorption and quite complex interpretation is necessary with each set of results. It is also possible to avoid self-absorption completely by measuring the relative intensities of lines in absorption. However, as explained in Chapter 1, this measurement involves a number of serious experimental difficulties and it does not appear to have been used for atomic spectra. An approximate application to CN band spectra is given in Section 3.6 and Kostkowski and Broida[104] used it with OH absorption bands.

In the previous work[93,94] line pairs unaffected by self-absorption were chosen on a rather empirical basis. Quite good results were obtained because the selection of lines improved quickly with experience, but the selection is tedious and open to criticism. In view of this a method of line selection based on sound theoretical principles has been developed and adapted for use with a simple computer programme. Another programme has been written to carry out the actual temperature calculations. The tables of results prepared by these two programmes may then be used to select line pairs and calculate temperatures with the minimum of effort.

3.5.2 Theory

The nomenclature to be used for transitions between the upper and lower levels of two spectral lines is illustrated in Fig. 3-8.

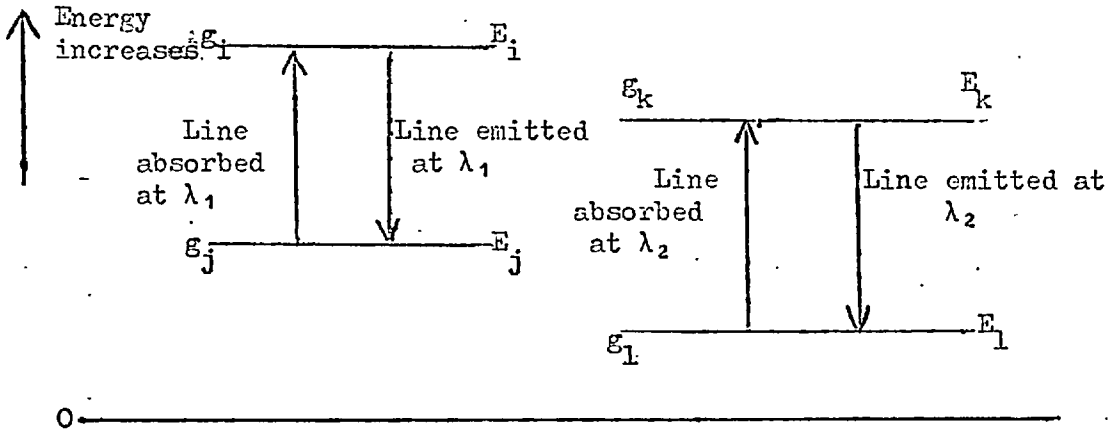


Fig. 3-8 Nomenclature Used For a Pair of Spectral Lines

For the two emission lines we may apply equation (1-17) directly, giving

$$I_1 = I_{ij} = \frac{h.c.N.}{F(T)} \frac{g_i . A_{ij}}{\lambda_1} . \exp(-E_i/kT) \qquad (3\text{-}1)$$

$$I_2 = I_{kl} = \frac{h.c.N.}{F(T)} \frac{g_k . A_{kl}}{\lambda_2} . \exp(-E_k/kT) \qquad (3\text{-}2)$$

where I_1 and I_2 are the integrated emission intensities.
The expression for I_1/I_2 is therefore:

$$\frac{I_1}{I_2} = \frac{g_i}{g_k} . \frac{A_{ij}}{A_{kl}} . \frac{\lambda_2}{\lambda_1} . \exp.[-(E_i - E_k)/kT] \qquad (3\text{-}3)$$

For the two absorption lines, equation (1-16) may be applied in simplified form since in flames at normal temperatures the population of the upper level is negligible.

i.e.

$$K = \frac{h}{\lambda} \cdot B_{ji} \cdot N_j$$

To make use of equation (3-4) we must substitute for N_j in terms of N using equation (1-14). This gives

$$K = \frac{h}{\lambda} \cdot B_{ji} \cdot N \cdot g_j \cdot \frac{\exp(-E_j/kT)}{F(T)} \qquad (3\text{-}5)$$

This is more useful if B_{ji} is replaced by A_{ij} using equation (1-5), i.e.

$$K = \frac{\lambda^2}{8\pi} \cdot g_i \cdot A_{ij} \cdot N \cdot \frac{\exp(-E_j/kT)}{F(T)} \qquad (3\text{-}6)$$

Hence, with the two lines in Fig. 3-8 we obtain:

$$\frac{K_1}{K_2} = \frac{g_i}{g_k} \cdot \frac{A_{ij}}{A_{kl}} \cdot \frac{\lambda_1^2}{\lambda_2^2} \cdot \exp[-(E_j - E_l)/kT] \qquad (3\text{-}7)$$

where K_1 and K_2 are the integrated absorption coefficients for the two lines.

In practice, it is more convenient to work in terms of the oscillator strength. Using equation (1-7), the expressions for I_1/I_2 and K_1/K_2 become

$$\frac{I_1}{I_2} = \frac{g_i \cdot f_{ij}}{g_k \cdot f_{kl}} \cdot \frac{\lambda_2^3}{\lambda_1^3} \cdot \exp[-(E_i - E_k)/kT] \qquad (3\text{-}8)$$

$$\frac{K_1}{K_2} = \frac{g_i \cdot f_{ij}}{g_k \cdot f_{kl}} \cdot \exp[-(E_j - E_l)/kT] \qquad (3\text{-}9)$$

Equation (3-8) is used to calculate temperatures from the intensities of the emission lines assuming that the ratio of the observed intensities is identical to that of the emitted intensities, i.e. assuming that self-absorption has no effect. This condition is found by using equation (3-9), since it can be seen that for a given

pair of lines there will only be one temperature where $K_1/K_2 = 1$ and this is calculated simply by substituting the spectral data for the lines into the equation.

The ratio of K_1/K_2 cannot be used to measure self-absorption because it can only be obtained by plotting the line profiles with an ultra-high resolution monochromator. It will also only give a quantitative result for the ratio of self-absorption with two lines whose intensities are measured using a conventional spectrograph or monochromator if the lines are assumed to be infinitely narrow. This is obviously not true for lines giving self-absorption in a flame. However, the ratio for two lines of the same atom, in the same source and whose wavelengths and intensities are similar will be a good guide to the relative degrees of self-absorption shown by the two lines. Therefore, we may assume that to a good approximation the intensity ratio of a line pair will be unaffected by self-absorption in a source whose temperature is such that $K_1 = K_2$ for those two lines.

3.5.3 Implementation of the method

In order to make temperature measurements by the original method,[93,94] spectra were photographed and for any particular temperature line pairs were chosen which exhibited the following properties:

(1) Intensities as similar as possible

(2) Wavelengths as close as possible

(3) Largest possible difference in upper energy levels to produce good sensitivity to changes in temperature and better accuracy.

(4) The smaller of the two lower energy levels as high as possible above the ground state, since this will help to minimise self-absorption.

(5) Lines whose wavelengths and intensities lie within the optimum range of the detector.

Conditions (1) and (2) form the well-known iso-intensity method which is frequently used for temperature determinations from band spectra[20].

Eliminating the gf values from equations (3-8) and (3-9) and substituting for the energy differences in terms of the wavelengths of the lines gives

$$\frac{I_1}{I_2} = \frac{K_1}{K_2} \cdot \frac{\lambda_2^3}{\lambda_1^3} \cdot \exp.\left[-\frac{h.c}{k.T.} \cdot \left(\frac{1}{\lambda_1} - \frac{1}{\lambda_2}\right)\right] \qquad (3\text{-}10)$$

Substitution of the two conditions into this equation gives the result $K_1/K_2 = 1$; i.e. our present method is in fact a derivation of the iso-intensity method. However, since the value of K_1/K_2 is readily calculated from equation (3-9) it provides a much more convenient means of finding the temperature at which any line pair will be least affected by self-absorption.

In practice, it is often not possible to obtain suitable line pairs with K_1/K_2 exactly equal to unity at any given temperature. However, provided that the self-absorption is not extremely serious this condition may be relaxed somewhat and line pairs whose K_1/K_2 value lies between fairly narrow limits either side of unity may be employed. It is not possible to specify a given temperature range for all line pairs because the rate of change of K_1/K_2 with temperature varies a great deal with different line pairs. In view of this the computer programme is used to calculate a table of K_1/K_2 values at suitable intervals within the required temperature range and the useful range for each line pair is determined by inspection. If the approximate temperature of the flame is known, the table may then be used to select a small set of line pairs which should be unaffected by self-absorption in the flame. Conditions (3), (4) and (5) are then easily applied to this small set to select the two or three line pairs which should give the best possible results for a particular flame.

3.5.4 SAECO: A computer programme to calculate self-absorption coefficients for pairs of spectral lines.

Equation (3-9) forms the entire calculation so that this occupies only a small part of the programme. The rest is designed to allow a set of data for a number of spectral lines (selected by taking a preliminary spectrum from the flame) to be read into the computer and automatically selected into suitable line pairs on which the calculation is performed. To prevent calculations on unsuitable line pairs, a minimum value is set for the difference between the upper energy levels of each line pair. The energy difference between the lower levels is also calculated because if it should be zero K_1/K_2 will be independent of temperature. If this should occur the programme is designed to print results for all temperatures but place an explanatory note below.

The actual programme listing is shown in Table 3-3. As well as the four variables for each spectral line, the data read includes the number of lines for a run; the initial and final temperatures and the temperature interval; and the minimum upper energy level difference for a usable line pair. For convenience, all data is printed out with the results, as shown in Table 3-4. An example of the block of results obtained for each line pair is also shown in Table 3-4. The total number of these blocks on any run is printed-out at the end as the number of line pairs.

The use of the programme should be clear from Tables 3-3 and 3-4. The data cards for the lines should be placed in order of increasing wavelength. The two "DO" loops are designed so that the results will then be given with the line of higher upper energy level first for each pair and with the first lines of the pairs arranged in order of increasing wavelength. To facilitate further the use of SAECO, its name list of variables is given below.

Table 3-3

```
C     SABCO.....A PROGRAM TO CALCULATE RATIOS OF SELF ABSORPTION
C                 COEFFICIENTS FOR PAIRS OF SPECTRAL LINES.
C
C
      DIMENSION  WAVEL(100), GF(100), ELOWER(100), EUPPER(100), IT(1000)
     1, T(1000), SAB(1000)
C
       NPAIRS = 0
C
      WRITE (6, 1000)
 1000 FORMAT (1H1, 27X, 81HCALCULATION OF RATIOS OF THE SELF ABSORPTION
     1COEFFICIENTS FOR PAIRS OF IRON LINES, // 64X, 9HM.SARGENT, ///)
C
      READ (5,1001) NLINES, ITEMPA, ITEMPB, ITINT, ENGMIN
 1001 FORMAT ( 10X, 4I10, F10.3 )
      WRITE (6,1002) NLINES, ITEMPA, ITEMPB, ITINT, ENGMIN
 1002 FORMAT ( 26X, 4HDATA, //  1X, I5, 5HLINES, 4X, 16HINITIAL TEMP, I
     15, I5,  5HDEG.K, 4X, 14HFINAL TEMP, I5, I5, 5HDEG.K, 4X, 17HTEMP,
     21NTERVAL I5, I5, 5HDEG.K, 4X, 19HMIN.ENERGY DIFF, I5, F6.3,2HEV,/)
C
      READ (5,1003) (WAVEL(I), GF(I), ELOWER(I), EUPPER(I), I=1,NLINES)
 1003 FORMAT ( 10X, F10.2, F10.4, 2F10.3 )
      WRITE (6,1004)
 1004 FORMAT(1H0,25X,14HWAVELENGTH (A), 15X, 2HGF, 15X, 12HE-LOWER (EV),
     1  15X, 12HE-UPPER (EV), // )
      WRITE (6,1005) (WAVEL(I), GF(I), ELOWER(I), EUPPER(I), I=1,NLINES)
 1005 FORMAT ( 26X, F10.2, 12X, F10.4, 11X, F10.3, 17X, F10.3 )
C
C
      WRITE (6,1006) ENGMIN
 1006 FORMAT(1H1,25X,7HRESULTS,// 11X, 80H(NO RESULTS PRINTED FOR LINE P
     1AIRS WITH UPPER ENERGY LEVEL DIFFERENCES LESS THAN, F6.3, 3HEV),/)
C
C
      NTEMPS = (ITEMPB - ITEMPA) / ITINT + 1
C
      DO 30 JJ = 1, NLINES
      I = JJ
C
      DO 20 KK = 1, NLINES
      I = KK
      ENGAP = EUPPER(JJ) - EUPPER(KK)
      IF ( ENGAP .LT. ENGMIN ) GO TO 20
      NPAIRS = NPAIRS + 1
C
      WRITE (6, 1007) WAVEL(JJ), WAVEL(KK), ENGAP
 1007 FORMAT (1H0, 5X, 5HLINES, F9.2, 1X, 3HAND, F9.2, 39H , ENERGY DIFF
     1ERENCE OF UPPER LEVELS IS, F6.3, 3HEV., ///, 8( 3X, 5HTEMP., 2X,
     25HK1/K2, ) // )
C
      M = 1
      ITS = ITEMPA
   10 IF ( ITS .GT. ITEMPB ) GO TO 15
      IT(M) = ITS
      T(M) = ITS
C
      XPON = ( ELOWER(KK) - ELOWER(JJ) ) / ( 0.0000862 * T(M) )
      SAB(M) = GF(JJ) * EXP(XPON) / GF(KK)
C
      ITS = ITS + ITINT
      M = M + 1
      GO TO 10
C
   15 WRITE (6, 1008) ( IT(M), SAB(M), M = 1, NTEMPS )
 1008 FORMAT ( 8( 3X, I4, 2X, F6.3 ) )
C
      ENGAPL = ELOWER(KK) - ELOWER(JJ)
      IF ( ENGAPL .NE. 0.0 ) GO TO 40
C
      WRITE (6, 1010)
 1010 FORMAT (1H0,114H(DIFFERENCE BETWEEN LOWER ENERGY LEVELS IS ZERO, T
     1HEREFORE K1/K2 IS INDEPENDENT OF TEMPERATURE FOR THIS LINE PAIR),)
C
   40 WRITE (6, 1011)
 1011 FORMAT (1H0, 60X, 12H************, /// )
   20 CONTINUE
   30 CONTINUE
C
C
      WRITE (6,1009) NPAIRS
 1009 FORMAT (1H0, 5X, 39HNUMBER OF LINE PAIRS ON THIS RUN EQUALS, I6 )
C
      STOP
      END
```

Table 3-4

CALCULATION OF RATIOS OF THE SELF ABSORPTION COEFFICIENTS FOR PAIRS OF IRON LINES

P.SARGEAT

DATA

18LINES INITIAL TEMP. IS 1500DEG.K FINAL TEMP. IS 3500DEG.K TEMP. INTERVAL IS 20DEG.K MIN.ENERGY DIFF. IS 0.30DEV

WAVELENGTH (A)	GF	E-LOWER (EV)	E-UPPER (EV)
3705.57	0.0794	0.052	3.396
3722.56	0.0955	0.087	3.417
3733.32	0.0661	0.110	3.432
3734.87	3.720C	0.859	4.137
3737.13	0.3160	0.052	4.3C1
3748.26	0.135C	0.110	3.417
3749.49	2.75C0	0.915	4.22C
3758.24	2.04C0	0.958	4.256
3820.43	2.5700	0.859	4.1C3
3824.44	0.0676	0.	3.241
3825.88	1.82C0	0.915	4.154
3856.37	0.0724	0.052	3.268
3878.57	0.0661	0.958	4.154
3895.66	0.0363	0.110	3.292
3859.71	0.0479	0.087	3.226
3920.26	0.0331	0.121	3.283
3922.91	0.0363	0.052	3.211
3927.92	0.05C1	0.110	3.266

RESULTS

(NO RESULTS PRINTED FOR LINE PAIRS WITH UPPER ENERGY LEVEL DIFFERENCES LESS THAN 0.30DEV)

LINES 3734.87 AND 3705.57 , ENERGY DIFFERENCE OF UPPER LEVELS IS 0.781EV.

TEMP.	K1/K2	TEMP.	K1/K2	TEMP.	K1/K2	TEMP.	K1/K2	TEMP.	K1/K2	TEMP.	K1/K2	TEMP.	K1/K2	TEMP.	K1/K2
1500	0.091	1520	0.099	1540	0.107	1560	0.116	1580	0.125	1600	0.135	1620	0.145	1640	0.155
1660	0.167	1680	0.178	1700	0.190	1720	0.203	1740	0.216	1760	0.229	1780	0.244	1800	0.258
1820	0.273	1840	0.289	1860	0.305	1880	0.322	1900	0.339	1920	0.357	1940	0.376	1960	0.395
1980	0.414	2000	0.434	2020	0.455	2040	0.476	2060	0.498	2080	0.520	2100	0.543	2120	0.566
2140	0.590	2160	0.614	2180	0.639	2200	0.665	2220	0.691	2240	0.717	2260	0.744	2280	0.772
2300	0.800	2320	0.828	2340	0.857	2360	0.887	2380	0.917	2400	0.948	2420	0.979	2440	1.010
2460	1.042	2480	1.075	2500	1.108	2520	1.141	2540	1.175	2560	1.209	2580	1.244	2600	1.279
2620	1.315	2640	1.351	2660	1.387	2680	1.424	2700	1.462	2720	1.499	2740	1.538	2760	1.576
2780	1.615	2800	1.654	2820	1.694	2840	1.734	2860	1.775	2880	1.815	2900	1.857	2920	1.898
2940	1.940	2960	1.982	2980	2.025	3000	2.067	3020	2.111	3040	2.154	3060	2.198	3080	2.242
3100	2.286	3120	2.331	3140	2.376	3160	2.421	3180	2.467	3200	2.513	3220	2.559	3240	2.605
3260	2.652	3280	2.699	3300	2.746	3320	2.793	3340	2.841	3360	2.888	3380	2.936	3400	2.985
3420	3.033	3440	3.082	3460	3.131	3480	3.180	3500	3.229						

WAVEL	Wavelength of line in Angstrom units.
GF	gf value of line.
ELOWER	Lower energy level of line in eV.
EUPPER	Upper energy level of line in eV.
NLINES	Number of lines put in as data.
ITEMPA	Initial temperature (^{0}K) used for a run.
ITEMPB	Final temperature (^{0}K) used for a run.
ITINT	Temperature interval used for a run.

ENGMIN Minimum upper level energy difference for a usable line pair.
ENGAP Energy difference between the upper levels of a line pair.
ENGAPL Energy difference between the lower levels of a line pair.
SAB Ratio of self-absorption coefficients.
NPAIRS Number of line pairs for which SAB is calculated.
NTEMP Number of temperatures for which SAB is calculated with each line pair.

IT, T, ITS } Intermediate temperatures used in the calculation.

XPON Intermediate value (the exponential term) used in the calculation.

3.5.5 IRTEMS: A computer programme to calculate the temperatures corresponding to the intensity ratios of pairs of spectral lines.

The method of reading in the data and of selecting line pairs is virtually identical to that used for SABCO. The main difference from the previous programme is that in this case the calculation performed is based on equation (3-8). There are also minor differences in the instructional data read in at the beginning and the warning notes printed in the output. The programme listing is shown in Table 3-5 and the data print-out and a sample of the results in Table 3-6. The name list is largely the same as for SABCO, but some additional variables are as follows.

FEIR Intensity ratio of a pair of lines.
FEIRA Initial intensity ratio used for a run.
FEIRB Final intensity ratio used for a run.
FEIRIN Intensity ratio interval used for a run.
FEIRS Intermediate intensity ratio used for a calculation.
EOTLOG Intermediate value (logarithmic term) used in a calculation.
DENOM Intermediate value (logarithm to the base ten of EOTLOG) used in a calculation.

Table 3-5

```
C      IRTEMS.....A PROGRAM TO CALCULATE THE TEMPERATURES CORRESPONDING
C                 TO THE INTENSITY RATIOS OF PAIRS OF SPECTRAL LINES.
C
       DIMENSION  WAVEL(100), GF(100), ELOWER(100), EUPPER(100),
     1           FEIR(1000), TEMP(1000)
C
C.
        NPAIRS = 0
C
C
       WRITE (6,1100)
 1100 FORMAT ( 1H1, 17X, 90HCALCULATION OF TEMPERATURES CORRESPONDING T
     1O GIVEN INTENSITY RATIOS OF PAIRS OF IRON LINES, // 64X,
     29HM.SARGENT, /// )
C
C
       READ (5,1101) NLINES, FEIRA, FEIRB, FEIRIN, ENGMIN
 1101 FORMAT ( 10X, I10, 4F10.3 )
C
       WRITE (6,1102) NLINES, FEIRA, FEIRB, FEIRIN, ENGMIN
 1102 FORMAT ( 26X, 4HDATA, / 26X, 4H****, /// 1X, 15, 6H LINES, 3X,
     116HINITIAL I1/I2 IS, F6.3, 3X, 14HFINAL I1/I2 IS, F6.3, 3X,
     221HINTERVAL FOR I1/I2 IS, F6.3, 3X, 19HMIN.ENERGY DIFF, IS, F6.3,
     33HEV., / )
C
       READ (5,1103) (WAVEL(I), GF(I), ELOWER(I), EUPPER(I), I=1,NLINES)
 1103 FORMAT ( 10X, F10.2, F10.4, 2F10.3 )
C
       WRITE (6,1104)
 1104 FORMAT(1H0,25X,14HWAVELENGTH (A), 15X, 2HGF, 15X, 12HE-LOWER (EV),
     1  15X, 12HE-UPPER (EV), // )
C
       WRITE (6,1105) (WAVEL(I), GF(I), ELOWER(I), EUPPER(I), I=1,NLINES)
 1105 FORMAT ( 26X, F10.2, 12X, F10.4, 11X, F10.3, 17X, F10.3 )
C
       WRITE (6,1106) ENGMIN
 1106 FORMAT(1H1,25X,7HRESULTS,// 1X, 80H(NO RESULTS PRINTED FOR LINE P
     1AIRS WITH UPPER ENERGY LEVEL DIFFERENCES LESS THAN, F6.3, 3HEV),/,
     211X, 81HI1/I2 IS INTENSITY OF FIRST LINE OVER INTENSITY OF SECOND
     3LINE FOR EACH LINE PAIR, /// )
C
       NTEMPS = ( FEIRB - FEIRA ) / FEIRIN + 1.0
C
       DO 130 JJ = 1, NLINES
       I = JJ
       DO 120 KK = 1, NLINES
       I = KK
C
       ENGAP = EUPPER(JJ) - EUPPER(KK)
       IF ( ENGAP .LT. ENGMIN ) GO TO 120
       NPAIRS = NPAIRS + 1
C
       WRITE (6, 1107) WAVEL(JJ), WAVEL(KK), ENGAP
 1107 FORMAT (1H0, 5X, 5HLINES, F9.2, 1X, 3HAND, F9.2, 39H , ENERGY DIFF
     1ERENCE OF UPPER LEVELS IS, F6.3, 3HEV., ///, 7( 4X, 5HI1/I2, 2X,
     27HT DEG.K, ) // )
C
C
       M = 1
C
       FEIRS = FEIRA
  110 IF ( FEIRS .GT. FEIRB ) GO TO 115
       FEIR(M) = FEIRS
       BOTLOG = GF(JJ)*WAVEL(KK)**3 / ((GF(KK)*WAVEL(JJ)**3) * FEIR(M) )
       DENOM = ALOG10 (BOTLOG)
       TEMP(M) = 5040.0 * ENGAP / DENOM
C
C
       FEIRS = FEIRS + FEIRIN
       M = M + 1
       GO TO 110
C
  115 WRITE ( 6, 1108) ( FEIR(M), TEMP(M), M = 1, NTEMPS )
 1108 FORMAT ( 7( 3X, F6.3, 2X, F7.2 ) )
C
       WRITE (6, 1111)
 1111 FORMAT (1H0, 60X, 12H**********, /// )
C
  120 CONTINUE
  130 CONTINUE
C
       WRITE (6,1109) NPAIRS
 1109 FORMAT (1H0, 5X, 39HNUMBER OF LINE PAIRS ON THIS RUN EQUALS, I6 )
C
       STOP
       END
```

TEMP Temperature corresponding to a given intensity ratio of a line pair.

3.5.6 Results

The two programmes were run for a small number of iron lines using the Imperial College IBM 7094 computer and the PUFFT (Purdue University Fast Fortran Translator) compiler system. The results were applied to the spectra used for the previous temperature determinations[93,94] to see whether the new system gave a significant change in the measured temperatures as well as being more convenient to use.

The previous measurements on the air-acetylene flame (Ref. 93, Table 7) had given a temperature of 2490 ± 65°K, based on nine different line pairs. Using the present system, it was found that only two of these line pairs could be recommended for that temperature region:

3749.49 - 3733.32
3734.87 - 3705.57

A third suitable pair had not been chosen by the previous procedure:

3734.87 - 37222.56

Using only the recommended line pairs and the more recent gf values from Ref. 95, the revised flame temperature becomes 2460 ± 25°K. i.e. a result well within the previously quoted limit of error.

As another example, a large number of measurements were previously made in the red interconal zone of a slightly fuel rich nitrous oxide-acetylene flame (Ref. 93 , Table 10). Temperatures at heights between 7.5mm and 17.5mm above the burner were measured using five different line pairs. The results lay within the range 2750 to 2850 °K. On the present system of line selection, only two of these line pairs could still be strongly recommended (3749.49 - 3705.57 and

3749.49 - 37222.56). A third pair (3820.43 - 3824.44) also gives its optimum results in this range but the 3824.44Å line is a ground state line and should be avoided if possible. Of the other two pairs used, one (3734.87 - 3748.26) is on the edge of its useful range and the other (3749.49 - 3733.32) is only recommended for lower temperatures. The new system also shows that one very suitable pair was missed (3758.24 - 3733.32) and two others could have been used with the available data (3820.43 - 3722.56 and 3825.88 - 3733.32) although they are rather widely spaced. However, since most of the previous measurements were concentrated on the two line pairs still recommended, no serious error appears to have been made.

The following conclusions may be drawn from these two examples:

(i) With the old system, even long experience was not always a guarantee that only suitable line pairs would be used and that no useful pairs would be missed.

(ii) The new system allows a much larger number of line pairs to be selected much more quickly without a great deal of practical experience.

(iii) With the new system the chance of using an unsuitable line pair is greatly reduced.

(iv) The new system should improve the precision of the temperature measurements somewhat, but more important is the greater certainty with which the reliability of the measurement may be assessed.

(v) Justification of the choice of a particular line pair (to someone using the results) is much easier with the new system.

In view of these facts, the method of choosing line pairs outlined here has been used extensively by Mr. S. Vetter[92] for the measurement of flame temperature profiles. He has rewritten the computer programme SABCO in a form which is capable of handling large numbers of spectral lines without printing enormous amounts of unwanted output and which may be run on the much larger University of London CDC 6600 computer. At the present time, the results are being applied to the measurement of the

Table 3-6

CALCULATION OF TEMPERATURES CORRESPONDING TO GIVEN INTENSITY RATIOS OF PAIRS OF IRON LINES

P.SARGENT

DATA
****

18 LINES INITIAL I1/I2 IS 0.500 FINAL I1/I2 IS 2.000 INTERVAL FOR I1/I2 IS 0.010 MIN.ENERGY DIFF. IS 0.300EV.

WAVELENGTH (A)	GF	E-LOWER (EV)	E-UPPER (EV)
3705.57	0.0794	0.052	3.398
3722.56	0.0955	0.087	3.417
3733.32	0.0661	0.110	3.430
3734.87	3.7200	0.859	4.177
3737.13	0.3160	0.052	4.361
3746.26	0.1350	0.110	3.417
3749.49	2.7500	0.915	4.220
3758.24	2.6400	0.958	4.256
3820.43	2.5700	0.859	4.103
3824.44	0.0676	0.	3.241
3825.88	1.8200	0.915	4.154
3856.37	0.0724	0.052	3.266
3878.57	0.0661	0.958	4.154
3895.66	0.0363	0.110	3.292
3899.71	0.0479	0.087	3.226
3920.26	0.0331	0.121	3.283
3922.91	0.0363	0.052	3.211
3927.92	0.0501	0.110	3.266

RESULTS

(NO RESULTS PRINTED FOR LINE PAIRS WITH UPPER ENERGY LEVEL DIFFERENCES LESS THAN 0.300EV)
I1/I2 IS INTENSITY OF FIRST LINE OVER INTENSITY OF SECOND LINE FOR EACH LINE PAIR

LINES 3734.87 AND 3705.57 , ENERGY DIFFERENCE OF UPPER LEVELS IS 0.781EV.

I1/I2	T DEG.K	I1/I2	T DEG.K	I1/I2	T DEG.K	I1/I2	T DEG.K	I1/I2	T DEG.K	I1/I2	T DEG.K	I1/I2	T DEG.K
0.500	2006.76	0.510	2015.60	0.520	2024.34	0.530	2032.99	0.540	2041.55	0.550	2050.02	0.560	2058.41
0.570	2066.72	0.580	2074.95	0.590	2083.10	0.600	2091.18	0.610	2099.18	0.620	2107.12	0.630	2114.98
0.640	2122.78	0.650	2130.52	0.660	2138.20	0.670	2145.81	0.680	2153.36	0.690	2160.86	0.700	2168.29
0.710	2175.68	0.720	2183.01	0.730	2190.28	0.740	2197.51	0.750	2204.68	0.760	2211.81	0.770	2218.89
0.780	2225.92	0.790	2232.90	0.800	2239.85	0.810	2246.74	0.820	2253.60	0.830	2260.41	0.840	2267.18
0.850	2273.91	0.860	2280.61	0.870	2287.26	0.880	2293.88	0.890	2300.45	0.900	2307.00	0.910	2313.50
0.920	2319.98	0.930	2326.41	0.940	2332.82	0.950	2339.19	0.960	2345.53	0.970	2351.83	0.980	2358.11
0.990	2364.36	1.000	2370.57	1.010	2376.76	1.020	2382.91	1.030	2389.04	1.040	2395.14	1.050	2401.21
1.060	2407.24	1.070	2413.28	1.080	2419.27	1.090	2425.23	1.100	2431.18	1.110	2437.09	1.120	2442.98
1.130	2448.85	1.140	2454.69	1.150	2460.51	1.160	2466.31	1.170	2472.09	1.180	2477.84	1.190	2483.57
1.200	2489.27	1.210	2494.96	1.220	2500.63	1.230	2506.27	1.240	2511.90	1.250	2517.50	1.260	2523.08
1.270	2528.65	1.280	2534.19	1.290	2539.72	1.300	2545.23	1.310	2550.72	1.320	2556.19	1.330	2561.64
1.340	2567.07	1.350	2572.49	1.360	2577.89	1.370	2583.27	1.380	2588.64	1.390	2593.99	1.400	2599.32
1.410	2604.64	1.420	2609.94	1.430	2615.22	1.440	2620.49	1.450	2625.75	1.460	2630.99	1.470	2636.21
1.480	2641.42	1.490	2646.61	1.500	2651.79	1.510	2656.96	1.520	2662.11	1.530	2667.25	1.540	2672.37
1.550	2677.48	1.560	2682.57	1.570	2687.66	1.580	2692.73	1.590	2697.78	1.600	2702.83	1.610	2707.86
1.620	2712.88	1.630	2717.88	1.640	2722.88	1.650	2727.86	1.660	2732.83	1.670	2737.79	1.680	2742.73
1.690	2747.67	1.700	2752.59	1.710	2757.50	1.720	2762.40	1.730	2767.29	1.740	2772.17	1.750	2777.04
1.760	2781.90	1.770	2786.74	1.780	2791.58	1.790	2796.40	1.800	2801.22	1.810	2806.02	1.820	2810.82
1.830	2815.60	1.840	2820.38	1.850	2825.14	1.860	2829.90	1.870	2834.64	1.880	2839.38	1.890	2844.11
1.900	2848.82	1.910	2853.53	1.920	2858.23	1.930	2862.92	1.940	2867.60	1.950	2872.27	1.960	2876.94
1.970	2881.59	1.980	2886.24	1.990	2890.88	2.000	2895.50						

****

temperature differences between conventional and separated air-acetylene and nitrous oxide-acetylene flames. Preliminary results are in good agreement with those outlined elsewhere in this thesis. They suggest that the temperature drop at the very centre of the long path flames is much smaller than that observed with the circular flames, but that quite large temperature drops occur near

the sides of the flames on separation.

3.6 The CN Vibrational Temperature of The Nitrous Oxide-Acetylene Flame.

A knowledge of the temperature of the nitrous oxide-acetylene flame and the way in which it changes on flame separation is a most useful aid in interpreting the results given in this chapter. Several different ways of measuring flame temperature have been tried by the author (see Sections 1.4.5 and 3.5), but the one described here is the most appropriate for the present purpose. It has a number of advantages:

(i) No additional substance need be added to the flames.

(ii) No CN is present in the outer cone of the flame so that there can be no confusion as to which area of the flame the temperature measurements apply.

(iii) It has been shown that CN vibrational temperatures appear to give a good approximation to the actual flame temperature (see below), even though this is not the case with many rotational and vibrational temperatures.

There are also some disadvantages. First, the method can only be used when sufficient CN is present. This is no real problem in our case because we are mainly interested in the "best red zone" flame used for the atomic emission and absorption spectroscopy of the refractory elements. Secondly, the method involves a number of experimental and theoretical uncertainties. These are discussed below.

3.6.1 Introduction

The measurement of effective flame temperature from the rotational and vibrational fine structure of band spectra of molecular species present in the flame gases is well known and has been reviewed

by Gaydon (Ref. 20, Ch.8). However, these methods mostly involve the use of large spectrographs which are capable of complete resolution of the bands and allow measurements to be made of individual rotational lines. (These are used directly for rotational temperatures or summed in the appropriate way to give the total band intensities for vibrational temperatures). Even when such apparatus is available, there are many difficulties which must be overcome. If rotational temperatures are required, it is usually possible to select sufficient isolated lines for a calculation, although this becomes more difficult if precautions are required to avoid self-absorption. For vibrational temperatures, the situation is much more complicated because all of the lines of each band must be measured and the vibrational bands almost always overlap. Alternatively, individual rotational lines of different vibrational bands may be compared, but the calculation of the vibrational temperature then requires a knowledge of the rotational temperature and transition probability as well as the vibrational transition probability (see Ref. 18, p. 527, eqn. 21-92). Unfortunately, only one or two studies of a flame band have been systemmatic enough for this method to be employed, even though it gives the most reliable vibration temperatures.

There is also another method of measuring vibrational temperatures which involves much less laborious work than the two methods above and, even more important, does not require the ultra-high resolution monochromator needed for the rotational temperatures. It requires measurement of some prominent feature of the vibrational bands, usually the maximum intensities of the band heads. These relative values can then be used to calculate vibrational temperatures just as if they were the true relative intensities of the whole bands. Great care must be taken in the selection of band heads used in this way, because for a given vibrational temperature the apparent intensity will vary with changes in the rotational temperature due to changes in the

pattern of the rotational fine structure. Since different vibrational bands of the same molecule can be affected in quite different ways, the errors in the relative intensities may often be large, leading to serious errors in the temperature unless corrections are again made from the rotational temperature.

Fortunately, several workers have shown that reasonable results may be obtained from one or two, at least, of the CN violet bands without making corrections and the bands recommended by them will be used here.

The first work on the method was carried out at Utrecht 1931 by Ornstein and Brinkman[105] who measured the temperature of a D.C. carbon arc using the emitted CN bands. In this first paper they were mainly concerned with obtaining the vibrational transition probabilities of the CN violet bands using a low dispersion prism spectrograph so that the values could be used with similar instruments for straightforward temperature determinations. They achieved the following results:-

(i) They photographed the spectrum of the $\Delta v = 0$ CN sequence (main head at 3883.4Å) in great detail using a large grating spectrograph. The results were used to calculate the rotational CN temperatures of the arc and the true relative intensities of the band heads (by summing the intensities of the lines, correcting for the rotational temperature, etc.).

(ii) They photographed the spectra of the $\Delta v = -1, 0, 1, 2$ CN sequences using a low resolution prism spectrograph and measured the relative intensities of the observed band heads, Good agreement was obtained for the $\Delta v = 0$ sequence between these results and those under (i), especially for the first two or three bands.

(iii) Using the results of (ii), they summed the intensities of all band heads within each progression for values of v^1 from 0 to 6 (some of the higher v^1 progressions required extrapolated values). By plotting these sums against the energies of the

levels corresponding to the different v^1 values, they were able to obtain a value of the CN vibrational temperature without a knowledge of the vibrational transition probabilities. The temperature was in reasonably good agreement with the rotational temperature obtained under (i).

(iv) Using this temperature value, they were able to calculate from the relative band head intensities the relative vibrational transition probabilities of all the CN violet bands.

In order to make use of these results, we require two further pieces of information. First, how accurate are these transition probabilities and which are the most reliable. Secondly, will the method also give accurate temperature values for flames and which of the CN bands will be most useful.

(a) Accuracy of the transition probability ratios.

1. A considerable amount of work on CN temperatures was carried out by the successors of Ornstein and Brinkman at Utrecht. Much of this was concerned with "calibrating" various features of the CN bands with respect to temperature, rather than direct use of intensity ratios as carried out above, and has been reviewed by J.A. Smit[106]. Although the calibrations were calculated theoretically, they still involved the experimental transition probabilities. Dr.Smit has stated (Ref. 106, p.698) that results with these calibrations indicate that the most reliable ratios of the set are $1 \rightarrow 1/0 \rightarrow 0$ and $1 \rightarrow 2/0 \rightarrow 1$.

2. Theoretical values of the same transition probabilities, obtained by numerical integration (and also by another technique) were published by Fraser, Jarmain and Nicholls[107]. The relevant experimental and theoretical values are listed side-by-side in Table 3-7, arranged in sequences. The ratio of the two values for each band is given in the last column. It can be seen that although the overall agreement between the two sets of values is not very high, the agreement within each sequence is good. This is particularly true

Table 3-7

λ(Å)	v^1	v^{11}	Δv	Transition Probability		Ratio:
				Ornstein, et.al	Fraser, et.al.	Ornstein / Fraser
4606.1	0	2	+2	0.003	0.005	0.6
4578.0	1	3	+2	0.007	0.014	0.5
4553.1	2	4	+2	0.009	-	-
4531.9	3	5	+2	0.012	-	-
4514.8	4	6	+2	0.016	-	-
4502.2	5	7	+2	0.02	-	-
4216.0	0	1	+1	0.055	0.074	0.74
4197.2	1	2	+1	0.095	0.121	0.78
4181.0	2	3	+1	0.12	0.147	0.81
4167.8	3	4	+1	0.15	-	-
4158.1	4	5	+1	0.19	-	-
4152.4	5	6	+1	0.23	-	-
3883.4	0	0	0	1.0	0.920	1.09
3871.4	1	1	0	0.87	0.787	1.10
3861.9	2	2	0	0.77	0.691	1.11
3854.7	3	3	0	0.67	0.625	1.07
3850.9	4	4	0	0.59	-	-
3590.4	1	0	-1	0.16	0.079	2.02
3585.9	2	1	-1	0.29	0.137	2.12
3583.9	3	2	-1	0.24	0.181	1.33

of the $\Delta v = 0$ sequence with differences of less than 1% for the ratios $0 \rightarrow 0/1 \rightarrow 1$ and $1 \rightarrow 1/2 \rightarrow 2$. Even with $0 \rightarrow 1/1 \rightarrow 2$ and $1 \rightarrow 0/2 \rightarrow 1$, the difference between the two sets of values is only 5%. It should also be remembered that Ornstein and Brinkman's data may be more suitable for our purposes, because any experimental errors due to overlapping of the band heads and change of the spacing

of the rotational lines when going from one band head to another should partly cancel out.

(b) Suitability of the method for flame temperatures.

1. As mentioned above, most of the work on this method has been carried out at Utrecht where the only interest was in the carbon arc. However, one or two workers have also applied it to other sources. Brewer, Templeton and Jenkins[108] measured CN equilibrium temperatures in a King furnace and found good agreement with those obtained by an optical pyrometer. Thomas, Gaydon and Brewer[109] measured the temperature of an oxygen-cyanogen flame using the main bands of the (0,1) and (0,0) sequences. They obtained good agreement with the calculated maximum temperature and with C_2 rotational temperatures obtained by the conventional method. Fishburne, Rao and Weinberg[110] measured temperatures of nitrous oxide-cyanogen flames using the infra-red CN rotational bands and obtained good agreement with calculated temperatures and those from the relative intensities of iron lines. Finally, Watson, Planet and Pitts[111] have suggested that the non-resolved CN violet bands may be used (by a different technique to that described here) to measure temperatures of a variety of hot gases, including those surrounding spacecraft on atmospheric re-entry. Thus, it would appear that, provided they are accurately made, CN temperature measurements should correspond closely to the "actual" temperatures in the equilibrium region of a flame.

2. From the author's experience with the iron two line temperatures (see Section 3.5) the main problem in using the CN bands for flame temperatures would seem to be self-absorption. This is less of a problem in arcs and other high temperature sources which can generally be considered as "optically thin". Even so, Ornstein and Brinkman's original work was criticised on this basis by Lochte-Holtgreven and Maecker[112]. This could be the cause of the discrepancy between the two sets of results in Table 3-7 when the different sequences are compared. Because of this and because of

the need to obtain sufficient intensity of the bands to be used, our measurements will be restricted to the 3883, 3871 and 3861 Å peaks. Thomas et. al.[109] reported no self-absorption effects on their emission measurements but this was mainly because their flame was much hotter (4800°K) so that the population of lower levels was much reduced. They also avoided where possible using transitions involving the zero vibrational state of the ground state. This is not possible in the present work and it will be shown experimentally that only temperatures measured in absorption are reliable.

3.6.2 Theory

The equations derived for atomic spectra in Section 3.5.2 may also be applied to molecular spectra. However the gA values must be replaced by a term $P\nu^3$ where P is the molecular transition probability of the form given in Table 3-7. The frequency, ν, of the transition must be introduced as a cubic term because P must now allow for the rotational, vibrational and electronic transition probabilities (see Ch. 21-4-3 of Ref. 18). Equations (3-3) and (3-7) may therefore be rewritten as:

$$\frac{I_1}{I_2} = \frac{P_1}{P_2} \cdot \frac{(\lambda_2)^4}{(\lambda_1)^4} \cdot \exp\left[\frac{-(E_1 - E_2)}{kT}\right] \qquad (3\text{-}11)$$

and

$$\frac{K_1}{k_2} = \frac{P_1}{P_2} \cdot \frac{\lambda_2}{\lambda_1} \cdot \exp\left[\frac{-(E_{L_1} - E_{L_2})}{kT}\right] \qquad (3\text{-}12)$$

where E_1 and E_2 are the upper energy levels of the two transitions and E_{L_1} and E_{L_2} the lower energy levels.

It should be noted that the reliability with which equation (3-11) can be applied to the relative intensities of the CN band heads will depend on the extent to which they represent the ratios of the total vibration band intensities. From the discussion of Section 3.6.1 it would appear that there is fairly good correlation,

but this obviously depends to a certain extent on the excitation source and the measuring apparatus. There is even less theoretical justification for applying equation (3-12) to the relative strengths of the absorption band heads. This is discussed further in Section 3.6.4.

3.6.3 Results.

As mentioned earlier, only the CN sequence with a head at 3883.4Å was used for temperature measurements. All measurements were made using the Techtron AA4 described in Section 3.1. The narrowest possible monochromator slit width was generally used and a typical scan obtained with the sequence in emission and a 15μ slit is shown in Fig. 3-9.. The energy levels corresponding to the transitions are shown diagrammatically in Fig. 3-10.

Equation (3-12) may be used to estimate the effects of self-absorption on the emission intensity ratios of the CN peaks just as was described for iron lines in Section 3.5. At 3000°K, this gives a ratio of K_1/K_2 of about 3 for both 3883 - 3871 and 3871 - 3861; i.e. neither of these pairs will be suitable for emission measurements of the temperature of the nitrous oxide-acetylene flame unless the CN concentration is very low or the optical path length is small. To illustrate the serious effect of self-absorption on the observed temperature, measurements were made in the slightly fuel rich nitrous oxide-acetylene flame giving the "best red zone". Different CN concentrations could be obtained by separating the flame and different path lengths by using either the circular burner (see Section 2.4.3) or the long path burner (see Section 2.4.4) in its "end-on" or "sideways-on" positions. The results are shown in Table 3-8. It should be noted that each temperature in the table is a mean of several determinations and is subject to considerable uncertainty (of the order of ± 5%). However, because of the high CN concentration in the fuel rich flames used the self-absorption

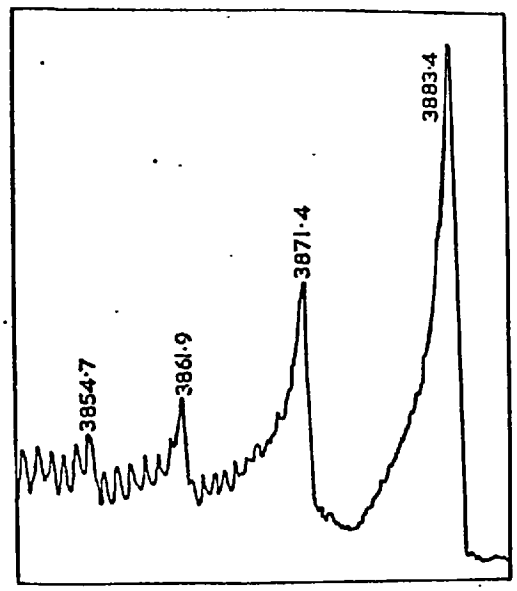


Fig. 3-9

CN 3883A Sequence Observed In Emission From a Circular Argon Separated Nitrous Oxide - Acetylene Flame.

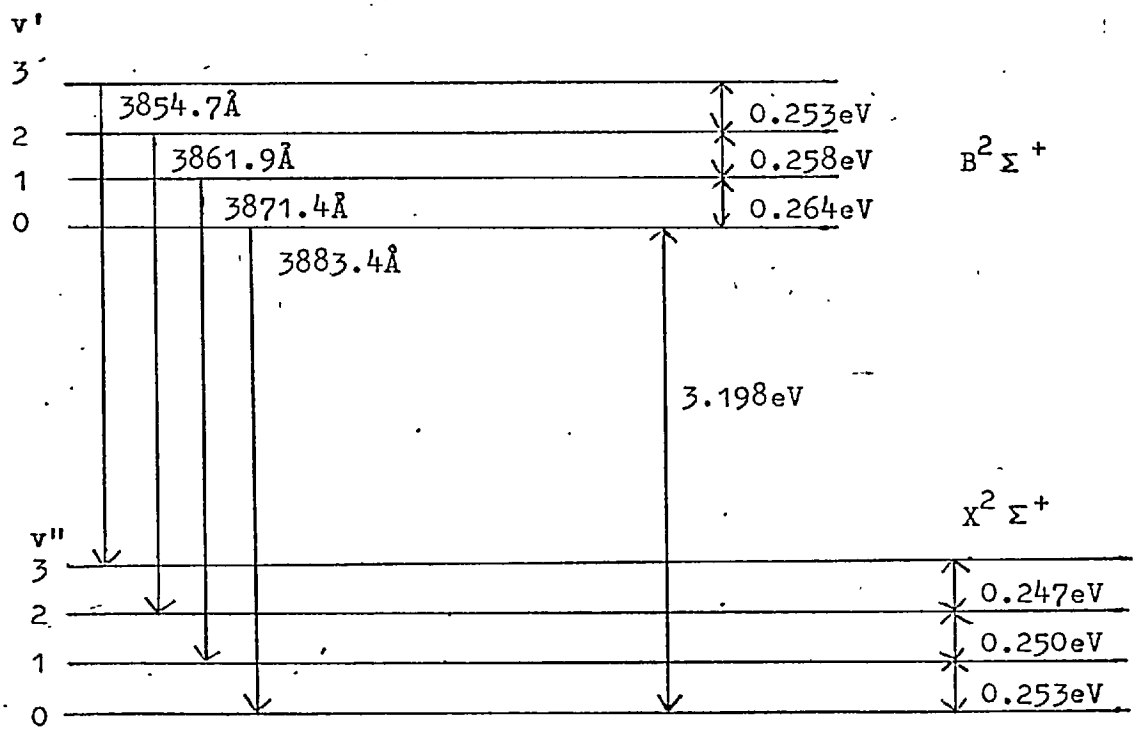


Fig.3-10 Vibrational Energy Levels of The CN 3883.4Å ($\Delta v = 0$) Sequence

Table 3-8

Burner Type	Apparent Temperature (°K)		
	Unseparated	Argon Separated	Nitrogen Separated
Circular	4730	4630	4150
Long path end on	6980	10200	3580
Long path sideways on	3545	4630	4220

is severe and significant differences may still be observed between different conditions. It may be seen that all of the results are well above the maximum flame temperature of 3228°K and that those with the long burner end on are particularly ludicrous. With the circular burner, separation reduces the observed temperature as expected but with the long slot burner separation gives an apparent increase in temperature due to the higher CN concentration. It should be clear from these results that a self-absorption effect is present which prevents any useful temperature determinations from the emission spectrum.

As mentioned earlier, more promising results were obtained by using the same method in absorption. Equation (3-12) was applied to the absorption spectra CN bands described in Section 3.4; i.e. those obtained from the slightly fuel rich nitrous oxide-acetylene flame on a circular burner. The 3883 and 3871Å peaks were sufficiently intense for accurate measurement in all three flames and gave the following temperatures:

Unseparated flame	3120°K
Argon separated flame	3060°K
Nitrogen separated flame	2990°K

The 3861 Å peak was only sufficiently well defined in the separated flames and for these two the 3871-3861 temperatures were:

Argon separated flame	3060°K
Nitrogen separated flame	2970°K

i.e. there is very good agreement between the two sets of results and the actual temperatures and their changes on separation are very close to those which were expected from previous experience with these flames.

3.6.4 Conclusions

A method has been described which, in theory, allows temperatures of flames containing CN to be measured with simple equipment and the minimum of experimental difficulty. In practice it has been found that successful results could not be obtained using the emission spectra because of the effects of self-absorption. It should be possible to avoid this for a number of useful flames. For example, the CN concentration drops markedly with a slightly more lean flame. The loss of intensity would be no real problem since the author would suggest using wider monochromator slits - ideally the best results should be obtained with a dispersion which completely separates the peaks to be measured but does not resolve any of the rotational fine structure. Under these conditions, the experience of the author and other workers suggests that the emission method should give temperatures close to the "actual" flame temperature, especially if the optical path length through the flame is kept to a minimum.

The absorption method appeared to give much more satisfactory results even under strong self-absorption conditions. However, it must be emphasized that the reason for this is somewhat uncertain since there are several theoretical difficulties to be resolved. First, Penner[25] has explained at some length (and, unfortunately, with extremely complicated mathematics) that conditions giving strong

self-absorption in emission may also affect the ratios of absorption intensities. In the author's opinion this effect should be very small under the conditions of measurement used here. Much more important is the theoretical basis by which the temperature is calculated from the heights of the absorption peaks. It was emphasized in Section 3.5 that ratios of K_1/K_2 should only be used qualitatively because they can only be measured from spectral line profiles using ultra-high resolution apparatus and that the same "integration" is not performed in absorption with the non-resolved peaks obtained with low dispersion apparatus. The situation is even more complicated with molecular vibrational bands since it is always uncertain whether the intensity ratios of band heads are the same as the ratios obtained by summing the intensities of all rotational peaks measured individually.

These problems will vary enormously with the experimental conditions. Therefore the absorption method requires calibration before it can be treated as reliable. This could be done by measuring the absorption spectrum under ultra-high resolution and calculating the true vibration band intensities for several bands. The work would be extremely laborious but if results in agreement with the "quick" method were obtained for several different flames the latter would prove very useful for future work. For the present, we may say that under the conditions used here the three flames should be subject to similar errors. The absorption method has, therefore, provided a useful estimate of the temperature drop on flame separation which is in good agreement with the "iron two line" results mentioned in Section 3.5.6.

Chapter IV

The Application of Separated Flames To Atomic Emission Spectroscopy

It has already been shown (Chapter 3) that flame separation considerably reduces the band and continuous emission of molecular species present in the secondary zone of a flame. As discussed in Chapter 2, this reduction in the signal strength and noise of the flame background is accompanied by the protection of reactive species in the interconal zone from attack by atmospheric oxygen. The combination of these effects has proved particularly advantageous in the determination of certain elements by flame emission spectroscopy. These advantages are illustrated and discussed below by way of some representative examples investigated by the author.

4.1 The Nitrogen Separated Air-Acetylene Flame For The Determination of Bismuth[113].

4.1.1 Introduction

Since the introduction of atomic absorption spectroscopy, the determination of bismuth at concentrations down to 1-2 ppm has presented no real problems. However, determination of trace quantities has, in the past, proved to be rather more difficult. The reason for this difficulty may be seen from the data given in Table 4-1, which shows the ten strongest bismuth emission lines obtained in flames, together with their approximate relative intensities.

By far the strongest line is the resonance line at 3067.7Å ($^4S_{1\frac{1}{2}} - {}^4P_{0\frac{1}{2}}$), but unfortunately this is extremely close to the strong

Table 4-1

Principal Flame Emission Lines of Bismuth

Wavelength Å	Intensity		gf	Energy Levels (eV)	
	Flame	Arc	Value	Lower	Upper
2228.3	17	100	0.010	0	5.562
2230.6	30	100	0.047	0	5.556
2276.6	7	100	0.014	0	5.444
2627.9	8	200	1.2	1.416	6.132
2898.0	35	500	4.0	1.416	5.692
2938.3	10	300	7.8	1.914	6.132
2989.0	10	250	2.3	1.416	5.562
3067.7	400	3000	0.99	0	4.040
3397.2	5	100	0.66	1.914	5.562

OH band heads at 3067.8 and 3063.7Å. Even the next strongest line at 2898.0Å lies on an OH band. Since most conventional flames which are hot enough to excite bismuth emission also give strong OH band emission from their secondary reaction zones, both of these lines shown poor signal to noise ratios. This is not the case with an oxy-cyanogen flame, and Gilbert[114] was able to obtain a detection limit of 3ppm for bismuth. However, this flame has several other disadvantages and at the present time has still not been used for routine analysis.
Dean and Carnes[115] were also able to obtain good results by using organic solvents and a special light guide and reported detection limits of 6.4 ppm at 2230.6Å in the primary zone of an oxy-acetylene flame and 2.8 ppm at 2898.0Å in an air-hydrogen flame. It has been possible to obtain a considerable improvement on these results by using the nitrogen separated air-acetylene flame, since this has a high enough temperature to excite the 3067.7Å line of bismuth but the OH band

emission is so low (see Section 3.2) that spectral interference becomes almost negligible. This effect can be seen in Fig. 4-1, which shows the spectra of the conventional and separated air-acetylene flames with 1000ppm bismuth solution aspirated. In the former, the bismuth 3067.7Å line cannot be distinguished from the OH peaks, but in the latter it stands out clearly against the flat background.

4.1.2 Experimental

Apparatus

The burner used is described in Section 2.4.1 and illustrated in Fig. 2-10. It was fitted in place of the standard emission burner on a Unicam SP900A flame spectrophotometer. This was used in its standard form in the emission mode, except that the photomultiplier tube was replaced by an EMI 9601B to give increased sensitivity in the ultraviolet region. Also, the needle valve/manometer assembly fitted to the instrument for monitoring the acetylene flow rate was sealed off and replaced by a calibrated rotameter (1-10 l./min.) fitted with a needle valve. Rotameters were also used to measure the air and nitrogen (shield) flow rates. The air was maintained at 7 l./min. for all of this work giving an atomizer pressure of 28 psig. This was found to give optimum results with the Unicam indirect atomizer and "cyclone" type spray chamber used to introduce sample solutions into the flame. The nitrogen shielding gas was usually set to about 10 l./min., but the exact flow rate was not critical. A Honeywell 0 → 10mV chart recorder was connected to the instrument for the measurement of noise levels and detection limits.

Reagents.

A 1000 ppm stock solution of bismuth was prepared by dissolution of the pure metal in a small volume of concentrated nitric acid and dilution with water. Working strength solutions of bismuth

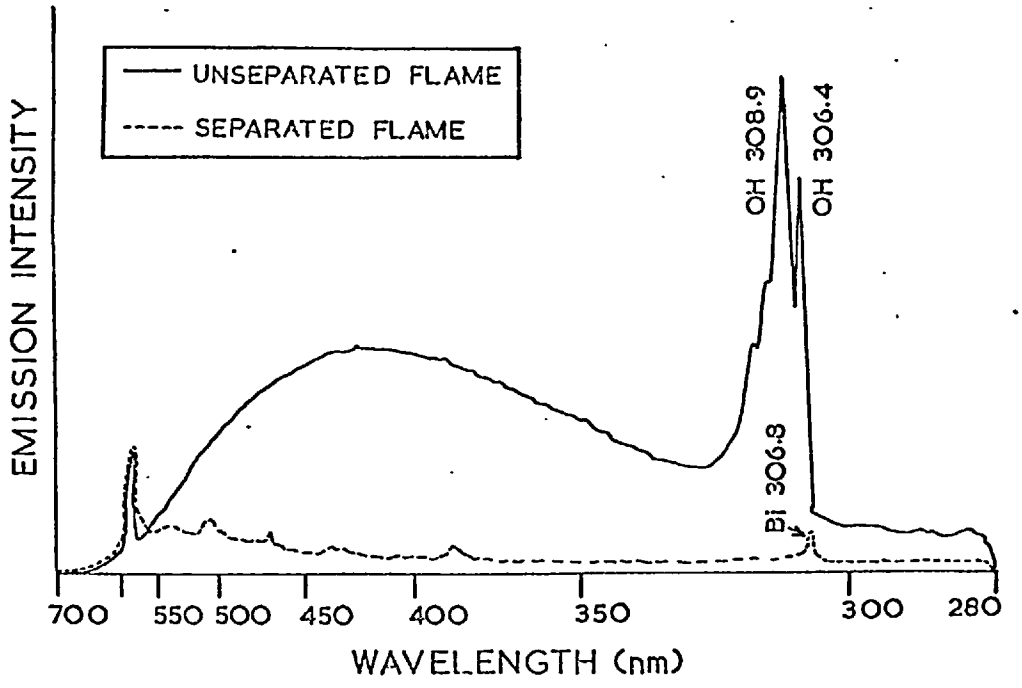


Fig. 4-1 Flame Spectra With 1000ppm Bismuth Solution Atomized

(The separated flame spectrum is shown with a scale four times greater than that for the conventional flame).

---

were prepared by further dilution of this solution. Ethanolic solutions containing up to 60% ethanol could be prepared simply by diluting the stock solution with the appropriate amounts of ethanol and water. However, if solutions containing higher percentages of ethanol were prepared, precipitation occurred after some hours.

4.1.3 Results

Height of observation in flame

The emission intensity in the separated flame decreases rapidly with height owing to the absence of the surrounding hot diffusion zone.

However, it was found that the maximum benefit from separating the flame was derived immediately above the primary zone, since the reduction of flame background is many times greater in the interconal zone than in the primary zone of the flame. It was also found that the position of maximum emission is relatively independent of the mixture strength and occurs just above the primary zone. In view of this, all measurements were made with the level of the bottom of the monochromator entrance slit just above the top of the primary zone, i.e. about 1 cm high in the separated flame. As the flame was merely placed about 5cm from the entrance slit without any lens system, stray radiation from the primary zone was screened from the slit by a small metal shield placed adjacent to the flame. The top of the flame was screened from the slit in a similar way so that the only radiation from the flame entering the slit was from a completely nitrogen-shielded region of the interconal zone ca. 2.5cm high.

Effect of acetylene flow rate

The effect of varying the acetylene flow rate on the emission signal at 3068Å is shown in Fig. 4-2. Results are plotted for (a) the flame background emission (i.e. OH), (b) the signal noise level and (c) the emission from an aqueous solution of bismuth. The results for (b) were obtained by taking the noise level as the distance between opposite extremities of a recorder trace produced during a period of 60 seconds by the flame emission at 3068Å from an aqueous (100ppm) bismuth solution.

It can be seen from Fig. 4-2 that the bismuth emission increases steadily as the acetylene flow is reduced until about 0.7 l./min. (this is simply due to the increasing flame temperature). However, Fig. 4-2 (a) and (b) show that both the OH emission and the signal noise level increase sharply when the fuel flow is reduced below about 0.9 l./min. The optimum fuel flow for the lowest detection limit was, therefore, chosen as 0.9 l./min.

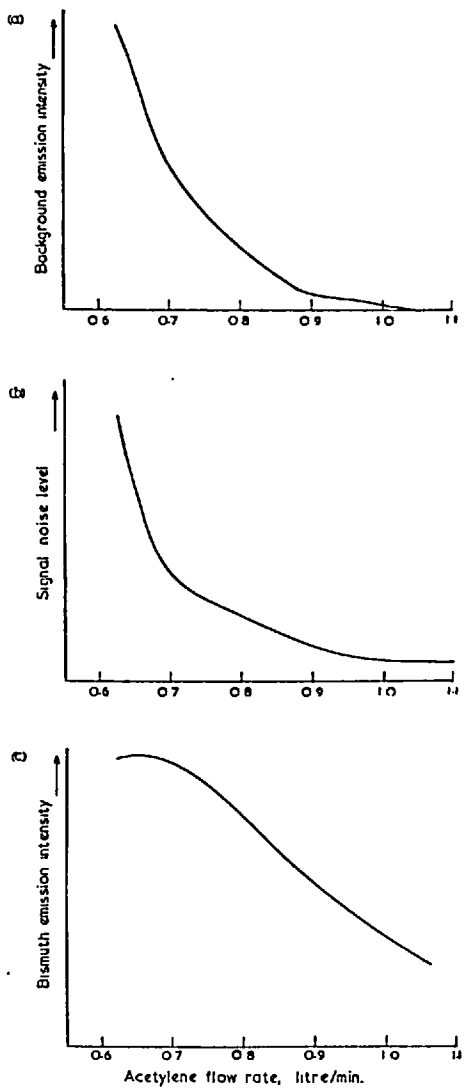


Fig. 4-2

Effect of Acetylene Flow Rate on Emission at 3068 Å

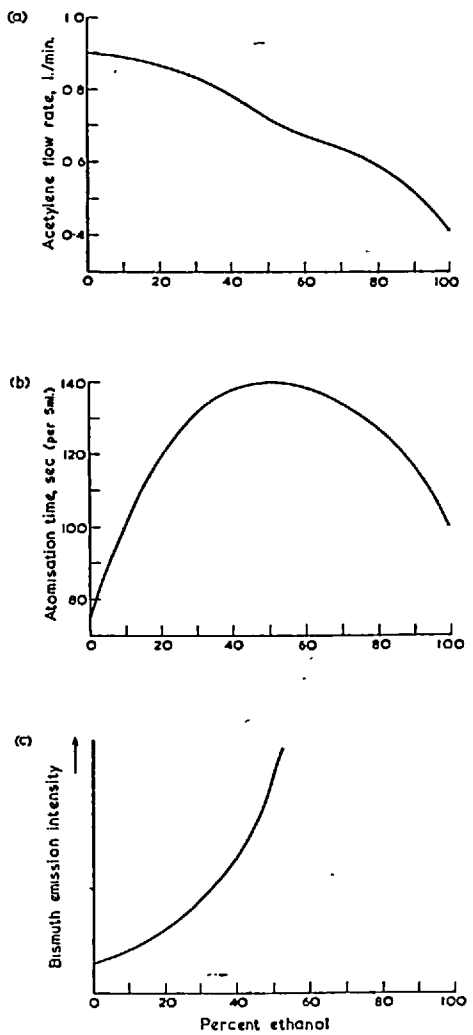


Fig. 4-3

Effect of Adding Ethanol To Aqueous Bismuth Samples

Effect of adding ethanol to samples

The most efficient use of organic solvents in flame spectrophotometry is obtained with a solvent extraction to increase the actual solution concentration of the sample which is nebulized. However, a significant improvement in detection limits may often be obtained simply by adding a water mixible organic solvent to the aqueous samples. This is principally because of the large increase in atomizer efficiency given by organic solvents. The effect of adding ethanol to the samples is shown in Fig. 4-3. Since the ethanol acts as a fuel, it is necessary to adjust the acetylene flow rate to maintain constant flame conditions. Fig. 4-3 (a) shows the acctylene flow rate needed with different percentages of ethanol to maintain the optimum flame conditions for bismuth determinations. Fig. 4-3 (b) shows the effect of ethanol on the uptake rate of the atomizer. A peak is reached at about 50%, but the efficiency of the atomizer (i.e. the percentage of sample actually reaching the flame) probably continues to increase with higher ethanol concentrations. The actual bismuth emission signal (Fig. 4-3 (c)) increases sharply up to about 55% ethanol, but then starts to level off. In view of this and because of the difficulty of preparing bismuth solutions containing higher concentrations of ethanol, samples of bismuth in 50% aqueous ethanol were used for detection limit measurements.

Detection limits

Bismuth detection limits in the nitrogen separated flame were measured with both aqueous solutions and solutions in 50% aqueous ethanol. The results were calculated on the basis of a 1:1 signal: noise ratio from recorder tracings obtained using 50ppm (aqueous solutions) or 5ppm (50% ethanol solutions) bismuth. The detection limits obtained were 2.0ppm in aqueous solution and 0.3ppm in ethanolic solution.

4.1.4 Conclusions

It has been shown that nitrogen separation of the air-acetylene flame reduces the bismuth detection limit at the 3067.7Å emission line from greater than 1000ppm to 2.0ppm (or 0.3ppm in ethanolic solutions). More important, these detection limits are somewhat better than the best values reported in the literature for any other emission line in any of the commonly used flames. Further, they compete very favourably with the best atomic absorption results reported for air-acetylene flames (0.1ppm[116]). Improved atomic absorption results may be obtained with air-hydrogen flames (0.03ppm[117]), but this flame is more prone to chemical interferences. Thus, the method described here provides a simple, sensitive determination of bismuth without the expense and inconvenience of providing the hollow cathode lamp needed for AAS and with only minor modifications to a standard flame spectrophotometer.

4.2 The Nitrogen or Argon Separated Nitrous Oxide-Acetylene Flame For The Determination of The Refractory Elements[118]

4.2.1 Introduction

The elements Al, Be, Ge, Hf, Mo, Nb, Si, Ta, Ti, V, W and Zr are usually grouped together as "the refractory metals" because of their common property of forming extremely stable, high melting point (i.e. refractory) oxides. They are used for a wide variety of industrial applications and in recent years several have become of even greater interest because of their applications to the aerospace and nuclear power industries. Thus, their precise and sensitive analysis is of particular importance. Unfortunately, their very refractory nature made the production of free atoms needed for atomic spectroscopic methods extremely difficult and only emission

spectrography in arcs or sparks could provide anything like the sensitivity needed. However, this technique is notorious as being more of an art than a science and by the early 1960's could no longer meet the demands of industry for ever more precise and sensitive determinations of these elements. Neither flame emission spectrophotometry, nor the then newly developed atomic absorption spectroscopy, could provide the solution since the flames available at that time were just not capable of breaking down the refractory oxides to form free metal atoms. The situation in flame photometry at that time is shown in Table 4-2. This table is made up of the best results taken from a large compilation published by Herrmann and Alkemade[119] and corrected to mid-1962 by P.T. Gilbert. It may be assumed that refractory elements for which no values are quoted give extremely poor sensitivities. The best results were obtained with molecular band emission in relatively cool flames, but in practice these would be of limited use because of the high level of chemical and spectral interferences. One or two good results were obtained for atomic lines by using a turbulent, oxygen sheathed oxy-acetylene flame with organic solvents (see also Section 2.2.4), but this flame is so noisy that the precision of determinations would have been very poor.

The situation was changed dramatically in 1965 with the introduction by Willis[120] of the nitrous oxide-acetylene flame for atomic absorption spectroscopy. This flame combines the high temperature associated with oxy-acetylene flames with an extremely reducing interconal zone and since 1965 has become as widely used in AAS as the air-acetylene flame (see Section 5.2.1 for a full discussion of AAS applications). The wide-spread interest in atomic absorption appears to have resulted in the overlooking of the fact that the refractory metal atoms formed in the nitrous oxide-acetylene flame could also be determined by their atomic emission. This situation was corrected in 1968 when Kirkbright, Semb and West showed (see Section 2.3.3 for full details) that by using a quartz-tube separated flame to reduce flame noise they could obtain by AES detection limits

Table 4-2

Element	Wavelength (Å)	Character (*)	Det. Limit (ppm)	Flame (**)	Solvent
Al	3961.5	A	0.3	OC	Water
	3961.5	A	0.05	OA	Hexone
	4842	B	0.15	OA	Hexone
Be	2348.6	A	0.4	OAO	Water
	4709	B	15	OH	Water
Ge	2592.5	A	14	AH	Isopropanol
Mo	5500	B	0.4	AH	Water
Nb	5500	B	2	AH	Water
Si	2516.1	A	7	OAO	Methanol
Ti	5450	B	0.22	OH	Water
V	5737	B	0.09	AH	Water
Zr	5740	B	8	OH	Water

* A : Atomic line emission
* B : Molecular band emission or a continuum

** AH: Air-hydrogen
** OC: Oxy-cyanogen
** OA: Oxy-acetylene
** OAO: Very fuel rich OA sheathed with oxygen
** OH: Oxy-hydrogen

---

which compared very favourably with those by AAS. Further proof of this was provided shortly afterwards by Pickett and Koirtyohann[121]. By using all the instrumental advances associated with AAS (in fact their prototype instrument was considerably better than most commercially available instruments) they were able to obtain extremely low detection limits for the refractory elements by AES using a standard, long path nitrous oxide-acetylene burner of the type supplied

for AAS. The case which can be made for the renewal of interest in AES for the analysis of the refractory elements is further advanced by the present work, in which it is hsown that by using a simple separated flame results equal to (and in some instances surpassing) those obtained by AAS can be obtained using a commercial flame spectrophotometer of relatively low resolution.

4.2.2 Experimental

Apparatus

Most of the work described in this section (including all measurements of detection limits) was carried out using the circular nitrous oxide-acetylene burner and separator described in Section 2.4.1 and illustrated in Fig. 2-10 in conjunction with the Unicam SP900A flame spectrophotometer described in Section 4.1.2. This was modified by fitting a heat shield made up of layers of asbestos and aluminium foil along the side nearest the flame. The shield was essential for preventing overheating of the monochromator, caused by the close proximity of the nitrous oxide-acetylene flame. This is necessary because no focussing system is used in the emission mode, the flame merely being placed as close to the entrance slit of the monochromator as possible. In fact, this caused the slit plates to overheat and resulted in rapid drifting of the signal. As a compromise, the flame was moved to about 10cm from the slit. Also, another asbestos shield was placed close to the burner with a hole cut in it such that only light from the red interconal zone of the flame could enter the monochromator. Although these precautions reduced the absolute intensity of the emission signals from elements nebulized into the flame, it was possible to obtain much more reproducible results and also lower detection limits (due to the reduced noise levels).

For comparison purposes, the effects of flame separation on the refractory metal emission were also measured using the long path

nitrous oxide-acetylene burner and separator described in Section 2.4.4 and illustrated in Fig. 2-15. This was used with the Techtron AA4 flame spectrophotometer described in Section 5.2.2. The instrument was used in the atomic absorption arrangement described there, except that the A.C. amplifier was short-circuited to allow it to amplify the D.C. emission signal from the flame. This avoided the use of the emission chopper accessory which would have restricted the light path and made a direct comparison between the different flames more difficult.

With both arrangements the standard nebulizer and spray chamber supplied with each instrument were used to atomize the sample solutions via the nitrous oxide supplied to the flame. However, in both cases all gas control units fitted to the instruments were by-passed, a set of three calibrated rotameters being used to control the flames. The outputs from the air and nitrous oxide rotameters were linked via a T-piece placed between them and the nebulizer so that the flames could be lit with air as oxidant before gradually changing over to nitrous oxide. The circular burner was used with a nitrous oxide flow rate of 4.0 l./min. giving a pressure of 15 psig at the Unicam nebulizer, but the long slot burner (which has a considerably larger exit slot area) was used with 8.5 l./min. giving a pressure of 25 psig. at the Techtron non-adjustable nebulizer. The acetylene flow rates used with these flames depended on the element being studied and are given in Section 4.2.3. The nitrogen or argon sheathing gas was used at about 10 l./min. with the circular separator and 20 l./min. with the rectangular one, although the exact flow rates were not critical.

Reagents

Analytical grade metals or their salts were used to prepare stock solutions of suitable strength. These were diluted with distilled water to provide working strength solutions except in the case of tungsten which was diluted with 0.2M hydrofluoric acid.

Molybdenum, 1000ppm.

Prepared by dissolution of ammonium molybdate in distilled water.

Aluminium, 1000ppm.

Prepared by dissolution of the metal foil in 1M hydrochloric acid.

Beryllium, 1000ppm.

Prepared by dissolution of the metal in the minimum quantity of aqua regia and dilution with distilled water.

Vanadium, 1000ppm.

Prepared by dissolution of the metal in 0.5M nitric acid.

Silicon, 50000ppm.

Prepared by dilution of B.D.H. reprecipitated silica in the minimum quantity of hydrofluoric acid.

Tungsten, titanium, niobium and ziranium, 5000ppm.

Prepared by dissolution of the metal in the minimum quantity of hydrofluoric acid and dilution with distilled water.

4.2.3 Results

Height of observation in flame

With the circular burner and the SP900A it was found that the best results with shielded or unshielded flames were obtained by setting the burner so that its top was exactly level with the bottom of the monochromator entrance slit and then adjusting the height of the aperture in the absestos shield until a position was reached where no light from the primary zone of the flame could reach the slit but light from the region immediately above it was not cut off - i.e. about the lower 1cm of the red zone was being used, With the long burner and the Techtron AA4, a more critical adjustment of the flame height for each element was necessitated by the focussing system used. The height was set to the optimum position as described for AAS in section 5.2.2.

Effect of acetylene flow rate

The effect of acetylene flow rate on refractory metal emission was measured in the circular flame using the SP900A, with a nitrous oxide flow rate of 4.0 l./min. The results are shown graphically in Fig. 4-4. The relative heights of the peaks for the different flames on each of these graphs should not be compared, since the amplifier gain was set to give approximately full scale deflection for the peak reading of each set.

It can be seen from Fig. 4-4 that the atomic emission intensities increase rapidly as the mixture is made more rich and that the maximum intensity is obtained for each element only within a very narrow range of fuel flows (particularly in the separated flames). With the separated flames this peak was usually obtained with fuel flows corresponding to a bright red zone. In the case of the conventional flame, a higher acetylene flow rate was always needed and usually the flame became quite luminous with streaks of incandescent carbon. In both types of flame, the decrease in signal occurring as the flame is made increasingly rich is largely due to the cooler flame obtained with such a mixture. However, it is also likely that efficiency of the flame in reducing the metal oxide deteriorates under these conditions (cf. the corresponding absorption results given in Section 5.2.3).

Effect of flame separation on atomic emission signals.

As was mentioned in Chapter III, the effects of flame separation depend a great deal on the nitrous oxide:acetylene ratio - if a lean flame is used, the signal from a refractory element may increase enormously whereas the same element in a very rich flame can actually show a decrease on shielding. To avoid the confusion resulting from this, all the measurements given below were recorded using the optimum fuel flow for the element/flame combination to which they refer. While this system has some disadvantages, it does allow

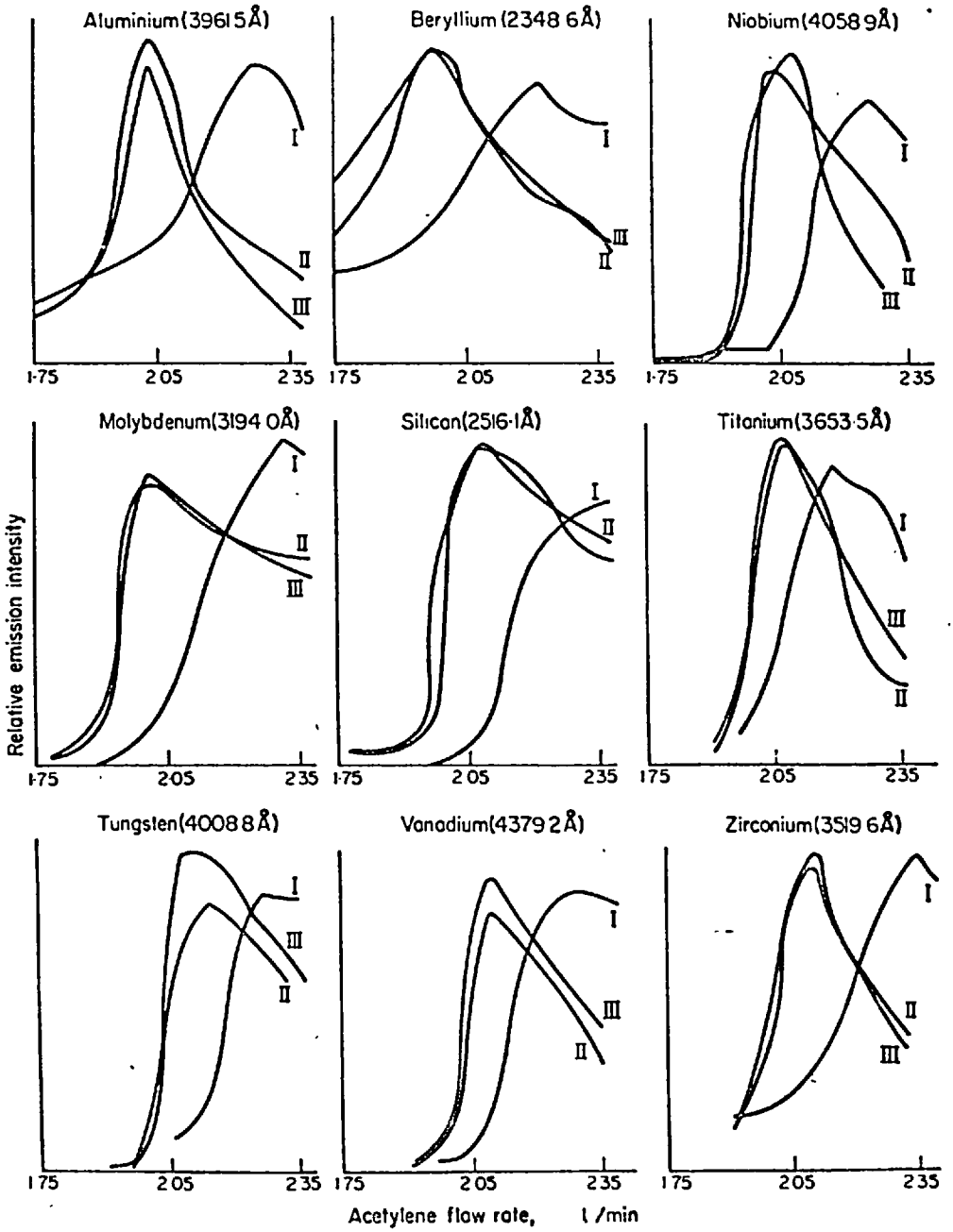


Fig. 4-4 Effect of Acetylene Flow Rate on Refractory Metal Emission

(I = conventional flame; II/III = nitrogen/argon separated flames).

the analyst to see the effect of flame separation on the best result obtainable (which is what he is interested in). In Table 4-3, the results are given for the circular burner/SP900A combination and for the long slot burner/Techtron AA4 combination. The latter were obtained at a later date and a number of extra results are given so that comparisons can be made with the AAS results quoted in Chapter V. For convenience, some of the AAS results from Section 5.2.3 have been converted to the same relative form as the emission results and are given in Table 4-3.

Table 4-3

Element	Wavelength (Å)	Relative Emission						Relative Absorption		
		Circular flame			Long flame					
		I	II	III	I	II	III	I	II	III
Al	3961.5	100	87	197	100	96	120			
	3092.7				100	106	128	100	131	150
Be	2348.6	100	41	62.5	100	67	79	100	124	132
Ge	2651.6				100	53	61	100	119	124
Mo	3194.0	100	61	103	100	106	127			
	3132.6				100	106	124	100	117	120
Nb	4058.9	100	127	334	100	103	148			
	3349.1				100	112	154			
Si	2516.1	100	43	96.5	100	43	57	100	117	135
Ti	3653.5	100	128	206	100	100	127			
	3998.6	100	133	208	100	106	139			
	3642.7				100	99	125	100	157	190
V	4379.2	100	124	254	100	104	125			
	3184.0				100	107	127	100	149	164
W	4008.8	100	118	235	100	110	122			
	2551.4				100	76	88			
Zr	3519.6	100	72	167	100	115	135			
	3601.2				100	104	125	100	122	165

I = Conventional, II = Nitrogen separation, III = Argon separation.

The following points should be noted in connection with the results shown in the table.

1. The best emission results in the long flame are almost always obtained with a slightly more lean flame than the best absorption results. This is true in the conventional or separated flames and suggests that the optimum absorption conditions correspond to the most reducing flame whereas the optimum emission conditions are the best compromise between a very reducing flame and the highest temperature.

2. Since the atomic absorption signal is a direct measure of the number of free atoms present, one would not expect the emission signals to show a larger increase on flame separation than the absorption signals (unless some emission was chemiluminescent and was enhanced by separating the flame). This is, in fact born out by the emission results from the long flame but not for several elements in the circular flame. This latter effect is almost certainly a result of the optical system of the SP900A; i.e. the monochromator field of view is sufficient to take in the whole flame, and as the red (reducing)zone is considerably enlarged on separation (especially with an argon sheath) the increase in signal is due to an increase in the number of free atoms in the field of view as well as to the increase in their actual concentration per unit volume of flame. Even if the circular flame were used with a focussing system such as that of the AA4 this effect would still be apparent, since the length of flame red zone along the optical path increases considerably on separation (whereas with the long slot burner this effect is negligible).

3. With the absorption signals, the effect of flame separation really just depends on the properties of the particular metal oxide. However, the relative size of the emission signals depends to an even greater extent on the particular wavelength being monitored. At long wavelengths, flame separation gives a large increase in the emission signal,whereas at short wavelengths a decrease is often recorded. This is simply a result of the drop in flame temperature

produced by separation (see Section 3.6); the shorter the wavelength of the line, the larger is the drop in emission signal produced by a given fall in temperature. In Fig. 45-(a) the results for the circular shielded flame given in Table 4-3 have been plotted against wavelength in the form of the change in emission relative to the conventional flame produced by separation. It can be seen that although an approximation to a straight line is obtained, the points are somewhat scattered. However, this is to be expected since the different elements used are not all equally refractory and will show different increases in atomic population on shielding. This can be corrected by using the absorption results given in Table 4-3, since these are a direct measure of the change in atomic population on flame separation. The values obtained after normalizing the emission results in this way (only for those elements which were used for absorption studies) are plotted in Fig. 4-5 (b) on the same scale as before. It can be seen that a much better straight line is obtained. This is fairly conclusive evidence that thermal equilibrium prevails in the red interconal zone of the circular flame, although the results are still too scattered to be absolutely certain of this.

4. The emission results from the long flame (obtained with the Techtron AA4) are plotted in exactly the same way in Fig. 4-6; (a) and (b) show the uncorrected results for nitrogen and argon separation respectively and (c) and (d) show some of the same results after normalizing with the atomic absorption results. These graphs look completely different from those given in Fig. 4-5 and at first sight the points plotted do, in fact, appear to be scattered rather at random. If, however, one allows for a high level of inaccuracy in the individual readings (which might be caused by varying self-absorption in the long flame), it may be possible that many of the points from 3000 - 4500 Å lie on a straight line <u>parallel</u> to the wavelength axis. This suggests, in effect, that the change in emission signal on separation no longer alters enough with wavelength to show up significantly. If this is indeed the case there are two immediate

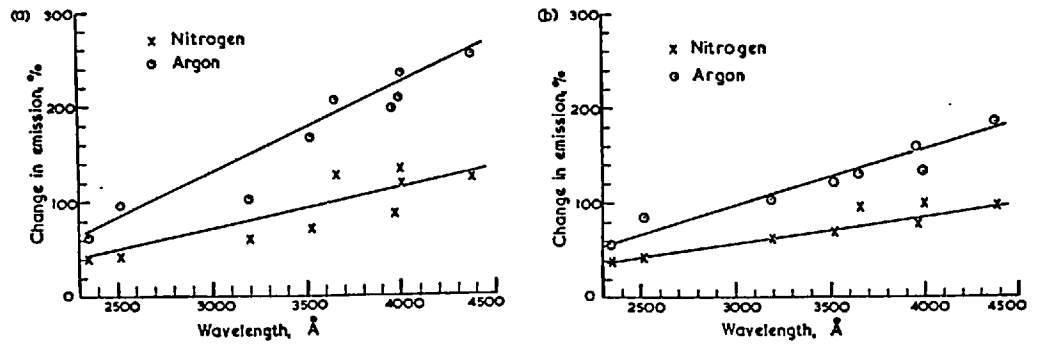


Fig. 4-5 Variation With Wavelength of Effect of Separation on Emission Signal With The Circular Flame

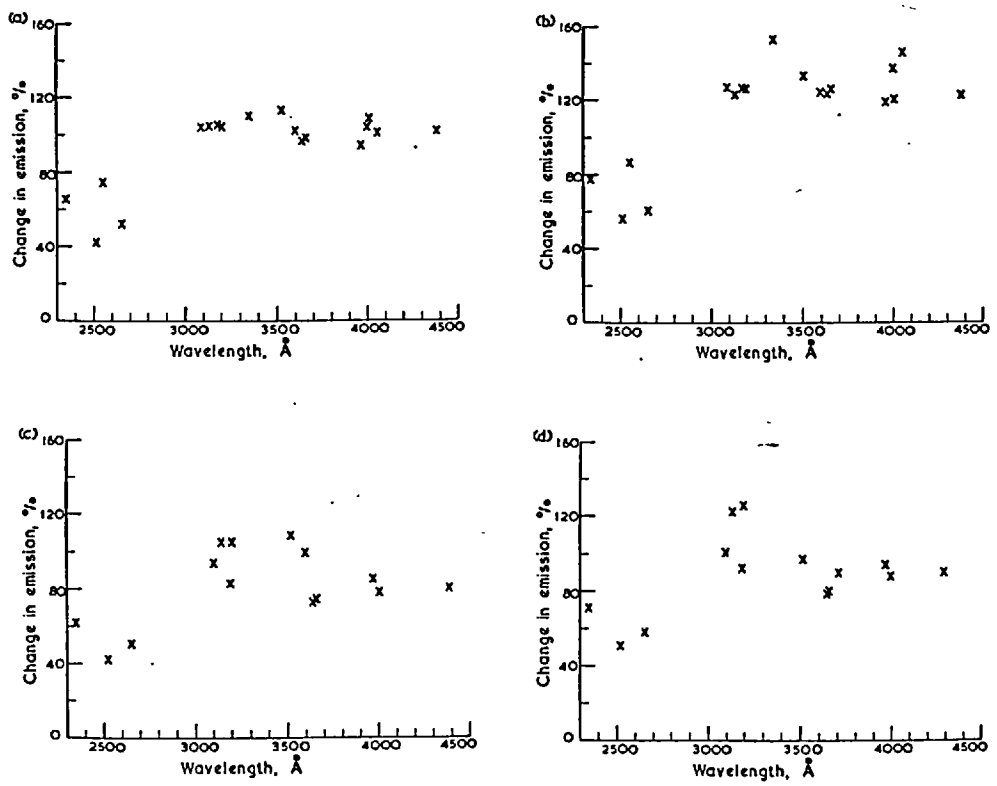


Fig. 4-6 Variation With Wavelength of Effect of Separation on Emission Signal With The Long Path Burner

(See p.165 for explanation of the diagrams).

possible explanations - either the flame is no longer in thermal equilibrium or there is only a small temperature change on separation. This then poses the question of why either of these factors should show up in the long flame but not the circular one. The most likely explanation lies in the optical arrangements used - with the long flame the Techtron AA4 monochromator was really viewing only the very centre of the red zone immediately above the primary zone. Thus any chemiluminescence would be more apparent and any temperature change would be kept to a minimum. On balance, appreciable changes in any chemiluminescence which might (if at all) be present seem unlikely and the small temperature change seems the most probably explanation of Fig. 4-6.

Notes on individual elements

The brief notes on each element given in this section are merely intended to record some useful facts observed during this work and which could not conveniently be fitted into the tables of results. They include such things as reasons for the choice of a particular line as the best one (this can sometimes vary with the monochromator used); choice of the best slit-width for each element; indications of the range of linearity of calibration graphs, etc. At this point it is worth noting that with a low resolution instrument such as the SP900A, the selection of the monochromator slit width giving the best detection limit is particularly difficult. This is because the size of the emission signal can be increased (until the noise level becomes too high) by either opening the slit further or by increasing the amplifier gain. In regions of low flame background the slit can be opened fully without causing too serious noise levels, but in other cases a small increase in slit width beyond the optimum may increase the spectral band pass of the monochromator sufficiently to encompass a nearby flame band and cause a serious increase in signal noise level. The empirical method used by the author to solve this problem was as follows. At a given slit width, the galvanometer of the

instrument was set to zero using the "backing-off" device provided while water was sprayed into the flame. A signal was then measured for an appropriate solution of the element being determined. The slit width was then altered and the galvanometer was rezeroed on water by using the amplifier gain control (the backing-off control being left untouched). A new signal from the same solution of the element was then measured. This was repeated at different slit widths and the combination of slit width/amplifier gain giving the best results was chosen. Operator judgement was necessary in some cases to decide when further increases in signal were accompanied by too large an increase in signal noise. Also, if two or more combinations gave similar signal size, the pen recorder was used to decide which gave the best signal to noise ratio.

Aluminium gives only three reasonably strong flame emission lines, even in this strongly reducing flame. These are 3961.5, 3944.0 and 3092.7 Å and the latter is much weaker than the other two. These lie rather close to the CN 3883Å band head and with the SP900A are observed on a sloping background. The 3961.5Å line is the stronger of the two and lies further from the band head so that it was chosen. Because of the proximity to the CN band, a narrow slit width was needed, 0.04mm being used for the conventional flame. The aluminium solution used for measuring detection limits was prepared using aluminium metal dissolved in hydrochloric acid because it was found that solutions prepared from the sulphate [$Al_2(SO_4)_3 . 16H_2O$] gave much smaller signals. A test calibration curve was found to be linear from 0.3 to 10ppm.

Beryllium gives only one strong flame emission line, at 2348.6Å. The low flame background from the separated flames in this region allowed the maximum slit width of 2.0mm to be used, but this had to be reduced to 0.3mm in the conventional flame. A linear calibration curve was observed up to 10ppm.

Molybdenum gives its principal flame emission lines at 3132.6, 3170.3, 3194.0, 3798.3, 3864.1 and 3903.0Å. The 3864.1Å line lies right on the 3883Å band and cannot be used. 3798.3 and 3903.0Å lines are the strongest of the others but lie too close to the CN band to be detected by the SP900A unless very strong solutions and a narrow slit width are used. The other three lines give approximately the same emission intensities but 3132.6 lies between the OH (3089Å) and CH (3143Å) band heads and 3170.3 also lies on a strong part of the OH band. Therefore, the 3194.0Å line was chosen as the most suitable (with a better monochromator such as on the AA4, the 3903 Å line would probably give better detection limits). A slit width of 0.065mm was used with the separated flames but was reduced to 0.04mm with the conventional flame because of the high noise level from the OH band.

Niobium gives a number of relatively strong emission lines in the nitrous oxide-acetylene flame. The most intense group is 4058.9, 4079.7, 4100.9 and 4152.6Å and of these the 4058.9Å line is the strongest and lies on the most level background. It was found that the slit width had little effect on the size of the signal and 0.02mm was chosen for the unshielded flame and 0.03 and 0.04mm for the argon and nitrogen separated flames.

Silicon gives several strong lines in the U.V. region of the spectrum, not all of which can be resolved with the SP900 monochromator. The main ones are 2881.6, 2528.5/2524.1, 2516.1/2514.3 and 2506.9Å and of these the most intense peak is 2516.1/2514.3. Because of the relatively low flame background emission at this wavelength, a wide monochromator slit could be used; 0.25mm being chosen for the conventional flame and 1.0mm for the separated flames.

Titanium gives two main groups of strong emission lines in this flame. The first (and more intense group) is made up of

3998.6, 3989.8 and 3958.2/3956.3Å, and of these the strongest is 3998.6Å. The second group is made up of the 3653.5, 3642.7 and 3635.5Å lines and of these the 3653.5Å line is slightly more intense. Although the 3998.6Å line is much more intense than 3653.5Å, the latter lies in a region of much lower flame background intensity so that both lines gave similar detection limits. Because of these differences in background emission a slit width of 0.03mm was used at 3998.6Å. whereas 0.05mm was possible at 3653.5Å.

Vanadium gives a large number of atomic emission lines, the strongest ones in the nitrous oxide-acetylene flame being at 4488.9, 4408.5/4406.1 and 4379.2Å. The latter is the strongest and as the flame background is no worse for this line than the others it was selected as the optimum wavelength. The optimum slit widths were found to be 0.04mm for the conventional flame and 0.05mm for the separated flames.

Tungsten gives several emission lines above 4000Å, but by far the strongest of those in this flame is 4008.8Å. This also lies in a region of reasonably low, level background in the separated flames so it was chosen for tungsten determinations. The slit width was found to have little effect on the sensitivity and 0.02mm was chosen for the conventional flame with 0.04 and 0.05mm for the argon and nitrogen separated flames. It was found that the tungsten emission signal depended quite strongly on the concentration of hydrofluoric acid present. Best results were obtained by using 1ml. of 40% hydrofluoric acid per 100ml. of 5, 10 or 20 ppm solutions (plus the trace already present from diluting the stock solution).

Zirconium gives a relatively large number of lines in the nitrous oxide-acetylene flame. The strongest ones lie at 3764.4, 3601.2 and 3547.7Å, but all are in regions of noisy, steeply sloping background emission and are not suitable for use with the low resolution monochromator of the SP900A. The next most intense lines are at 3663.7, 3623.9 and 3519.6Å and of these the latter probably gives the best compromise between high intensity and low noise levels.

It allowed a slit width of 0.03mm to be used with the conventional flame and 0.06mm and 0.08mm with the argon and nitrogen shielded flames. The calibrations were observed to be linear up to 100ppm. It was found that, as with aluminium, addition of sulphate gave a large depression of the emission signals.

Detection limits

The detection limit of each element studied was measured in the conventional and nitrogen and argon separated flames. This was done by recording a signal using a solution of the metal which was relatively close to the detection limit then calculating the concentration in ppm which would give a signal to noise ratio of 2:1. The maximum damping provided by the SP900A was used, but no extra damping was provided to the recorder output: so that realistic time-constants were maintained. The results are summarized in Table 4-4.

Table 4-4

Element	Wavelength (Å)	Detection Limit (ppm)		
		Conventional	Nitrogen	Argon
Al	3961.5	0.4	0.04	0.02
Be	2348.6	1.5	0.3	0.15
Mo	3194.0	20	0.5	0.3
Nb	4058.9	0.5	0.09	0.06
Si	2516.1	60	10	6
Ti	3653.5	7	1	0.5
Ti	3998.6	5	0.4	0.2
V	4379.2	2	0.08	0.05
W	4008.8	10	0.8	0.4
Zr	3519.6	9	2	1.2

4.2.4 Conclusions

An extensive study has been conducted on the effect of separation of the nitrous oxide-acetylene flame on the flame emission signals from the so-called refractory elements. It has been shown that with a flame spectrophotometer such as the Unicam SP900A, this technique results in improvements in detection limit ranging from 7 to 60-fold (depending on the element being determined). Experimental evidence has also been obtained on the reasons for these improvements, the conclusions from which may be summarized as follows.

1. Flame separation greatly reduces the amount of OH and CO emission received by the SP900A detector over a wide range of wavelengths. The reduction in signal noise associated with this, combined with the fact that flame separation allows less fuel rich mixtures to be used, gives a considerable improvement in the signal to noise ratios recorded for all of the refractory elements. This is in spite of the fact that separation actually increases the strength of the CN, C_2 and CH emission observed from the interconal zone of the flame and that it decreases the absolute emission signal observed at some analytical lines in the ultra-violet.

2. Further, the improvement in the reducing power of the flame resulting from flame separation produces a higher-concentration of refractory metal atoms in the flame and, in the case of the SP900A, it is possible to observe these free atoms over a wider area of the flame. This means that in spite of the drop in flame temperature associated with flame separation, an increase in the absolute emission intensity is actually observed for many of the refractory elements.

3. The approximately two-fold improvement of argon separation over nitrogen separation observed with the SP900A has been shown to be caused by two main factors. Firstly, monatomic argon removes

less heat from the flame than diatomic nitrogen, thus causing a smaller drop in flame temperature. Secondly, argon appears to cause less disturbance to the flame gases than nitrogen, possibly again because of its lighter weight. The effect of this may tentatively be said to result in less entrainment of air and dilution of the reducing atmosphere at the outside of the flame. This is observed as an increase in the overall size of the red zone and hence of the "useful" flame area viewed by the monochromator of the SP900A. It is also possible that to a small extent some improvement of reducing nature is obtained throughout the red zone (since the rates of diffusion of all species concerned are extremely high).

4. When a high resolution monochromator and elaborate focussing system are used, as with the Techtron AA4, the effects of reduced signal noise and larger useful flame area are no longer so pronounced. However, the enhanced reducing power of the flame is still important and this combined with a useful (if somewhat smaller) reduction in signal noise is sufficient to retain the analytical utility of flame separation. This is, indeed, borne out by the results to be presented in Section 4.3).

4.3 The Use of The Separated Nitrous Oxide-Acetylene Flame For The Removal of Interferences In Flame Emission Spectroscopy.

4.3.1 Introduction

The work presented in Section 4.2 has shown how separation of the nitrous oxide-acetylene flame extends to flame emission spectroscopy its utility for the determination of refractory elements which had previously been reported by other workers for atomic

absorption spectroscopy. Another well known application of the nitrous oxide-acetylene flame in AAS has been for the determination of those elements which are particularly prone to chemical interferences in cooler, less reducing flames. The classic examples of this type of element are calcium and magnesium. Their determination is essential in a wide range of sample types, ranging from biological fluids to mineral ores. In almost all cases these determinations are necessary in the presence of large concentrations of elements and anions which cause severe interferences in conventional flames (particularly with calcium) - e.g. Al, PO_4, Fe, Na, V and each other. Although some of these interferences are spectral in nature, most of them can be attributed to the presence in the flame of stable species (e.g. mixed oxides) which prevent the formation of free atoms of the element being determined. Amos and Willis[122] indicated in their first full paper on the use of the nitrous oxide-acetylene flame for AAS how its highly reducing atmosphere was capable of breaking down these species and removing many of the interferences observed in the air-acetylene flame. Shortly afterwards, Manning and Capacho-Delgado[123] illustrated that most of the interferences still observed in the nitrous oxide flame were ionization effects and could be removed by ensuring that an excess of an easily ionizable element (e.g., potassium) was always present. Fleming[124] showed that several elements still interfered with magnesium (which does not give significant ionization), but that this could be avoided by diluting the nitrous oxide with the correct percentage of air to give a flame of exactly the right temperature. In the past year or two many workers have reported that the alkaline earths may be determined by AAS with a nitrous oxide-acetylene flame in a wide variety of matrices without elaborate sample preparation. For example, Taylor and Belcher[125] found that by using the nitrous oxide-acetylene flame they could determine calcium and magnesium in steels with good sensitivity and freedom from interferences simply by

adding 1500ppm (Sr + Na) to samples. The most detailed study of interferences to be observed in the AAS determination of calcium and magnesium is that by Ramakrishna et. al.[126].

Obviously, all of these advantages reported for AAS will also apply to atomic emission spectroscopy. As with the determination of the refractory elements, this fact occurred to both the present author and to Koirtyohann and Pickett (see Section 4.2.1). Shortly after the work described below was completed, these authors reported in some detail[127] on the use of a conventional, long path nitrous oxide-acetylene flame for the determination of Ca, Mg and the other alkaline earths by AES. As mentioned earlier (Section 4.2.1) the main difficulty with using this flame for emission work is the high background intensity and noise, and Koirtyohann and Pickett overcame this by using a specially built instrument with a high resolution monochromator and high gain amplifier. In the present work, the alternative approach of flame separation has been used, thus allowing a conventional flame spectrophotometer (the Techtron AA4) to be employed. It will be shown that AES provides a simple determination of calcium and magnesium with good sensitivity and the same freedom from interferences as AAS. Iron has been studied under the same conditions, both as a "control" element and because its determination is often required in the same samples as the alkaline earths. In all cases a full comparison with the air-acetylene flame has been made as this is also useful for the determination of these elements if interfering species are absent and it is desirable to compare fully the relative merits of the two flames.

4.3.2 Experimental

Apparatus

The work with calcium and magnesium was carried out with the

shortened circular separator described in Section 2.4.2. This was used with a standard Meker-type head for air-acetylene flames and with the special head described in Section 2.4.3 for nitrous oxide-acetylene flames. Both burner heads were fitted with brass adaptors so that they could be fitted directly into the burner/atomizer unit of the Techtron AA4 spectrophotometer with which this work was carried out. Apart from the burner, this instrument was used in its standard form, one of the lenses supplied for AAS being used to focus the flame on to the monochromator entrance slit. The detection system was used in its D.C. form, as described previously. A Servoscribe chart recorder was fitted for the measurement of detection limits. Calibrated rotameters were used to control the air, nitrous oxide and acetylene flow rates. Sample solutions were sprayed via a Techtron adjustable atomizer using either air at 15 psig (6 l./min.) or nitrous oxide at 10 psig. (4 l./min.). The acetylene flow rates requires for the various elements and flames are given in Section 4.3.3.

Reagents

Stock 10,000ppm solutions of the elements to be studied were prepared as shown in Table 4-5, using analytical grade metals or their salts.

Table 4-5

Element	A.W.	Compound Used	M.W.	Wt. taken*	Dissolved in
Ca	40.1	$CaCO_3$	100.1	12.5 gm.	0.5N HCl
Mg	24.3	$MgCl_2.6H_2O$	203.3	41.8	Water
Fe	55.9	Electrolytic iron powder	-	5.0	0.5N HCl
Al	27.0	Analar metal foil	-	5.0	3.5N HCl
Na	23.0	NaCl	58.5	12.7	Water
K	39.1	KCl	74.5	9.5	Water
PO_4^{3-}	-	Analar phosphoric acid (H_3PO_4)	-	-	-

(* For 500ml. of 10,000ppm solution).

N.B.1. All the solutions (except the phosphoric acid) have the chloride ion as their common anion. This was chosen because :

(a) Previous workers have shown that this is the only common acid anion which does not interfere with Ca and Mg determinations even in the cool air-hydrogen flame (see for example Ref. 128).

(b) It is often present in high concentrations in samples used for Ca and Mg determinations (e.g. blood plasma).

N.B.2. There is some confusion in the literature as to which species should be used to express the concentration of the interfering ion when measuring the effect of phosphoric acid on Ca, Mg, etc. To avoid this here, all phosphate solution concentrations are given as molarities and the approximate relations to ppm "(PO_4^{3-})" and ppm "P" are shown in Table 4-6.

Table 4-6

Molarity of H_3PO_4	Approx. ppm PO_4^{3-}	Approx, ppm P
0.0001	1	0.33
0.001	10	3.3
0.01	100	33
0.1	1000	330
0.5	5000	1650
1.0	10000	3300

4.3.3 Results

Optimum conditions

The instrumental and flame settings giving the best sensitivities and detection limits for the three elements are summarized in Table 4-7. The optimum flame heights are not quoted

because it was found more convenient to optimize the position of the flame each time before taking a set of readings. The fuel flow values given in Table 4-7 were also used with the interference measurements so that a completely fair picture could be presented. This was sometimes a disadvantage as explained later.

Table 4-7

Condition	Ca	Mg	Fe
Wavelength of line (Å)	4226.7	2852.1	3719.9
Monochromator slit width:			
Air-acetylene flames (μ)	100	125	125
Nitrous oxide-acetylene flames (μ)	50	125	125
Acetylene flow rate (l./min.):			
Air-acetylene flames	0.83	0.70	0.73
Nitrous oxide-acetylene flames	1.52	1.56	1.48

Detection limits

These were measured for all three elements in all four flames (i.e. conventional and separated air-acetylene and nitrous oxide-acetylene). The results were calculated on the basis of a signal to noise ratio of 2:1. The amplification of the signal was increased until the noise level was easily measurable (using both the Techtron amplifier gain control and, if necessary, the sensitivity control of the Servoscribe recorder). The detection limits obtained are summarized in Table 4-8. It can be seen that, merely from the point of view of the best detection limits, the air-acetylene flame is superior to conventional nitrous oxide-acetylene for all three elements. This is entirely due to the high noise levels of the latter and if the separated nitrous-oxide-acetylene flame is used it offers a very worthwhile improvement in detection limit for Ca and Mg and only a small increase in detection limit for Fe.

Table 4-8

Flame	Detection Limit (ppm)		
	Ca*	Mg	Fe
Conventional air-acetylene	0.022	0.235	0.715
Separated air-acetylene (N_2)	0.008	0.235	0.50
Conventional N_2O-acetylene	0.03	2.1	5.0
Separated N_2O-acetylene (N_2)	0.0017	0.1	2.06
" " " (Argon)	0.0027	0.077	1.1

(* All values in presence of 1000 x excess of K+ to suppress ionization).

Interferences

The detailed interference studies made for each element are summarized in tabular form. Unless otherwise stated, all readings were zeroed using distilled water. Also, all readings shown are normalized to a value of 50 with no interfering anions present. This makes the trend of the results easier to interpret but, of course, prevents comparisons between relative signal strengths of the different flames. Some brief explanatory notes are given after each table as to the types of interferences observed and any special circumstances are noted. The key letters used in each table are:

A: Conventional air-acetylene flame.

B: Separated air-acetylene flame.

C: Conventional nitrous oxide-acetylene flame.

D: Separated nitrous oxide-acetylene flame.

(a) Calcium

All readings were taken using 1ppm Ca. Except for the test for K interference, all Ca solutions including the standard contained an excess of 1000ppm K to suppress ionization. This allows all the interferences recorded for the other elements to be unaffected by changes in Ca ionization. The readings are given in Table 4-9.

Table 4-9

Interfering Element	Concentration	Relative Signal			
		A	B	C	D
-	-	50	50	50	50
K	10 ppm			80	80
"	50			92½	92
"	100			96	95½
"	500			96	95½
Mg	10	59½	66	52½	51
"	100	63	71½	52½	52½
Al	5	8	5	51½	50½
"	10	14	11½	50	49
"	80	48	50	54½	52½
Fe	50	49½	48	50½	50
"	100	48½	47	50½	51
"	500	41½	30	49½	50½
"	800	37	26	50	50
* PO_4^{3-}	0.0001M	48½	48	49	49½
"	0.0005	47	43	50	50½
"	0.001	46	39	49½	49½
"	0.010	39	34	46	46
"	0.015	40	34	43	44
"	0.100	26½	19½	41	40
"	0.500	20	17½	32	33

(* Results were corrected using a blank solution for the zero reading because of Ca in the phosphoric acid used).

It can be seen that all the elements give serious interference in the air-acetylene flame, Mg giving an enhancement of signal and Al, Fe and PO_4 a depression. The interferences caused by Mg, Al and Fe are almost completely removed when the nitrous oxide-acetylene flame is used and that due to PO_4 is greatly reduced. It was found that by using a much more fuel rich nitrous oxide flame (i.e. more reducing), almost all interference by the PO_4 could be removed as well, although this advantage was off-set by a poorer detection limit.

The interference caused by Mg is due to band emission from MgO and MgOH. The depression caused by the other elements is due to the formation of complex mixed compounds and is well known. The result with Al whereby the depression decreases as the Al concentration increases is most odd. If it were due to the presence of Ca in the Al solution, one would expect a large enhancement of signal in the nitrous oxide flame and this was not observed. One possible explanation is that when excess Al is present the complex formed between the two elements and oxygen starts to break up releasing Ca atoms. This has been discussed in detail by Herrmann and Alkemade(Ref. 119, p. 302ff.).

(b) Magnesium

All readings were taken using 10ppm Mg. The results are given in Table 4-10.

It can be seen that interferences in the air-acetylene flame are much less serious than for Ca and that there is no ionization effect, even in the nitrous oxide flame. Ca and PO_4 do not interfere at all, and the interferences from Al and Fe are not too serious. All interferences are removed by using the nitrous oxide-acetylene flame.

The depression of the Mg signal by Al is caused by compound formation. This has been studied in detail by Harrison and Wadlin[129]. They conclude that the interference is caused by the formation of the spinel $MgO.Al_2O_3$, and they too found that the nitrous oxide flame would break down the spinel if conditions were carefully chosen. They

also point out that under certain flame conditions this type of interference can appear as either an enhancement or depression of the signal, but offer no explanation. This was in fact observed by the author for the effect of Fe on the Mg signal in the air-acetylene flame (see Table 4-10).

Table 4-10

Interfering Element	Concentration	Relative Signal A	B	C	D
-	-	50	50	50	50
K	100 ppm	50	50½	50	50
"	500	48	48	48½	48
"	1000	50½	50	50	50
"	5000	51	50½	51	51
* Ca	100	52	50	50	50
"	500	50	49½	50	50
"	1000	52	51	50	50
Al	100	45	46	50	50
"	500	41½	41½	52	50½
"	1000	25	40	50	50
Fe	100	55	56	50½	50½
"	500	46½	44	50	50
"	1000	51½	52	50	50½
PO_4	0.001M	50	50	50	50
"	0.01M	49	51	52	50½
"	0.1M	47	50	50	49½
"	0.5M	50	49	50	45½

(* Results were corrected using a blank solution for the zero reading because of Mg in the Ca stock solution).

(c) Iron

All readings were taken using 10ppm Fe. The results are given in Table 4-11.

Table 4-11

Interfering Element	Concentration	Relative Signal A	B	C	D
-	-	50	50	50	50
K	100 ppm	51½	52	51	52
"	500	49½	50	50	50
"	1000	50	50½	50	50
"	5000	50	50	50½	50
Ca	100	53	54	50½	50
"	500	58½	58	52	52½
"	1000	67	67½	56	56½
Mg	100	100	96	50	50
"	500	140	>200	51	50
"	1000	>200	>200	57	58
Al	100	50	50	50	50
"	500	51½	52	51	51½
"	1000	53	52	50	50
PO_4	0.001M	54	55	50½	50
"	0.01	53	62	50	50
"	0.1	60	60	51	51½
"	0.5	75	74	50	50

It can be seen that again there is no ionization effect and that Ca and Mg show only a small interference in the nitrous oxide-acetylene flame. This could be removed by using a more reducing flame (i.e. more fuel rich) at the expense of a worse detection limit. In the air-acetylene flame, Al gives only a small interference but

Ca, Mg and PO_4 give large enhancements of signal. These are due to band emission coinciding with the Fe atomic line. The species primarily responsible for the band emission are CaO, MgO/MgOH and HPO/PO.

4.3.4 Conclusions

The results presented have shown that the determination of Ca and Mg by flame emission spectrometry in the presence of a number of important extraneous ions presents considerable difficulty when the air-acetylene flame is used as a source of atoms. This difficulty has been largely overcome by the application of the separated nitrous oxide-acetylene flame to the problem. The use of this flame removes almost all of the interferences from elements which are important in biological and metallurgical samples, and at the same time affords a considerable improvement in detection limits over those obtained with the air-acetylene. Further, it has been shown that elements such as Fe which are also important species in the samples mentioned (e.g. Fe, Co and Ni in steel samples) may be determined simultaneously with good sensitivity and freedom from interference. This capability should provide a useful alternative to the widely quoted AAS methods, especially in laboratories where such samples are only encountered occasionally.

Chapter V

The Application of Separated Flames To Atomic Absorption Spectroscopy

It should be obvious from the work presented in Chapter IV that one of the major advantages of applying separated flames to emission spectroscopy is the large reduction in signal noise levels. This advantage is no longer valid in many AAS applications because the use of high intensity sources and modulated detection systems (see Section 1.3) has effectively banished flame noise. However, there are still one or two AAS applications in which separated flames can offer an advantage over their conventional counterparts and the most obvious examples are studied in detail below. These applications to the determination of arsenic and selenium and of the refractory elements were chosen by the author as the most useful at the present time; when the occasion arises others will doubtless be found.

5.1 The Nitrogen Separated Air-Acetylene Flame For The Determination of Arsenic and Selenium[130]

5.1.1 Introduction

The determination of arsenic and selenium by flame emission spectroscopy is extremely difficult because the resonance lines of both elements require excitation energies above 6 eV, which is unobtainable with normal flames. In fact, the only reported direct determinations by this method appear to be those of arsenic by Deans and co-workers[115, 131]. By using the arsenic chemiluminescent emission

obtained from the reaction zone of a fuel-rich oxy-acetylene flame when organic solvents are aspirated, they were able to obtain a detection limit of 2.2ppm at the 2350 Å line.

The application of AAS to the problem has improved matters but up to now not to the significant extent observed with elements such as zinc. Two reasons can be put forward to explain this. First, the preparation of hollow cathode lamps for As and Se has so far proved to be rather difficult, mainly because of the volatility of the elements. Secondly, the most sensitive absorption lines of both elements lie below 2000Å in a region of high background absorbance for the commonly used flames. This has aggravated the problem of the rather dim hollow cathode lamps and the high level of flame noise has led to poor detection limits. In spite of these difficulties, successful determinations using hollow cathode lamps and air-acetylene flames have been reported in the literature. For example, Slavin, Sebens and Sprague[132] were able to obtain a sensitivity of 2ppm for As at 1937Å and Chakrabarti[133] has reported a sensitivity of 0.72ppm for Se at 1960Å.

Several workers have attempted to improve the detection limits by using a hydrogen-argon-entrained air flame which gives much lower background absorbance and noise in the region of the As and Se resonance lines[134,135]. This flame works well with samples in pure solution, but unfortunately its low temperature results in chemical interference from many species, especially if a turbulent, total consumption burner is used[135,136]. Attempts have also been made to improve detection limits by using an electrodeless discharge tube to give a much brighter source e.g. Menis and Rains[135] have obtained a detection limit of 0.1ppm for As and Rann and Hambly[137] obtained 1ppm for Se. The most successful results using EDT's were by Dagnall, Thompson and West. They have obtained detection limits for Se[138] in an air-propane flame of 1.0ppm by AAS and 0.25ppm by AFS and for As[139] in a nitrogen-hydrogen flame of 0.9ppm by AAS and

0.15ppm by AFS.

In the present study, it was hoped to improve the detection limits for As and Se without increasing the chemical interferences by using a nitrogen separated air-acetylene flame. As was described in Section 2.4 this flame gives a much lower background absorbance below 2000Å without a significant drop in flame temperature. At the same time, it was decided to use EDT's as the background source, since the work cited above would suggest that these are more reliable than the hollow cathode lamps for As and Se available at the time.

5.1.2 Experimental

Apparatus

A Techtron AA4 atomic absorption spectrophotometer as described previously was used. The standard air-acetylene burner was replaced by the separated burner described in Section 2.4.4 and illustrated in Fig. 2-15. The air and acetylene flow rates were controlled by calibrated rotameters as usual, the air flow being maintained at 7 l./min. giving an atomizer pressure of 20 psig. The EDT's used as line sources were prepared as described by Dagnall, Thompson and West[138,139]. For the Se tube, ca.10mg. of the metal were used in a quartz bulb 3.5cm long with an argon pressure of ca. 0.1 torr. The As tube was prepared using ca. 10mg. of a mixture of arsenic and iodine (ratio 2:1 W/W) in a bulb 4cm long with an argon pressure of ca. 1 torr. Both tubes were used without cooling in conjunction with a 200-watt microwave generator (2450 MHz) and a model 210L (3/4-wave) resonant cavity (Electro-Medical Supplies Ltd.). Modulation of the light at 285 Hz was obtained by means of the standard Techtron rotating sector placed between the source and the flame.

Reagents

Standards were prepared by dilution of 1000ppm stock solutions of As or Se.

As : 1.320g of analytical reagent grade arsenious oxide (As_2O_3) was dissolved in 500ml.of distilled water containing a little sodium hydroxide.

Se : 0.9959g of analytical reagent grade anhydrous sodium selenite was dissolved in 500ml. of distilled water.

Stock 100,000ppm solutions of the anions and cations used for interference studies were prepared using the compounds shown in Table 5-5. Where possible, the cations were used as aqueous solutions of their salts; where the presence of an acid was essential its concentration was kept to a minimum.

5.1.3 Results

Optimum conditions

All variables were optimized in the usual manner. The resulting sets of optimum conditions are shown in Table 5-1 and the effects of EDT power are shown in Tables 5-2 (arsenic) and 5-3 (selenium). The oscillations referred to in Table 5-2 were observed as large regular pulses in the output of the tube, accompanied by a colour change between pink and blue. They appeared to be the result of vapour alternately condensing and vapourising inside the tube.

Table 5-1

Optimum Conditions For Determination of Arsenic and Selenium

Variable	Arsenic	Selenium
Wavelength	1937Å	1961Å
Monochromator slit width	35μ	100μ
Height of optical path above burner	5mm	2mm
EDT power	35 watts	25 watts
Acetylene flow rate:conventional flame	1.5 l./min.	0.7 l./min.
Acetylene flow rate: separated flame	0.8 l./min.	0.7 l./min.

Table 5-2

Effect of Power on Arsenic EDT at 1937Å

Power (watts)	Signal	Absorbance*
20	1	Tube colour pink instead
25	3	of blue
30	6	Still pink and oscillating
35	60	0.230
40	80	0.200
50	77	0.170
60	77	0.160
75	65	Tube oscillating; more than before.

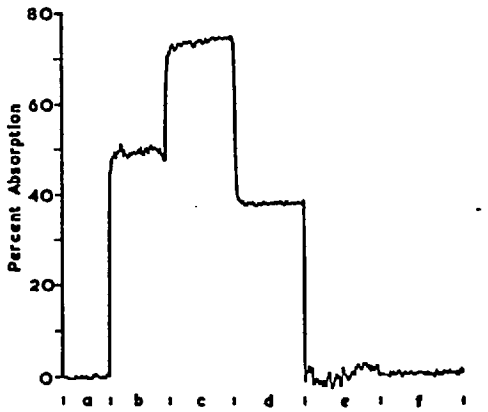
Table 5-3

Effect of Power on Selenium EDT at 1961Å

Power (watts)	Amplifier Gain	Absorbance*
20	$20\frac{1}{2}$	0.520
25	17,3/4	0.500
30	$15\frac{1}{2}$	0.400
35	$14\frac{1}{2}$	0.150

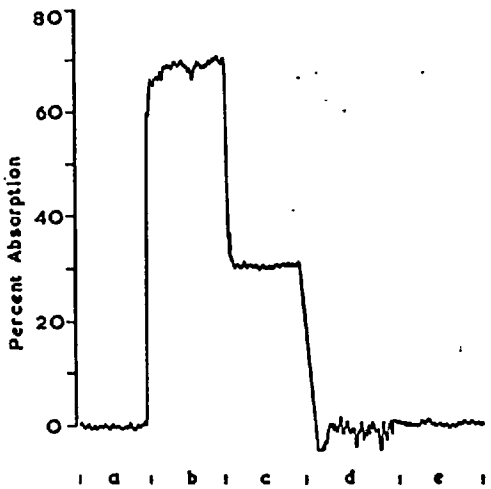
(* Recorded in nitrogen separated flame under optimum conditions).

The selenium EDT was the easier of the two to use, giving a stable output at all the operating powers tested. However, it can be seen from the tables that the absorbance for both elements dropped off quickly if the power was increased very much above the minimum. This was attributed to line broadening and self reversal caused by the high volatility of the two elements.



Background absorbance at the arsenic 1937 mμ line.
a) No flame
b) Conventional flame, optimum fuel flow for arsenic determinations
c) Conventional flame, same fuel flow as d)
d) Separated flame, optimum fuel flow for arsenic determination
e) Conventional flame, absorbance set to zero (by increasing gain)
f) Separated flame, absorbance set to zero

Fig. 5-1



Background absorbance at the selenium 1961 mμ line.
a) No flame
b) Conventional flame, optimum fuel flow for selenium determinations
c) Separated flame, optimum fuel flow for selenium determinations
d) Conventional flame, absorbance set to zero (by increasing gain)
e) Separated flame, absorbance set to zero

Fig. 5-2

Effect of flame separation on background absorbance

The background absorption and noise levels under optimum conditions are shown in Fig. 5-1 for the arsenic 1937 Å line and Fig. 5-2 for the selenium 1961 Å line. It can be seen that there is a considerable reduction in the level of background absorption on flame separation, especially for selenium which requires the same fuel flow in both flames. The level of signal noise (recorded with the absorbance set to zero on distilled water prior to taking a reading) is also significantly reduced at both wavelengths —— of the order of three-fold.

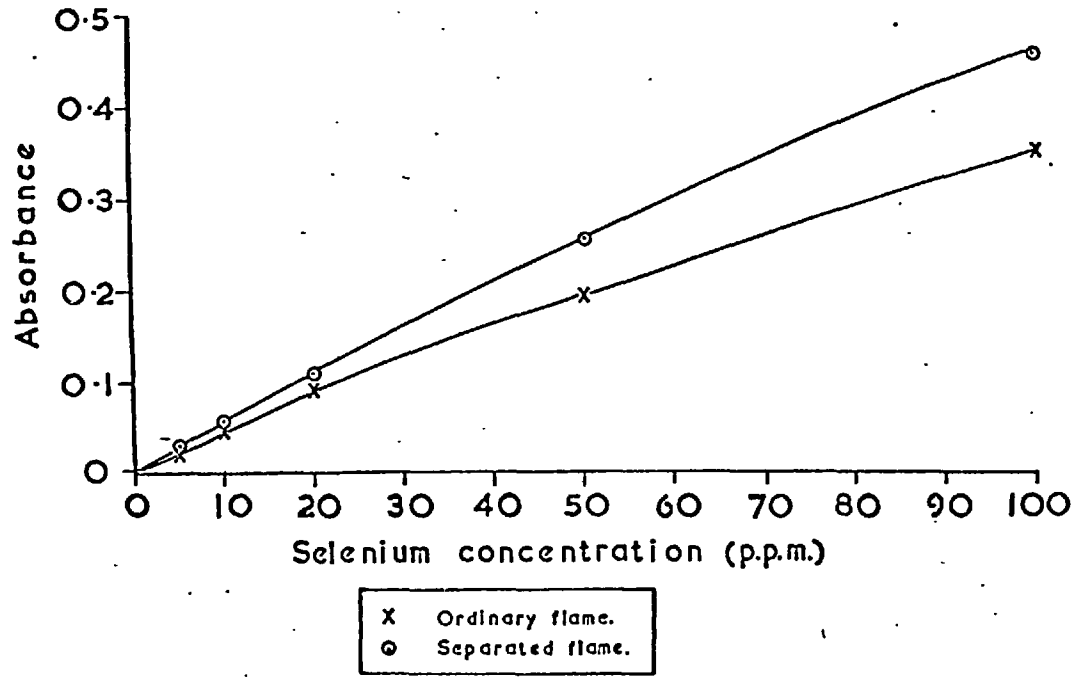


Fig. 5-3 Selenium Calibration Graphs

Calibration curves, sensitivities and detection limits

Arsenic was found to give linear calibration graphs between 1 and 100ppm in both the conventional and separated flames. The selenium calibration graphs, which are shown in Fig. 5-3 were found to be linear in both flames from 1 to 20ppm but to slope slightly towards the concentration axis from 20 to 100ppm.

The sensitivities for both elements were calculated for the two flames from the slopes of the calibration graphs, using the linear portion for selenium. The results are shown in Table 5-4 together with the corresponding detection limits. These were calculated on the basis of a signal:noise ratio of 2:1, using the chart recorder to give a permanent record of the signal noise levels.

Table 5-4

Sensitivities and Detection Limits of Arsenic and Selenium

Flame	Arsenic		Selenium	
	Sensitivity	Detection Limit	Sensitivity	Detection Limit
Conventional	1.5ppm	7.8ppm	0.9ppm	3.6ppm
Separated	1.6ppm	3.2ppm	0.6ppm	1.2ppm

It can be seen that in all cases the detection limit is worse than the sensitivity. This is rather unusual in AAS and was due to the high noise level of the signal from the EDT's. However, with both elements the reduction in flame noise on separation was sufficient to give a three-fold improvement in the detection limits. As expected, flame separation had only a small effect on the sensitivity.

Interferences

The interference effects of various anions and cations on the absorption of arsenic and selenium were measured in the separated flames using the optimum conditions established above. All interferences were recorded for 100-fold weight excesses of the diverse ions using 100ppm solutions of arsenic or selenium. The results obtained are shown in Table 5-5. After allowing for the standard deviations in absorbance readings, it was decided to accept only changes in absorbance greater than 0.030 as true interferences. On this basis, out of 28 potential interferences tested, only 10 interfered with arsenic and 11 with selenium.

5.1.4 Conclusions

Use of the nitrogen separated air-acetylene flame has been shown to allow the determination of arsenic and selenium with good

Table 5-5

Potential Interferences on 100 μg/ml Arsenic and 100 μg/ml Selenium

Ion Added	Compound Used	Arsenic			Selenium		
		Absorb.	Δ Abs.	Interf.	Absorb.	Δ Abs.	Interf.
—	—	0.320	—	—	0.480	—	—
NO_3^-	HNO_3	0.320	−0.002	Nil	0.480	0	Nil
SO_4^{3-}	H_2SO_4	0.320	0	Nil	0.485	+0.005	Nil
PO_4^{3-}	H_3PO_4	0.320	0	Nil	0.480	0	Nil
Cl^-	HCl	0.320	0	Nil	0.475	−0.005	Nil
F^-	HF	0.315	−0.005	Nil	0.483	+0.003	Nil
NH_4^+	NH_4Cl	0.320	0	Nil	0.485	+0.005	Nil
Mg^{2+}	$Mg(NO_3)_2$	0.200	−0.120	—	0.390	−0.090	—
Al^{3+}	$AlCl_3$	0.215	−0.105	—	0.400	−0.080	—
K^+	KCl	0.320	0	Nil	0.460	−0.020	Nil
Ca^{2+}	$CaCl_2$	0.275	−0.045	—	0.375	−0.105	—
Ti^{4+}	Ti/HF*	0.290	−0.030	Nil	0.390	−0.090	—
V^{5+}	V/HF*	0.210	−0.110	—	0.310	−0.170	—
Cr^{6+}	$K_2Cr_2O_7$	0.235	−0.085	—	0.340	−0.140	—
Mn^{2+}	$MnSO_4$	0.300	−0.020	Nil	0.475	−0.005	Nil
Fe^{3+}	$FeCl_3$	0.230	−0.090	—	0.315	−0.165	—
Co^{2+}	$CoCl_2$	0.280	−0.040	—	0.395	−0.085	—
Ni^{2+}	$NiCl_2$	0.205	−0.115	—	0.320	−0.160	—
Cu^{2+}	$CuCl_2$	0.285	−0.035	—	0.450	−0.030	Nil
Zn^{2+}	$ZnSO_4$	0.310	−0.010	Nil	0.480	0	Nil
Zr^{4+}	$Zr(SO_4)_2$	0.320	0	Nil	0.480	0	Nil
Mo^{6+}	$(NH_4)_2MoO_4$	0.260	−0.060	—	0.300	−0.180	—
Ag^+	$AgNO_3$	0.315	−0.005	Nil	0.475	−0.005	Nil
Cd^{2+}	$CdCl_2$	0.295	−0.025	Nil	0.450	−0.030	Nil
Te^{4+}	Na_2TeO_3	0.315	−0.005	Nil	0.480	0	Nil
Ta^{5+}	Ta/HF*	0.290	−0.030	Nil	0.400	−0.080	—
Hg^{2+}	$Hg(NO_3)_2$	0.320	0	Nil	0.450	−0.030	Nil
Pb^{2+}	$Pb(NO_3)_2$	0.320	0	Nil	0.475	−0.005	Nil
Bi^{3+}	$Bi(NO_3)_3$	0.310	−0.010	Nil	0.465	−0.015	Nil

*Pure metals dissolved in minimum 40% HF.

sensitivity combined with relatively high freedom from chemical interferences. This should prove useful in many practical applications, since the only flame offering better sensitivity at the present time is the argon-hydrogen diffusion flame which suffers interference effects from almost all elements. For example, Menis and Rains[135] have recently reported the determination

of As in cast iron by AAS using this flame. They were forced to use an extraction with diethylammonium diethyldithiocarbonate because it was found that all elements interfered at concentrations greater than 1000ppm due to scattering. Further, they found it necessary to use a stripping process to obtain an aqueous sample of arsenic because spraying organic solvents caused a new interference near 1937Å from the CH and C_2 radicals introduced into the flame.

5.2 The Nitrogen or Argon Separated Nitrous Oxide-Acetylene Flame For The Determination of The Refractory Elements[140]

5.2.1 Introduction

The nitrous oxide-acetylene flame has already been discussed in some detail in this thesis and reference has been made to many of the developments reported in the literature since its introduction in 1965 (see, for example, Sections 1.4, 3.5, 4.2.1 and 4.3.1). On several of these occasions, it was mentioned that by far the most wide-spread application of the flame has been in its 5cm long slot form for atomic absorption spectroscopy. Since the literature references on this subject must by now run into the hundreds, it would obviously be unwise to attempt a review of the subject here. It is sufficient to say that almost all atomic absorption spectrophotometers are now available with the nitrous oxide-acetylene flame, either as standard or as an optional accessory. Until recently, most of these burners were very similar to the original one described by Willis[120] and published investigations were mainly concerned with extending its applications. An extensive summary of these developments and applications has been given by Willis[141]. The various possibilities in this direction are now becoming exhausted and several attempts have been made to improve the burners themselves. For example, attempts

have been made to reduce the burner clogging associated with fuel-rich flames by water cooling the burner[142] and by cutting away the top edge of the plates so as to maintain a high temperature and to entrain more air[143]. Attempts have also been made to improve detection limits by heating the burner chamber[143,144]. In the present work, it is hoped to show that the use of a separated nitrous oxide-acetylene flame can greatly improve the burner clogging situation and at the same time give an improvement in the detection limits of the refractory elements by AAS.

5.2.2 Experimental

Apparatus

A Techtron AA4 spectrophotometer was used as described previously with its optical bar realigned to allow the standard absorption burner head and stand to be replaced by a larger one. This burner is described in detail in Section 2.4.4. To allow the flame to be positioned accurately and reproducibly with respect to the optical path of the instrument, the burner was supported by a stand fitted with horizontal and vertical screw adjustments giving an accuracy better than 0.5mm. The "zero" positions were set by forming an illuminated image of the monochromator entrance slit over the burner and aligning the bottom of this image with the top of the burner plate and with the centre of the burner slot. All vertical measurements could then be recorded as "the height of the base of the optical path above the burner" using a scale attached to the stand. The Techtron indirect nebulizer and expansion chamber were retained, but the acetylene inlet to the expansion chamber was sealed off because the burner used had an independent acetylene inlet at its base (see Fig. 2-15).

The gas control unit of the instrument was replaced by a set

of calibrated rotameters fitted with needle valves. The burner was used with a nitrous oxide flow rate of 6.75 l/min. The nitrous oxide was used to nebulize the sample solutions and this flow rate resulted in a nebulizer pressure of 22.5 psig. This gave a solution uptake rate of ca. 5.5 ml./min. and was found to be the most efficient setting with the nebulizer employed. Acetylene flow rates in the range 3.2 to 4.6 l./min. were found to be the most useful for atomic absorption studies of the refractory elements.

Hollow cathode lamps of the following types were used as the absorption light sources:-

Al, Be, Ge, C	:	Atomic Spectral Lamps Pty. Ltd.
Mo, Si	:	Atomic Spectral Lamps Pty. Ltd. High Intensity Lamps (in conjunction with Techtron XLS-2 auxiliary power supply).
Zr	:	Perkin-Elmer Corporation
Ti	:	Perkin-Elmer Corporation high intensity "Intensitron" lamp.

A Servoscribe potentiometric chart recorder was used for the measurement of detection limits.

Reagents

Analytical reagent grade metals or their salts were used to prepare 1000 or 5000ppm stock solutions of the ions of the elements studied. Be, Si, Ti and Zr solutions were prepared by dissolution of the elements in the minimum quantity of 40% hydrofluoric acid and dilution with distilled water. Al and V solutions were prepared by dissolution of the metals in 1M HCl and 0.5M HNO_3 respectively. Ge solutions were prepared from germanium dioxide in 2% KOH and dilution with distilled water, while Mo solutions were obtained by dissolving ammonium molybdate in distilled water.

A stock 100,000ppm solution of potassium was prepared from analytical reagent grade KCl.

Table 5-6

Optimum Operating Conditions For Elements Studied

Element	Wavelength, *nm*	Slitwidth, *μm*	Lamp current, *mA*
Aluminium	309·27	100	8
Beryllium	234·86	100	6
Germanium	265·16	35	15
Molybdenum*	313·26	50	8†
Silicon*	251·61	50	16†
Titanium	364·27	35	18
Vanadium	318·40	100	20
Zirconium	360·12	50	20

* High intensity lamps of Sullivan and Walsh type
† Current to auxiliary electrodes 400 mA.

5.2.3 Results

Optimum conditions

The conditions giving the best compromise between high sensitivity and low detection limits (i.e. low signal noise levels) were established for each element. The instrumental variables (absorption line, monochromator slit width and hollow cathode lamp current) are summarized in Table 5-6.

The flame variables (height and fuel flow) were studied in some detail over a wide range. The effect for each element of height of measurement in the flame on the absorbance over a large part of the red interconal zone is shown in Fig. 5-4. The readings were recorded at the optimum fuel flow for each element.

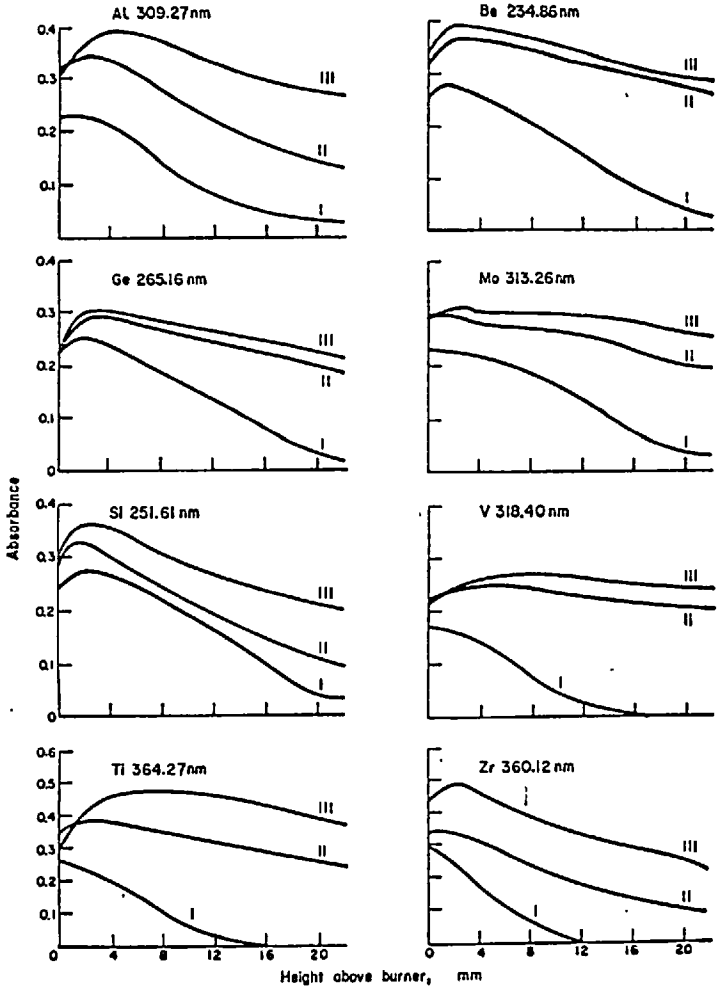
Two differences between the conventional and separated flames are immediately apparent. First, the peak absorbance in the conventional flame is invariably obtained with the base of the optical path less than 2mm above the burner. With the separated flames this distance may be increased to as much as 6 or 8mm (e.g. V and Ti). Secondly, the rate of decrease of absorbance with height is much more rapid in the conventional flame, so that the effect of shielding at, say, 20mm above the burner is extremely large. These results illustrate how significant is the effect of diffusion of atmospheric oxygen into the centre of the conventional flame.

The effect of acetylene flow rate on absorbance is shown in Fig. 5-5. The readings were recorded at the optimum height in the flame for each element. As shown, the peak absorbance in the conventional flame is always obtained with a more fuel-rich mixture than is required for the separated flames. This is an advantage of the latter, since rich flames are associated with higher noise levels and are subject to carbon deposition. On the other hand, the separated flames do show a sharper absorption peak so that the setting of the optimum fuel flow must be more closely regulated. This was not found to be a serious problem in practice, however, and was far outweighed by the freedom from carbon deposition during operation.

Absorption characteristics of individual elements.

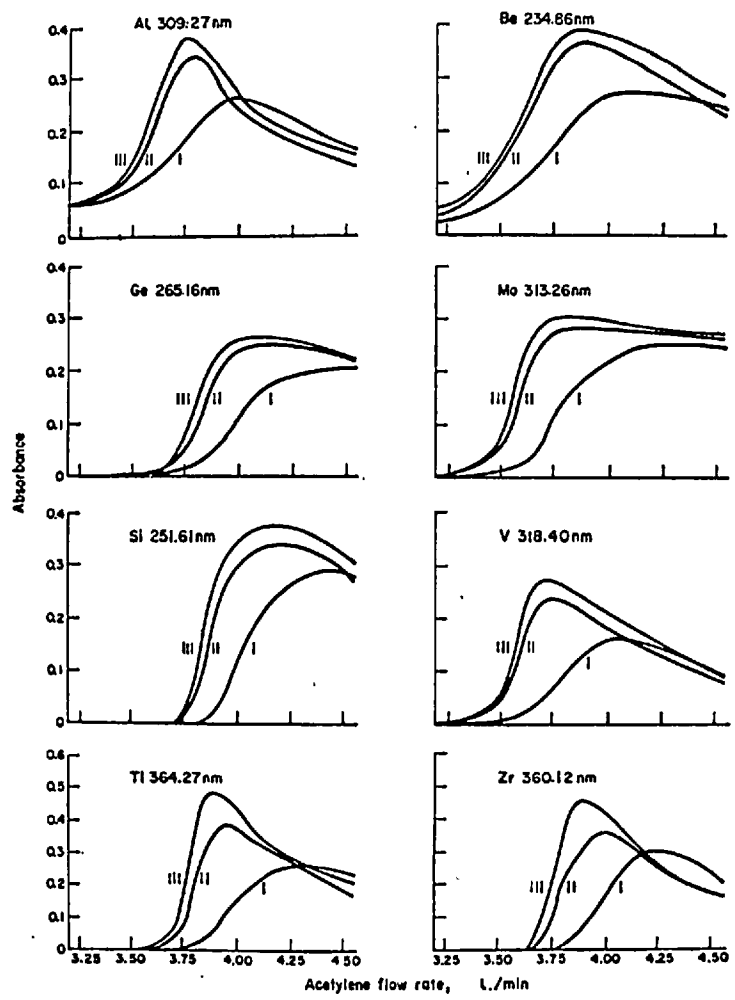
The following notes indicate the concentration range studied for each element, the shapes of the calibration graphs; the existence of any ionization for the metal in the flame, (i.e. whether the addition of 10,000ppm of K^+ to the samples increased the absorption); and any other significant facts recorded during the work with that element.

Aluminium The calibration graphs were linear over the range 5 to 50ppm, but curvature towards the concentration axis occurred from 50 to 200ppm (12% deviation from linearity at 200ppm). The addition of KCl gave a significant increase in absorbance but did not



Variation of absorbance with height above burner.
I Conventional flame; II nitrogen shielded flame; III argon shielded flame.

Fig. 5-4



Variation of absorbance with acetylene flow-rate.
I Conventional flame; II nitrogen shielded flame; III argon shielded flame.

Fig. 5-5

significantly alter the shape of the calibration graph for each flame.

Beryllium The calibration graphs were linear from 0.05 to 2.5ppm; a slight curvature towards the concentration axis occurred between 2.5 and 5ppm (5% deviation from linearity at 5ppm). This was most noticeable with the conventional flame.

Germanium The calibration graphs were linear from 5 to 200ppm with the separated flames, but only from 5 to 150ppm with the conventional flame. The latter exhibited slight curvature towards the concentration axis between 150 and 200ppm (2.3% deviation at 200ppm).

Molybdenum The calibration graphs were linear from 2.5 to 50ppm, but curvature towards the concentration axis occurred from 50 to 100ppm. This was only very slight in the separated flames but quite marked in the conventional flame ($5\frac{1}{2}$% deviation at 100ppm).

Silicon The calibration graphs were linear from 5 to 200ppm. The very refractory nature of this element demanded an unusually high fuel flow for the separated flame. This resulted in an instability at the ends of the burner slot with the nitrogen shielded flame; this effect was not experienced with argon shielding. Hence, the latter gave a much more pronounced improvement in detection limit than nitrogen shielding. This effect was not found with the other elements studied.

Titanium The calibration graphs were linear from 10 to 250ppm. The addition of KCl gave an increase in absorbance at all concentrations of titanium but had no effect on the linearity of the calibrations.

Vanadium The calibration graphs were linear in the range 5 to 100ppm but between 100 and 200ppm curvature away from the concentration axis was observed (4% deviation at 200ppm). The addition of KCl increased the absorbance and resulted in a curvature towards the concentration axis between 100 and 200ppm (5% deviation at 200ppm).

Zirconium The calibration graphs were linear from 500 to 1000ppm, but over the range 50 to 500ppm sloped away from the concentration axis. The addition of KCl increased the absorbance but had no effect on the shape of the calibration graphs. In both instances argon shielding was found to produce a larger improvement in absorbance relative to nitrogen shielding than was observed for the other elements studied.

Sensitivity and detection limits.

These were recorded for each element in all three flames and the results are listed in Table 5-7. Where appropriate, the values with a concentration of 10,000ppm K^+ (as KCl) present were also measured. A typical set of calibrations is shown in Fig. 5-6 to illustrate the effect of separation on the sensitivity. The linear portions of the graphs were used to calculate the sensitivity. The detection limits were defined as the concentrations giving a signal to noise ratio of 1:1. They were measured using the chart recorder and an appropriate degree of scale expansion. Sample solution concentrations were chosen so as to give less than 5% absorption (i.e. the range where concentration is linearly related to percent absorption), and detection limits were calculated by extrapolation of the signals and noise levels recorded. The recorder was damped with a 2000μF condenser so as to provide a time constant of 1cm/second over a chart width of 20cm.

5.2.4 Conclusions

The use of a separated nitrous oxide-acetylene flame on a water cooled burner as described here allows the determination of the refractory elements by AAS with much less fuel rich conditions than usual. This results in lower noise levels, giving better detection limits and precision and also removes the sooting up of the burner experienced with the conventional flame. The latter effect also

Table 5-7

SENSITIVITIES AND DETECTION LIMITS OBTAINED IN CONVENTIONAL AND SHIELDED FLAMES

Element	Sensitivity, *ppm*			Detection limit, *ppm*		
	Normal	N_2 separation	Ar separation	Normal	N_2 separation	Ar separation
Aluminium	1·6	1·3	1·1	0·29	0·14	0·11
Aluminium*	1·4	1·1	0·98	0·24	0·12	0·10
Beryllium	0·033	0·026	0·024	0·006	0·003	0·003
Germanium	2·8	2·4	2·3	0·20	0·12	0·11
Molybdenum	0·70	0·62	0·59	0·18	0·10	0·10
Silicon	3·6	2·8	2·5	0·45	0·37	0·24
Titanium	4·1	2·6	2·1	0·14	0·045	0·041
Titanium*	3·2	2·1	1·7	0·11	0·036	0·034
Vanadium	2·5	1·7	1·6	0·18	0·053	0·045
Vanadium*	1·9	1·4	1·4	0·14	0·04	0·04
Zirconium	16	13	9·7	0·83	0·38	0·26
Zirconium*	14	12	8·9	0·74	0·35	0·24

* Results with potassium chloride added to sample.

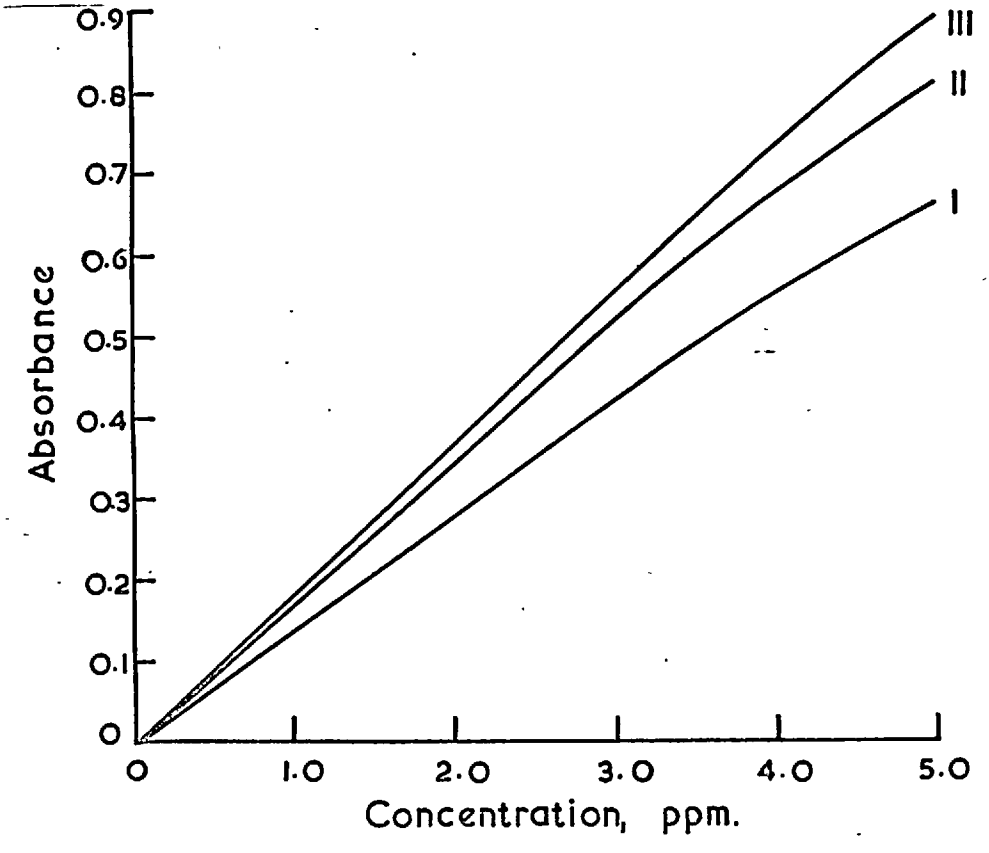


Fig. 5-6 Calibration Graphs For Beryllium

increases the precision, but more important is the considerable reduction in inconvenience during the determination of these elements. Thus, a significant saving in time is achieved during a routine set of analyses. If the full benefit of this saving is to be obtained, it is essential to control the gas flows with reliable rotameters and needle valves (as was done here) so that resetting of optimum conditions is unnecessary during the processing of a set of samples. A smaller, but still useful, advantage of the flame separation is the improvement of the actual sensitivity of determinations by between 15 and 50% for elements such as Al, Be, Ge, Mo, Si, Ti, V and Zr. Except for Si and Zr, argon shielding offers no significant advantage over nitrogen shielding. Since the latter is far cheaper, it would probably prove the best choice for most routine analytical purposes.

Chapter VI

High Resolution Spectroscopy With A Fabry-Perot Interferometer

6.1 Introduction

Mention has already been made several times in this work of the importance of spectral line widths in atomic absorption and fluorescence spectroscopy. In spite of this importance and the great interest in recent years of producing improved spectral sources for AAS and AFS, very few analytical chemists have attempted measurements of the actual profiles of the lines from their spectral sources (see Chapter VII for details).

Testing of a new source usually involves use of a conventional, low resolution monochromator to measure the intensity and stability of its output. Measurements of absorption sensitivity may also be made under standardized conditions since with conventional analytical equipment the sensitivity will generally increase with decreasing line width. Unfortunately, this can provide no more than an indication of the processes occurring within the source and the information is easily misinterpreted unless the results are evaluated very carefully. Furthermore, it is almost impossible to correlate the results with actual measurements of line profiles made by spectroscopers under quite different conditions.

In view of these facts, a project to study the line profiles of spectral sources used by analytical chemists appeared to be most desirable. A preliminary study soon dispelled any ideas that accurate measurement of line widths would simply involve purchasing a more expensive spectrometer than is usually used in the department. The difficulties of obtaining an ultra-high resolution instrument

which is not prohibitively large or expensive and which gives a reasonably high light transmission are discussed below.

Even when a suitable instrument has been selected a number of experimental difficulties remain. The observed profile of the spectral line always includes a contribution due to the instrument; the relation between the actual and observed profiles varies not only with the instrument but also with the type of intensity distribution in the source lines. Hence considerable expertise is necessary to decide on the broadening factors within the source before any attempt can be made to measure line widths. Furthermore, many spectral lines have a hyperfine structure (see Section 1.2.4) which complicates measurements and makes it difficult to relate actual line widths to the quantities important in AAS. Thus any quantitative measurement of spectral line widths requires considerable background knowledge and a detailed study of each line of each element - rapid progress through a long list of elements is not possible. Fortunately, less sophisticated results are often sufficient for the analyst and, as will be shown later, quite rapid evaluations of the suitability of light sources for AAS and AFS may be made by qualitative techniques.

6.2 Historical

6.2.1 High resolution spectroscopy

Early work on high resolution spectroscopy was mainly concerned with practical optics. Towards the end of the last century and during the early 1900's a number of workers were actively searching for means of obtaining better resolution than is possible with the conventional prism spectrograph. This resulted in the introduction and refinement of several new ways of dispersing spectra, including the diffraction grating, the echelon grating and a number

of interferometers. Thus, Michelson was first able to view the hyperfine structure (hfs) of a spectral line in 1881 and the structures of other lines were published in the literature from time to time. However, the main interest lay in the instruments themselves and line structures were merely used as convenient examples to show how further progress had been made towards the three main goals (high resolution, good light transmission and coverage of wide wavelength regions without overlap).

This situation changed dramatically in the late 1920's when the introduction of the quantum theory (see Section 1.2.2) and the discovery of nuclear spin led to a wide interest in hyperfine structure studies. It was then found that the factor retarding progress was no longer the lack of instrumental resolving power but the non-existence of light sources giving lines intense enough to study yet sharp enough for all of the hfs components to be separated. Thus, for the next twenty or so years most work was concerned with the analysis of the hfs of large numbers of lines and the development of spectral sources giving ultra-narrow lines; improvements to instruments were largely confined to the level of practical detail. The more exotic of these sources, such as the atomic beam, are of little interest in the present work where we are concerned with routine atomic absorption and fluorescence spectroscopy. However, some of the earlier measures taken to provide sharp, intense lines would appear to have direct applications to AAS and it is unfortunate that this important branch of high resolution spectroscopy has largely been overlooked by current workers in this field.

In recent years the situation has once again reversed; by the end of the 1940's sources had been developed giving lines so sharp that it was difficult to find instruments to take full advantage of them. Furthermore, most of the interesting hfs analyses had been completed and work was largely restricted to improving the accuracy of the measured line separations. This has led to a renewed interest in instrument development and a number of sophisticated interferometers

have been introduced, often using computers to control their wavelength scanning or for the interpretation of results. Apart from this instrument development, the most popular high resolution work during the past few years has been the measurement of spectral line widths for comparison with calculated values (to test the theory). Most of these measurements have been made with simple Fabry-Perot interferometers rather than the most recent sophisticated instruments.

Before describing further the reasons for the choice of the instrumental techniques which have been applied to high resolution spectroscopy, it is necessary to define exactly what is meant by high resolution and to outline the practical requirements. These points have been discussed in detail by Tolansky[145] and only a brief summary will be given here.

The resolving limit of an instrument is the smallest wavelength interval, $d\lambda$, which can be separated at a particular wavelength (or, of course, we can use $d\sigma$ or $d\nu$). The actual point at which separation can be said to cease must be defined in a standard way and it is usual to use the original value given by Rayleigh (see Ref. 145, p. 86). For historical reasons the resolving limit of conventional spectroscopes and spectrographs is usually replaced by another quantity due to Rayleigh and known as the resolving power. This is simply $\lambda/d\lambda$ at any wavelength λ. With high resolution instruments it is generally more helpful to quote the resolving limit and this will be used in the present work.

The resolving limit at which an instrument is said to be of high (or ultra-high) resolution instead of just conventional good quality is obviously quite arbitrary. For present day purposes a useful definition is : "high resolution spectroscopy involves an interest in the hyperfine structure and energy distribution of the lines of the electronic spectra which with conventional equipment would be regarded as single, uniform, sharp lines". From the discussion of spectral line widths given in Section 1.2.4 it will be seen that for most purposes this will require a resolving limit

better than 0.05Å. This corresponds to a resolving power of 100,000 at 5000Å. Generally, instruments with this capability would be intended only for high resolution work as defined above, although the best general purpose instruments used for, say, studies of molecular band spectra would give a resolving power of this order.

Apart from a very small resolving limit, there are two other requirements for a high resolution instrument. First, the light transmission at the required resolution must be sufficiently high to allow convenient study of the spectral sources to be used. Secondly, many of the instruments work by interference (including diffraction) of light and hence give spectra corresponding to the order of interference. If these spectra overlap in such a way as to make individual lines coincide a small resolving limit will be of little use. Both of these difficulties are high-lighted when attempts are made to obtain high resolution by using a conventional instrument at its maximum resolving power; e.g. a grating spectrograph used in the third order with 5μ slits.

The best compromise between these requirements and the greatest versatility was given for many years by the Fabry-Perot interferometer and it has been used for the majority of hyperfine structure investigations. The introduction during the past twenty years of adaptations permitting scanning of spectral lines has given it a new lease of life and this type of instrument is used in the present work. A detailed description of its development will be found in Sections 6.2.2 and 6.2.3. The diffraction grating offers a much wider wavelength range without overlap and is more convenient for routine use but its performance has always been restricted by the quality of the gratings. Although these have improved enormously in recent years the combination of resolution and light transmission is still inferior to that of the Fabry-Perot. The reflection echelon grating offers better performance but gives problems of order overlap similar to those of the Fabry-Perot. In any case its high cost has

restricted its use. It is described by Tolansky[145] together with some other interferometric devices which have had limited application to high resolution spectroscopy in the past. The most modern derivatives of these interferometers have been reviewed by Jacquinot[146] but, as mentioned earlier, they are extremely complicated when compared with the scanning Fabry-Perot and have not been widely applied to routine high resolution work.

6.2.2 The Fabry-Perot interferometer

The instrument introduced in 1897 by Fabry and Perot[147] is probably the best known of the interferometers and is certainly the most versatile. In its standard form it has been used for high resolution spectroscopy; absolute wavelength measurements; evaluation of the metre; determination of the refractive index of gases; measurement of small displacements; etc.

In spite of this the instrument is simple in design and contains only a small number of components. It consists of two thick plane parallel glass or quartz plates rigidly mounted in a frame. The two inner surfaces are polished as plane as possible and coated with a suitable reflecting film. This film is such that it has a high reflection coefficient, a small transmission coefficient and the smallest possible absorption coefficient. Thus when a beam of light is passed through the two plates multiple reflections occur in the space between them and some of the light is transmitted to the far side. This is made up of a large number of coherent light beams of different path length so that interference will occur at infinity. Therefore if the light is collected by a lens (such as that in the eye) an interference pattern is seen. As explained in Section 6.3, this is a set of rings because there is circular symmetry about the optical axis.

If the light is monochromatic each ring will correspond to a different order of interference; with a number of wavelengths in the

incident light each will give a similar set of rings so that the observed fringe pattern is extremely complicated. For this reason it is nearly always necessary to isolate the spectral line of interest when the interferometer is used for high resolution work. Although a filter may be suitable for simple spectra, the classical technique is to combine the instrument with a normal spectrograph. If the spectrum is photographed using light which has passed through the interferometer, a conventional spectrum is obtained across the photographic plate but it is found that in the perpendicular direction each line consists of a narrow section of its own ring system. If there is a hyperfine structure this ring system will contain one set of rings for each hyperfine component.

When attempts are made to use this ring system to analyse an unknown hyperfine structure, one of the main difficulties of the Fabry-Perot interferometer becomes obvious. The resolving limit for a given experimental arrangement and a particular wavelength is a fixed function of the wavelength range which may be covered without overlap of orders. The wider the plate separation the narrower is the range covered and the better is the resolution. Since the wavelength range is usually only 10 to 100 times greater than the resolving limit (depending on the quality of the instrument) overlap of orders can be a serious problem even for an isolated spectral line. For this reason the most useful type of plate mounting for high resolution work is one which allows a variable gap with a suitable means of adjusting the plates for parallelism. The optimum wavelength range for any spectral line may then be selected.

Even variable mounts are a fairly simple problem and the photographic Fabry-Perot interferometer has changed little in this respect since its introduction. The main area for improvements has been in the plate surfaces and their coatings. The object is to obtain a surface which is absolutely flat and a coating which gives extremely low absorption of light. Glass plates have been quite

widely used but quartz or fused silica allow better quality surfaces and may also be used at wavelengths down to 2000Å. The flatness of the plates is usually quoted as a fraction of a wavelength for green light; λ green/50 has been accepted as the minimum for good quality plates for many years. This corresponds to a flatness of about 100Å and, of course, the shorter the wavelength of the line used the worse is the relative flatness of the plates. The main improvement has been to increase the size of the plates (to give a better light gathering power) and commercial plates of 5 to 6cm diameter are now available with this flatness. The very best modern plates are flat to λgreen/200 with λgreen/70 possible for the whole area of a plate 10 to 15cm in diameter. Unfortunately these are only produced in a few specialist laboratories and are very expensive.

Much greater improvements have been possible in the coatings of the mirror surfaces. Traditionally the coatings are obtained by sputtering on a layer of silver or aluminium (i.e. using an electrical discharge at low pressure). Silver gives between 90 and 98% reflection in the visible but cannot be used below about 4000Å. Aluminium gives a maximum of about 90% but is much more uniform with respect to wavelength and gives good results down to about 2000Å. A high reflection coefficient is useless if almost no light is transmitted and during the first 40 or 50 years of this century the main interest in Fabry-Perot development was in depositing extremely thin uniform layers of these metals so as to obtain very low absorption of light. Even so, the best results which can be reproducibly obtained (with green light) are about 94% reflection and 5% absorption for silver and 90% and 9% for aluminium. In view of this a major development during the last twenty or so years has been the introduction of coatings made up of multiple layers of dielectric materials such as ZnS, Mg_2F and $PbCl_2$. In the visible it is quite possible to produce coatings giving less than 0.1% absorption even with 99% reflection. Although such high reflection coefficients are not normally needed (see Section 6.3.3) the very low absorption gives an enormous improvement in light

transmission. The combination of resolving power and luminosity obtainable using dielectric plates is far superior to that which can be obtained with even the most expensive grating spectrometers. Current research on dielectric coatings is concerned with two main problems. First, each particular coating only gives its optimum results over a fairly narrow wavelength range of, say 500Å and may only be usable over 1000 to 2000Å. Secondly, much poorer results are obtained in the ultra-violet because of the difficulty of obtaining sufficiently transparent dielectric materials. Fortunately, this problem applies to the widely used interference filters as well as Fabry-Perot plates so that it is receiving considerable attention. It should soon be possible to obtain excellent results over the whole range covered by aluminium mirrors at the present time.

6.2.3. The Fabry-Perot spectrometer

Although the combination of a Fabry-Perot interferometer with a spectrograph has been widely used and given excellent service it has a number of serious drawbacks:

(i) The rings may only be recorded photographically.

(ii) The rings obey a parabolic law; measuring the separation of the rings will not give directly the wavelength separation or widths of the components which produced them. Reduction of the observations is extremely laborious (see Tolansky[145], Ch. 9).

(iii) These reduction methods normally require measurements to be made on several orders, which means using rings some distance from the centre of the pattern. However, the resolving limit grows larger with increasing distance from the centre because of lens aberrations, loss of light beams etc.

(iv) The intensity of the rings falls off with distance from the centre so that accurate relative intensity measurements are difficult, quite apart from the need to calibrate the photographic plate.

The problem of photo-electric recording could easily be overcome using the techniques applied to prism and grating spectrometers (i.e. alter the angle of incidence of the light, either by rotation of the interferometer or of the diaphragm through which observations are made). However, this does not remove the other difficulties. A much better method which removes all of the drawbacks listed above was proposed in 1948 by Jacquinot and Dufour[148]. They suggested replacing the photographic plate by a small aperture placed on the optical axis so that only the central fringe of the system is observed. The order of the observed fringe is then changed by changing the optical retardation, i.e. the effective optical path length between the two plates. Each change of $\lambda/2$ in the optical path results in a scan through one order (see Section 6.3.1) so that only minute changes are needed. If the light passing through the aperture is recorded photoelectrically a scan is obtained which is linear with respect to both the wavelength and the intensity of the incident light. Thus the laborious reduction of observations necessary with the F-P interferometer is no longer required. At the same time, all of the advantages of the F-P over other instruments are retained and its optical quality is actually improved by using only the central fringe.

There are two ways of varying the optical path length. Jacquinot and Dufour[148] suggested altering the refractive index (μ) of the gas between the plates by changing its pressure. This method has been used by many workers and most high resolution applications of the F-P during the past twenty years have employed pressure scanning instruments. In theory the method is simple because any commercial photographic F-P may be converted to pressure scanning by placing it in an air-tight box and there are no special problems of maintaining the

plates parallel during a scan. In practice a number of difficulties are encountered:

(i) If the gas used is air, a pressure change of 1 atm. is just sufficient to scan one order with a wavelength range of 1Å. If larger ranges or more orders are required either another gas (such as freon) or high pressures must be used.

(ii) It is difficult to change the pressure uniformly with time so as to obtain a linear wavelength scale.

(iii) Adjustments to the parallelism of the plates cannot readily be made during scanning and in any case are only possible by the traditional methods of viewing fringes visually. The construction of the vacuum system often makes this difficult and tedious.

(iv) The windows of the vacuum box lead to light losses.

(v) The fastest scanning speed is usally around 1 order per second (to avoid heat effects and uneven pressure changes). Even at slower speeds most instrumental arrangements do not allow continuous repetitive scanning.

In view of these difficulties pressure scanning instruments have not been available commercially and were not considered suitable for the present project (even though they have been widely used for the type of measurements envisaged).

The other method of changing the optical path length is simply to move one of the plates. The main problems are to produce linearly and reproducibly movements of the order of a few thousand Angstroms(i.e. 0.001mm) while maintaining the two plates absolutely parallel. Several workers have managed to achieve this with mechanical systems based on springs, the most useful instrument probably being that of Tolansky and Bradley[149]. However, most interest in this field has been concerned with instruments capable of

fast scanning and this is much easier to achieve using a piezoelectric transducer to move the interferometer plate. The first really successful instrument using this principle was designed by Cooper and Greig[150,151]. It was intended for ultra-high speed scanning rather than really high resolution and was mainly operated at the resonance frequency (15KHz) of the ceramic transducer. It is the prototype of the commercial instrument used in the present project and has been found to work equally well at slow scanning speeds. A more sophisticated instrument was produced at about the same time by Ramsay[152]. He used three ceramic transducers to oscillate the moving plate with a complicated servo-mechanism linking them so that the parallelism of the two plates could be maintained. A piezoelectric F-P designed for use with slow scanning has been described by Mielenz, et. al.[153]. They avoided the problems of maintaining parallelism by having the plates and the transducer permanently mounted within a quartz tube.

During the last five years a number of workers have produced F-P spectrometers using change of plate separation, mostly by piezoelectric transducers and with variable space etalons, Most report that a major advantage over the pressure scanning instruments even for slow scanning is the ability to observe a line profile on an oscilloscope while the instrument oscillates continuously. Fine adjustments to the parallelism may then be made much more easily than with the stationary interferometer. The instruments are also much more compact than the pressure scanning type and are certainly more versatile. As a result of these advantages several commercial instruments have recently been introduced, one of which features two piezoelectric transducers for the non-oscillating plate so that fine adjustments to the parallelism may be made without disturbing the instrument. This last feature is particularly important because the main disadvantage of these instruments over the pressure scanning type is their susceptibility to vibrations (since one of the plates is

not rigidly mounted). Under most conditions they must be placed on an anti-vibration mounting.

6.3 Interferometry Theory

6.3.1 Interference spectroscopy

The principles of the interference of light are well known and will not be repeated here. However, it is useful to summarize one or two topics which help to avoid any misunderstanding of the working of the Fabry-Perot interferometer and which illustrate its similarities with other spectrometers. Several equations needed for the experimental work will also be introduced.

Interference fringes are obtained from two or more light beams which have different path lengths but the same frequency and the same initial phase, i.e. which originate from coherent sources. This generally implies that the origin of the light is a single source and the different path lengths may be obtained by (a) dividing the wavefront into two or more parts or by (b) using a semi-reflecting surface to divide the amplitude of the light beam. With both methods it is possible to use just two different path lengths (e.g. the Rayleigh refractometer for (a) and the Michelson interferometer for (b), or many different path lengths (e.g. the diffraction grating for (a) and the Fabry-Perot interferometer for (b). In the latter case, instruments of type (b) are usually referred to as multiple beam or multiple reflection interferometers.

Method (a) usually involves the use of very narrow apertures or surfaces so that the interference pattern is complicated by a diffraction pattern (diffraction is simply interference which arises from mutual interactions of different parts of the same wavefront so that it can be obtained at a single slit wire, etc.). The classic example is the diffraction grating. (Although this is generally

thought of as just an alternative dispersive system to the prism, other instruments using division of wavefront, such as the Rayleigh refractometer, are always classed as interferometers). The fringe pattern is complicated by the combined interference and diffraction but if the grating is illuminated normally by light of wavelength λ, the angles at which the principle maxima occur are given by

$$\mu(a+b)\sin\theta = n\lambda \qquad (6\text{-}1)$$

where a and b are the widths of the two types of spaces on the grating, μ is the refractive index and n is an integer known as the order of interference. The sharp line seen at each maximum is an image of the entrance slit used as a light source and spectra may be scanned by changing θ.

Method (b) gives a more simple fringe pattern because there is no diffraction. All of the maxima are now of equal brightness and the equation corresponding to (6-1) is

$$2\mu t\cos\theta = n\lambda \qquad (6\text{-}2)$$

where t would be the plate separation in the case of the Fabry-Perot interferometer. Since the straight line symmetry imposed by the diffraction grating and its slit source no longer apply, each value of $n\lambda$ now corresponds to a cone of transmitted light rays all of which make an angle θ with the axis. Hence the fringes are seen as a series of concentric rings. As explained in Section 6.2.3 the F-P spectrometer uses only the central fringe for which $\theta = 0$. Hence equation (6-2) becomes

$$2\mu t = n\lambda \qquad (6\text{-}3)$$

The change needed to scan one order with either the diffraction grating or F-P spectrometers is found by substituting $n = 1$ into equations (6-1) or (6-3) respectively. If the F-P is scanned by changing the plate separation (and μ is taken as 1 in air) it can be seen that t must be changed by $\lambda/2$. For either type of spectrometer the wavelength range corresponding to one order (i.e. the wavelength range without overlap) may be found by using the fact that if everything else is kept constant, two wavelengths λ' and λ'' corresponding to

orders n' and n'' are related by

$$n'\lambda' = n''\lambda'' \qquad (6\text{-}4)$$

Hence

$$(\lambda' - \lambda'') = \lambda'(n'' - n')/n'' \qquad (6\text{-}5)$$

Some results of this for $\lambda = 5000\text{Å}$ are given in Table 6-1. It can be seen that

Table 6-1

n'	n''	$(n'' - n')/n''$	$(\lambda' - \lambda'')$ in Å
1	2	$\frac{1}{2}$	2500
2	3	1/3	1667
9	10	1/10	500
99	100	1/100	50
999	1000	1/1000	5
		etc.	

the higher the order the smaller is the wavelength range. This is the only reason for the difference between the two types of spectrometer; the diffraction grating spectrometer is used at very low orders whereas the F-P is used at very high orders. The actual F-P order may be found by substituting the value of t into equation (6-3). However, the wavelength range is such an important factor with the F-P that it is generally referred to as the free spectral range (FSR) and found from the formula obtained by substituting $n'' = 2t/\lambda$ into equation (6-5). This gives

$$\text{FSR} = \Delta\lambda = \lambda^2/2t \qquad (6\text{-}6)$$

The wavelength range depends on the wavelength and this is inconvenient for the F-P where it is small and changes rapidly. The problem can be avoided by working with wavenumbers. Equation (6-3) for the F-P then becomes $n = 2\mu t\sigma$ and by the same method it is found that

$$FSR = \Delta\sigma = {}^{1}/_{2t} \qquad (6\text{-}7)$$

which is independent of wavelength.

6.3.2 Theoretical resolving power.

We have already defined the practical resolving power of a spectrometer in Section 6.2.1. However, the instruments also have a theoretical resolving power which assumes that all of the optical components are perfect (e.g. infinitely narrow slits, perfectly flat surfaces, etc.). This depends only on the optical retardation of the dispersing system and with interferometric instruments is determined by the maximum path difference possible between two rays for which interference occurs. It may be shown that for all of these instruments the theoretical resolving power is the product of the order of interference and the number of different light paths.

Thus for a diffraction grating the theoretical resolving power is found by multiplying the order and the number of lines on the grating. Low orders are used with a large number of lines so that a fairly wide wavelength range can be obtained without overlap. e.g. a grating with 50,000 lines will give a theoretical resolving power of 50,000 in the first order, 100,000 in the second, etc. It can be seen that there is a limit to the combination of large wavelength range and high resolution which may be obtained. Equation (6-1) shows that n is directly related to θ and (a+b). Since $\sin\theta$ cannot exceed 1, the smaller (a+b) becomes (i.e. the closer the lines on the grating) the smaller is the maximum value of n for the grating. Therefore to obtain really high resolution with n in the range 10 to 20 it is necessary to use an extremely large grating so as to have a large number of lines which are not too closely spaced. Apart from this the diffraction pattern of the fringes means that about $1/n^2\pi^2$ of the incident light goes into each order. Therefore in

higher orders the problem is not simply one of overlap with other orders of equal intensity (as in the F-P spectrometer) but with much more intense orders. The problem is greatly reduced by using blazed gratings in which the rulings are specially shaped grooves. These can be made so that for any desired wavelength region most of the light is concentrated in the order required. Even so this should help to illustrate that the diffraction grating is not such an attractive alternative to the F-P as it might appear at first sight.

With interferometers a much larger order of interference is used with many fewer path lengths. Since the resolving power is still the product of the order and the number of light beams, instruments such as the Michelson interferometer with only two beams are generally greatly inferior for high resolution work when compared with multiple beam interferometers such as the F-P and the reflection echelon grating. With the two beam devices and the multiple beam ones like the echelon, the number of light paths is known. The theoretical resolving power can therefore be found with the same simple multiplication used for the diffraction grating. However, with multiple beam devices using semi-reflecting surfaces (such as the F-P spectrometer) the maximum number of path lengths possible for one ray will depend on the number of reflections which can be obtained before the intensity becomes too low; i.e. the higher the reflection coefficient of the surfaces the greater the number of reflections and the better the theoretical resolving power becomes.

There is no absolute number of reflections since the limit is reached only when the intensity becomes too small to have any effect. It is, therefore, not possible to define a theoretical resolving power for the F-P spectrometer using the method above. This can only be done in terms of a practical resolving limit as explained in Section 6.2.1. However, it is still possible to have a theoretical factor based only on the reflection coefficient of the mirrors and a practical factor taking into account all deviations from perfect optical quality. To avoid confusion with the resolving power of other spectrometers a special factor known as the <u>finesse</u> is used.

6.3.3 The Fabry-Perot finesse

We shall first consider the "theoretical" finesse of the instrument. Since this depends only on the reflection coefficient of the mirror surfaces it is usually referred to as the reflection finesse, N_R. This is calculated using the Airy function which describes the fringe intensity in terms of the reflection and transmission coefficients, R and T, of the mirror surfaces. For the transmitted fringes it takes the form

$$G_T = \left(\frac{T}{1-R}\right)^2 \left\{1 + \frac{4R}{(1-R)^2} \sin^2 \pi\sigma\Delta\right\} \qquad (6\text{-}8)$$

where G_T is the fraction of the incident light which is transmitted, σ is $1/\lambda$ and Δ is the optical retardation. This is equal to the left hand side of equation (6-2). Hence, transmission maxima occur when $\Delta = n\lambda$. Since n is an integer, sin $n\pi$ is zero. Therefore the transmission factor at each maximum is simply

$$G_m = \frac{T^2}{(1-R)^2} \qquad (6\text{-}9)$$

It can be seen that if the plates absorbed no light we should have $T + R = 1$, giving $G_m = 1$; i.e. the intensity of each peak would equal that of the incident light. This explains why the F-P gives such high luminosity even though it is working at very high orders of interference. In practice, of course, the plates always have an absorption coefficient A giving $T + R + A = 1$. G_m may then also be calculated from the alternative expressions

$$G_m = \left(\frac{1-A-R}{1-R}\right)^2 = \left(\frac{T}{A+T}\right)^2 \qquad (6\text{-}10)$$

The resolution of the instrument will depend on the sharpness of the fringes and this in turn will depend on the rate at which G_T falls to a minimum (obtained when $\sin(\pi\sigma\Delta)$ equals unity). From equation (6-8) it can be seen that this depends solely on the factor $4R/(1-R)^2$. This was therefore termed the coefficient of finesse, F, by Fabry. However, it is not very useful in practice because it neither has any relation to the resolving power of other spectrometers nor illustrates the relation between the resolving power and FSR of the F-P (which is very important with such a small FSR).

In view of this, the finesse, N, is defined as the free spectral range divided by the observed half-width of a fringe obtained from an infinitely narrow source line. Thus for N_R the half-width used will be that due to the value of the reflection coefficient. It may therefore be found using the value of Δ obtained when $G_T = G_m/2$ is substituted into equation (6-8). This gives

$$N_R = \frac{\pi R^{\frac{1}{2}}}{1-R} \qquad (6\text{-}11)$$

(In the older literature the reflection finesse is often given on the basis of Rayleigh's criterion for the resolving limit. This results in the slightly smaller value

$$N_R' = \frac{2.98 R^{\frac{1}{2}}}{1-R} \qquad (6\text{-}12)$$

but is rarely used with the F-P spectrometer. It corresponds to a resolving limit slightly larger than the half-width of the fringe).

Values of N_R corresponding to some different values of R are shown in Table 6-2. Also given are the values of G_m for different values of A. It can be seen that, except at very low absorption levels, increasing R decreases the peak intensity much more than it increases the finesse even if the absorption of the plates is kept constant; e.g. for plates giving 6% absorption, increasing N_R from 18 to 38 reduces the peak intensity 6.5 fold. The situation is even worse if the higher value of R is achieved at the expense of an increase in plate absorption. For example, if the same increase in N_R were obtained by increasing the plate absorption from 2% to 6%, there would be almost a 13 fold reduction in the peak intensity. It will be shown below that because no instrument is optically perfect values of N_R greater than 30 to 40 seldom give a significant improvement in the overall finesse of the instrument. Therefore, unless the plates give very low absorption (much less than 1%) it is always best to use the minimum acceptable value of N_R with the lowest possible absorption of light by the plates.

Table 6-2

(The numbers in the main part of the table are values of G_m).

A		R = 0.80	0.84	0.88	0.92	0.96	0.98
	N_R =	14.1	18.0	24.6	37.6	77.0	156
0.18		0.01	-	-	-	-	-
0.14		0.09	0.02	-	-	-	-
0.10		0.25	0.14	0.03	-	-	-
0.06		0.49	0.39	0.25	0.06	-	-
0.02		0.81	0.77	0.69	0.56	0.25	-
0.01		0.90	0.88	0.84	0.77	0.56	0.25
0.005		0.95	0.94	0.92	0.88	0.77	0.56
0.001		0.99	0.99	0.98	0.98	0.95	0.90

Deviations from optical perfection

As mentioned above, the value of N_R calculated from the plate reflectivity would only represent the practical finesse of the instrument if all components were optically perfect. The most serious deviation from perfection is the fact that the plates have a finite flatness and can never be set exactly parallel (especially when one is moved to scan fringes). Less important is the finite size of the scanning aperture which adds to the recorded width of the fringes. Both of these factors may be expressed in terms of a finesse.

The surface defects finesse, N_D will be affected by the original grinding of the plates, the setting of plate parallelism, bowing of the moving plate due to fixing to the piezoelectric transducer and the forces on it while it oscillates, etc. It may be shown (Ref. 146, Section 3.2) that if the flatness of the plates is expressed in the form λ/m then $N_D = m/2$; e.g. if the plates are flat to $\lambda_{green}/50$

then N_D will be 25 for green light. It is almost always the limiting finesse for the instrument, especially when light of shorter wavelength is used (plates specified as flat to $\lambda/50$ at 5461Å will give N_D values of only 18 at 4000Å and 11.5 at 2500Å). Some improvement may usually be obtained by using a stop so that only the centre area of the plates is utilised. This is because it is easier to set and maintain plate parallelism over a small area at the centre and because commercial plates usually exceed their specified flatness in this region.

The scanning finesse, N_F depends on the size of the solid angle accepted by the scanning aperture used to record the fringes; i.e. on the diameter of the hole and the focal length of the lens used to focus the fringes. It is defined as

$$N_F = \frac{2.\pi.\Delta\sigma}{\Omega.\sigma} \qquad (6\text{-}13)$$

where $\Delta\sigma$ = FSR (in cm^{-1}).

σ = wavenumber of light used (in cm^{-1})

Ω = the solid angle associated with the diaphragm hole.

If the radius of the hole is r, the focal length of the lens f and we define an angle α such that $\tan\alpha = r/f$, the solid angle is given by $2\pi(1-\cos\alpha)$.

Hence,

$$N_F = \frac{\Delta\sigma}{\sigma(1-\cos\alpha)} \qquad (6\text{-}14)$$

It is difficult to evaluate equation (6-14) directly because α is always extremely small. However, this fact allows a useful approximation. Substituting $2\sin^2\alpha/2 = (1-\cos\alpha)$ into equation (6-14) gives

$$N_F = \frac{\Delta\sigma}{2.\sigma.\sin^2\alpha/2} \qquad (6\text{-}15)$$

But for small α, $\sin\alpha \rightarrow \alpha$. Hence we have

$$N_F = \frac{\Delta\sigma}{2.\sigma.(\alpha/2)^2} = \frac{2.\Delta\sigma}{\sigma.\alpha^2} \qquad (6\text{-}16)$$

But for small α, $\tan\alpha \to \alpha$. Therefore,

$$N_F = \frac{2.\Delta\sigma}{\sigma(\tan\alpha)^2} \qquad (6\text{-}17)$$

Substituting $\tan\alpha = r/f$ gives

$$N_F = 2.\left(\frac{\Delta\sigma}{\sigma}.\frac{f}{r}\right)^2 \qquad (6\text{-}18)$$

This approximation works well even for quite large values of r/f (i.e. small N_F); e.g. $N_F = 1.5$ is obtained to five significant figures. Some values of N_F obtained using equation (6-18) with $\Delta\sigma = 1\text{cm}^{-1}$, $\sigma = 20000\text{cm}^{-1}$ (i.e. $\lambda = 5000\text{Å}$) and useful values of r and f are given in Table 6-3. It can be seen that N_F will not be the limiting finesse since large values are easily obtained. N_F should not be made unnecessarily large as this reduces the luminosity of the instrument, but it must be sufficient to cover the FSR's likely to be used.

Table 6-3

f (cm)	r(mm) 0.1	0.2	0.3	0.5	0.7	1.0
25	625	141	69	25	13	6
30	900	225	100	36	18	9
35	1225	306	136	49	25	12
40	1600	400	178	64	33	16
45	2025	506	225	81	41	20
50	2500	625	277	100	51	25
55	3025	756	336	121	62	30
60	3600	900	400	144	73	36

Practical instrumental finesse, N

The combination of N_R, N_D and N_F to give a resultant finesse N depends on their relative values. However, it may be shown[154] that to a good approximation

$$\frac{1}{N^2} = \frac{1}{N_R^2} + \frac{1}{N_D^2} + \frac{1}{N_F^2} \qquad (6\text{-}19)$$

This has several very important consequences:

(i) The maximum value of N can never exceed the smallest of the three component values. Furthermore, it would only equal this one even if the other two were infinitely large, which is unlikely.

(ii) Making one component very much larger than the others will only cause a small increase in N. If this were done at the expense of the reducing of the light transmission (e.g. by increasing the reflectivity of the plates), the small increase in N would be accompanied by a large reduction in the luminosity of the instrument.

The best compromise between high finesse and good luminosity is to have $N_R = N_D = N_F$. This gives N as approximately $0.6N_R$ (etc.). In practice it is inconvenient to change N_F for each different scan and usually N_F is made sufficiently large so that $1/N_F^2 = 0$ under most conditions. Then putting $N_R = N_D$ gives N as about $0.7N_R$ or $0.7N_D$. Since it is difficult to obtain values of N_D higher than about 35 even with green or yellow light, values of R greater than 0.92 to 0.94 are unnecessary for most purposes. The corresponding value of N would be about 25.

6.4 The Apparatus

6.4.1 The basic interferometer

The instrumentation is constructed around the Hilger and Watts N250 Fabry-Perot interferometer which, as mentioned earlier, is based very closely on the prototype instrument of Cooper and Greig.

(The design and construction of the prototype is described extensively in part II of Ref. 155). For our purposes the instrument provides three basic facilities:

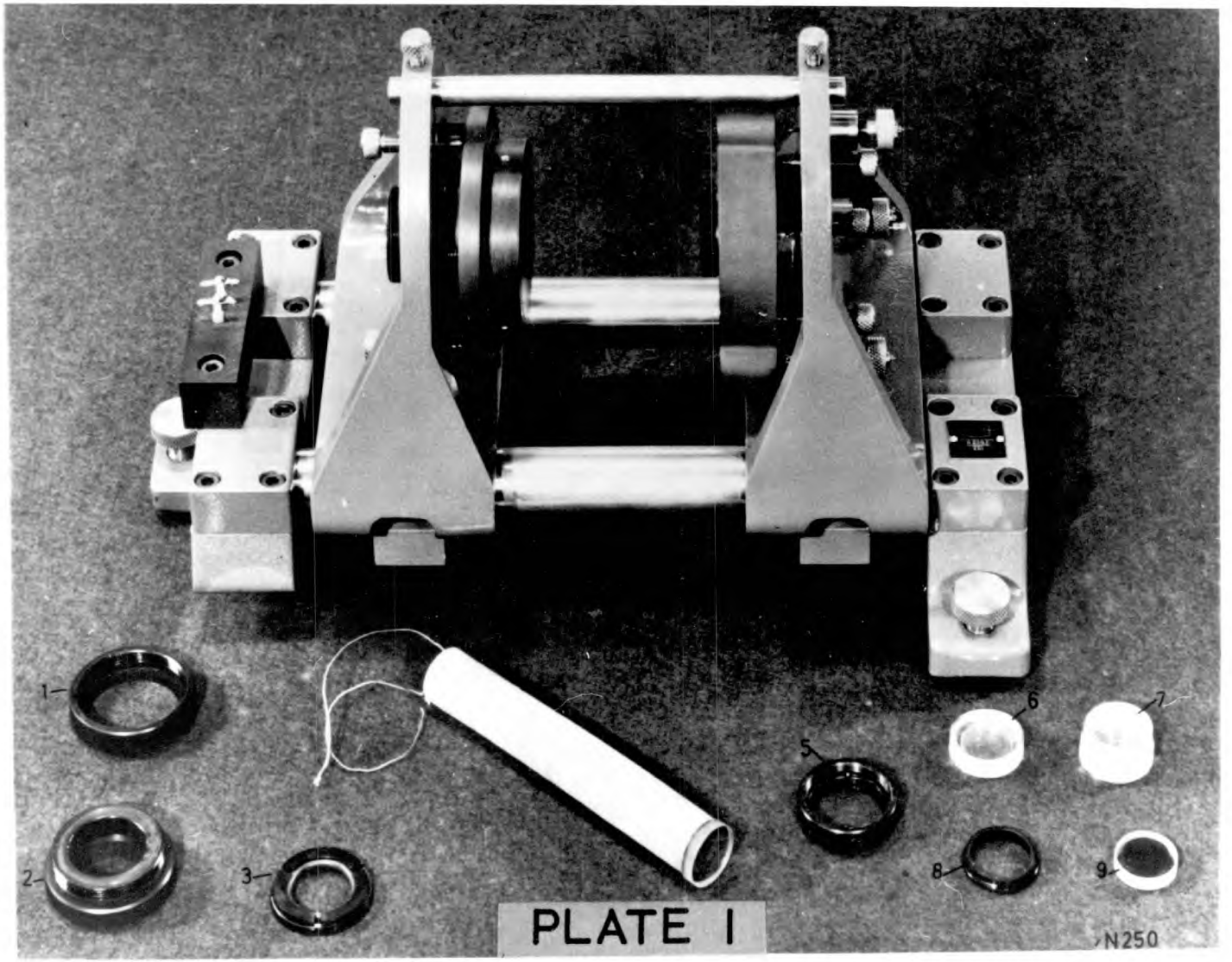
(i) A rigid framework which supports the interferometer plates and allows a variable FSR.

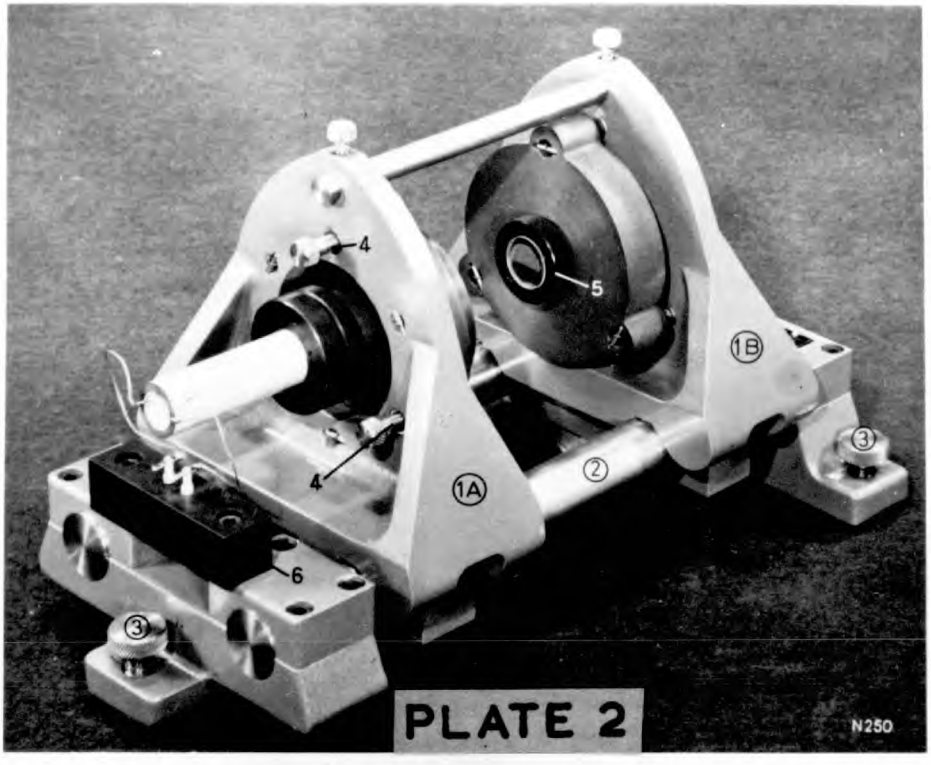
(ii) Spring adjusted mounts to allow the mirror surfaces to be set accurately parallel.

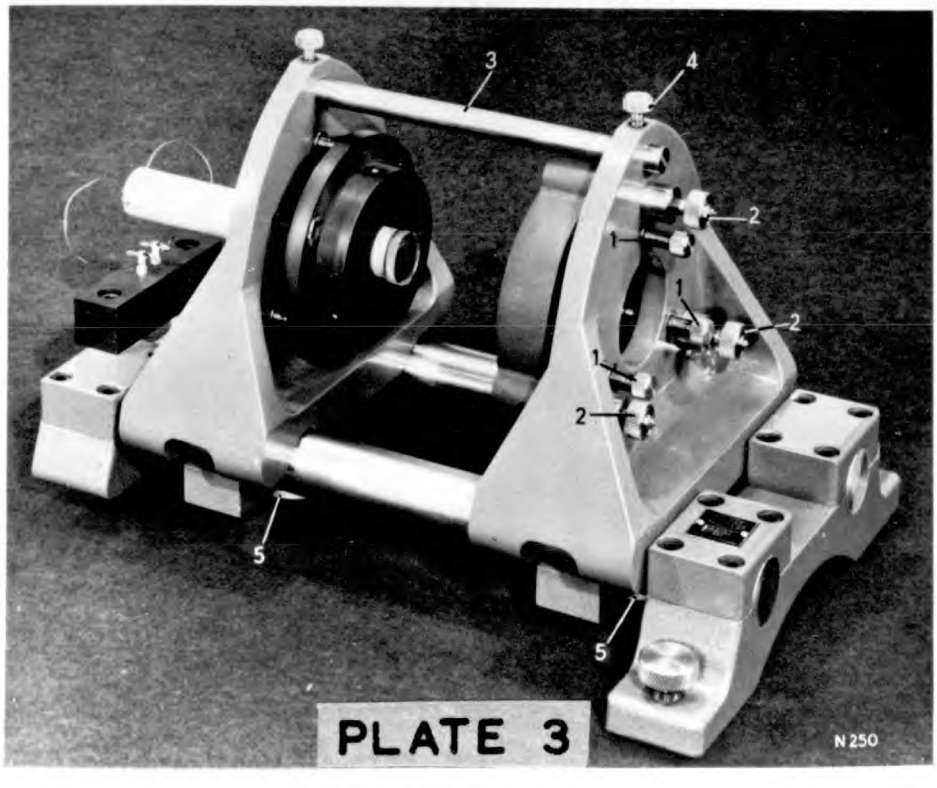
(iii) A piezoelectric transducer which allows the plate separation to be altered by distances of the order of $\lambda/2$ while accurately maintaining the mirror parallelism.

The construction of the N250 interferometer is shown in Plates 1,2 and 3. In the description below the components will be referred to using notation of the type 2/5, which means the part numbered 5 in Plate 2.

The base of the instrument is made up of two heavy stainless steel bars (2/2) held together at their ends by two clamps. These clamps rest on three adjustable feet (2/3) by which the instrument may be leveled. The interferometer plates and their mounts are supported in two frames (2/1A and 2/1B) which slide along the steel bars so that any plate separation from 0 to 75mm may be used. The frames are clamped to the bars by capstan screws (3/5) when in the required position. A small bar (3/3) with locking screws (3/4) is fitted between the tops of the frames to damp any vibrations which may occur. The frame 2/1A is used to support the piezoelectric transducer and the oscillating plate and is fitted with three adjusting screws (2/4) used to set the exact position of the plate. The other frame supports the stationary plate (2/5) and its mount and has three similar screws (3/1). However, it also carries three other screw controls (3/2). These alter the tension of the springs which hold the mirror mount to the frame. They therefore provide a very fine


1
2
3
5
6
7
8
9
PLATE 1
N250


4
5
1B
3
4
1A
2
6
3
PLATE 2
N250


3
4
2
1
1
2
1
2
5
5
PLATE 3
N250

adjustment and are used to make the final trimming of the plate so that the two mirror surfaces are exactly parallel.

The method of supporting the two interferometer plates in their mounts can be seen from Plate 1. The stationary mirror (1/9) is placed inside a split ring (1/8) which has one side bevelled. The ring is fitted into a locking ring (1/5) with a matching bevelled surface. When this ring is screwed to the mount the plate is locked rigidly in place by the contraction of the split ring. (The components 1/6 and 1/7 are spacers used to hold the two plates face to face for storage purposes). The other plate is cemented with epoxy resin to one end of the piezoelectric transducer (1/4). This is a barium titanate tube of length 75mm and internal and external diameter of 19mm and 25mm respectively. (The tube in the photographs is a different one 150mm long). Silver is plated on to the inner and outer surfaces of the tube to form two electrodes to which two thin copper wires are soldered, as shown. A rubber 'O' ring inside a bevelled split ring (1/3) is fitted over the ceramic tube and set so that it is exactly at the centre of mass of the tube and plate. Two locking rings (1/1 and 1/2) are then added from opposite ends of the tube and screwed together so that the split ring contracts and the ceramic tube is locked in place. The larger of the two rings (1/2) also has an internal thread on the opposite side and this is used to screw the whole assembly to its mount. The two copper wires are supported by two terminals mounted on an insulating block (2/6). When a voltage is applied across the two wires, the piezoelectric expands or contracts. This movement moves the interferometer plate and gives the required change in plate separation to scan fringes.

The interferometer plates used in the present work were Hilger and Watts type B358. These are vitreous silica of 26mm diameter and specified flat to $\lambda/50$ at 5461Å. The mirror coatings were also supplied by Hilger and Watts. They are aluminium giving a usable wavelength range of at least 2000 to 8000Å. They are specified only as giving 2% transmission. From the attainable finesse

at 5461Å (see Section 6.5) it was estimated that the plates are probably flat to about $\lambda/60$ over their central 1cm and that their surfaces give about 86% reflection and 12% absorption, i.e. $N_R = 21$ and $G_m = 0.02$.

6.4.2 Arrangement of optical components

The interferometer and all ancillary optical components were mounted on a 180cm optical bar of the standard spectrographic type. This bar was fitted with three feet so that it could be leveled and rested on antivibration mounts. The interferometer was mounted on the optical bar with the Hilger and Watts F1565 stand which also incorporates rubber pads to damp vibrations. The arrangement of the optical components on the bar is shown schematically in Fig. 6-1.

All lenses employed were of fused silica and the focal lengths were chosen to give a convenient arrangement of the optical bar. It was intended to use the instrument with a variety of sources, including HCL's, VDL's and EDT's. To facilitate the interchange of sources the light from the source was focussed on to a source aperture which provides a reproducible secondary source for alignment purposes. Its diameter is arbitrary but .2mm was useful for studying selected areas of the emission source. The sources used for experiments are described in Chapter VI. For setting up and testing the instrument a mercury EDT was used. The maximum usable diameter of the interferometer plates is limited to 19mm by the internal diameter of the ceramic tube but it was further reduced by the use of an iris diaphragm to improve the finesse and reduce flare at the lens. A diameter of 10mm was used for most work. The diameter of the scanning aperture is very important and 0.5mm was chosen in conjunction with the 300mm lens to give $N_F = 144$. This is sufficiently large to have a negligible effect on the total finesse, N, but only a small increase in light intensity would be obtained with a larger hole because the maximum slit-width of the monochromator used is only 0.3mm.

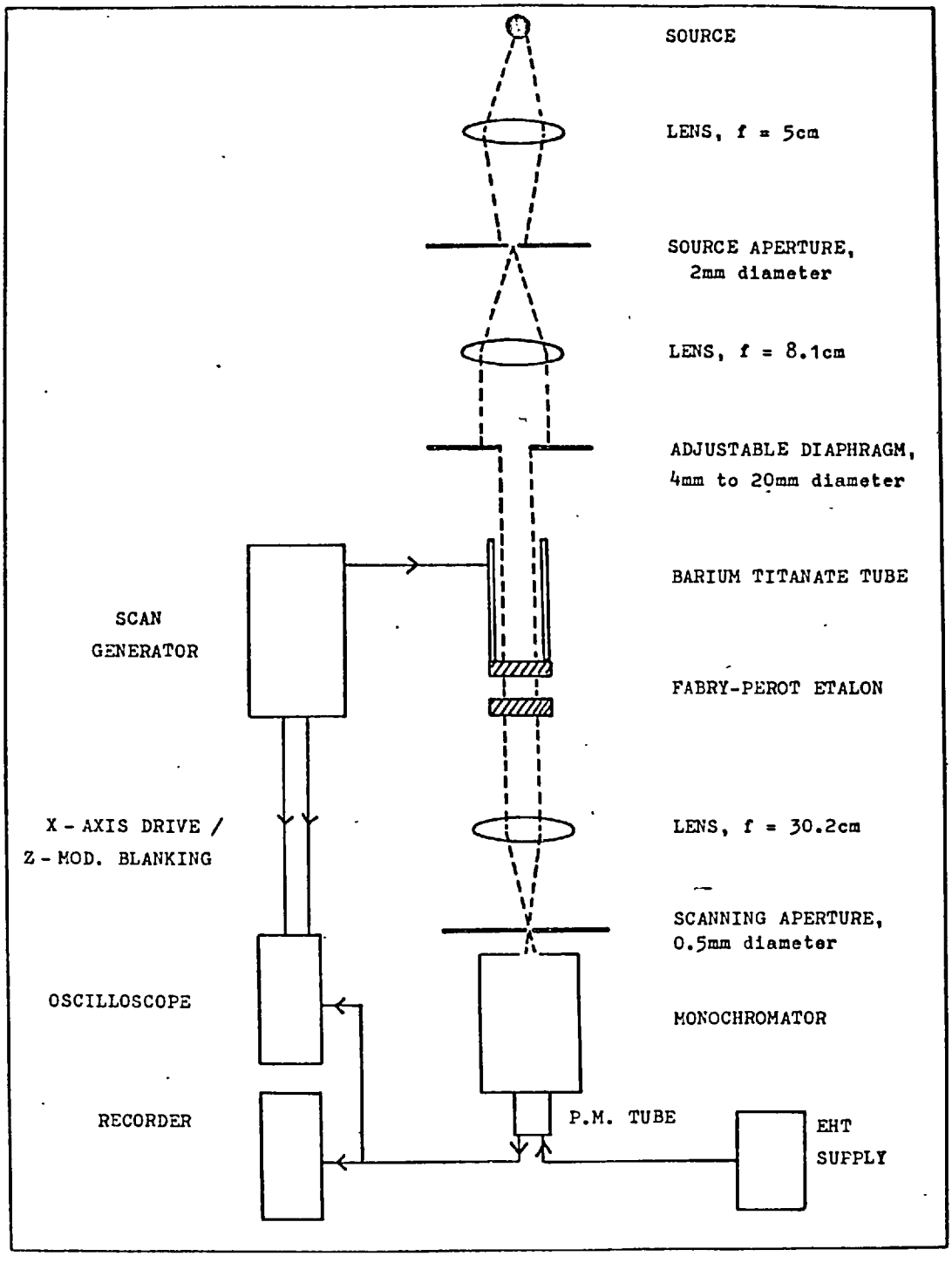


Fig. 6-1 Schematic Diagram of The Fabry-Perot Spectrometer

The plate containing the scanning aperture was cemented directly over the entrance slit of the monochromator which is a Si-Ro-Spec grating instrument normally supplied with the Techtron AA4 atomic absorption spectrometer. It has a reciprocal linear dispersion of 33Å/mm and an aperture of f10. A nine-stage side-window photomultiplier tube (Hamamatsu R213) was mounted immediately in front of the exit slit of the monochromator and used as the radiation detector.

The 300mm lens used to focus the fringes was placed about 40cm from the end of the interferometer. This allowed space for the head to be inserted to study the fringes visually (almost essential when setting up the instrument). The extra space also meant that when this lens was removed a Hilger and Watts N306 fringe intensity viewer could be fitted to the optical bar. This instrument is a highly corrected achromatic telescope focussed on infinity and fitted with a beam splitter and eyepiece. The latter is in a side tube so that it is extremely convenient for viewing the fringes. It is also fitted with a scanning aperture and photomultiplier housing so that it may be used directly with the scanning interferometer. This was not done in the present work because of the need for auxiliary equipment to isolate a spectral line and because the glass optics only allow lines down to about 3800Å to be used. However, the viewer was always used to set the alignment of the components on the optical bar, as described in Section 6.5.1. The eyepiece is fitted with a graticule which sets the optical axis exactly 18cm above the centre of the optical bar. This corresponds to the centre of the interferometer plates when all of the recommended accessories are used and all components on the bar were adjusted to this standard height. The viewer also incorporates a lamp to illuminate the graticule. The interferometer plates may be adjusted perpendicular to the optical axis by viewing the image of this graticule reflected from them.

6.4.3 The electrical system of the spectrometer

(a) The scanning power supply

Although it is only necessary to alter the length of the ceramic tube by $\lambda/2$ to scan one order fairly high voltages are required to do this. It was found that the plate separation is altered by about 25Å per volt applied to the tube; e.g. at 5461Å about 110v is required to scan one order. In view of this a conventional signal generator is unsuitable for use in the rapid scanning mode and a special generator was required. This was therefore designed to provide both slow and rapid scanning power supplies. The unit is mounted in a standard "nineteen inch" rack and is made up of the following modules:

(i) An Aim Electronics PSU 101 stabilised power supply which provides +20/-20v at 1Amp and +150/-150v at 50mA and is used to power the other modules.

(ii) An Aim Electronics SSG 212 slow scan generator which provides a triangular wave output with a peak to peak voltage continuously variable from 0 to 20v. The time taken to scan one wave (i.e. the peak to peak voltage) is also continuously variable in two calibrated ranges which provide frequencies of 1 cycle in 5 seconds to 1 cycle in 55 seconds and 1 cycle in 50 seconds to 1 cycle in 550 seconds. The generator may be stopped and held at any required position on the ramp.

(iii) A Chelsea Instruments TWG10 rapid scan generator which provides a triangular waveform with a peak to peak voltage continuously variable from 0 to 10v. The frequency is also continuously variable in two switched ranges of 0.2 Hz to 16.5 Hz and 6.25 Hz to 500 Hz. This generator also supplies a fixed amplitude square wave output which is used to switch off the oscilloscope cathode ray tube during each return trace (to prevent a double image being seen).

(iv) A Chelsea Instruments HVA 10 amplifier. This is driven by either of the above generators and amplifies the voltage 100 times so that the ceramic tube may be conveniently driven. It will supply a maximum of ± 400 volts to the tube, which is sufficient to scan about 7 orders at 5461Å and correspondingly more at shorter wavelengths. The amplifier is only capable of following the rapid scan generator up to about 100 Hz and a distorted waveform is obtained if higher frequencies are used. The unit may also be switched to an internal voltage control which provides a manual control of the voltage applied to the tube over the full range of +400 to -400v.

(v) An output module fitted with a moving coil DC meter (0-25μA, calibrated 0-500v on a 5-inch scale) to measure the slow scan voltage applied to the tube. The unit is also fitted with a reversing switch for the meter, input and output connections for the other modules and a switch to select slow or fast scan inputs for the amplifier.

(b) The read-out equipment

The R213 photomultiplier tube was powered by a Hilger and Watts FA187 EHT supply unit. This provides a continuously variable voltage in two ranges of 350V to 1050V and 750V to 2100V, the lower range being suitable for this type of photomultiplier. The output from the photomultiplier was switched to either an oscilloscope or a chart recorder, depending on the scan speed. The oscilloscope used was a Telequipment D53A fitted with two independent y-axis amplifiers. The signal is fed directly into the second input of a type B differential amplifier. This input features reversed polarity so that the negative signal from the photomultiplier is displayed on the screen as fringes which are the "correct way up". No extra amplification of

the signal was required since the amplifier has a sensitivity range of 1mV-5V per cm. and the observed signal is very noisy even when 5mV per cm is used. The time base of the oscilloscope was generally switched to external and driven by an auxiliary triangular wave output from the oscillator. This waveform was also fed into the input of the second amplifier (type J) so that it could be monitored when required. The oscilloscope was also fitted with a "Z-mod" input so that the square wave output from the oscillator could be used to blank out the return trace during each cycle.

At slow scan speeds the DC signal from the photomultiplier was amplified by a microammeter unit (RCA Type 84C) before being passed to a unit providing variable degrees of backing-off and a range of time constants. The circuit diagram of this unit is shown in Fig. 6-2. S_1 is a single pole switch used to switch off the battery if the recorder is to be used without any backing off. S_2 is a double pole, double throw, centre-off switch which is used to select two backing-off ranges or to switch off simultaneously the battery and the signal. The two ranges provided are 9v to 18v (when the fixed 10K resistor is switched into circuit) or 0v to 18v (when the 10K resistor is switched out). Since the same amount of control is available over both ranges, the former provides a finer degree of control at high backing-off voltages than would be possible with a simple 0-18v range. In both cases a ten turn precision 10K potentiometer provides the course voltage adjustment and a ten turn precision 1K potentiometer is used for fine adjustment. The circuit is arranged so that this fine control allows the same percentage voltage change no matter what backing off voltage is used (10% on the 0-18v range and 5% on the 9-18v range).

The variable condenser, C, which provides variable signal damping is actually a wafer switch fitted with condensers so that 0, 5, 10, 25, 50, 100, 250 or 500μF may be selected to provide damping. In use it was found that condensers up to 50μF had little effect on the recorder time constant with the present system; factors such as the

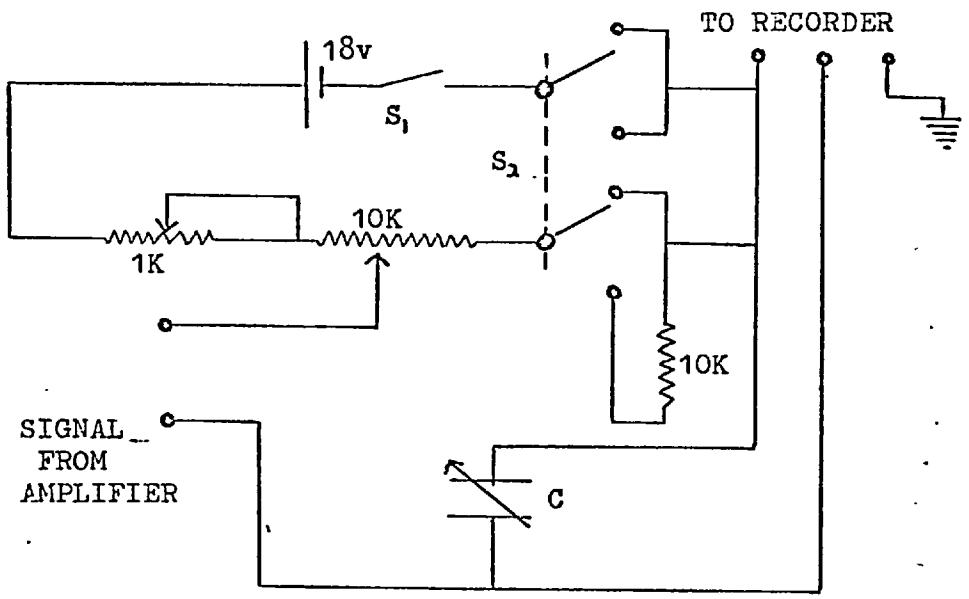


Fig. 6-2 Circuit Diagram of Backing-off and Damping Unit

signal size and the combination of amplifier and recorder settings were much more important. With the larger condensers the capacity used was the controlling factor. The time constants for 90% of full scale deflection were approximately 3.5, 9.5 and 20 seconds for the 100, 250 and 500μF condensers respectively. These large time constants could be used with only extremely slow scan speeds to avoid distortion of the recorded fringes.

The unit was connected to the chart recorder (Servoscibe Desk Type) by a twin core shielded cable. The shield was used to link the metal case of the unit to the earth terminal of the recorder and greatly reduced signal noise and drift. The combination of a wide range of recorder sensitivities (2, 5, 10, 20, 50, 100, 200, 500mV, 1, 5, 20V) with those of the amplifier (X0.01, 0.1, 1.0, 10, 100, 1000) meant that relative peak intensities could be measured over large variations of intensity.

(c) Source power supplies

The HCL's were powered by a Techtron MLS1-A power supply unit of the type fitted to the AA4 spectrometer. This is able to provide a 3-25mA DC warm-up output on three channels and a 3-30mA stabilized DC output on one channel. The VDL's were powered by a half wave rectifier connected to a "Variac" adjustable transformer. The latter was used to vary the current supplied to the VDL's, the normal range being 0.3 to 1.5A. Since only half-wave rectification is used, the VDL's could not be normally used to observe a profile on the oscilloscope. The EDT's were powered by a Microtron 200 microwave generator which provides an output of 20 to 200 watt at 2450 MHz. The generator was normally used in conjunction with a standard 9ft microwave cable and a 210L discharge cavity (Electromedical Supplies). The optimum conditions for EDT's were usually found using the optional portable reflected power meter which may be connected between the generator and the cable.

6.5 Adjustment and Use of The Interferometer

6.5.1 Setting-up

If the highest resolution is to be obtained from the interferometer it is essential that no unnecessary distortion of the fringes be produced. This requires that the components on the optical bar be aligned extremely carefully. However, it was found that the necessary adjustments could be completed quickly and easily using the following systematic approach.

Initially the interferometer is removed from its stand on the optical bar and all components on the source side of the system are positioned approximately by measurement. The fringe viewer is placed on the bar and the source aperture is illuminated using a mercury EDT and a green optical filter. The positions of the source aperture and

the 8cm lens are then varied until a sharp image of the aperture is seen exactly on the optical axis of the graticule in the viewer. The adjustable diaphragm is then placed centrally in the light beam and set to about 1cm to reduce the flare at the lenses. The final adjustment to the focussing may then be made.

The fringe viewer is now removed and the 30cm lens and the monochromator adjusted until a sharp image of the source aperture is obtained on the plate containing the scanning aperture. The latter should lie at the centre of the circle of light. The exact position of the 30cm lens is marked so that it may again be replaced by the fringe viewer. The interferometer is then placed on its stand on the optical bar but with only the movable plate and ceramic tube in position. The lamp in the viewer is now switched on so that an image of the graticule reflected from the surface of the plate may be seen. The adjusting screws (2/4) are now moved until the two images of the graticule exactly coincide. The interferometer plate is now normal to the optical axis. The second interferometer plate is now mounted, the approximate plate separation set and the locking screws (3/4 and 3/5) tightened. The illuminated graticule is again used to set the position of the plate, using the screws 3/1.

The two plates are now parallel, but only approximately by interferometric standards. The fringe viewer is again replaced by the 30cm. lens and the head is placed between the interferometer and the lens so that fringes may be viewed directly. The screws 3/1 are again used until a set of sharp concentric rings is observed. If the ceramic tube is now oscillated at 20 to 30 Hz and the green filter removed.it should be possible to see a series of broad fringes on the oscilloscope at the 5461Å line. The oscillator voltage level should be set to give four or five fringes and the fine adjustment screws (3/2) must now be used until the fringes are as tall and sharp as possible and give approximately equal peak heights in successive orders. It will be necessary to repeat the fine adjustments from time to time to maintain optimum results.

The complete resetting of all components should not be necessary unless one component is accidentally moved. Similarly, it will only be necessary to use the illuminated graticule in the fringe viewer if the plates are demounted. If the plate separation is changed, or if the spectrometer is not used for several days, it will probably be necessary to reset the parallelism using the screws 3/1 while viewing the fringes visually. In all other cases adjustments are made using only the fine screws 3/2 while watching the oscilloscope trace. If care is taken to tension all springs equally the setting should give optimum results for up to two hours and the mirrors should remain sufficiently parallel to observe a line profile for at least 48 hours.

6.5.2 Scanning spectra

With the interferometer accurately set up using the above procedure, it was in a suitable form to scan spectra using the selected FSR. Routine testing of spectral sources was usually carried out with rapid scanning at about 25Hz. At higher speeds it is more difficult to maintain plate parallelism and the sharpness of the peaks is reduced. At slower speeds much better quality is obtained but "flicker" of the oscilloscope trace makes study of the line profile difficult. Rapid scanning also allows study of the line profile from sources giving an unsteady output; for example, during warm-up. In view of this, rapid scans at 25Hz were extremely useful for studying the suitability of sources used in AAS and AFS and some examples of the technique are given in Chapter VII.

The main disadvantages of fast scanning using the oscilloscope for readout are the difficulty of making accurate measurements on the line profiles and the fact that low signal noise levels are only obtained using relatively intense sources. These problems are easily overcome using the slow scanning mode (say, one cycle per minute or

slower) and a chart recorder. A tracing of the scan is then permanent and immediately available for accurate measurements. It was also found that slow scanning allowed the use of much less intense sources without excessively high noise levels due to the signal integration and damping inherent in the system. Apart from this, the slower scans result in considerably higher finesse than is possible using the oscilloscope. Some examples of the accurate measurements and low intensity levels allowed by slow scanning are again given in Chapter VII.

It should be noted that before any meaningful results can be obtained from a spectral source by either rapid or slow scanning a literature check on the required line is essential to determine the nature of any hyperfine structure (hfs) which may exist. If the line width greatly exceeds the selected FSR it will be extremely difficult to identify the peaks obtained on the scan unless a full analysis is made by measuring the actual separations on a recorder chart. Even if the FSR is sufficiently large, some practice is usually necessary before individual peaks can be quickly identified. This is because it is extemely unlikely that all hfs components of a line will be resolved, so that each observed peak may be the integrated intensity of several components. The amount of separation obtained will depend on both the line broadening in the source and the instrumental width of the spectrometer.

These aspects of high resolution work which apply, of course, to all types of spectrometers, are well illustrated by scans of the mercury 5461Å line. The hyperfine structure of the line is shown in Fig. 6-3. It is extremely complicated because mercury has six abundant isotopes and two of these are odd giving an additional nuclear spin fine structure. The total width of the line is almost 1600mK (i.e. 0.535Å at this wavelength). However, the extreme component (201a) is very weak and the line may be scanned without serious overlap using a FSR of 1500mK, as shown in Fig. 6-4.

It can be seen that none of the central components are resolved

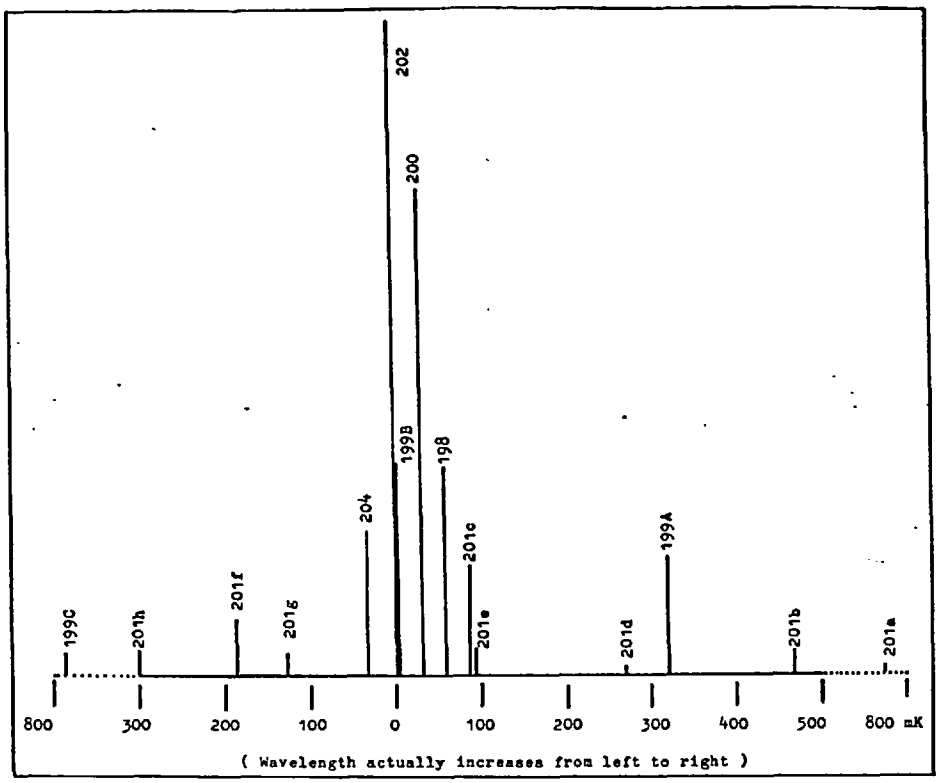


Fig. 6-3 Hyperfine Structure of The Mercury 5461A Line

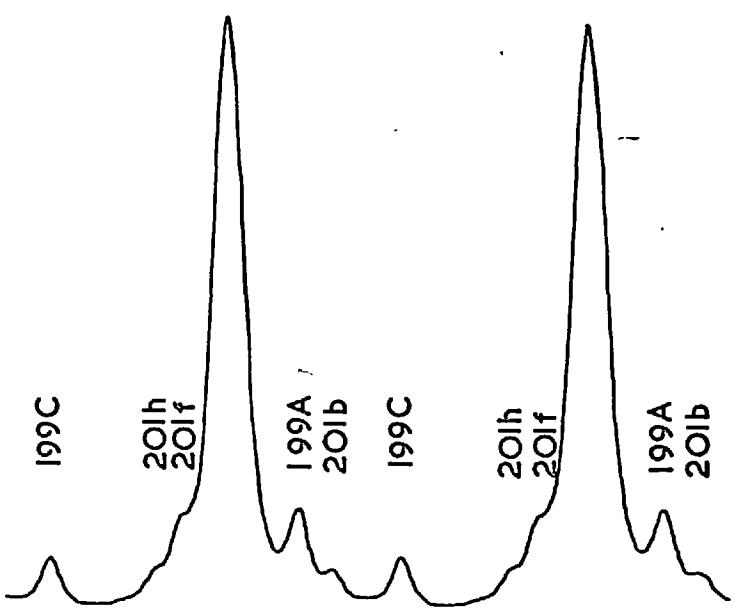


Fig. 6-4 Slow Scan of The Mercury 5461A Line With a FSR of 1500mK or 0.5A (Two Orders)

but the true structure of the line is easily recognised.

When overlap of orders is used it is essential that the exact FSR to be used is calculated so that no overlap of the major components is obtained. Suitable values for the 5461Å line are 650mK and 490mK. However, the technique is only successful if the individual components are fairly sharp and quite widely spaced. That this is not the case with this line can be seen from the two scans shown in Fig. 6-5. None of the peaks shown are produced by a single component and the scans are of little practical use. The components forming each peak could only be found by accurate measurements of the separations and calculation of the theoretical pattern. For 650mK they are (for the three smaller peaks, starting from the left) : 199A-201h; 201f-201b; 201g-199C. For 490mK the two smaller peaks are made up of 201-199C; 201f-199A-201g. (The components forming each peak are not, of course, all from the same order).

6.5.3 Attainable finesse

As mentioned earlier, the finesse of the instrument is a function of both the reflectivity of the mirror surfaces and the flatness and parallelism of the plates (together with the size of the scanning aperture if this is not made negligibly small). Since both of these factors vary in relative importance with wavelength, the calculation of the overall finesse is difficult and it is usually found experimentally by measuring the instrument profile. Ideally this is carried out by scanning an extremely sharp single line, such as that obtained from a single isotope of even atomic number (i.e. no nuclear spin hfs). Such a source was not available during the present work, but a good approximation may be obtained by scanning any source line using an extremely large FSR. This is obtained by setting the plate separation to a few thousandths of an inch.

An example of the results which may be obtained is given in Fig. 6-6 which shows three orders of a scan of the sodium D-lines

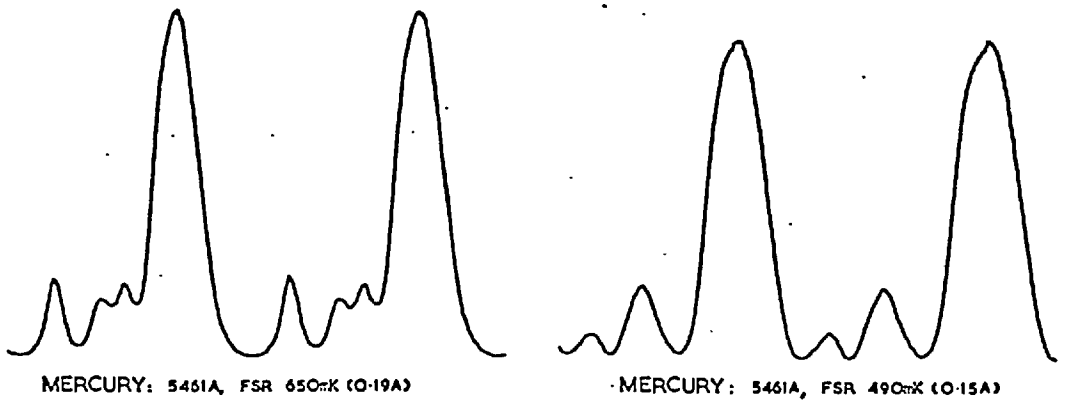
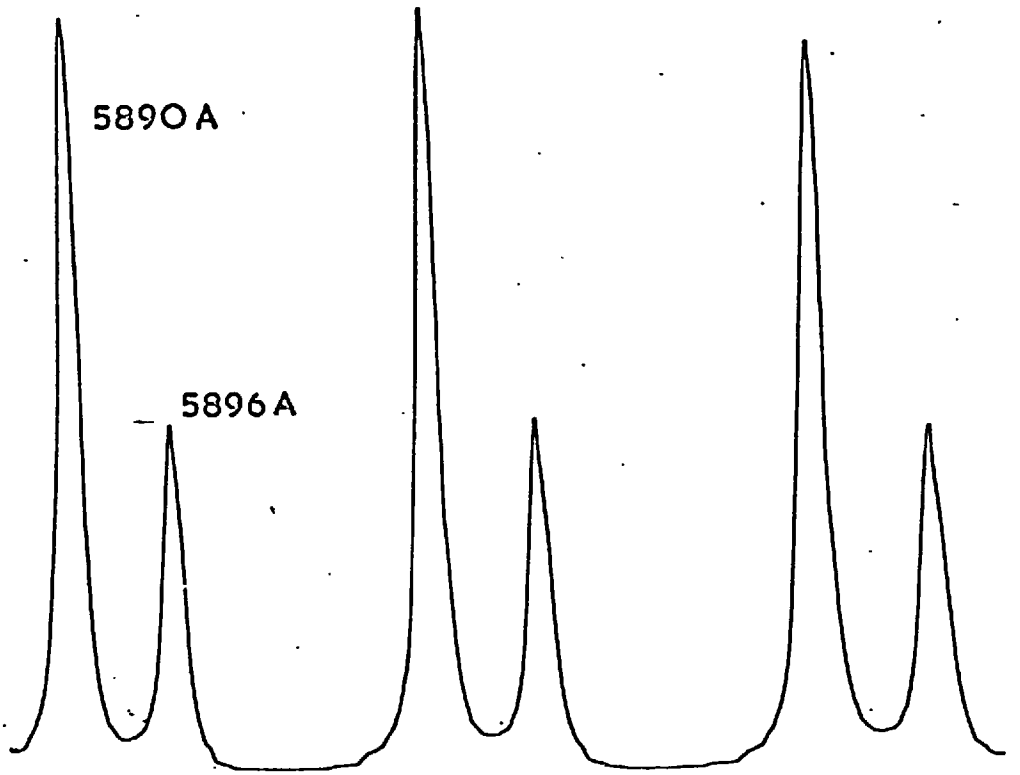


Fig. 6-5 Slow Scans Made With Overlap of Orders (Two Orders)

(obtained from a Wotan VDL). The plate separation was too small to measure accurately using a travelling microscope, but the FSR may be calculated from the order separation of the two lines, which corresponds to 6Å. The FSR is then found to be 20Å or 58K, which corresponds to a plate separation of only 0.086mm or 0.0035". The finesse calculated by measuring the half-width of the 5890Å line is 18. This means that the limit of resolution is just over 1Å at this FSR. However, it should be noted that the value of the finesse will apply to all values of the FSR at this particular wavelength (provided the plates are reset with the same precision). Therefore, values of the finesse obtained in this way may be used to calculate the instrumental line width for line width measurements made at much smaller FSR.

In view of the importance of the finesse if accurate measurements of line widths are to be made, its variation with wavelength was found by making measurements at a number of mercury lines. A scan of three orders of the 5461Å line (using the same plate separation as with the sodium D lines) is shown in Fig. 6-7. The finesse of 17·5 obtained is only possible with a slow scan; under the



SODIUM D LINES (FSR 20A or 58K)

Fig. 6-6

same conditions an oscilloscope trace obtained at 25Hz showed a finesse of 13. Hence, rapid scanning usually results in approximately a 20% reduction of the finesse values shown in Fig. 6-8 for the wavelength range 2500 to 5500Å. It can be seen that the finesse shows a reproducible decrease with decreasing wavelength. The irregularity in the region of 4000Å was quite reproducible (even a measurement made at the calcium 4226.7Å line and described in Chapter VII lay on the curve shown) and is probably characteristic of the particular plate coating.

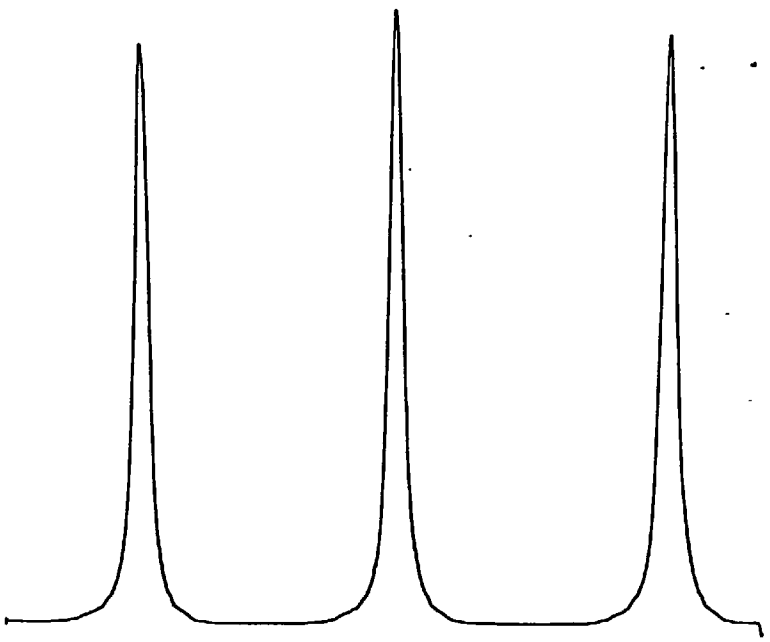


Fig. 6-7

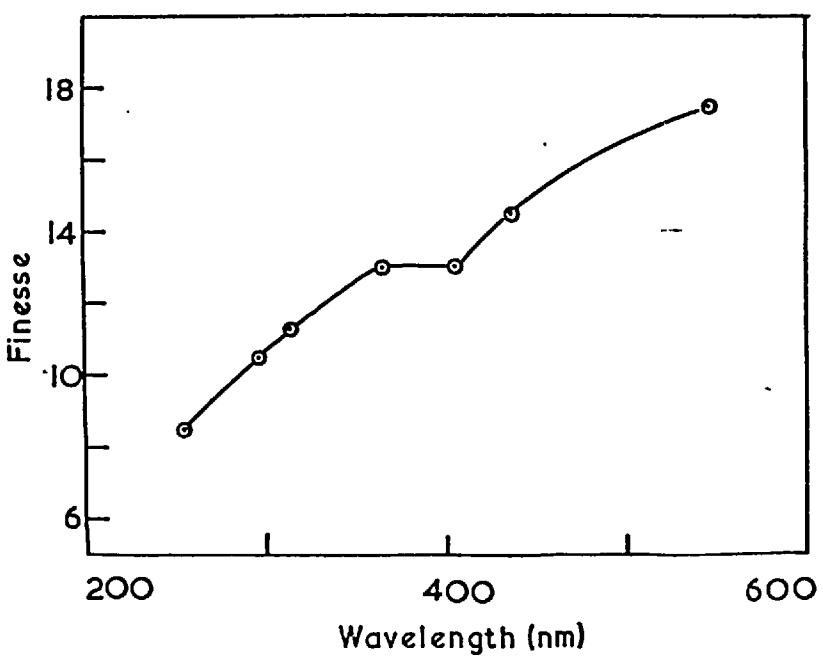


Fig. 6-8 Variation of Finesse With Wavelength For The Spectrometer Employed In The Slow-Scanning Mode

Chapter VII

The Evaluation of Spectral Sources By Measurement of Line Profiles

7.1 Introduction

Over the years many papers have been published on the widths of spectral lines, concerning both theoretical studies and practical spectroscopic measurements. The measurements have been used both to check the increasingly sophisticated calculations of line widths and for more practical purposes, such as studies of plasma temperatures or stellar gases. However, as mentioned in Section 6.2, work of direct interest to the analytical chemist using atomic absorption or fluorescence spectroscopy has been rather limited. A short list of the most useful of the recent papers in this area should help to indicate the scope of the work which has been carried out. There are also many papers by analytical chemists on isotopic analysis by optical spectroscopy (usually using very large grating spectrographs or pressure scanned F-P spectrometers) and some of these contain useful information on spectral sources suitable for AAS.

Several workers have attempted theoretical calculations of line widths and of the effect on calibration curves of changing the source and absorption line widths (see, for example, L'vov[156], Parsons et. al.[157] and Rann[158]). Some of these results are very useful but much confusion has resulted from their use outside of their original context. Probably actual practical measurements are of greater interest. In an early paper, Russell, Shelton and Walsh[159] used an echelle spectrum of the cadmium 2288Å line to illustrate the unsuitability of vapour discharge lamps as sources for the AAS determination of this element. Shimazu and Hashimoto[160] used a pressure scanned F-P to study the relationship between the source line profile from a sodium VDL and the shape of the analytical calibration curve. Atkinson and co-workers[161] compared

Osram VDL's with their own electrodeless discharge tubes for potassium and rubidium. They tested their suitability for excitation of atomic fluorescence by measurement of the effects of lamp current and temperature on self-reversal, line widths, hfs intensities and integrated intensities using a photographic F-P. Bodretsova, L'vov and co-workers[162,163] used a pressure scanned F-P to measure line widths of metals excited in conventional HCL's and those with an auxiliary high frequency discharge. They also reported that self-absorption was a major broadening factor and estimated the amount of absorption from the relative intensities of hfs components, as in the present work. Yasuda[164] also used a pressure scanned F-P to make a detailed study of the profile of the calcium 4226.7Å resonance line in emission from a HCL and a flame and also in absorption from both sources. Unfortunately, some of the assumptions made during the evaluation of his results appear to be open to criticism. Davies[165] investigated the mechanism of the Sullivan and Walsh type of high-intensity hollow cathode lamp by observation of the line profile and self-absorption of the copper 3247.5Å resonance line using a pressure scanned F-P. He also derived an expression (for this particular case) which relates the amount of absorption given by a sample to the relative intensities of the hfs groups in the source line (i.e. to the amount of self-absorption within the source) so that comparisons could be made with the intensity ratios measured at different lamp currents. Recently Human and co-workers studies the profile of the calcium 4226.7Å line from several sources during an investigation of multielement sources for AAS[26] and also carried out a theoretical study[166] on the effect of line width on AAS calibration curves.

In the present work, line profile measurements have been used in two ways to evaluate the suitability of spectral sources for AAS and AFS. For elements such as thallium, which have a well-defined hyperfine structure, amounts of self-absorption within the source have been estimated by visual inspection of the observed profile and by relative intensity measurements on the hfs peaks. In the case of

elements such as calcium, which have no hfs detectable on the existing instrument, evaluation has been carried out by accurate measurement of line widths and also by visual observation of very serious self-absorption and self-reversal.

7.2 Estimation of self-absorption effects in thallium sources from the relative intensities of the hyperfine components.

7.2.1 General

The thallium atomic spectrum is well-suited to the type of studies envisaged for the present work. It is simple, with a few well separated and intense lines. Of these, the resonance line at 3775.72Å is within the useful range of our instrument and was easily studied. The well known green line at 5350.46Å lies at the optimum wavelength region for study with the instrument and, since its lower level lies only 0.966eV above the ground state, shows self-absorption like thatobtained at the resonance line. Both lines have a well-defined hfs which assumes a useful and easily recognized pattern with the resolving power of our instrument., Furthermore, VDL, HCL and EDT sources are readily available for thallium so that a comprehensive comparative study is possible.

The instrumental arrangement used was exactly as described in Section 6.4. Commercial VDL and HCL sources were employed (Wotan lamps and Atomic Spectral Pty. Ltd., respectively) but the EDT was prepared in the laboratory. The vacuum line and method of preparation used has been described in detail by Thompson[167]. The tubes were made by using transparent quartz tubing (Jencons Ltd.) of 8mm internal diameter and 1.1mm wall thickness with argon as the filler gas. EDT's were prepared using extremely small quantities (less than 5mg) of thallium metal, thallium metal + iodine, thallium iodide and thallium chloride. Discharge tubes using the metal alone would only emit a

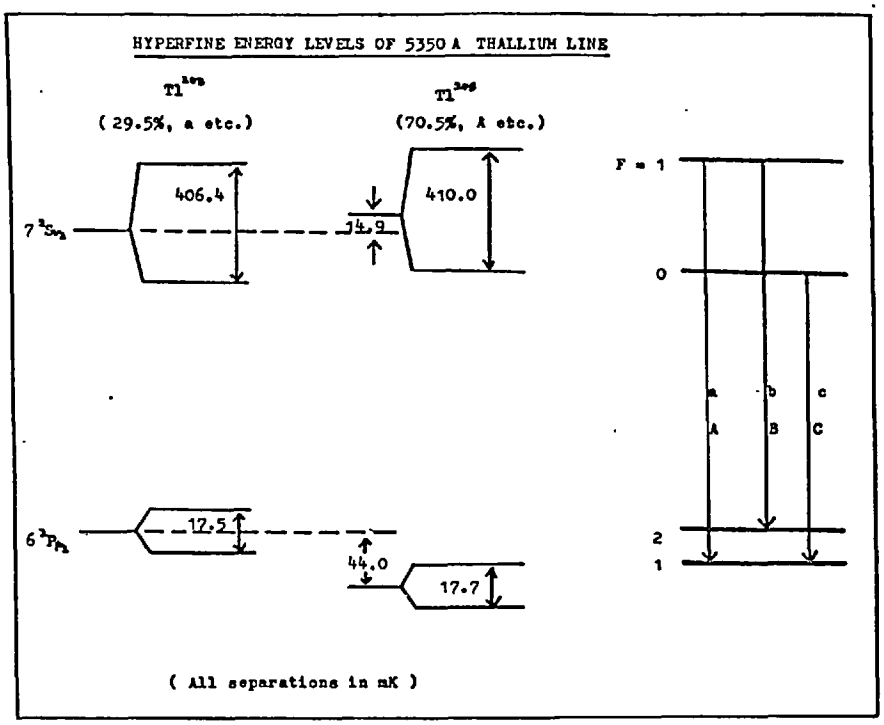
sufficiently intense spectrum at very high power and were very unstable. Those made with the metal and iodine were also of little use. They were troublesome to prepare and invariably contained too much iodine. No significant differences could be detected between good tubes made with the iodide or chloride. Since it was generally easier to prepare a good tube using the iodide, an EDT of this type was used for the results given here. It worked well with an argon pressure of 5 to 7 torr. A short bulb was essential to keep all of the bulb well within the discharge region of the cavity (this prevents condensation of solid material at the ends of the bulb) and best results were obtained with a length of about 2.5cm. The tube would give a thallium spectrum at the minimum power of 20 watts, but only assumed the characteristic intense green discharge at about 30 to 35 watts.

7.2.2 Results

Measurements were made at both 5350Å and 3776Å since although the former is a non-resonance line it indirectly provides useful information concerning self-reversal of the resonance line. This is important since with many Fabry-Perot interferometers only non-resonance lines in the visible region are accessible to study (because of the restrictions due to the nature of the plate-material and mirror coatings).

The hyperfine structure of both lines contains a number of components due to the existence of two stable isotopes (Tl^{203} and Tl^{205}) both of which have a nuclear spin. The accepted hyperfine splittings of the energy levels of the two lines and the resulting configuration of the hyperfine structure are shown in Figures 7-1 and 7-2.

The experimental values for the splitting of the energy levels are taken from the work of Schuler, et. al.[168] but the relative intensities shown are the theoretical values calculated from the tables


HYPERFINE ENERGY LEVELS OF 5350 A THALLIUM LINE
Tl^205
(29.5%, a etc.)
Tl^203
(70.5%, A etc.)
406.4
410.0
14.9
7 ²S½
12.5
6 ²P½
44.0
17.7
F = 1
0
2
1
a
b
c
A
B
C
(All separations in mK)

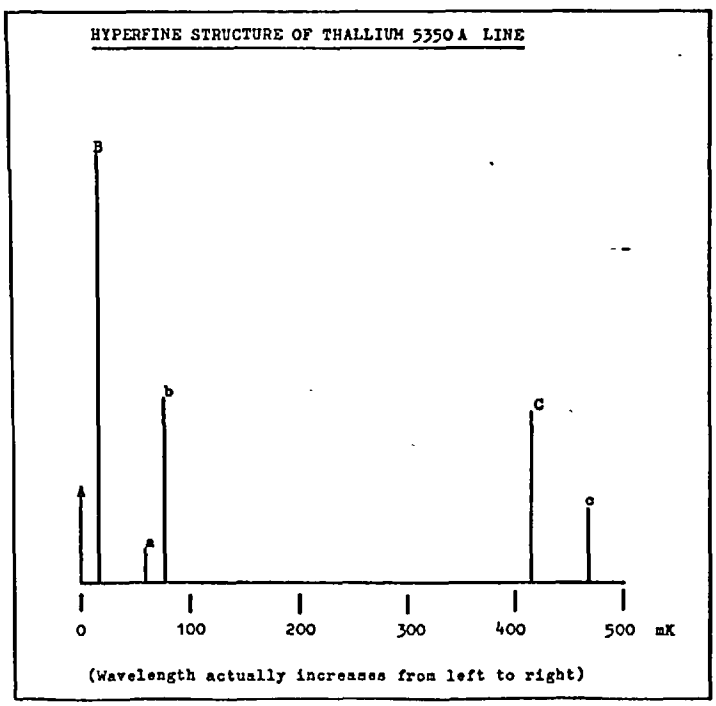
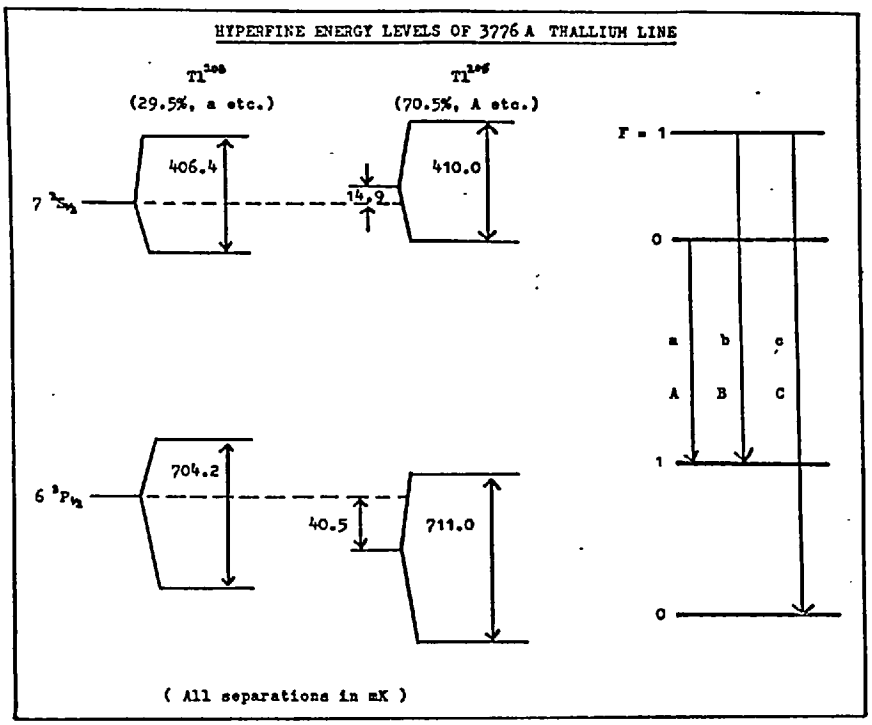

HYPERFINE STRUCTURE OF THALLIUM 5350 A LINE
B
b
C
A
a
c
0
100
200
300
400
500
mK
(Wavelength actually increases from left to right)

Fig. 7-1


HYPERFINE ENERGY LEVELS OF 3776 A THALLIUM LINE
Tl^205
(29.5%, a etc.)
Tl^203
(70.5%, A etc.)
406.4
410.0
14.9
7 ²S½
704.2
711.0
40.5
6 ²P½
F = 1
0
1
0
a
b
c
A
B
C
(All separations in mK)

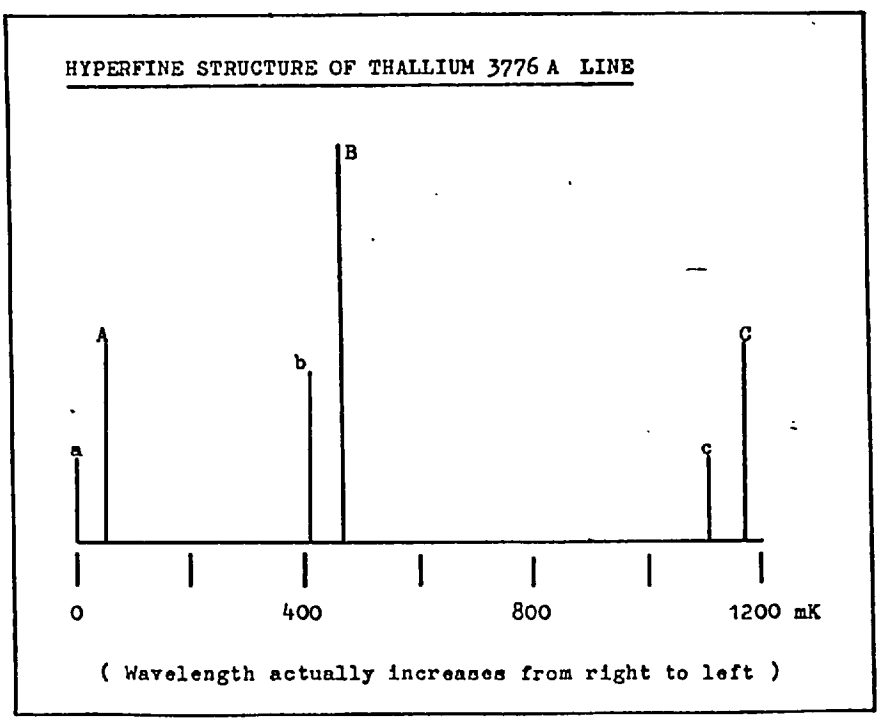

HYPERFINE STRUCTURE OF THALLIUM 3776 A LINE
a
A
b
B
c
C
0
400
800
1200 mK
(Wavelength actually increases from right to left)

Fig. 7-2

of White and Eliason[23], As a result of the line broadening within our sources, and to some degree the limited finesse of the interferometer, not all of the components could be resolved. The 5350Å line was observed as two peaks (a/A/b/B and c/C using the symbols of the diagrams). The 3776Å line was recorded as three peaks, each of which includes the corresponding component from the two isotopes. The hfs of both lines is very useful in assisting the rapid evaluation of conditions inside the spectral sources. This arises from the fact that the principal reason for loss of atomic absorption sensitivity when, for example, the current to a hollow cathode lamp is increased appears to be an increase in the self-absorption which occurs. The increase in broadening due to other causes (Doppler and collisional) seems to be quite small in these instances. The relative intensities of the hyperfine structure components of the two thallium lines studied are quite sensitive to self-absorption effects. It is therefore unnecessary to make accurate measurements of line widths or of absolute intensities to evaluate the conditions which prevail within the source and its suitability for AAS. (This is only true under the conditions commonly found in sources used for AAS. In many other situations, where self-absorption is less important (especially for non-resonance lines), the changes of Doppler and collisional half-widths with operating parameters etc. may have much greater significance).

Changes in the degree of self-absorption within the sources are manifested as changes in relative intensity of the hyperfine structure components in two ways. First, if two lines have very similar energy levels any difference in intensity will depend on their relative transition probabilities. Thus if one line is twice as intense as the other the amount of absorption at those lines will be approximately in the same ratio. This applies quite accurately to hyperfine structure components where the differences in excitation and wavelength have a negligible effect on intensity. As the most intense line is not only proportionally more strongly absorbed but also suffers from a larger absolute change in intensity, a rapid change in the intensity ratio occurs

as the self-absorption increases. Thus, for example, if the two hfs components have true intensities of 100 and 50 units and the smaller peak suffers 20% self-absorption, its observed intensity is 40 units (50 - 20/100 x 50) while that of the larger peak is 60 units (100 - 40/100 x 100), i.e. the ratio changes from 2:1 to 1.5:1 for only a moderate level of self-absorption. The calculated change in the intensity ratio of such a line pair is plotted in Fig. 7-3 over a wide range of self-absorption. It is emphasized that this is only a qualitative guide to conditions within the source and the method cannot give a rigorous evaluation of the effect of self-absorption on line intensities.

The a/A and b/B peaks of the 3776Å thallium line shown in Fig. 7-2 may be used as an example of this method of estimating the degree of self-absorption. The c/C and b/B peaks may not be used in this way because the lower energy level of the former line is a different state to that of the other two peaks. However, this allows the second method of noting changes in self-absorption to be applied. It has been shown by Turkin[169] that the upper of the two levels ($6\ ^2P_{\frac{1}{2}}$, F = 1) is actually metastable and has a higher population. Therefore, even without the effect outlined above, c/C would show less self-absorption than b/B. Thus, except at zero self-absorption the intensity ratio of b/B and c/C will not be identical to that of b/B and a/A. However, since a/A and c/C have the same theoretical intensities they will show only the effect of the metastable level. The increase in the intensity ratio (c/C : a/A) with self-absorption therefore gives an indication of the relative populations of the two levels as well as the degree of self-absorption.

Although a change in the ratio of the intensities of the two peaks observed for the 5350Å line will occur as self-absorption increases, it is more difficult to make an accurate evaluation of the results. This arises from the fact that the larger of the two peaks incorporates hyperfine structure components due to two different transitions (nuclear spin splitting) as well as to two isotopes.

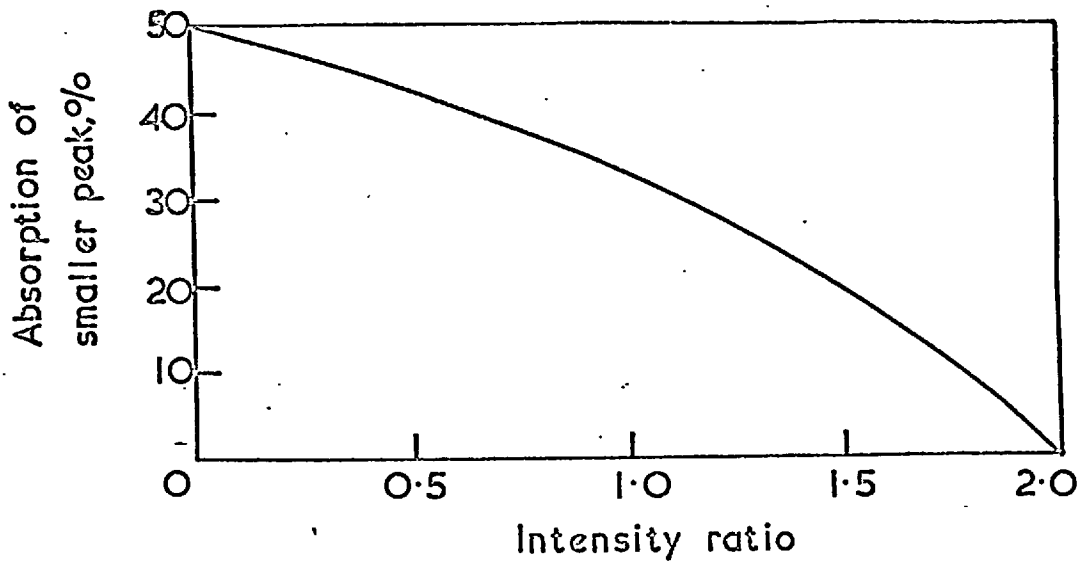


Fig. 7-3 Effect of Self-Absorption on The Intensity Ratio of a Pair of Hyperfine Structure Components With a Theoretical Intensity Ratio of 2:1

A graphical integration of the components of each peak using the known separations and intensities and an estimate of the line width (including the effect of instrumental half-width) indicates that the ratio of the observed peak heights at zero self-absorption should be in the region of 2.75 to 3.0 : 1. The change in the ratio will therefore be more rapid than with the 3776Å line as self-absorption increases. To some extent this effect compensates for the lower degree of self-absorption at 5350Å line, whose lower level is 0.966eV above the ground state, and a useful indication of self-absorption is still provided.

The hyperfine structure intensity measurements were carried out using a FSR of 750mK at the 5350Å line and 1500mK at the 3776Å line, i.e. ca. 0.2Å at both lines. These values give maximum resolution of the components before overlap of adjacent orders becomes a problem.

The results obtained for the HCL and VDL sources are shown in Tables 7-1 and 7-2. The results obtained with high operating currents for the vapour discharge lamp are not very precise, particularly at 3776Å, because under these conditions with this source the separate peaks were not well resolved. All of the hyperfine structure intensities in both tables are shown relative to each other. The intensities shown are uncorrected for change in photomultiplier and instrumental sensitivity between 5350 and 3776Å. The "conventional" intensity measurements shown at the right hand side of each table were made using the same instrumental arrangement as for the other measurements with the exception that the interferometer was removed from the optical bar. The tables also show the values obtained for the intensity ratios discussed above. Several of the scans from which the data of Tables 7-1 and 7-2 were taken are shown in Figures 7-4 and 7-5 since they illustrate very clearly the effect of increasing the lamp current.

An attempt was made to obtain similar data for the thallium electrodeless discharge tube. Unfortunately, the reproducibility of the EDT source (with respect to intensity, self-absorption and power input) was not sufficiently good to warrant a comprehensive tabulation of intensity measurements. The effect of variation in the power input to the EDT source employed is, however, illustrated in the scans shown in Figures 7-6 and 7-7. These are reproduced from photographs obtained using the fast scan facility in conjunction with the oscilloscope. No difficulties are encountered from drift of signal intensity during each measurement when photographs are taken using the instrument at fast scan rates. The vertical axis gain is given for each photograph so that the changes in intensity produced under different operating conditions may be gauged. These operating modes are indicated only as "low absorption", high absorption" modes etc., rather than by the power settings from the microwave generator employed as the power settings vary somewhat with the position of the compound in the tube and the tube within the cavity used. Typically the conditions shown were obtainable over the range 20 to 60 watts input power.
As an approximate guide, the EDT source gives about the same

Table 7-1

Effect of Lamp Current at Thallium 5350Å Line

Current (mA)	Intensity of hfs* a/A/b/B	c/C	(a/A/b/B): (c/C)	Conventional** Intensity
(a) Hollow cathode lamp.				
10	-	-	-	16.5
12	-	-	-	30
15	260	100	2.6	100
17	520	200	2.6	179
20	661	269	2.5	446
22	792	334	2.4	850
25	1430	637	2.3	1240
(b) Vapour discharge lamp.				
300	60	22	2.8	14
400	391	159	2.5	106
500	1290	727	1.8	369
600	1845	1145	1.6	1295
700	2160	1580	1.4	2550
800	2200	1870	1.2	3950
900	2250	2260	1.0	5800
1000	2070	2200	0.9	6150
1100	2030	2180	0.9	6600

* All to the same scale relative to an intensity of 100 for the c/C hyperfine structure component from the Tl 5350Å line emitted from the HCL source at 15mA.

** All to the same scale relative to an intensity of 100 for the 5350Å line emitted from the HCL source at 15mA.

Table 7-2

Effect of Lamp Current at Thallium 3776Å Line

Current (mA)	Intensity of hfs* a/A	b/B	c/C	(b/B): (c/C)	(c/C): (a/A)	Conventional** Intensity
(a) Hollow cathode lamp.						
10	45.5	86.5	44.5	1.9	1.0	29
12	97	182	97	1.9	1.0	52.5
15	234	422	236	1.8	1.0	172
17	436	773	443	1.8	1.0	330
18	513	910	530	1.8	1.0	490
20	744	1262	773	1.7	1.0	835
22	925	1545	985	1.7	1.1	1670
25	1260	2055	1400	1.6	1.1	2460
(b) Vapour discharge lamp.						
300	53	97.5	52	1.8	1.0	18
400	364	670	422	1.8	1.2	154
500	1010	1690	1320	1.7	1.3	530
600	2560	3480	3420	1.4	1.3	1860
700	3410	4150	4260	1.2	1.3	3350
800	4510	4430	5150	1.0	1.1	4750
900	3510	3350	3900	1.0	1.1	5700
1000	3180	3060	3480	1.0	1.1	5670
1100	2980	2860	3140	1.0	1.1	5720

* All to the same scale relative to an intensity of 100 for the c/C hyperfine structure component from the Tl 5350Å line from the HCL source at 15mA.

** All to the same scale relative to an intensity of 100 for the Tl 5350Å line emitted from the HCL source at 15mA.

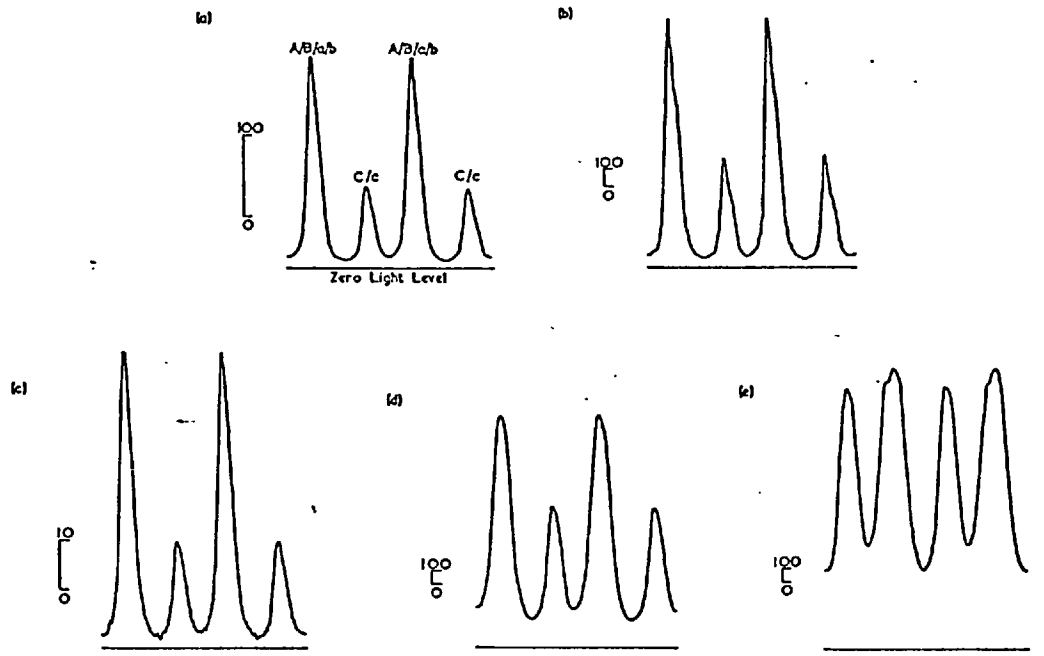


Fig. 7-4 Interferometer Scans of The Thallium 5350A Line

FSR = 750mK, two orders shown, relative intensity scale on left.
(a) HCL at 15mA (b) HCL at 25mA (c) VDL at 300mA
(d) VDL at 600mA (e) VDL at 1000mA

intensity as the HCL source when operated at the lowest self-absorption, but produces greater intensity for a given degree of self-absorption than the VDL source at the high power end of the operating range.

7.2.3. Discussion

The results of Table 7-2 provide an accurate guide to the effect on the resonance line of changing the current to the HCL and VDL sources. The graph of Fig. 7-3 may be used to convert the ratio b/B : a/A for the HCL source to approximate degrees of self-absorption.

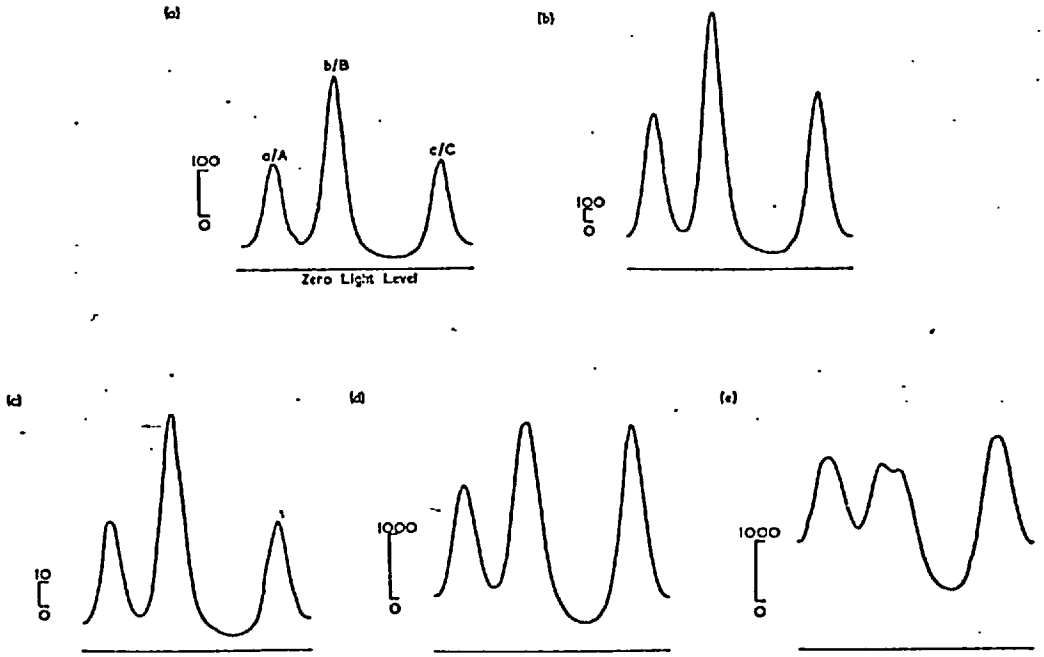


Fig. 7-5 . Interferometer Scans of The Thallium 3776A Line

FSR = 1500mK, one order shown, relative intensity scale on left. (a) to (e) for HCL and VDL as in Fig. 7-4.

This is only possible at very low operating currents for the VDL source as the overlap of the components due to line broadening/self-absorption becomes too large to allow the individual peaks to be accurately measured; hence the constant values achieved for both ratios in Table 7-2(b) when the self-absorption is obviously increasing rapidly. This is shown by the continued change in the ratio in Table 7-1 (b) which arises because measurements are still possible at the 5350Å hfs due to the better separation of the peaks. The results of Table 7-1 also show that, except at very low self-absorption, the 5350Å line is well able to indicate changes in self-absorption occurring at the 3776Å resonance line. It does, therefore, provide a useful alternative if measurements cannot be made at 3776Å.

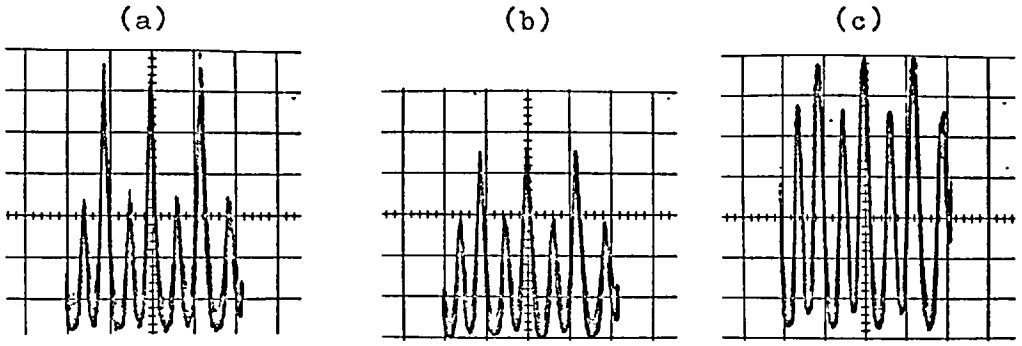


Fig. 7-6 Oscilloscope Traces of The Thallium 5350Å Line From an EDT Source

FSR = 750mK, identification of peaks as in Fig. 7-4(a).

(a) Low self-absorption (y axis 10mV/cm.)
(b) Medium self-absorption (y axis 20mV/cm.)
(c) High self-absorption (y axis 50mV/cm.)

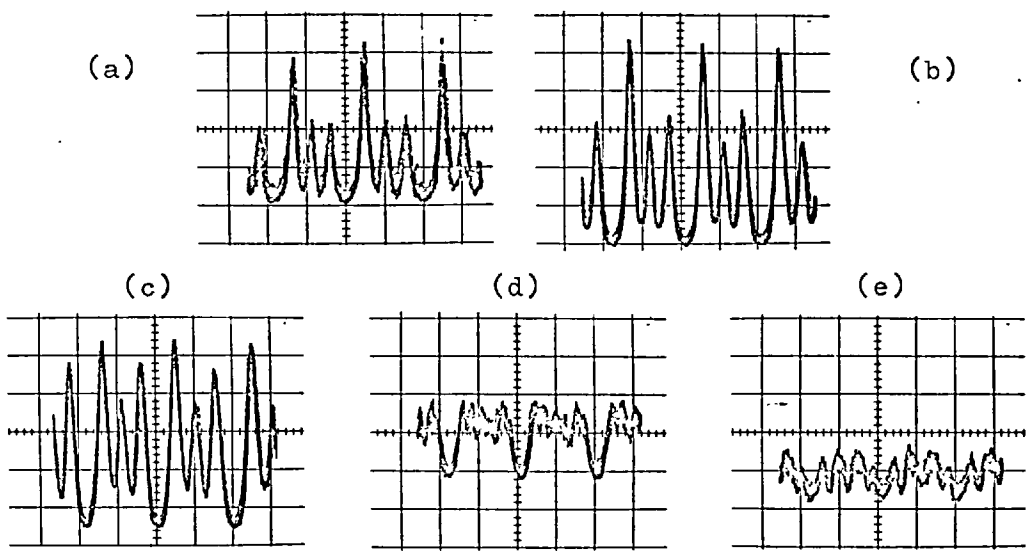


Fig. 7-7 Oscilloscope Traces of The Thallium 3776Å Line From an EDT Source

FSR = 1500mK, identification of peaks as in Fig. 7-5(a)

(a) Very low self-absorption (y axis 5mV/cm.)
(b) Low self-absorption (y axis 20mV/cm.)
(c) Medium self-absorption (y axis 50mV/cm.)
(d) Self-reversal (y axis 50mV/cm.)
(e) Serious self-reversal (y axis 50mV/cm.)

It can be seen from the tables and Figures 7-4 and 7-5, that self-absorption is low within the HCL at the operating currents recommended by the manufacturers (15 to 20mA) and changes only slowly with current variation. Conversely, the VDL shows severe self-absorption at its recommended operating current of 1Amp and the change in self-absorption with variation in the operating current is very marked. The VDL does give self-absorption and line-width comparable to the HCL, however, if it is operated at very low currents, but it is then less intense than the HCL (cf. VDL at 300mA and HCL at 18mA in Table 7-2).

As mentioned above, the behaviour of the thallium EDT was less predictable than that of the other two types of source. The relationship between the output intensity and degree of self-absorption can vary with the operating conditions, whereas it appears to be substantially constant for a particular HCL or VDL. The main reason for this appears to be that the conditions within the EDT change considerably dependent upon the position of the solid compound in the tube and this varies each time the EDT is used. Thus it is possible under favourable conditions to obtain from the thallium EDT a resonance line which is as narrow as that from a HCL and of at least equal intensity. At other times, however, the self-absorption may be worse than that with a VDL. Under most operating conditions the EDT was found to be very sensitive to changes in coupled power input, and may rapidly change from a "low intensity" mode, suitable for application to AAS, to the well-known "high intensity" mode. It should also be mentioned that under certain conditions the compound in the tube will condense out of the hot discharge region and a resonance line of the type shown in Fig. 7-7 (a) and 7-7 (b) can be obtained over a wide range of input power. From observations of the line profiles made when the EDT was working at its best, it would seem that an EDT is capable of giving a better combination of intensity and small half-width than the standard HCL. However, these benefits will only be obtained by design of a tube configuration which gives such results reliably, reproducibly and with stable output.

7.3 Accurate Measurements of Changes In Line Width

7.3.1 General

The method outlined in Section 7.2 for the evaluation of a spectral source is obviously inapplicable for an element whose spectral lines have no hyperfine structure. However, useful results may still be obtained and calcium will be used as an example to illustrate the measurements which are necessary. The main calcium isotope, Ca^{40}, has an abundance of 97% so that any isotopic fine structure in the calcium spectral lines is negligible for our purposes. Since calcium also has an even atomic number (20) there is no nuclear spin hyperfine structure. The main calcium resonance line lies at 4226.73Å which is well within the useful range of the F-P spectrometer employed for this work. The only difficulty is the provision of a suitable source. A calcium HCL (Atomic Spectral Lamps Pty.) was used at a current of 10mA (although the recommended setting for AAS is 5mA) to obtain a sufficiently high signal to noise ratio. Calcium EDT's with a useful operating lifetime are extremely difficult to prepare but it was possible to obtain a tube suitable for line width measurements (but not for AAS) by using the following technique.

The tube was prepared in the same way as those for thallium using a bulb of quartz tubing 2.0 to 2.5cm in length (8mm diameter, 1.1mm wall thickness) and an argon pressure of 5 torr. The calcium was added to the blank in the form of a solution of calcium chloride. This was prepared at a concentration of 10,000 ppm calcium by dissolving analytical grade calcium carbonate in 0.5 N hydrochloric acid, approximately 1 µl. of the solution being added to each tube (i.e. 10 µg of calcium). Some of the water was evaporated off by gently warming the tube at atmospheric pressure and the rest removed under vacuum. Care was taken to remove all traces of water vapour by repeated evacuation, flushing with argon and gentle warming before sealing off the bulb. For use with the interferometer the calcium EDT was used in

the power range 100 to 150 watts, reflected power being approximately 15 to 5 watts (the lowest reflected power being obtained at the highest incident power, presumably due to more efficient coupling in the untuned microwave cavity). Under these conditions the tubes produced an intense pink discharge which is mainly due to strong calcium oxide band emission. This does, of course, have no effect on the calcium resonance line at 4227Å which is observed with an extremely high signal to background ratio using a conventional monochromator. Except at the lower end of the power range, the discharge occupied the full width of the bulb only at the ends, taking the form of a narrow "neck" over the main part of the bulb. This constriction was normally observed to occupy a width of about 2mm at the centre of the bulb and was quite stable. Several tubes were prepared and in each case the ends of the bulb became partially coated with a white layer after a short period of running, leaving the centre part (around the constricted discharge) transparent. Thereafter this condition became stable and no change was observed in the operation of each EDT even after 50 to 100 hours of use.

7.3.2 Results

The line profile of the 4226.73Å line emitted by the calcium EDT was recorded at several different operating conditions. The operating condition of the EDT was taken as "standard" using the emission from the constricted part of the discharge at 130 watts (Fig. 7-8). The less intense output obtained from the same part of the discharge at 120 watts was classified as low power (Fig. 7-9). Some scans of the line profile obtained from the two distinctive regions of the EDT at high power are shown in Fig. 7-10. It may be seen, even without a hyperfine structure to study, that serious self-absorption and the onset of self-reversal are clearly visible. Smaller increases in line width may also be noted by carefully choosing the FSR so that it is only slightly larger than the observed line width.

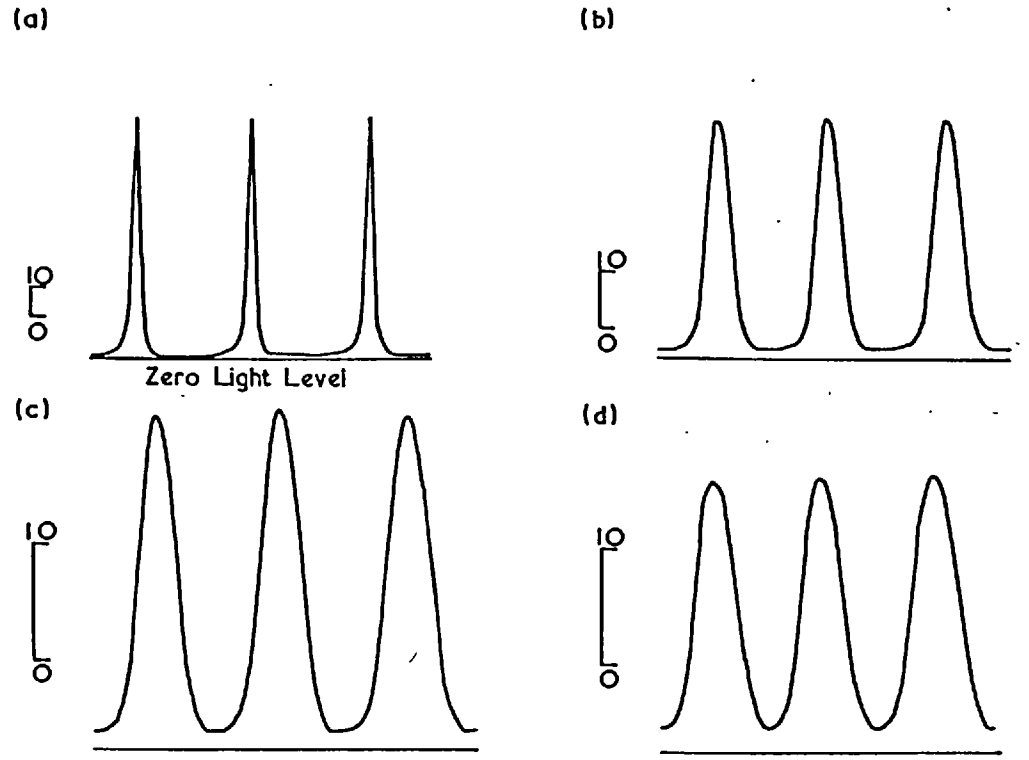


Fig. 7-8 Profile of The Calcium 4226.7Å Line From an EDT Source at Standard Power (130watts).

(a) Very large FSR (b) FSR = 1113mK
(c) FSR = 807mK (d) FSR = 603mK

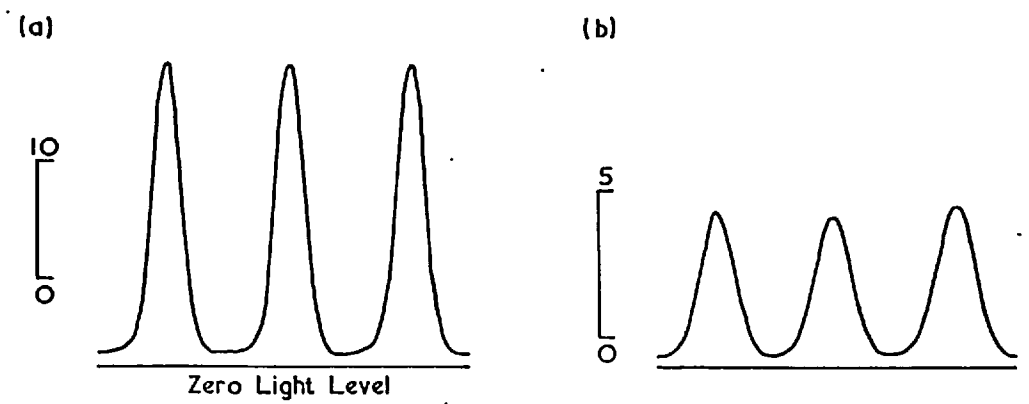


Fig. 7-9 Profile of The Calcium 4226.7Å From an EDT Source at Low Power (120watts).

(a) FSR = 890mK (b) FSR = 603mK

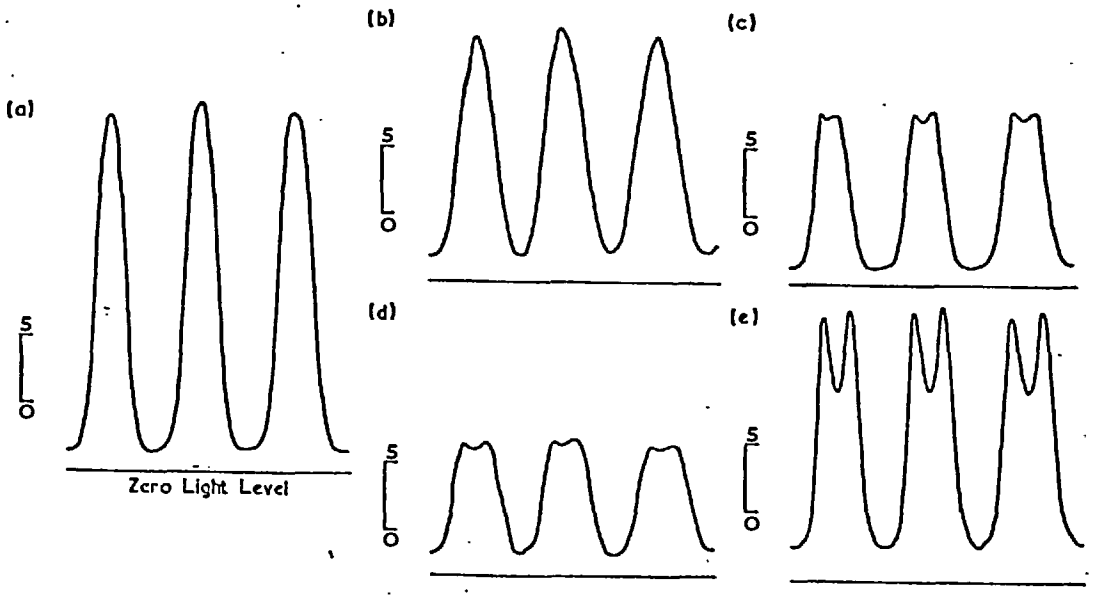


Fig. 7-10 Profile of The Calcium 4226.7A Line From an EDT Source at High Power

(a) FSR = 807mK, 140watts, constricted region of discharge.
(b) FSR = 603mK, " " " "
(c) FSR = 807mK, 140watts, full width region of discharge.
(d) FSR = 603mK, " " " "
(e) FSR = 900mK, 150watts, full width region of discharge.

Increases in line width are then quite easily seen by the smaller separation between orders near the zero light level. Several different FSR's were used for the scans in the diagrams and this effect may be seen by studying the scans made with a FSR of 603mK; even the small change between 120 watts in Fig. 7-9 (b) and 130 watts in Fig. 7-8 (d) is quite clear.

To indicate the very large half-width of these lines from the calcium EDT, some scans from the calcium HCL are shown in Fig. 7-11. Six different FSR's were used and the lamp was run at 10mA, which is a good compromise between the manufacturer's recommended current of 5mA (giving a signal of insufficient intensity) and the maximum current of 20mA. Comparison of Fig. 7-8 (c) and 7-11 (b) which were

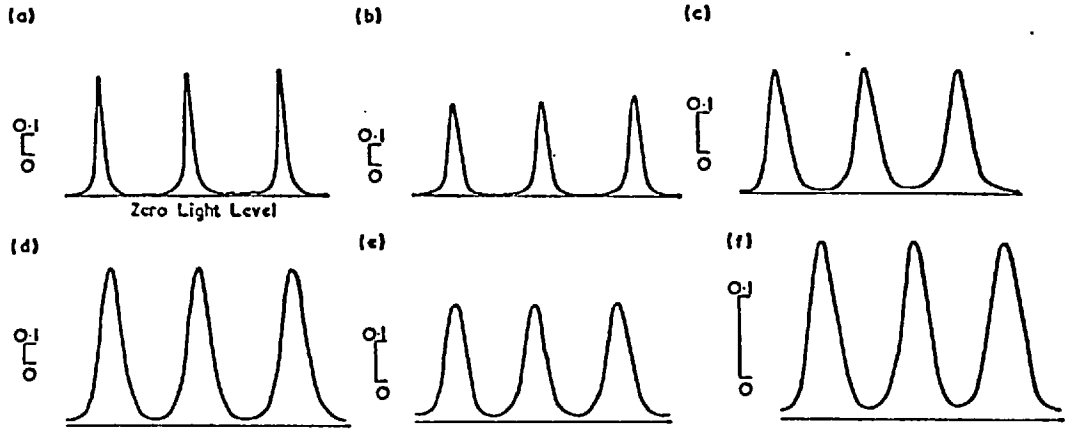


Fig. 7-11 Profile of The Calcium 4226.73A Line From A Hollow Cathode Lamp Source at 10mA.

(a) FSR = 1610mK (b) FSR = 800mK (c) FSR = 400mK
(d) FSR = 265mK (e) FSR = 249mK (f) FSR = 216mK

made using approximately the same FSR, shows very clearly the large difference in the line widths of the two sources. Similarly, the separation of the peaks in Figs. 7-8 (c) and 7-11 (f) is approximately the same even though the latter was recorded using a FSR almost four times smaller. Thus it may be seen that even without a hfs to study it is possible to detect a wide variety of changes in the line profile simply by visual observation. Rapid evaluation of new sources using fast scanning and the oscilloscope should, therefore, still be possible in many cases.

More precise information may be obtained, however, by making actual measurements of the half-width of the line. As mentioned earlier, this involves a number of problems. The observed width is easily obtained from the profile by measuring the fraction of an order to which it corresponds. This fraction is then converted to the

half-width by multiplying it by the FSR. The values of this shown in the diagrams were found by measuring the plate separation with a travelling microscope and are sufficiently accurate for the present experiment. The instrumental width may also be calculated fairly easily by measuring the finesse. This was calculated from the scan in Fig. 7-8 (a) which was recorded using a very large FSR. The value of 14 obtained for the finesse is in good agreement with that given in Fig. 6-8. Thus, for each scan the instrumental width is taken as simply (FSR/14). The calculation of the true half-width of the line from the observed and instrumental widths is a far more serious problem and can, in fact, only be overcome by using a source carefully chosen to give a certain type of profile. Even with a very sophisticated technique involving complex theoretical calculations it is extremely difficult to measure the line width of a source chosen completely at random.

This problem arises because the relation between the true and observed widths of the line depends upon the distribution curve of the line; i.e. on the mathematical expression which may be used to represent the variation of intensity with wavelength. The simplest case is with the so-called Lorentzian profile which results from natural broadening, collision broadening and resonance broadening. To a good approximation the observed width is then given by direct addition of the true and instrumental widths, i.e.

$$W = w + b \qquad (7\text{-}1)$$

where w is the true half-width of the line and b is the instrumental half-width. Although the lines from all normal sources will have some Doppler broadening, equation (7-1) will give fairly good results if the profile of a line is mainly due to, say, resonance broadening.

With lines having a Doppler broadened profile, the situation is much more complicated; the relationship between the true and observed widths varies with the ratio of the instrumental and true widths. Fortunately, all of these relationships were summarized in the form of a

plot of w/W versus b/W by Minkowski and Bruck[170]. Although more sophisticated treatments have been given by later workers, this simple graphical solution is quite sufficient for our purposes. Since the Doppler broadened profile is Gaussian, its combination with the Lorentzian one when both types of broadening are present becomes extremely complex (especially as there is still the instrumental function to take into account). Several solutions of the problem have been published with suitable tables or graphs to allow the interpretation of results. Unfortunately they may only be used if the ratio of Doppler to collisional (etc.) broadening is already known. They are, therefore, of no use in the present work.

The measured half-widths obtained from the line profiles in Figures 7-8 to 7-11 are given in Table 7-3. This shows the observed width, the true width assuming pure Doppler broadening (w_D) and the true width assuming pure resonance broadening (w_R). As would be expected, w_D and w_R are never equal, the latter in general being somewhat smaller. Unless there is pure Doppler broadening or a pure Lorentzian profile neither value will be correct and the true half-width presumably lies somewhere between the two values. This is discussed further below. It should also be noted that the error in each value will depend on the FSR used to measure it. Thus these values cannot be used directly even to measure changes in line width. Table 7-4 shows some of these changes calculated from the half-widths given in Table 7-3. It can be seen that from this point of view calculation of w_D and w_R serves no purpose since they both give the same change as simply using W. Also the indicated change in half-width depends very largely on the FSR used. For this reason great care must be taken when consulting papers which give only uncorrected half-widths for "comparison of relative values" (see, for example, Ref. 162); when conditions are varied these relative values may have no simple relationship.

Table 7-3

Half-Width of The Calcium 4226.73Å Line

Type of Source	FSR (mK)	Half-Width (mK)* b	W	W_D	W_R
1) EDT at 120 watts.	890	63.5	239	214	175.5
	603	43	220.5	204	176.5
2) EDT at 130 watts	1113	79.5	280	248	200.5
	807	57.5	267.5	245	210
	603	43	244.5	228	201.5
3) EDT at 140 watts (discharge centre)	807	57.5	303	282	245.5
	603	43	306	291	263
4) EDT at 140 watts (discharge end)	807	57.5	346	325	288.5
	603	43	354	338	311
5) EDT at 150 watts	900	64.3	462	438	398
6) HCL at 10mA	1610	115	159	87.5	44
	800	57	111.5	83	54.5
	400	28.6	92	80	63.4
	265	19	77	69.5	58
	249	18	76.5	70	58.5
	216	15.5	75.5	69.5	60

* Refer to text for definitions of the symbols.

Table 7-4

Effect of FSR on Measured Changes in Half-Width

Sources being compared	Change in half-width (mK)					
	FSR = 807 mK			FSR = 603 mK		
	W	w_D	w_R	W	w_D	w_R
1 - 2	-	-	-	24	24	25
2 - 3	35.5	37	35.5	61.5	63	61.5
2 - 4	78.5	80	78.5	109.5	110	111
3 - 4	43	43	43	48	47	48

7.3.3 Discussion.

The difference between the values of w_D and w_R obtained from a given value of W will depend on two factors. First, the larger the FSR the larger will be the difference (although the difference relative to the FSR should, of course, be constant). Secondly, the closer the true line profile approaches one of these two extremes the larger will be the difference (since the error in the other value will be that much greater). Both of these possibilities are illustrated in Table 7-5. This lists the results of Table 7-3. recalculated in the form of two coefficients, x and y, which are defined as

$$x = 100(w_D - w_R)/w_R \qquad (7\text{-}2)$$

$$y = 100\ (w_D - w_R)/w_D \qquad (7\text{-}3)$$

The effect of FSR on these coefficients is removed by dividing each value by its corresponding FSR and the results obtained are shown in the last two columns of Table 7-5. The reference numbers for the different types of source are those given in Table 7-3.

Table 7-5

Source	FSR (mK)	x	y	100x/FSR	100y/FSR
1	890	22	18	2.5	2.0
	603	15.6	13.5	2.5	2.2
2	1113	23.7	19.2	2.1	1.7
	807	16.7	14.3	2.1	1.8
	603	13.2	11.6	2.2	1.9
3	807	12.8	11.2	1.6	1.4
	603	10.6	9.6	1.8	1.6
4	807	12.6	11.2	1.6	1.4
	603	8.7	8.0	1.4	1.3
5	900	10	9.1	1.1	1.0
6	1610	99	49.8	6.1	3.1
	800	52.6	34.4	6.6	4.3
	400	26.2	20.8	6.5	5.2
	265	19.8	16.5	7.5	6.3
	249	19.2	16.1	7.7	6.5
	216	15.8	13.7	7.3	6.3

It can be seen that for each source fairly good agreement is obtained after this correction for the effect of FSR. This shows that good accuracy is being obtained in the measurement of W, the errors arising during its interpretation. Generally speaking the highest accuracy in W would be expected with smaller FSR for the narrow lines and with the larger FSR for the wide lines (due to errors caused by overlap of orders). Another much more interesting observation which can be made from Table 7-5 concerns the change in the corrected values of x or y between the different sources; i.e. as

the line width changes. The coefficients are largest for source 6 (i.e. the HCL giving a very sharp line) and drop sharply to their next largest value with source 1. Going from source 1 to source 5 (i.e. gradually increasing line width for the EDT) they show a steady decline. Thus the HCL line approximates much more closely to one extreme type of profile than that from the EDT. Furthermore, as the line width from the EDT increases the relative importance of the two types of broadening becomes even more similar.

These facts may be interpreted more readily by considering the line broadening theoretically. The natural width will be negligible as will pressure broadening (due to the low filler gas pressure in the lamps) and Stark broadening (due to the low electric fields). This leaves Doppler, resonance and self-absorption broadening. The Doppler half-width may be calculated using the equation

$$\Delta\sigma_D = 2\sigma_o \left(\frac{2kT\ln 2}{mc^2}\right)^{\frac{1}{2}} \qquad (7\text{-}4)$$

where σ_o is the wavenumber of the line centre, k is the Boltzmann constant, T the absolute temperature, m the mass of the atom and c the velocity of light. Equation (7-4) reduces to

$$\Delta\sigma_D = (7.162 \times 10^{-7}).\ \sigma_o.\ (T/M)^{\frac{1}{2}} \qquad (7\text{-}5)$$

where M is the atomic weight of the atom. Values of $\Delta\sigma_D$ for the calcium 4227Å line over a range of temperatures are shown in Fig. 7-12.

The value of w_D obtained for the HCL was about 70mK (using the results with small FSR since these should be the most accurate). Assuming that other broadening factors account for no more than about 5mK, it can be seen from Fig. 7-12 that the temperature of the HCL is in the range 600 to 700°K (i.e. 325 to 425°C). This is a very reasonable result for a HCL of this type running at 10mA and we may assume that Doppler broadening is by far the most important factor. The value of w_D obtained should, therefore, be quite close to the true width of the line. At this wavelength, a half-width of 70mK is equal to about 0.0125Å, which is considerably less than the value of

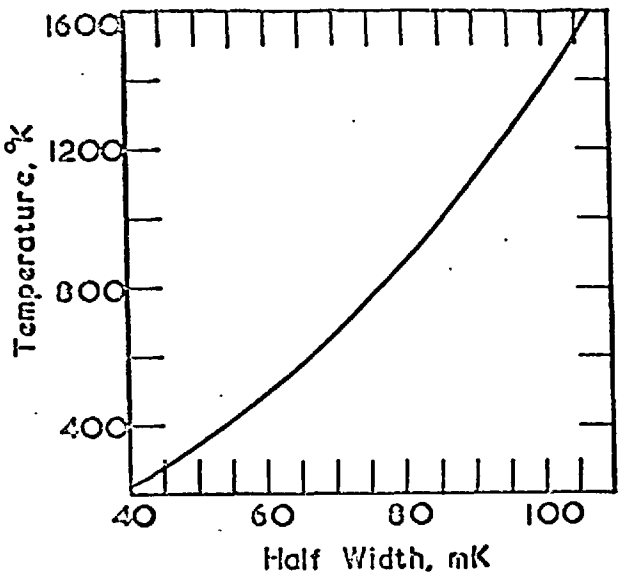


Fig. 7-12 Variation of Doppler Half-Width With Temperature For The Calcium 4226.73A Line

0.04Å often quoted as an approximate width of the lines emitted by HCL's.

The situation with the EDT is more difficult to interpret. Although under the conditions used the quartz bulb normally glowed red, it never became white hot or softened. Its temperature could not, therefore, have exceeded 1000°C at the most. Referring to Fig.7-12 it may be seen that the maximum possible Doppler width of the line is of the order of 95mK. Furthermore, the effect of self-absorption on a Doppler profile is such that it can only approximately double the half-width even when self-reversal has become quite pronounced. Therefore, it may be concluded that the largest likely half-width resulting from Doppler and self-absorption broadening is about 190 mK and this is less than the value of w_D given for even source 1 in Table 7-3. Thus there must be a considerable contribution from resonance broadening even when the EDT is run at 120 watts. This

contribution will increase with higher power, since the resonance broadening depends directly on the number of atoms present. Fig. 7-12 shows that the increase in Doppler width between 120 and 150 watts would be no more than about 20 mK even for a temperature change of about 500^0, so that changes in resonance broadening are probably more important than changes in Doppler broadening as the power is increased. However, increases in self-absorption broadening will probably be even more important than either of these, since it must be remembered that the self-absorption effect acts on the combined broadening of all other facts. This increase with increasing atom population in the EDT is made even more pronounced by the fact that a given degree of self-absorption causes a larger change in half-width with a Lorentzian profile than with a Gaussian one; i.e. the greater the resonance broadening contribution to the half-width the more serious is the effect of self-absorption.

In view of these considerations, it seems likely that for the "standard" calcium EDT (i.e. operating at 130 watts), the Doppler half-width is about 80mK, the resonance half-width is somewhat less than 50% of this value (remember that they cannot be summed by direct addition) and self-absorption approximately doubles the effect of these two factors. Thus a good estimate of the half-width at this power would lie in the range 210 to 220 mK; i.e. about three times the line width obtained from the HCL. The EDT would, therefore, be quite unsuitable as a source for AAS when used in this way. However, it should give good results for AFS since the line is both intense and has a profile which should give efficient transfer of energy to the absorbing atom.

7.4 Conclusions

A scanning Fabry-Perot interferometer has been employed for the routine evaluation by several different methods of spectral sources

used in atomic absorption and fluorescence spectroscopy. It has been found that using this instrument simple qualitative techniques are capable of giving a considerable amount of useful information on a spectral source. However, to avoid errors it has proved to be essential to take into consideration the limitations of the instrument and to carry out a preliminary survey of the source and spectral line to be studied. Even with considerable experience it is rarely possible to make an immediate useful evaluation of an "unknown" source. An exception to this rule is the identification of serious self-reversal, such as is often obtained from an EDT operated in the so-called high intensity mode, which has proved to be a facile problem with most sources.

Experience has shown that if a detailed study is to be carried out on a particular source, results may be most easily obtained when a simple, easily identified hyperfine structure is present. Detailed information on self-absorption within the source may then be obtained from relative intensity measurements on the components. On the other hand, an accurate measurement of the actual line width may only be obtained if there is no hfs or if the components are widely separated. Even then the interpretation of results is difficult with most sources. It would seem that accurate measurement of line widths is not a realistic method of evaluating spectral sources and in any case is often of little added advantage. However, it would be a useful exercise to prepare several examples of the most widely used sources in a form optimised for line width measurements of different types. It would then be possible to obtain detailed information on line widths for applications in AAS research.

A number of possible improvements to the Fabry-Perot interferometer have become apparent while carrying out the work described above. Perhaps the most important of these would be to improve the light transmission of the mirror surfaces. This would make the study of all types of HCL much easier and would also allow the use of sources such as flames. A very worthwhile improvement can be achieved by using

interferometer plates with dielectric mirror surfaces rather than aluminium and these can, in fact, be obtained at very little extra expense provided that a restricted wavelength range can be tolerated. This would be no real problem if a detailed study of, say, line widths were carried out at a few carefully chosen spectral lines. Vibrations have also proved a problem but again the solution should be quite simple; ideally the instrument should be located in a basement laboratory with a stone floor.

Finally mention must be made of spectral sources studied with the instrument. It is obviously unwise to make broad general assumptions on the basis of one or two examples. However, from the results given here it does seem that self-absorption is a most serious factor in reducing the suitability of sources for AAS; it would certainly appear to have a much greater effect than increases in Doppler broadening when lamp currents are increased. It would, therefore, be advantageous to develop sources which kept to a minimum the number of free atoms present, the number of "cool" atoms within the light beam, and the optical path length within the source. The other important point made clear by the interferometer in connection with the development of light sources concerns the stability and intensity of EDT's. As discussed in Section 7.2, an EDT designed to give maximum intensity and stability when measured with a conventional monochromator will often also give extremely wide lines. If these sources are to be used for AAS it is essential that measurements of the line profile be carried out as a routine part of the development programme in conjunction with the more usual checks on intensity and stability.

References

1. I. Newton, "Opticks, or a Treatise of the Reflections, Refractions, Inflections and Colours of Light". 1st Ed. 1704, reissued by Dover Publications, New York, 1952.
2. G. Kirchhof and R. Bunsen, Phil. Mag., 20, 89-109, (1860).
3. G. Kirchhoff and R. Bunsen, Phil. Mag., 22, 329-49, (1861).
4. P. Champion, H. Pellet and M. Grenier, Compt. Rend., 76, 707-11, (1873).
5. H. Lundegårdh, "The Quantitative Spectral Analysis of the Elements", Vol. I, 1929 and Vol. II, 1934. (G. Fischer, Jena).
6. A.C.G. Mitchell and M.W. Zemansky, "Resonance Radiation and Excited Atoms", University Press, Cambridge, 1934 (republished 1961).
7. A. Walsh, Australian Patent 23041, (1953).
8. C.T.J. Alkemade and J.M.W. Milatz, Appl. Sci. Res., 4B, 288-99, (1955).
9. R.W. Wood, Phil. Mag., 10, 513, (1905).
10. P. Pringsheim, "Fluorescence and Phosphorescence", Interscience, New York, 1949.
11. E.L. Nichols and H.L. Howes, Phys. Rev., 22, 425, (1923) and 23, 472, (1924).
12. R.M. Badger, Z.f. Phys., 55, 56, (1929).
13. R. Mannkopff, Verhandl. d. Deutsch. Phys. Ges., 14, 16, (1933).
14. A.L. Boers, C.T.J. Alkemade and J.A. Smit, Physica, 22, 358-60, (1956).
15. C.T.J. Alkemade, pp. 143-170 of Proc. Xth Colloq. Spectros. Inter., Maryland, U.S.A., 1962. (Spartan Books, Washington, 1963).
16. J.D. Winefordner and T.J. Vickers, Anal. Chem., 36, 161-5, (1964).
17. J.D. Winefordner and R.A. Staab, Anal. Chem., 36, 165-8, (1964).
18. R. Mavrodineanu and H. Boiteux, "Flame Spectroscopy", Wiley, New York, 1965.

19. A.G. Gaydon and H.G. Wolfhard, "Flames, Their Structure Radiation and Temperature", 2nd Ed., Chapman and Hall, London, 1960.

20. A.G. Gaydon, "The Spectroscopy of Flames" Chapman and Hall, London, 1957.

21. H.E. White, "Introduction To Atomic Spectra", McGraw-Hill, New York, 1934.

22. R.C. Gibbs, D.T. Wilber and H.E. White, Phys. Rev., 29, 790, (1927).

23. H.E. White and A.Y. Eliason, Phys. Rev., 44, 753-6, (1933).

24. G.F. Kirkbright and M. Sargent, "Atomic Absorption and Fluorescence Spectroscopy" in "Comprehensive Analytical Chemistry", Vol. III, Ed. by C.L. Wilson and D.W. Wilson, Elsevier, Amsterdam, to be published.

25. S.S. Penner, "Quantitative Molecular Spectroscopy and Gas Emissivities", Addison-Wesley, Reading, 1959.

26. H.G.C. Human, L.R.P. Butler and A. Strasheim, Paper presented at XVth Colloq. Spectros. Inter., Madrid, 1969.

27. A. Smithells and H. Ingle, J. Chem. Soc., 61, 204-16, (1892).

28. N. Teclu, J. Prakt. Chem., 44, 246-55, (1891).

29. A. Smithells and F. Dent, J. Chem. Soc., 65, 603-10, (1894).

30. G.A. Hemsalech, Phil. Mag., 34, 221-42, (1917).

31. F.A. Smith and S.F. Pickering, Ind. Eng. Chem., 20, 1012-3, (1928).

32. E.B. Ludlam, J. Chem. Phys., 3, 617-20, (1935).

33. M. Honma and C.L. Smith, Anal. Chem., 26, 458-62, (1954).

34. J.C. Street and A.C. Thomas, Fuel, 34, 4-36, (1955).

35. O.H. Drager, Brit. Pat. 872671 (Filed 21-8-59, published 12-7-61). Also German Pat. 1095552 (Dec. 1960) and U.S. Pat. 3025141 (Mar. 1962).

36. P.T. Gilbert, Anal. Chem., 38, 1920-2, (1966).

37. B. Gutsche, R. Herrmann and K. Rüdiger, Z. Anal. Chem., 241, 54-66, (1968).

38. O.H. Drager, Brit. Pat. 998532 (Filed 19-1-62, published 14-7-65). Also German Pat. 1133918 (July 1962) and U.S. Pat. 3213747 (Oct. 1965).

39. U.S. Naval Applied Science Laboratory, Brooklyn, N.Y. in a brochure presented at Instrum. Soc. Am. Exhib., Chicago, (Sept. 1963).

40. Illinois Institute of Technology Research Institute, Technical Documentary Report No. RTD-TDR-63-1072, (1963).

41. W.L. Crider, Anal. Chem., 37, 1770-3, (1965).

42. S.S. Brody and J.E. Chaney, J. Gas Chromatography, 4, 42-6, (1966).

43. R.M. Dagnall, K.C. Thompson and T.S. West, Analyst, 92, 506-12, (1967).

44. A. Syty and J.A. Dean, Applied Optics, 7, 1331-6, (1968).

45. R. Mavrodineanu, Develop. Applied Spectros., 5, 371-401, (1965).

46. B.F. Scribner, J. Opt. Soc. Am., 39, (T), 1059, (1949).

47. C.K. Matocha and J. Petit, Applied Spectros., 22, 562-71, (1968).

48. E.C. Hinck, T.F.Seamans, M. VanPee and H.G. Wolfhard, Proc. 10th Symp. (Inter.) on Combustion, pp. 21-32, (Cambridge), 1964).

49. R.P. Porter, A.H. Clarke, W.E. Kaskan and W.E. Browner, Proc. 11th Symp. (Inter.) on Combustion, pp. 907-17, Berkely, 1966).

50. R.M. Fristrom, R. Prescott, R.K. Neumann and W.H. Avery, Proc. 4th Symp. (Inter.) on Combustion, pp. 267-74, (Massachusetts, 1952).

51. G.M. Hieftje and H.V. Malmstadt, Anal. Chem., 40, 1860-7, (1968).

52. A. Egerton and S.K. Thabet, Proc. Roy. Soc., A211, 445-71, (1952).

53. P.J. Padley and T.M. Sugden, Proc. Roy. Soc., A248, 248-65, (1958).

54. D.R. Jenkins, Proc. Roy. Soc., A293, 493-511, (1966).

55. C.T.J. Alkemade, Proc. Xth Colloq. Spectros. Inter., pp. 143-70, (Spartan Books, Washington, 1963).

56. P.J.T. Zeegers and C.T.J. Alkemade, Proc. 10th Symp. (Inter.) on Combustion, pp. 33-40, (Cambridge, 1964).

57. P.J.T. Zeegers and C.T.J. Alkemade, Combustion and Flame, 9, 247-57, (1965).

58. P.J.T. Zeegers and C.T.J. Alkemade, Proc. XIIth Colloq. Spectros. Inter., pp. 290-6, (Exeter, 1965).

59. P.J.T. Zeegers, Ph.D. Thesis, Utrecht, 1966.

60. H.M. Strong, F.P. Bundy and D.A. Larson, Proc. 3rd Symp. on Combustion and Flame, pp. 641-7, (Baltimore, 1949).

61. E. Hinnov and H. Kohn, J. Opt. Soc. Am., 47, 156-62, (1957).

62. F.W. Hofmann, H. Kohn and J. Schneider, J. Opt. Soc. Am., 51, 508-11, (1961).

63. F.W. Hofmann and H. Kohn, J. Opt. Soc. Am., 51, 512-21, (1961).

64. W. Behmenburg, H. Kohn and M. Mailänder, J. Quant. Spectros. Radiat. Transfer, 4, 149-61, (1964).

65. T. Hollander, Ph.D. Thesis, Utrecht, 1964.

66. W. Snelleman, Ph.D. Thesis, Utrecht, 1965.

67. H.P. Hooymayers and C.T.J. Alkemade, J. Quant. Spectros. Radiat. Transfer, 6, 847-74, (1966).

68. C.T.J. Alkemade and H.P. Hooymayers, J. Quant. Spectros. Radiat. Transfer, 7, 495-504, (1967).

69. T. Hollander, P.J. Kalff and C.T.J. Alkemade, J. Chem. Phys., 39, 2558-64, (1963).

70. T. Hollander, P.J. Kalff and C.T.J. Alkemade, J. Quant. Spectros. Radiat. Transfer, 4, 577-9, (1964).

71. C.T.J. Alkemade, T. Hollander and P. Kalff, Combustion and Flame, 9, 101-3, (1965).

72. P.J. Kalff, T.J. Hollander and C.T.J. Alkemade, J. Chem. Phys., 43, 2299-307, (1965).

73. C. van Trigt, T.J. Hollander and C.T.J. Alkemade, J. Quant. Spectros. Radiat. Transfer, 5, 813-33, (1965).

74. E.M. Bulewicz and T.M. Sugden, Proc. VIth Colloq. Spectros. Inter., pp. 20-27, (Amsterdam, 1956).

75. K. Schofield and T.M. Sugden, Proc. 10th Symp. (Inter.) on Combustion, pp. 589-604, (Cambridge, 1964).

76. S.I. Bogdan and W.G. Zinman, Rev. Sci. Instr., 33, 766-7, (1962).

77. T.E. Weichselbaum and P.L. Varney, Proc. Soc. Exptl. Biol. Med., 71, 570-2, (1949).

78. J.A. Ramsay, S.W.H. Falloon and K.E. Machin, J. Sci. Instr., 28, 75-80, (1951).

79. P.T. Gilbert, Analyzer (Beckman Instruments Inc.), 2, 3-6, (1961).

80. Bulletin 3063, Beckman Instruments Inc. (March 1962) and Supplement 3063-1 (Sept. 1963).

81. P.T. Gilbert, Proc. Xth Colloq. Spectros. Inter., pp. 171-215, (Spartan Books, Washington, 1963).

82. P.T. Gilbert, Proc. 10th National Analysis Instrumentation Symposium, pp. 193-233, (Plenum Press, New York, 1964).

83. M.S.W. Webb and M.L. Wordingham, Anal. Chim. Acta, 28, 450-6, (1963).

84. J.F. Byrne, Proc. 4th Symp. (Inter.) on Combustion, pp. 345-8. (Massachusetts, 1952).

85. G.F. Kirkbright, A. Semb and T.S. West, Talanta, 14, 1011-19, (1967).

86. D.N. Hingle, G.F. Kirkbright and T.S. West, Talanta, 15, 199-206, (1968).

87. G.F. Kirkbright, A. Semb and T.S. West, Talanta, 15, 441-50, (1968).

88. G.F. Kirkbright, A. Semb and T.S. West, Spectroscopy Letters, 1, 7-11, (1968).

89. D.N. Hingle, G.F. Kirkbright and T.S. West, Analyst, 93, 522-7, (1968).

90. D.N. Hingle, G.F. Kirkbright and T.S. West, Analyst, 94, 864-70, (1969).

91. D.N. Hingle, G.F. Kirkbright, M. Sargent and T.S. West, Laboratory Practice, 18, 1069-70, (1969).

92. G.F. Kirkbright, M. Sargent and S. Vetter, Spectrochim. Acta, To be published.

93. M. Sargent "The Spectroscopic Determination of Temperatures", Research report, Imperial College, June 1967 (unpublished).

94. G.F. Kirkbright, M.K. Peters, M. Sargent and T.S. West, Talanta, 15, 663-75, (1968).

95. C.H. Corliss and J.L. Tech, NBS Monograph 108, (March 1968).

96. D. Robinson and P.D. Lenn, Applied Optics, 6, 983-1000, (1967).

97. G.H. Dieke and H.M. Crosswhite, Quarterly Report, Oct. 1 - Dec. 31, 1950, Dept. of Physics, The Johns Hopkins University.

98. H.P. Broida and K.E. Shuler, J. Chem. Phys., 27, 933-9, (1957).

99. W.J. Pearce, pp. 125-165 of "Optical Spectrometric Measurements of High Temperatures", Edited by P.J. Dickermann, Univ. of Chicago Press, 1961.

100. L. de Galan and J.D. Winefordner, J. Quant. Spectros. Radiat. Transfer, 7, 703-13, (1967).

101. R. Hefferlin, J. Opt. Soc. Am., 49, 680, (1959).

102. V. Leftus, Bull. Astron. Inst. Czech., 12, 161, (1961).

103. R. Hefferlin, J. Opt. Soc. Am., 52, 338-9, (1962).

104. H.J. Kostkowski and H.P. Broida, J. Opt. Soc. Am., 46, 246-54, (1956).

105. L.S. Ornstein and H. Brinkman, Proc. Amsterdam Acad. Sci. 34, 33-41, (1931).

106. J.A. Smit, Physica, 12, 683-700, (1946).

107. P.A. Fraser, W.R. Jarmain and R.W. Nicholls, Astrophys. J., 119, 286-90, (1954).

108. L. Brewer, L.K. Templeton and F.A. Jenkins, J. Am. Chem. Soc., 73, 1462-5, (1951).

109. N. Thomas, A.G. Gaydon and L. Brewer, J. Chem. Physics, 20, 369-74, (1952).

110. E.S. Fishburne, K.N. Rao and J.M. Weinberg, Combustion and Flame, 9, 425-6, (1965).

111. R. Watson, W.G. Planet and C.C. Pitts, Applied Optics, 7, 1941-7, (1968).

112. W. Lochte-Holtgreven and H. Maecker, Z. Physik, 105, 1, (1937).

113. R.S. Hobbs, G.F. Kirkbright, M. Sargent and T.S. West, Talanta, 15, 997-1007, (1968).

114. P.T. Gilbert, Bulletin 753A, Beckman Instruments Inc., Fullerton, California, (1961).

115. J.A. Dean and W.J. Carnes, Analyst, 87, 743-7, (1962).

116. D.C. Manning, J. Vollmer and F. Fernandez, Atomic Abscrption Newsletter, 6, 17-18, (1967).

117. J.E. Schallis and H.L. Kahn, Atomic Absorption Newsletter, 7, 75-9, (1968).

118. G.F. Kirkbright, M. Sargent and T.S. West, Talanta, 16, 245-53, (1969).

119. R. Herrmann and C.T.J. Alkemade, "Chemical Analysis By Flame Photometry", Interscience, New York, 1963.

120. J.B. Willis, Nature, 207, 715-6, (1965).

121. E.E. Pickett and S.R. Koirtyohann, Spectrochim. Acta, 23B, 235-44, (1968).

122. M.D. Amos and J.B. Willis, Spectrochim. Acta, 22, 1325-43, (1966).

123. D.C. Manning and L. Capacho-Delgado, Anal. Chim. Acta, 36, 312-18, (1966).

124. H.D. Fleming, Spectrochim. Acta, 23B, 207-13, (1967).

125. M.L. Taylor and C.B. Belcher, Anal. Chim. Acta, 45, 219-26, (1969).

126. T.V. Ramakrishna, J.W. Robinson and P.W. West, Anal. Chim. Acta, 40, 347-50, (1968).

127. S.R. Koirtyohann, and E.E. Pickett, Spectrochim. Acta, 23B, 673-85, (1968).

128. D.R. Demers and D.W. Ellis, Anal. Chem., 40, 860-3, (1968).

129. W.W. Harrison and W.H. Wadlin, Anal. Chem., 41, 374-6, (1969).

130. G.F. Kirkbright, M. Sargent and T.S. West, Atomic Absorption Newsletter, 8, 34-7, (1969).

131. J.A. Dean and R.E. Fues, Anal. Letters, 2, 105-10, (1969).

132. W. Slavin, C. Sebens and S. Sprague, Atomic Absorption Newsletter, 4, 341, (1965).

133. C.L. Chakrabarti, Anal. Chim. Acta, 42, 379-87, (1968).

134. H.L. Kahn and J.E. Schallis, Atomic Absorption Newsletter, 7, 5-9, (1968).

135. O. Menis and T.C. Rains, Anal. Chem., 41, 952-4, (1969).

136. R. Smith, C.M. Stafford and J.D. Winefordner, Anal. Chim. Acta, 42, 523-31, (1968).

137. C.S. Rann and A.W. Hambly, Anal. Chim. Acta, 32, 346, (1965).

138. R.M. Dagnall, K.C. Thompson and T.S. West, Talanta, 14, 557-63, (1967).

139. R.M. Dagnall, K.C. Thompson and T.S. West, Talanta, 15, 677-87, (1968).

140. G.F. Kirkbright, M. Sargent and T.S. West, Talanta, 16, 1467-75, (1969).

141. J.B. Willis, Applied Optics, 7, 1295-1304, (1968).

142. R. Neybron and B. Rey-Coquais, Atomic Absorption Newsletter, 6, 92, (1967).

143. A. Hell, W.F. Ulrich, N. Shifrin and J. Ramirez-Munoz, Applied Optics, 7, 1317-23, (1968).

144. A.A. Venghiattis, Applied Optics, 7, 1313-16, (1968).

145. S. Tolansky, "High Resolution Spectroscopy", Methuen, London, 1947.

146. P. Jacquinot, Reports Progr. Phys., 23, 268-312, (1960).

147. C. Fabry and A. Perot, Ann. de Chim. et de Phys., 12, 459, (1897).

148. P. Jacquinot and C. Dufour, J. Rech. Centre Nat. Rech. Sci., 6, 1, (1948).

149. S. Tolansky and D.J. Bradley, pp. 375-84 of Interferometry; National Physical Laboratory Symposium No. 11, Teddington, 1959.

150. J. Cooper and J.R. Greig, Nature, 195, 371, (1962).

151. J. Cooper and J.R. Greig, J. Sci. Instrum., 40, 433-7, (1963).

152. J.V. Ramsay, Applied Optics, 1, 411-3, (1962).

153. K.D. Mielenz, R.B. Stephens and K.F. Nefflen, J. Res. Nat. Bur. Stand., 68C, 1-6, (1964).

154. R. Chabbal, J. Rech. Centre Nat. Rech. Sci.,24, 138, (1953).

155. J.R. Greig, Ph.D. Thesis, London University, 1964.

156. B.V. L'vov, Industrial Laboratory, 28, 987-93, (1963).

157. M.L. Parsons, W.J. McCarthy and J.D. Winefordner, Applied Spectrosc., 20, 223-30, (1966).

158. C.S. Rann, Spectrochim. Acta, 23B, 827-47, (1968).

159. B.J. Russell, J.P. Shelton and A. Walsh, Spectrochim. Acta, 8, 317-28, (1957).

160. M. Shimazu and A. Hashimoto, Science of Light (Tokyo), 11, 131-41, (1962).

161. R.J. Atkinson, G.D. Chapman and L. Krause, J. Opt. Soc. Am. 55, 1269-74, (1965).

162. A.I. Bodretsova, B.V. L'vov, E.N. Pavlovskaya and V.K. Prokof'ev, J. Appl. Spectrosc., 2, 62-7, (1965).

163. A.I. Bodretsova, B.V. L'vov and V.I. Mosichev, J. Appl. Spectrosc., 4, 149-52, (1966).

164. K. Yasuda, Anal. Chem., 38, 592-9, (1966).

165. D.K. Davies, J. Applied Physics, 38, 4713-20, (1967).

166. H.G.C. Human, A. Strasheim and L.R.P. Butler, paper presented at the International Atomic Absorption Spectroscopy Conference, Sheffield, 1969.

167. K.C. Thompson, Ph.D. Thesis, Ch. 2, London University, 1968.

168. C.J. Schuler, M. Ciftan, L.C. Bradley and H.H. Stroke, J. Opt. Soc. Am., 52, 501-3, (1962).

169. I.I. Turkin, Optics and Spectroscopy, 7, 5-6, (1959).

170. R. Minkowski and H. Bruck, Z. Physik, 95, 299, (1935).

Publications

Temperature Profiles in Nitrous Oxide Supported Acetylene Flames at Atmospheric Pressure.

Talanta, 15, 663-675, (1968)

Application of The Nitrogen-Separated Air-Acetylene Flame in Flame Emission and Atomic Fluorescence Spectroscopy.

Talanta, 15, 997-1007, (1968)

Measurement of Gas Flow-Rates and Calibration of Flow Meters For Flame Spectroscopy.

Analyst, 93, 552-554, (1968).

The Argon- or Nitrogen-Sheathed Nitrous Oxide - Acetylene Flame In Flame Emission Spectroscopy.

Talanta, 16, 245-253, (1969).

The Determination of Arsenic and Selenium by Atomic Absorption Spectroscopy in a Nitrogen-Separated Air-Acetylene Flame.

Atomic Absorption Newsletter, 8, 34-37, (1969).

Shielded Flame Emission Burner Assembly For Use With Atomic Absorption Spectrophotometers.

Laboratory Practice, 18, 1069-1070, (1969).

The Argon- or Nitrogen-Sheathed Nitrous Oxide - Acetylene Flame in Atomic Absorption Spectroscopy.

Talanta, 16, 1467-1475, (1969).

The Selection of Line-Pairs For The Iron 'Two-Line' Method of Flame Temperature Measurement.

Spectrochimica Acta, 25B, (1970), In Press.

The Application of A Piezoelectric Scanning Fabry-Perot Interferometer To The Study of Atomic Line Sources.

Spectrochimica Acta, To Be Published.

Errata

Page	Line	
12	22	For announced read enounced.
24	30	For factory read factor.
25	7	For There read These.
30	8	For absorping read absorbing.
50	25	For as read and.
55	24	Delete very.
105	16	For frome read from.
113	27	For smae read same.
119	21	For disoocation read dissociation.
154	6	For mixible read miscible.
158	3	For hsown read shown.
159	5	For exceot read except.
165	3	For 45-(a) read 4-5(a).
167	11	For probably read probable.
176	16	For requires read required.
215	19	For , read .